BEHAVIOR OF SHORT CONCRETE COLUMNS STRENGTHENED WITH FERROCEMENT

A THESIS

SUBMITTED TO THE COLLEGE OF ENGINEERING

OF THE UNIVERSITY OF BASRAH IN

PARTIAL FULFILLMENT OF

THE REQUIREMENTS FOR THE DEGREE

OF DOCTOR OF PHILOSOPHY IN CIVIL ENGINEERING

(STRUCTURES)

By

Abdulkhaliq Abdulyimah Jaafer

M.Sc. Civil Engineering (2008)

February, 2012

بِسْمِ اللهِ الرَّحْمنِ الرَّحِيمِ

إِنَّا أَعْطَيْنَاكَ الْكَوْثَرَ ﴿١﴾

فَصَلِّ لِرَبِّكَ وَانْحَرْ ﴿٢﴾ إِنَّ شَانِئَكَ هُوَ الْأَبْتَرُ ﴿٣﴾

صدق الله العلي العظيم

سورة الكوثر (١-٣)

To

My Family

Parents, brothers, Sisters

And wife

To all my friends

CERTIFICATION

I certify that the thesis entitled (**Behavior of Short Concrete Columns Strengthened with Ferrocement**) which is being submitted by ***Abdulkhaliq Abdulyimah Jaafer*** is prepared under my supervision at the University of Basrah in partial fulfillment of the requirements for the Degree of Doctor of Philosophy in Civil Engineering (Structures).

Signature:
Prof. Dr.Nabeel Abdulrazzaq Jasim
Date:

In view of the available recommendations, I forward this thesis for debate by examining committee.

Signature:
Dr. Ahmad M. Al-Kadhimi
Head of the Department of Civil Engineering
Date:

EXAMINING COMMITTEE'S REPORT

We certify that we, the examining committee, have read the thesis titled (***Behavior of Short Concrete Columns Strengthened with Ferrocement***) which is being submitted by (***Abdulkhaliq Abdulyimah Jaafer***), and examined the student in its content and in what is connected with it, and that in our opinion, it meets the standard of a thesis for the degree of Doctor of Philosophy in Civil Engineering (Structures).

Signature:
Name: **Dr. Nabeel Abdulrazzaq Jasim**
(Professor)
(supervisor)

Signature:
Name: **Dr. Ammar Yaser Ali**
(Professor)
(Member)

Signature:
Name: **Dr. Haithem H. Muteb**
(Professor)
(Member)

Signature:
Name: **Dr. Mustafa B. Dawood**
(Assist. Professor)
(Member)

Signature:
Name: **Dr. Jamal A. Khudair**
(Assist. Professor)
(Member)

Signature:
Name: **Dr. Nameer A. Alwash**
(Professor)
(Chairman)

Approval of the College of Engineering

Signature:
Name: **Prof. Dr. Nabeel Abdulrazzaq Jasim**
Dean, College of Engineering

ABSTRACT

One of the major requirements for strengthening or upgrading existing reinforced concrete structures is to increase their column capacities to withstand larger expected loads. There are different techniques to increase existing column capacities; however, such techniques differ in their advantages and disadvantages.

The main objective of the present study is to investigate the efficiency of confining plain concrete column with ferrocement jacket.

The study consists of two parts, experimental and theoretical. The main purpose of the experimental program was to investigate the structural behavior of concrete column strengthened with ferrocement jackets under monotonic and cyclic compression loading conditions. The experimental phase of this investigation consists of 48 short concrete columns. The main variables considered in this study were the volume fraction (number of wire mesh layers), the mortar compressive strength, column size, and column loading type. It was found that the ferrocement jacket provided sufficient lateral support to the concrete core and significantly increases both the strength and ductility of the specimens under axial loading. The ratio of strength of concrete column strengthened with ferrocement jacket to strength of plain concrete column ranged between 1.132 and 2.291 for columns with 35 MPa mortar compressive strength, whereas it was between 1.364 and 2.34 for columns strengthened with 45 MPa. Also, the validity of an envelope curve to describe cyclic behavior is discussed.

In the second part of the study, the tested columns are analyzed using nonlinear three dimensional finite element models. ANSYS (11.0) program is used to analyze the three dimensional model. Concrete core and ferrocement shell is modeled by using the 8-noded isoparametric brick elements (SOLID 65), while the loading steel plate as isoparametric brick elements (SOLID 45) with 8-nodes. Reinforcement in the ferrocement shell is assumed to be smeared throughout the concrete element. Perfect bond between concrete core and

ferrocement shell is assumed. The adopted finite element models are found to give results in a good agreement with the test results. It is found that the ratios of experimental to theoretical values of ultimate loads are between 0.88 to 1.094 with average of 0.983 for strengthened concrete columns with ferrocement jackets.

Several parametric studies have been carried out to investigate the effect of some important parameters on the predicted finite element results. The effects of concrete compressive strength, modulus of elasticity of ferrocement shell and applied load on ferrocement shell have been investigated.

The research also proposed new models for stress-strain relationship of concrete column strengthened with ferrocement jacket under monotonic load and for envelope curve, unloading and reloading.

Acknowledgement

First and always first, thank you to the almighty God for many blessings, past, present and future.

Words cannot express my sincere gratitude and appreciation to my supervisor Prof. Dr. Nabeel Abdulrazzaq Jasim for his guidance, assistance and encouragement offered continually during the various stages of this work.

Many thanks and appreciation are due to Prof. Dr. Nabeel Abdulrazzaq Jasim, dean of the College of Engineering, and Dr. Ahmad M. Al-Kadhimi, head of the Department of Civil Engineering, for providing facilities for conducting this investigation.

I would also like to use this opportunity to convey my gratitude to the staff of the Construction Materials Laboratory in the Department of Civil Engineering.

Thanks and respects are extend to my friends who helped me in my work specially Dr. Ahmad S. Saadon, Mr. Ali A. Khalaf and Mr. Sa'ad Fahad.

Especial thanks to Dr. Hayder Kamunna at University of Kufa for their help.

Last but not least, my thanks go to my family and friend for their support throughout the period of work.

Abdulkhaliq A. Jaafer

2012

CONTENTS

Notation

Symbol	Description
A_{sp}	Cross sectional area of spiral reinforcement
D	Diameter of column
D/t	Length to thickness ratio
D_b	Bar diameter of wire mesh
D_l	Centre to centre spacing of wires aligned longitudinally in reinforcement mesh
D_t	Centre to centre spacing of wires aligned transversely in reinforcement mesh
E_c	Modulus of elasticity of concrete
E_s	Modulus of elasticity of ferrocement shell
$E_{sec.}$	Secant modulus of elasticity of confining concrete
FE	Finite element
F	A function of the principal stress state (σ_1, σ_2, σ_3).
f	Yield function
f_c'	Uniaxial compressive strength of concrete
f'_{cc}	Axial compressive strength of strengthened column with ferrocement jacket
f'_{cm}	Compressive strength of mortar
f'_{co}	Axial compressive strength of unconfined concrete
f_r	Lateral confining pressure
f_{re}	Reloading stress
f_t'	Uniaxial tensile strength of concrete
f_y	yield strength of wire mesh reinforcement
f_{sy}	Yield stress of stirrup reinforcement
f_{un}	Unloading stress
h	thickness or ferrocement shell
k_1	constant
k_c	Confinement coefficent
L	Length (height) of column
L/D	Height to diameter ratio

Symbol	Description
L/r	Column slenderness ratio
N	Number of layers of mesh reinforcement
P	Axial load, kN
P_{cc}	Ultimate strength of concrete column strengthened with ferrocement jacket, kN
P_{co}	Ultimate strength of plain concrete column, kN
R^2	Correlation coefficient
w/c	Water to cement ratio
u,v,w	Displacement components
V_f	volume fraction of wire mesh
X,Y,Z	Global coordinate system at sampling point
β	Shear transfer coefficient
ε	strain
ε_c	Concrete strain
ε_{cc}	Strain at ultimate strength of strengthened concrete column with ferrocement jacket
ε_{co}	Strain at ultimate strength of plain concrete column
ε_{cu}	Concrete ultimate strain
ε_p	Plastic strain
ε_{un}	Unloading strain
$\varepsilon_1, \varepsilon_2, \varepsilon_3$	Principal strains
ε_o	Strain corresponding to peak uniaxial concrete compressive stress
ϵ'	Normalized unloading strain
ϵ_y	Yield strain of wire mesh
ν	Poisson's ratio
σ	Stress
σ_h	Hydrostatic stress
$\sigma_1, \sigma_2, \sigma_3$	Principal stresses
Matrices	
[A]	Displacement gradient matrix

Symbol	Description
[B]	Strain displacement matrix
[D]	Constitutive matrix
[J]	Jacobian matrix
|J|	Jacobian determinant
[K]	Stiffness matrix
[L]	Differential operator matrix
[N]	Shape function matrix
Vector	
{a}	Nodal displacement or flow vector
{b}	Body force
{f}	External load vector
{F}	Vector of applied loads
$\{F^a\}$	Total applied force vector
$\{F^{nr}\}$	Restoring force vector
{R}	Residual vector
{u}	Displacement vector (u,v,w) at node k
{σ}	Stress vector at sampling point
{ε}	General strain vector at sampling point

List of Figures

List of Tables

List of Plates

Abbreviations

ACI	American Concrete Institute
ASTM	American Society for Testing and Materials
CFFT	Concrete filled FRP tube
CFRP	Carbon fiber reinforced polymer
CFST	Concrete filled steel tube
FRP	Fiber reinforced plastic
GFRP	Glass fiber reinforced plastic
PVC	Polyvinyl chloride
RACFST	Recycled aggregate concrete filled steel tube
SL	Static load
VRL	Variable repeated load
WWM	Welded wire mesh

CHAPTER ONE
INTRODUCTION

1.1General

Compression members are the key elements of all skeletal structures, and the study of their behavior is usually based on testing of concentrically loaded columns. Compression members, or columns, may be defined as a members that carry axial compressive loads, and whose length is considerably greater than cross-sectional dimensions. Such members may carry other types of loadings, and may have end conditions and end moment of different kinds [1].

In buildings, bridges and other structures, columns play the vital role of transferring the vertical and lateral loads to the foundation. They are often reinforced with reinforcement consisting of longitudinal and transverse steel. The longitudinal reinforcement contributes to axial and flexural resistance. The transverse reinforcement contributes to improving shear (diagonal tension) capacity, preventing or delaying buckling of longitudinal reinforcement in compression, and confining concrete to improve strength and deformability of concrete. While the amount of longitudinal reinforcement affects flexural and axial strength, it does not play a significant role on column deformability. However, the transverse reinforcement plays a vital role on column shear strength and deformability [2]. Columns are often required to be designed with sufficient transverse reinforcement, in the form of ties, hoops, overlapping hoops and cross ties for excess shear capacity to prevent premature shear failure, which is regarded as a brittle form of failure. Hence, in properly designed concrete columns, brittle shear failure never precedes ductile flexural failure [2].

The same transverse reinforcement also improves flexural performance if placed with sufficiently small spacing. Closely spaced transverse reinforcement

provides a reinforcement cage which confines the compression concrete. Performances of reinforced concrete buildings and bridges located in earthquake regions have demonstrated that columns, especially at the first story level, suffer significant damage during strong earthquakes [2]. The damage also may be caused by the effects of missile impact, blast pressure, air raid, fire or vehicle collision. If any of these situations or others should arise, it needs to determine whether it is more economic to strengthen and rehabilitate the existing structure or to replace it [3].

Although the current design practice calls for strong columns and weak beams to dissipate seismic induced energy by yielding of the beams, it is difficult to prevent inelastic deformation in lower story columns during a strong earthquake [4]. Therefore, for earthquake resistant design, columns are proportioned to sustain a large number of inelastic deformation reversals without a significant loss of strength. This is referred to as inelastic deformability of columns and can be attained through the confinement or strengthening of core concrete [4]. Confined or strengthened concrete column is laterally restrained against possible expansion. Axially compressed concrete cannot crush unless it expands laterally due to the Poisson effect and develops vertical tensile cracks. The lateral pressure provided by confinement overcomes the tendency to expand, improving strength and ductility of concrete. In order to predict the behavior of concrete members with confinement throughout their loading range, the knowledge of the complete stress-strain relationship of confined concrete under various loading history is needed. The stress strain characteristics of confined concrete are distinctly different from those of uniaxially stressed concrete [5].

As a result of concrete column confinement, both the compressive strength and the ultimate strain of concrete can be enhanced. In all types of applications of strengthening techniques, the stress-strain behavior of confined concrete, under both monotonic and cyclic compression, needs to be properly understood and modeled [6]. The stress-strain behavior of confined concrete

under cyclic compression is of particular interest in the seismic retrofit and design of concrete structures.

1.2 Strengthening and Retrofitting Techniques of a Reinforced Concrete Element

One of the challenges in strengthening and rehabilitation of concrete structures is the selection of a method that will enhance the strength and serviceability of the structure while addressing limitation such as constructability, building operations, and budget. Strengthening and rehabilitation are accomplished either by reducing the magnitude of the internal forces or by enhancing the resistance of the existing structure to them [3].

The common confinement techniques that are used for strengthening and rehabilitation of the concrete structures are [7]:

1) Encasing concrete in steel jackets;
2) Lateral reinforcement in the form of steel ties or spirals (Section Enlargement);
3) External fiber composite wraps; or
4) Encasing concrete in fiber composite tubes.

The confinement of concrete columns by these means is passive by nature. The activation of these means depends on the lateral expansion due to axial compressive load. The lateral strain or the dilation of the column increases as the axial strain increases with increasing amount of compressive load. At the instant when concrete starts to crack due to the axial load carried by the column with strengthening means, the strengthening materials will experience tensile hoop stresses [4].

The most commonly method used for column retrofitting is steel jacketing as shown in plate (1.1). Steel jacketing involves covering the column surface by steel plates, welding the plates to form a sleeve, and filling the gap between the steel and concrete by pressure injected grout. The steel jacket overcomes diagonal tensile and compressive stresses generated by shear, while also

restraining concrete against lateral expansion, thereby confining the column for improved deformability [2]. In circular columns, passive confinement pressure is developed from hoop tension in the steel jacket as the concrete expands laterally. However, the same mechanism cannot be utilized in square and rectangular columns, unless the column is first re-shaped to have an elliptical or circular shape before a steel jacket is put in place [2]. The steel jacketing can be quite costly because of the large amounts of steel used and each steel jacket has to be custom made especially for non-circular columns.

Jacketing concrete columns can be done by providing a reinforced concrete sleeve around existing columns as shown in plate (1.2). This technique requires placement of reinforcement cage around the existing column which may be quite cumbersome especially because of the substantial amount of closely spaced transverse reinforcement that has to be placed around the column. Another complication is to provide the formwork and place concrete in the sleeve [2]. The mechanism of confinement and shear force resistance remains the same as that for steel jacketing. This technique results in a larger column size that may not be convenient and needing more space for the structure, which is not always possible. Therefore, section enlargement may require longer installation time than other strengthening method; however using reinforced concrete jackets results in a relatively lower cost [8].

All the previous strengthening and rehabilitation techniques are both labor intensive because of using heavy materials and vulnerable to future corrosion. Therefore, the other retrofitting techniques, that are being researched and developed for concrete columns, are FRP wraps and FRP tubes, involving fiber reinforced polymer (FRP) materials [2]. FRP can be used in strengthening systems because of its superior combination of properties with respect to weight, strength, stiffness, durability, fatigue, impact and corrosion resistance. Its ease in handling and application, and its light weight eliminates the need of mechanical lifting or anchoring devices, hence minimizing disruption to service for the duration of strengthening and maintenance process [3]. These techniques

involve covering the surface of concrete column by an FRP wrap or FRP tube, which provides passive confinement pressure as the concrete expands laterally under compression. While these techniques were proven to be effective for concrete confinement, its use against diagonal tension caused by shear is still questionable [3]. These techniques results in a higher load capacity without increasing section size, and can be done in a shorter construction time beside that it can be used while the building under operation; however such techniques results in a relatively high cost [8]. Plate (1.3) shows the concrete column wraps with FRP composite.

1.3 Ferrocement

Ferrocement was invented by a Frenchman, Joseph Louis Lambot, in 1848. It was a form of reinforced concrete, and it was used for the first time in making boats. Since the 1940's its application in the civil engineering field has widened. Definition of ferrocement reported by ACI Committee 549 [9] is a form of thin reinforced concrete structure in which a brittle cement-sand mortar matrix is reinforced with closely spaced multiple layers of thin wire mesh and /or small diameter rods, uniformly dispersed throughout the matrix of the composite. Figure (1.1) depicts the typical steel wire meshes used in ferrocement applications [10].

Ferrocement is a special form of reinforced concrete, which exhibits a behavior differing much from conventional reinforced concrete in strength performance and potential application. Therefore, the uniform dispersion of reinforcement in the matrix offers in achieving improvement in many of the engineering properties of the material, such as tensile and flexural strength, toughness, fracture, crack control, fatigue resistance and an impact resistance and in addition it provides advantages in fabrication [11]. In developing countries, the raw materials for ferrocement construction are easily available, and also it could be constructed in any complicated shape. The skill required is of low level and it has superior strength properties as compared to conventional reinforced concrete [11]. These are the reasons for which the ferrocement is

considered to be an appropriate confinement material in developing countries [11].

The ranges recommended for common ferrocement applications are: sand-cement ratio by weight, 1.5 to 2.5, and water-cement ratio by weight 0.35 to 0.5. The mix should be as stiff as possible, provided it does not prevent full penetration of the mesh. For most applications, the 28-day compressive strength of (75 ×150 mm) moist-cured cylinders should not be less than 35 MPa [9].

Welded Wire Fabric (WWF) and Welded Wire Mesh (WWM) with either hexagonal or square opening are commonly used as ferrocement reinforcements. Meshes with square openings are made out of straight wires in both the longitudinal and transverse directions welded at points of intersections. Figure (1.4) shows different types of wire meshes reinforcement used in ferrocement applications. Woven mesh is made of longitudinal wires woven around straight transverse wires. Welded-wire meshes have a higher modulus and hence higher stiffness than woven meshes. The major differences between Welded Wire Mesh (WWM) and Welded Wire Fabric (WWF) are the size and spacing of wires. Welded Wire Fabric normally contains larger diameter wires (2mm or more) spaced at 25mm or more [9].

In its role as a thin reinforced concrete product and as laminated cement-based composite, ferrocement can be used in numerous applications, including agricultural applications, applications in water supply and sanitation, housing, rural energy, and repair and rehabilitation. Details of these applications are given below [10].

a. Agricultural applications: grain storage bins and silos, water tanks, lining for underground pits and irrigation channels pipes, shells for fish and chicken farms, and pedestrian bridges.
b. Rural energy applications: biogas digestors, biogas holders, incinerators and panels for solar energy collectors.

c. Water supply and sanitation: water tanks, sedimentation tanks, well casings, service modules, sanitary tanks, linings for swimming pools, and fuel tanks.
d. Housing applications: house, commonly centers, museums, mosque domes and other worship place, domes structures, precast housing element, wall panels, sandwich panels, corrugated roofing sheets, hollow-core slabs, permanent formwork and repair and rehabilitation of existing housing.
e. Building Industry: Roofing element, wall element, lintels, beams, and columns.

1.4 Concrete under Cyclic Loading

Reinforced concrete structures may be subjected to various repeated loads that normally cover load ranges from dead load only to dead load plus live load during their service life [12].

Concrete under variable loading behaves differently compared to that under monotonic loading because the former includes considerations of the loading history that the concrete has experienced [13]. The effects of variable loads on structures can be divided into two categories. The first is the incremental deformations which occur under a relatively small number of load cycles but of rather high stress. The second is the fatigue effect which is due to a large number of cycles of loadings of relatively low stress level. The fatigue phenomenon may occur in concrete and reinforcement. It should be noted that the important factor in fatigue is stress repetition, not the rate of strain as in the first kind. Thus, failure of second kind might occur under static loading (of cyclic nature) as well as under dynamic loading [14].

1.5 Objectives of the Study

The main objective of this study is to investigate the behavior of short concrete columns strengthened with ferrocement jacket under axial monotonic and cyclic compressive loadings. For this purpose, experiments have been

performed on plain concrete columns confined externally with different layers of Welded Wire Mesh (WWM) and covered with external mortar layer subjected to various axial monotonic and cyclic compressive loadings. The volume fraction of reinforcements (number of wire mesh layer), compressive strength of the mortar (two target strengths), specimen size, and four different load regimes are used in order to assess the effect of these variables on the strength of columns.

The tested columns were analyzed by using nonlinear three-dimensional finite element method using ANSYS (version 11), and the predicted behavior was compared with the experimental one.

1.6 Thesis Layout

The thesis is organized in six chapters. The current chapter is being the ***first***, which gives a general introduction on the strengthening techniques of concrete columns.

Chapter two presents literature review concerning the experimental and theoretical studies of the confined concrete columns.

Chapter three concerns with the experimental work. In this chapter the properties and testing of the materials used in the investigation, details of test columns, instrumentation, and test procedure, are illustrated.

The finite element formulation and description of the model proposed to predict the strengthened column behavior is presented in ***chapter four***.

The results and behavior of the tested concrete columns are demonstrated and discussed in ***chapter five*** and the predicted behavior of the column using the finite element method is also presented and compared with the experimental behavior.

Finally, the main conclusions of the project in this thesis are given in ***Chapter six***. Recommendations are also given for further research.

Plate (1.1) Strengthened concrete column with steel plate.

Plate (1.2) Size enlargement of concrete columns.

Plate (1.3) FRP wrapped around concrete

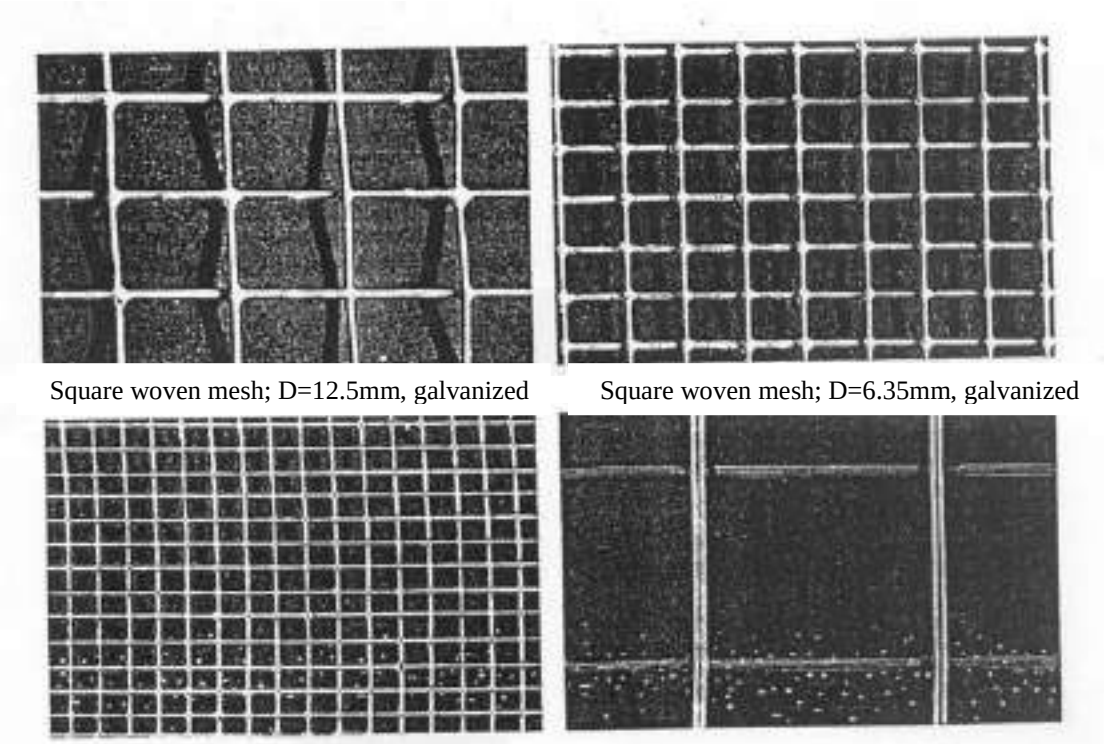

Square woven mesh; D=12.5mm, galvanized

Square woven mesh; D=6.35mm, galvanized

Square woven mesh; D=3.18mm, galvanized

Square welded mesh; D=25.4mm, non -galvanized

Square woven mesh; D=12.7mm, non -galvanized

Expanded metal mesh, non- galvanized

Figure (1.1): Typical steel meshes used in ferrocement [10]

CHAPTER TWO
Literature Review

2.1 Introduction

The common retrofit techniques that are used for strengthening concrete structures are concrete, fiber reinforcement polymer (FRP), and steel jackets. Concrete jackets are constructed by enlarging the existing cross section with a new layer of concrete and reinforcement. This reinforcement is traditionally provided by hoop or spiral rebar, or welded wire fabric. FRP reinforcement is typically applied in two ways: prefabricated (tubes) jackets or wraps. Steel jackets are constructed by placing a steel sheet or tube with a slightly larger diameter around the member to be retrofitted.

In this chapter, a literature review is presented of the research performed in the area of confinement of concrete columns, with a special emphasis on the commonly used confinement models. The confinement of concrete columns is reviewed in the first part of the chapter, followed by the behavior of concrete under cyclic loadings in the second part.

2.2 Confinement of Concrete Columns

2.2.1 Confinement by Reinforcement Concrete Jackets

Some research was conducted in order to evaluate the enhanced strength of concrete due to confinement. The early tests mainly considered the `active' state of confinement, in which the confining pressure was kept constant during the entire loading process.

Considere (1903) as cited in [7] tested the triaxial behavior of (80 x 300 mm) mortar cylinders, in which the lateral confinement was provided by constant hydraulic pressure. From the test results, proposed the following relationship to predict the compressive strength of confined concrete:

$$f'_{cc} = k_1 f'_{co} + k_c f_r \qquad (2.1)$$

where, f'_{cc} and f'_{co} are the compressive peak stress of the confined and unconfined concrete (in psi), respectively, k_1 is a constant varying between 1 and 1.5, k_c is the confinement coefficient equal to 4.8, and f_r , is the lateral confining pressure.

Considere's findings were further investigated by Richart et al. [15]. (1928) for concrete cylinders. They subjected (101.5x 203 mm) normal-weight concrete cylinders to constant hydraulic pressure while applying the axial compressive load until failure. The unconfined strength of the concrete varied from 1 to 3.8 ksi, while the applied lateral pressure varied from 550 and 4090 psi. They defined the confined strength of concrete as:

$$f'_{cc} = f'_{co} + k_c f_r \tag{2.2}$$

where the average value of k_c for the tests they conducted was 4.1.

Balmer in 1949, as cited in Ref. [7], tested (150 x 300 mm) concrete cylinders under triaxial compression. A maximum confining ratio f_r/f'_{co} of 6.8 was applied. Later, Chinn and Zimmerman (1965) as cited in [7] found out that for high confining pressures ($f_r/f'_{co} \leq 17$) the confinement coefficient k_c is a function of the lateral pressure. They proposed the following formula for k_c:

$$k_c = 3.65 f_r^{-0.117} \quad \text{(in ksi)} \tag{2.3}$$

In 1972, Iyengar et al. [16] tested a series of spiral-reinforced normal-weight concrete cylinders under concentric compression. The specimens were of two sizes: (101.5 x 203 mm) with spiral pitches ranging from 30 mm to 98mm, and (150 x 300 mm) with pitches ranging from 30 mm to 118 mm. They concluded that the strength enhancement due to the spiral confinement could still be represented by the expression of Richart et al., yet with a confinement coefficient of 4.6 instead of 4.1. They suggested a modified expression for the confining pressure f_r, as:

$$f_r = \frac{2A_{sp} f_{sy}}{D\, S_{sp}} \tag{2.4}$$

where A_{sp}, f_{sy}, S_{sp} are the cross-sectional area, yielding stress, and pitch of the spiral, respectively, and D is the inside diameter of the column.

Ahmad and Shah [17], in 1982a, developed a constitutive relationship for plain concrete subjected to triaxial compressive stresses. They proposed an equation to predict the complete stress-strain curve of `actively' confined concrete. They arrived at a bilinear relationship in lieu of the linear equation of Richart et al.. According to their procedure, the confined compressive strength was expressed as follows:

$$\begin{aligned} f'_{cc} &= f'_{co} + 4.256\, f_r \qquad (\text{for } f_r \le 0.679\, f'_{co}) \\ f'_{cc} &= 1.776\, f'_{co} + 3.117\, f_r \qquad (\text{for } f_r \le 0.679\, f'_{co}) \end{aligned} \tag{2.5}$$

They also established a procedure to predict the behavior of `passively' confined concrete using their model for 'active' confinement (Ahmad and Shah [18]1982b). Experimental data of their own [17, 18] and of Iyengar et al. on short concrete columns confined by steel stirrups, were used to verify their model. Experimental and predicted results compared favorably.

In 1988, Mander et al. [19] developed a more simplified confinement model applicable to concrete confined by circular or rectangular transverse reinforcement. The proposed stress-strain model is based on an equation proposed by Popovics for plain concrete. The axial compressive stress in concrete f'_c is expressed in terms of the axial strain ϵ_c, the peak strength f'_{cc} and the corresponding strain ϵ_{cc}, as follows:

$$f'_C = \frac{r f'_{cc}}{r - 1 + x^r} \tag{2.6}$$

where $x = \frac{\varepsilon_C}{\varepsilon_{cc}}$, $r = \frac{E_C}{E_C - E_{sec}}$, E_c is the tangent modulus of elasticity of concrete, and $E_{sec} = \frac{f'_{cc}}{\varepsilon_{cc}}$. The value of f'_{cc} is determined based on the multi-axial failure surface by William and Warnke, and for circular sections it is given by [19]:

$$f'_{cc} = f'_{co}\left(-1.254+2.254\sqrt{1+\frac{7.94\,f_r}{f'_{co}}}-2\frac{f_r}{f'_{co}}\right) \quad \text{(MPa)} \qquad (2.7)$$

and the value of ϵ_{cc} is given by [19]:

$$\varepsilon_{cc} = \varepsilon_{co}\left[1+5\left(\frac{f'_{cc}}{f'_{co}}-1\right)\right] \qquad (2.8)$$

The model assumes a constant confining pressure throughout the loading history and it is insensitive to variation of the Poisson's ratio of concrete, and thus it does not satisfy the strain compatibility condition at peak stress. In other words, it presents a solution for the active confinement problem rather than the passive confinement [19].

Bett et al. [20] in (1988) conducted testing on square columns repaired and strengthened by concrete jackets under compressive axial loading as well as lateral loading. Three square column test specimens were constructed, retrofitted with a concrete jacket, and then tested. One of the specimens was tested, repaired, and then retested. The other two specimens were strengthened before testing. Specimens were tested under axial and lateral loads simultaneously to simulate earthquake loading. Again, the experiment determined that a damaged retrofitted column has nearly the same strength and stiffness as an undamaged retrofitted column with a similar concrete jacket.

Ersoy et al. [21] in 1993 carried out two series of tests to study the behavior of strengthened and repaired concrete jacketed columns. The first series compares the behavior of jacketed columns with a monolithic reference specimen under monotonic axial loading. All the concrete for the monolithic specimen was cast with the base column and retrofit reinforcement in place, to provide a specimen with perfect interaction and bond between the base columns and retrofit material. Hoop reinforcement was used in the base column and retrofit reinforcement, as shown in Fig. (2.1). The jackets were applied under two conditions: after the compression loading was applied and removed, as well as while the axial load was still applied. It was determined that columns jacketed

after unloading performed well, reaching 80 to 90 percent of the strength of the monolithic reference specimen. Repair jackets applied while the column was still under load did not perform as well and only reached 50 percent of the axial load carried by the monolithic specimen. The second series of tests studied the effectiveness of concrete jackets with columns tested under combined axial load and bending. Both repaired and strengthened jackets behaved adequately under monotonic and reversed cyclic loading. From the results it was obvious that the strengthened specimens perform adequately and carry axial loads comparable to the monolithic reference specimen.

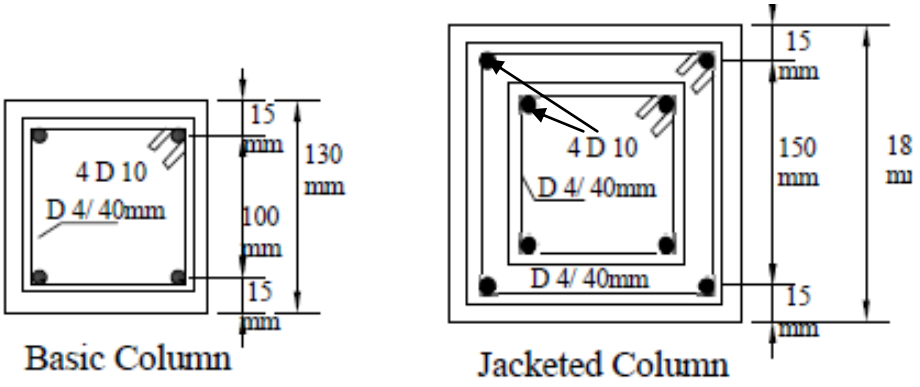

Figure (2.1) Cross section dimension for retrofitted specimens [21].

Rodriguez and Park [22] in (1994) conducted further testing on rectangular columns repaired and strengthened by concrete jackets under compressive axial loading as well as lateral loading. Rebar hoops were provided as the retrofit reinforcement for the concrete jackets. Concrete jackets increased the strength and stiffness of the as-built (unretrofitted or base) columns by up to three times. It was also shown that damage before the retrofit has no significant influence on the performance of the jacketed columns. Overall, concrete jackets with rebar reinforcement significantly improved stiffness, strength, and ductility of typical reinforced concrete columns, but construction was very labor intensive.

Lehman et al. [23] in 2001 used concrete jackets to repair severely damaged columns. Three repair methods were considered and implemented for the damaged columns, which were built to modern seismic specifications. Initial

damage to the columns included crushing of concrete, buckling and fracture of longitudinal reinforcement, and fracture of the spiral reinforcement, which was the result of axial and lateral loading. Concrete jacketed columns were reinforced with spiral transverse reinforcement, as shown in Fig. (2.2). Loose concrete was removed from the cover as well as the base column. The concrete jacket retrofitted column displayed increased stiffness and strength, comparable to the original column before damage.

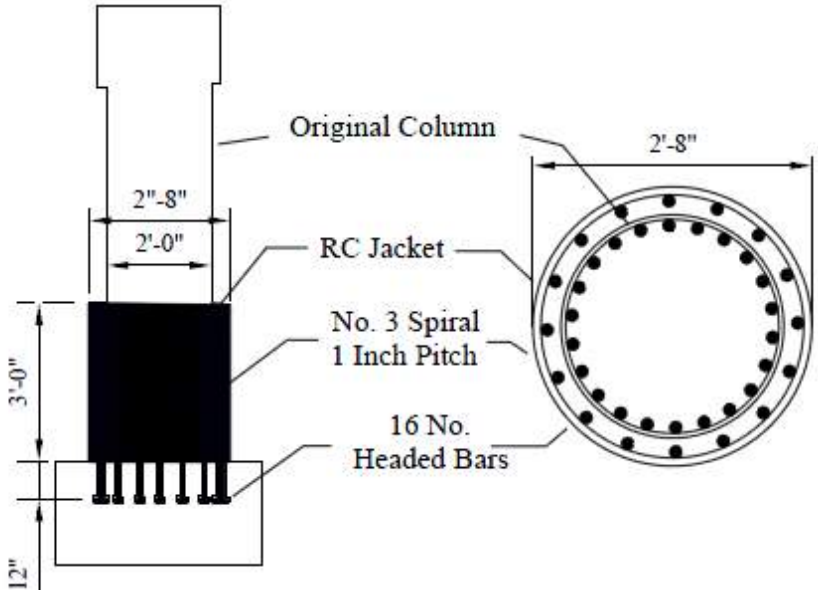

Fig. (2.2) geometry and reinforcement of columns 430SR with spiral reinforcement [23].

2.2.2 Confinement by Ferrocement Jackets

Balaguru [24] in1989 presented the results of an investigation on the behavior of plain concrete cylinders confined in ferrocement shell. The experimental investigation consisted of strength tests using $(150 \times 300\, mm)$ cylinders. The primary variables were: compressive strength of concrete in the range of (20-40 MPa) and one to four layers of wire mesh. The wire mesh provided effect confinement, resulting in an increase of compressive strength and increase in ductility. The increase in number of wire mesh resulted in consistent increase in both strength and ductility. The increase in compressive strengths estimated using constitutive models for confined concrete compares well with the experimental results.

Mansur and Paramasiva [25] in 1990 studied the behavior and strength of ferrocement box sections with and without concrete infill under axial and eccentric compression. It was concluded that ferrocement in the form of a box section in which reinforcing wire meshes are folded in the form of a cage may be used as a structural column, and its strength can be enhanced with concrete infill.

A method was presented by Fahmy et al. [26] in 1999 for repairing reinforced concrete columns using ferrocement laminates as a viable economic alternative to the highly expensive conventional jacketing methods. The experimental results demonstrated that irrespective of the pre-loading level or the mesh type, better behavior and load carrying capacity for all test specimens could be achieved compared to their original behavior.

Kabir and Hasan [27] in 1999 presented the test results performed on thirty two axially loaded brick masonry columns. These columns were divided into four sets. The first set of columns were completely bare, the second set of columns were plastered, the third set had precast ferrocement jackets divided into two equal halves, around the columns and the fourth set had precast ferrocement jackets divided into three segments, around the columns. All the columns were tested under increasing load until failure. Compared to bare brick masonry columns and plastered columns, precast ferrocement jacketed columns had better cracking resistance and higher ultimate load carrying capacity. They also exhibited more ductile behavior at failure.

Takiguchi et al. [28] in 2001 reported the result of an experimental investigation carried out on strengthening and repairing of shear failure type reinforced concrete columns by using circular ferrocement jacket. Four identical original reinforced concrete columns were constructed. Two original columns were tested as control specimens. The remaining two columns were tested after being strengthened with four and six layers of wire mesh respectively. Unless failure occurred at an earlier stage, all columns were tested under cyclic lateral forces and constant axial load. The conclusions were drawn from the test results

that circular ferrocement jacket was effective in preventing the shear failure that occurred on control specimens, in restoring the flexural strength, and enhancing the ductility of concrete columns.

Keisuke et al. [29] in 2002 tested a total of nine square cross section specimens ($120 \times 120 \times 240\ mm$) which was prepared and tested to study the strength and behavior of concrete confined by ferrocement boxes. Three identical specimens were prepared as control specimens in series 1. All specimens in series 2 were reinforced with wire meshes only. Besides being confined with wire meshes, specimens in series 3 were reinforced with laterally hoop bars of 2 mm diameter and containing four longitudinal bars of 2 mm diameter, one at each corner. Five millimeters gaps were provided at both ends of specimens confined with ferrocement boxes to avoid the confining box from bearing direct axial load. Two main variables considered in this investigation were: volume fraction of wire mesh and combination of confining reinforcement, hoop and ferrocement box. Based on test results of this investigation, it was found that deterioration of stiffness of concrete filled ferrocement boxes specimens began when crack formed. Also, the use of ferrocement boxes provided various degrees of confinement to the core concrete which resulted in improving strength and ductility significantly. The proposed method to calculate strength of concrete confined by ferrocement box agreed well with test results.

Abdullah and Takiguchi [30] in 2003 presented behavior and strength of reinforced concrete (RC) columns strengthened with ferrocement jackets. A total of six identical reference columns were prepared and tested after being strengthened with circular or square ferrocement jackets. Other than the ratio of axial load, parameters studied included the jacketing schemes, and the number of layers of wire mesh. Unless failure occurred at an earlier stage of loading, the columns were tested under cyclic lateral forces and constant axial load. Test results showed that by providing external confinement over the entire length of the RC columns, the ductility was enhanced tremendously. Also, test results of

this investigation revealed that the design method, proposed earlier by the authors, was very effective.

Kumar et al. [31] in 2005 conducted an experimental investigation to strengthen shear deficient reinforced concrete columns using ferrocement jacketing. Three scale model specimens, identical to the actual bridge piers, were tested. One of the piers was tested under as-built condition while the other two were strengthened with layers of wire mesh before being tested. All the specimens were subjected to a simulated seismic loading and constant axial load. It was observed from the experimental results that the ferrocement-jacketed specimens exhibited enhanced stiffness, strength, energy dissipation and ductility and the mode of failure changed from brittle shear failure to a ductile flexural failure. The control specimens failed by shear at a relatively low lateral displacement. A finite element model was developed and the results obtained from the numerical analysis compared with the experimental results. A design methodology for strengthening piers and square/rectangular columns with inadequate shear strength using ferrocement jackets was also presented.

Kazemi and Morshed [32] in 2005 presented results of an experimental study to evaluate a retrofit technique for strengthening shear deficient short concrete columns. In that technique a ferrocement jacket reinforced with expanded steel meshes was used for retrofitting. Six short concrete columns, including four strengthened specimens, were tested. Specimens were under a constant compressive axial force of 15% of column axial load capacity based on original concrete gross, and the concrete compressive strength. Main variables were the spacing of ties in original specimens and the volume fraction of expanded metal in jackets. Original specimens failed before reaching their nominal calculated flexural strength, and had very poor ductility. Strengthened specimens reached nominal flexural strength and had a ductility capacity factor of up to 5.5. Based on the test results, it was concluded that ferrocement jackets reinforced with expanded steel meshes can be used effectively to strengthen shear deficient concrete columns.

Mourad [8] in 2006 investigated the efficiency of confining plain concrete with different layers of Welded Wire Mesh (WWM) and different methods of attachment of the (WWM) around the concrete specimen. An experimental program was conducted on different plain concrete cylinders ($150 \times 300\ mm$) confined with ferrocement jackets that have different WWM layers and different methods of attaching the WWM to the concrete cylinders. The tested specimens were divided into three different groups namely, group A, B and C, according to the method of WWM attachment to the concrete cylinder. Group A specimens were prepared by attaching the WWM to the concrete specimens by means of L-shaped fasteners screwed in pre-drilled holes, group B specimens were prepared by attaching only the edge of WWM by fast setting epoxy, while group C specimens were prepared by wrapping the first two layers of WWM around the concrete specimen by applying Sikadur-31 on the concrete surface and between the first two layers of WWM. All WWM wrapped specimens were covered with a mortar layer to form the ferrocement jacket. All specimens were tested under axial loads. Stress-strain relationships were plotted and the ultimate load capacities were recorded and the failure modes were observed and compared to the unconfined specimens, in order to investigate the effect of confinement of the specimens with ferrocement Jackets. It was concluded that confining plain concrete cylinders with ferrocement jackets provided remarkable lateral confinement pressure that in turns increases its axial load carrying capacity. However, such increase depended mainly on the method of attaching the WWM on the specimen and the number of layers used in the ferrocement jacket.

Kumar et al. [33] in 2007 investigated reinforced concrete and ferrocement jacketed columns subjected to simulate seismic loading. The experimental program consisted of three scale model bridge pier specimens designed as shear deficient specimens, tested under different axial loads, before and after retrofitting with ferrocement jackets. The specimens were reinforced with 6 bars of 16mm diameter distributed evenly around the perimeter of the

pier cross section. 6 mm diameter ties at 300mm spacing were used as the transverse reinforcement. The three RC columns were strengthened with six layers of ferrocement jackets (V_f =3.46%) after their failure. Woven wire mesh of 2.76mm square opening and 0.44mm diameter were used as reinforcement for ferrocement jackets throughout the test program. The specimen used was 500 mm long, 70 mm wide, 120 mm thick, and symmetrically reinforced. The test specimen was a cantilever with the fixed end framing into a footing. All the specimens were subjected to a cyclic lateral load at the tip of the cantilever. The main variable parameter in the study was the axial load ratio. Cyclic lateral loading was applied on the scale model test piers while being simultaneously subjected to axial loads of 100, 150 and 200kN respectively. They concluded that the external confinement using ferrocement resulted in enhanced stiffness, ductility, strength and energy dissipation capacity. The mode of failure changed from brittle shear failure to ductile flexural failure. The axial loads influenced the hysteretic response of columns and the energy absorption capacity. The effect of axial compression on response was the acceleration of strength and stiffness degradation under repeated inelastic load cycles.

Kondraivendhan and Pradhan [11] in 2009 studied the use of ferrocement as an external confinement to concrete specimens. The effectiveness of confinement was achieved by comparing the behavior of retrofitted specimens with that of conventional specimens. The primary test variables considered in this study was the concrete compressive strength. All the other parameters, such as size, shape, number of layers of wire mesh, and height to diameter (L/D) ratio of the specimens, were kept constant. The sections chosen were circular cylinders with a size of (150 ×900 mm) and L/D ratio of 6:1. The test results showed that the confining of concrete specimens can enhance the ultimate concrete compressive strengths and failure strains.

Experimental study was made on burnt clay brick column specimens by Shah [34] in 2011. Burnt clay bricks of 221 mm x 110 mm x 55 mm were used. Ordinary Portland cement and alkaline free sand were mixed together to cast

cement mortar joint of 4.6 mm. In addition, 24 gage steel wire having tensile strength of 276 MPa was used in the ferrocement. Masonry columns of 221 mm x 221 mm x 784 mm, were prepared. After a period of one week of wet curing, steel wire was manually wrapped around column in both directions. Cement mortar was then applied as plastering and cured for minimum of 10 days before testing in compression. The type of mortar for brick masonry joint was same for all specimens. Specimens without ferrocement application were also constructed for comparison. The parameters such as cement mortar thickness, gage-wire spacing and bond at the interface of ferrocement and brick columns have been altered to study their effects on overall behavior. In this experimental study, it was found that the first crack load and ultimate load of a ferrocement encased masonry column was increased by 119% and 121% respectively. Cracks developed in ferrocement encased column were finer and well distributed as compared to plain specimen. However, premature failure was possible when bond at the interface of brick masonry column and ferrocement was poor. At higher reinforcement ratio, severe spalling and delamination was expected.

2.2.3 Confinement by Steel Jacketing

Knowles and Park [35, 36] (1969, 1970) conducted a series of tests on concrete-filled steel tubes of different slenderness ratios, and concluded that in most cases buckling of the tube dictated the overall failure of the composite column. They recommended avoiding loading the steel tube in the longitudinal direction in order to achieve its full utilization in the circumferential direction.

In 1994, Prion and Boehme [37] performed a series of tests on concrete-filled circular steel tubes. They reported that the enhancement of strength is noticeable for a slenderness ratio, L/D, less than 15, where L and D are the height and diameter of the column, respectively. The failure mode for short columns ($L/D < 15$) was a shear failure of the concrete core.

Schneider [38] in 1998 presented an experimental and analytical study on the behavior of short, concrete filled steel tube columns concentrically loaded in

compression to failure. Fourteen specimens were tested to investigate the effect of the steel tube shape and wall thickness on the ultimate strength of the composite column. Depth-to-tube wall thickness ratios between $17 < D/t < 50$, and the length-to-tube depth ratios of $4 < L/D < 5$ were investigated. Nonlinear finite element models were developed and verified using experimental results. It was shown that, the circular tubes offer substantial post-yield strength and stiffness, not available in most square or rectangular cross sections.

Uy [39] in 2001, presented experimental tests on the behavior of concrete filled high strength steel box columns. The experimental results were used to calibrate a numerical model developed elsewhere. Both the model and the experiments were then compared with the approach adopted in Eurocode 4. It was shown that whilst the numerical model is conservative, the Eurocode 4 model needs modifications in order to provide a conservative result in estimating the member cross-sectional strength. A mixed analysis approach was therefore suggested which was found to provide a conservative but reasonable estimate of the cross-section strength, which is more suitable for design applications.

Johansson and Gylltoft, [40] in 2002, studied the mechanical behavior of circular steel–concrete composite columns. Thirteen specimens, with L=650mm and D=159mm, were tested. To examine different types of mechanical behavior of the columns, three loading conditions were studied. Three dimensional nonlinear finite-element models were established and verified with the experimental results. The results obtained from the tests and the finite-element analyses showed that the mechanical behavior of the column was greatly influenced by the method used to apply the load to the column section. The bond strength had no influence on transformation of load on the behavior when the steel and concrete sections were loaded simultaneously. On the contrary, for the columns with the load applied only to the concrete section, the bond strength highly affected the mechanical behavior of the columns.

Liu [41] 2004 presented an experimental study on the behavior of 12 high strength rectangular concrete-filled steel hollow section columns subjected to eccentric loading. The primary test parameters were the cross-sectional aspect ratio, slenderness and load eccentricity. The specimens with cross-sectional aspect ratios of 1.0, 1.5 and 2.0 were fabricated from high strength materials (f_y = 550 MPa; f_{cu} = 70.8 and 82.1 MPa). The slenderness ratios of the specimens were 20 and 50, while the load eccentricity ratios (e/B; e is the load eccentricity, B is the breadth of cross-section) varied between 0.17 and 0.40. Favorable ductility performance was observed for all specimens during the test. The experimental ultimate capacities of the specimens were compared with the design strengths predicted by the codes. Comparison of results showed that Eurocode 4 overestimated the ultimate capacities of the columns with a difference of 3%. ACI and AISC, on the other hand, conservatively predicted the failure loads by 11% and 25%, respectively.

In 2005, Lam and Wong [42] performed a series of tests to consider the behavior of short composite concrete stainless steel columns under axial compressive loading. The columns were constructed of stainless steel square hollow sections filled with normal and high strength concrete. Eight specimens, of 100 x 100 mm stainless steel square hollow sections, were tested with various concrete strength (30, 60, and 100 N/mm^2) and wall thickness (2 and 5 mm). Results showed that the standard rules for composite columns design gave a reasonable prediction of the compressive strength, with the Eurocode 4 appeared to over-estimate the specimens filled with high strength concrete, while the ACI-318 and Australian standards would appear to under-estimate the compressive strength of the composite columns filled with normal strength concrete.

Ellobody et al. [43] in 2006 presented the behavior and design of axially loaded concrete-filled steel tube circular stub columns. The study was conducted over a wide range of concrete cube strengths ranging from 30 to 110 MPa. The external diameter of the steel tube-to-plate thickness (*D/t)* ratio ranged from 15 to 80 covering compact steel tube sections. An accurate finite element model

was developed to carry out the analysis. Accurate nonlinear material models for confined concrete and steel tubes were used. The column strengths and load-axial shortening curves were evaluated. An extensive parametric study was conducted to investigate the effects of different concrete strengths and cross-section geometries on the strength and behavior of concrete-filled compact steel tube circular stub columns. The column strengths predicted from the finite element analysis were compared with the design strengths calculated using the American, Australian and European specifications. Based on the results of the parametric study, it was found that the design strengths given by the American Specifications and Australian Standards are conservative, while those of the European Code are generally unconservative. Reliability analysis was performed to evaluate the current composite column design rules.

Yang and Han, [44] in 2006 studied the behavior of steel tubular columns of circular and square section filled with normal concrete and recycled aggregate concrete. Thirty specimens, including 24 recycled aggregate concrete filled steel tubular (RACFST) columns and 6 normal concrete filled steel tubular (CFST) columns, were tested to investigate the influence of variations in the tube shape, circular or square, concrete type, normal concrete and recycled aggregate concrete, and load eccentricity ratio, from 0 to 0.53 on the performance of such composite columns. The test results showed that both types of filled columns failed due to overall buckling. Comparisons were made with predicted ultimate strengths of RACFST columns using the existing codes. The predicted load versus deformation relationships were in good agreement with test results.

Gupta et al. [45] in (2007), studied the behavior of circular concentrically loaded concrete filled steel tube columns. Eighty-one specimens were tested to investigate the effect of diameter and D/t ratio of a steel tube on the load carrying capacity of the concrete filled tubular columns. Diameter to wall thickness ratios between $25 < D/t < 39$, and the length to tube diameter ratios of $3 < L/D < 8$ were investigated. Results were compared with the corresponding findings of the available literature. Also a nonlinear finite element model was

developed to study the load carrying capacity using the finite element code ANSYS. This model was validated by comparison of the experimental and computational results of load-deformation curves and their corresponding modes of collapse. They concluded that for smaller *D/t* ratio, the steel tube provided good enhancement in the concrete strength, and that the load carrying capacity of the columns decreased as the *D/t* ratio increases.

In 2007, Ellobody [46] investigated the nonlinear behavior of concrete-filled high strength stainless steel stiffened slender square and rectangular hollow section columns. The stiffened slender tubes had overall depth-to-plate thickness (*D/t*) ratios ranging 60–160. The concrete strengths covered normal and high-strength concrete. The investigation was focused on short axially loaded columns. A nonlinear finite element (FE) model had been developed to study the behavior of the concrete-filled stiffened tube columns. The results of the concrete-filled stiffened tube columns were compared with the results of the companion concrete-filled unstiffened tube columns. It was shown that the concrete-filled stiffened slender tube columns offer a considerable increase in the column strength and ductility than the concrete-filled unstiffened slender tube columns. The column strengths obtained from the FE analysis were compared with the design strengths calculated using the American specifications and Australian/New Zealand standards. A design equation was proposed for concrete-filled stainless steel stiffened slender tube columns. It was shown that the proposed modified equation provides more accurate design strengths compared to the American and Australian/New Zealand predictions.

2.2.4 Confinements by Fiber Reinforcement Polymers (FRP)

2.2.4.1 Confinements by FRP Wraps

Shahawy et al. [47] in 2000. A total of 45 carbon-wrapped and 10 unconfined control concrete cylinders with 152.5 mm diameter and 305 mm height were tested under uniaxial compression. Two concrete batches of normal and high-strength concrete and five different numbers of wraps (from 1 to 5

layers) were used. A nonlinear finite element model was developed. Model compared favorably with test results. It was concluded that the adhesive bond between concrete and the wrap would not significantly affect the confinement behavior. The same confinement model can be applied to carbon and glass fibers, as long as the model has incorporated the dilation tendency of concrete as a function of the stiffness of the jacket. It is of outmost importance to establish the effective hoop rupture strain of the wrap through a reliability analysis by settingproper confidence level for design purposes.

Li et al. [48] in 2003 presented a study on the behavior of concrete columns repaired by FRP under axial load. The RC column dimensions were (152.4×609.6 mm). A finite element analysis using ANSYS was utilized to conduct a parametric analysis. Experiments were also conducted to justify the finite element analysis results. A reasonable agreement was found between the finite element analysis and the test results. The effect of the thickness, stiffness, and fiber orientation of the FRP layers as well as the interfacial bonding between the FRP wraps and the concrete on the strength and stiffness of the repaired columns was evaluated using the finite element modeling.

Lin and Liao [49] in 2004 presented experimental and the numerical model to predict the compressive strength of concrete columns confined by composite materials. FRP was wrapped around plain concrete columns and RC columns to determine the difference between their behavior under uniaxial compression. Experimental results indicated that the FRP confinements of the two specimen types were similar. Accordingly, a method for analyzing the behavior of an FRP-wrapped plain concrete column can be used also to analyze that of an FRP-wrapped RC column. Its stress-strain plot was bilinear. The study presented a theoretical stress-strain model. Some comparisons between experimental stress and the stress predicted using a model indicated that the presented model was good to predict the fracture stress of FRP-wrapped concrete column.

Li [50] in 2006 studied the behavior of FRP concrete columns under axial compression. Two types of fiber reinforced polymer (FRP) confined concrete cylinders were used in this study. One was FRP jacketed concrete cylinders; the other was FRP tube encased concrete cylinders. A total of 24 jacketed cylinders and 15 encased cylinders were prepared. It was found that insufficiently confined cylinders behave similar to unconfined cylinders. FRP cannot confine the concrete core until the concrete is damaged (cracked or crushed) due to the larger transverse Poisson's ratio and lower axial stiffness of FRP. The rate of increase in confinement effectiveness decreased nonlinearly as confinement ratio increases. A considerable deviation was found between the prediction by existing design-oriented confinement models and test results.

Hadi [51] in 2007 presented results of testing eccentrically loaded columns externally wrapped with two types of materials. Six cylindrical (205 mm diameter and 925 mm height) plain columns were cast and tested. Half of the columns were wrapped with GFRP and the other half with CFRP. All columns were tested by applying an axial load at 50 mm eccentricity. In each group GFRP or CFRP wrapped of columns, one column did not have any vertical straps, one had vertical straps made of one layer of wrapping material and one column had vertical straps made of three layers of wrapping material. The vertical straps were made of 50 mm GFRP or CFRP and were glued to the columns at an equal spacing of 57.5 mm. All columns were horizontally wrapped with three layers of material GFRP or CFRP. One column was reinforced longitudinally and helically with steel bars to serve as a reference column. Based on testing the columns it was concluded that considerable gain in strength and ductility was obtained when reinforcing the columns with CFRP vertical straps and horizontally wrapped. Although being tested under eccentric loads, the CFRP columns outperformed both the GFRP and the steel reinforced columns.

Wu et al. [52] in 2008 studied the behavior of concrete cylinders confined with hybrid FRP composites. A total of 35 cylindrical specimens with

dimensions of (150× 300mm) were tested, which included three plain concrete cylinders as control specimens, 12 concrete cylinders confined with one kind of FRP sheet and 20 specimens confined with hybrid FRP sheets. The experimental parameters included the different types of FRP sheets, the number of layers of FRP sheets and the different kinds of hybridization with two or three types of FRP composites. First, the characteristics of the stress-strain curves of hybrid FRP-confined concrete were described based on previous studies. Then, in order to describe the main mechanical features of hybrid FRP-confined concrete cylinders including stress and strain behavior, some simple models were suggested based on a number of empirical equations determined from mechanical tests. Finally, a multi-linear model was proposed to predict the axial stress-strain model of concrete cylinders confined with hybrid FRP composite. The proposed model closely agreed with the experimental results of the presented study.

Chakrabarti et al. [53] in 2008 developed a nonlinear finite element model for the analysis of plain and reinforced concrete column confined by FRP sheets. The column sections chosen for the analysis were either circular or square in shape. The behavior of small and large scale FRP wrapped concrete columns under uniaxial compression was investigated using the developed model. A detail parametric study was done to quantify the effect of the thickness, stiffness and fiber orientation of the FRP sheets as well as unconfined concrete strength on confinement and stiffness of the strengthened columns using the proposed model. Based on the analysis results, accurate stress distribution in concrete and FRP was also obtained which improves understanding of the confinement mechanism.

Benzaid et al. [54] in 2008 tested a total of twenty-one prisms of size (100 × 100 × 300 mm) concrete column confined with GFRP composite wrap under axial compression, in order to study the effect of confinement. The parameters considered were the number of composite layers and the corner radius for a square shape. Based on the analysis of experimental results obtained from tests

on square concrete column, it concluded that composite wrapping can enhance the structural performance of concrete columns under axial loading. The number of layers of GFRP materials and the corner radius having a significant influence on the behaviour of specimens. Applying multiple layers of GFRP led to increase the stiffness of column. A larger radius expanded the strong constraint zone and diminished the stress concentration. So the reduced confining pressure in a square section due to the concentration of stresses at the corners was solved by using a square section with circular corners.

Sadeghian and Rahai [55] in 2008 presented the results of numerical analyses of concrete cylinders (i.e., columns) confined in composites jackets. The specimens were subjected to uniaxial compression and the analysis was carried out using a non-linear finite element method. Various parameters such as wrap thickness, fiber orientation, concrete strength, and interfacial bonding were considered. The finite element analysis results were in good agreement with experimental data presented by other researchers. The numerical analysis results demonstrated significant enhancement in the compressive strength, stiffness, and ductility of the CFRP-wrapped concrete cylinders compared to unconfined concrete cylinders. The stress-strain response of cylinders was greatly affected by analysis parameters.

Sadeghian et al. [56] in 2009 presented the results of experimental studies about concrete cylinders confined with high-strength Carbon Fiber Reinforced Polymer (CFRP) composites. Forty small scale specimens (150 × 300 mm) were subjected to uniaxial compression up to failure and stress-strain behavior was recorded. The various parameters such as wrap thickness and fiber orientation were considered. Different wrap thicknesses (1, 2, 3, and 4 layers), fiber orientation of 0^o, 90^o, $\pm 45^o$ and combinations of them were investigated. The results demonstrated significant enhancement in the compressive strength, stiffness, and ductility of the CFRP wrapped concrete cylinders as compared to unconfined concrete cylinders. An analytical model for ultimate stress and strain of confined concrete has been proposed.

Yu and Niu [57] in 2010 presented a calculating model of the load-carrying capacity of PVC-FRP confined concrete column. The influences of the hoop spacing of FRP strips and equivalent confinement effect coefficient on load-carrying capacity were well considered. According to the regression of experimental data, a formula of the ultimate axial strain was also put forward. For this last case, a bilinear stress-strain model of PVC-FRP confined concrete column in axial and lateral directions was established. The comparison between experimental and numerical results indicated that the model provides satisfactory predictions of the stress-strain response of the columns.

Mostofinejad and Saadatmand [58] in 2010 described how to predict the behavior of concrete confined with Carbon Fiber Reinforced Polymers (CFRP) using non-linear analysis. The results of 29 experimental studies were used, where confining composites have been unidirectional CFRP. The stress-strain behavior of the concrete members from these experiments was estimated as bilinear curves and, by extracting the necessary data, specific expressions for modeling of the nonlinear behavior of confined concrete were presented. The presented relationships were verified using the results of 29 distinct experiments. The relationships were applicable in the confinement modeling by considering the hoop rupture strain of the CFRP attached to the concrete, and by using the Tsai-Wu failure criterion. As part of the study, concrete specimens confined with a CFRP composite were modeled with ANSYS software using the presented relationships. The results showed the suitability of the model selected, such that the stress-strain curves obtained from the software are properly applicable in the parametric studies conducted on the confined concrete subjected to axial load and flexural moment.

2.2.4.2 Confinements by FRP Tubes

Harmon et al. [59] in 1995, tested small scale fiber reinforced plastic (FRP) tubes filled with concrete under axial compression. Glass/epoxy and carbon/epoxy circular 50.8 x 101.6mm tubes were used and filled with high

strength concrete (64 MPa). Fibers to concrete volume ratios ranging from 0 to 0.06 were used. Bi-linear stress-strain responses were obtained for all the glass and carbon specimens. The following observations were reported: 1) the second slope of the axial stress-strain curves was proportional to the tube stiffness; and 2) the axial stress at the bend-point of the bilinear stress-strain curve was proportional to the tube stiffness.

Mirmiran and Shahawy [60] in 1995 proposed a concrete-filled FRP tube (CFFT), in which the tube acts as: formwork for the encased concrete, hoop and longitudinal reinforcement, and corrosion-resistant casing for the concrete. The CFFT was proposed for bridge columns as well as for pile splicing.

Kargahi [61] in 1995 investigated the strength of CFFT under uniaxial compression. A total of 12 circular specimens were tested, nine CFFTs and three (152.4 x 304.8mm) plain concrete cylinders. Filament-wound E-glass/polyester tubes were used, with winding angle of ±75° with respect to the longitudinal axis of the tube. Three different tube thicknesses were included, namely, 1.88, 3.3, and 6mm. An enhancement in the concrete strength, in the order of 2.5-3.5 times the unconfined strength, was reported. A parametric study was also performed on the effect of ply thickness and winding angle. It was concluded that the thickness of the tube enhances the pure axial strength. Moreover, the pure flexural capacity was maximum at a winding angle of ±45°.

In 1997, Pico [62] tested a total of 9 (152.4mm x 152.4mm x 304.8mm) square concrete-filled FRP tubes under axial compression, in order to study the effect of cross section of the CFFT. No bond was provided between the concrete core and the FRP tube. A marginal increase in strength was observed independent of the jacket thickness.

El Echary [63] in 1997 evaluated the effects of length-to-diameter (*L/D*) and diameter-to-thickness (*D/t*) ratios on the behavior of the CFFT. A total of 24 circular CFFTs (D_{inner} =145mm) with three different tube thicknesses (6, 10, and 14 layers) and four different lengths (304.8, 457.2, 609.6, and 762mm) were tested. No buckling was observed during the tests. The analysis of the test

results indicated that the reduction in strength was not significant. It was concluded that up to a ratio *L/D* of 5:1, slenderness effects are negligible.

In 1998, Kanatharana and Lu [64] studied the behavior of FRP reinforced concrete composite columns under uniaxial compression. Two types of FRP tubes were used in this study; namely the filament-wound FRP (FFRP) and the pultruded FRP (PFRP) tubes. The FFRP has continuous glass fibers winding at 53° and 127° from its circumference, whereas the PFRP has continuous fibers running along its axis. The experimental results showed that significant increases in concrete ductility and FRP strength occurred in all the FFRP specimens but not in the PFRP specimens. Detailed examination revealed that the inclined orientations of the glass fibers enable strength and ductility gains in the FFRP specimens.

In 1999, Saafi et al. [65] tested FRP tubes filled with concrete under axial compression. Glass and carbon circular tubes were used. It was proved that the increase in axial stress over the plain specimen ranged from 51 to 137 percent for the concrete-filled glass tubes and 57 to 177 percent for the concrete-filled carbon tubes.

Marzouk and Sennah [66] in 2002 conducted an experimental study in which four concrete filled PVC columns were tested up to failure. All specimens were of 100 mm diameter and of different heights (270, 416, 562, and 758 mm) and were subjected to monotonically increasing axial load until compression failure occurred. They concluded that the use of PVC tube provides considerable lateral confinement to the concrete columns and as the slenderness ratio increases, the compressive strength of the concrete filled PVC tubes decreases.

Hong and Kim [67] in 2004, presented experimental and analytical investigations of axial behavior of large-scale circular and square concrete filled carbon composite tube columns. The specimens were filament-wound carbon composite with (±90°, ±60°, ±45°, and ±30°) winding angles with respect to a longitudinal axis of a tube. The influence of winding angle, thickness of a tube, as well as shape of the column section on stress-strain relationships of the

composite columns was identified and discussed. Proposed equations to predict both strength and ductility of concrete filled carbon composite tubes demonstrated good correlation with test data obtained from large-scale specimens.

In 2005 Li et al. [68] tested twenty-seven 101.6 x 304.8 mm composite columns with FRP tube. The composite columns were divided into three equal groups. The first group was prepared using 35 MPa concrete, the second group using 50 MPa concrete, and the third one using 80 MPa concrete. FRP tubes with 5 mm wall thickness were used. They found that the structural behavior of the tested columns depends on the concrete strength. The tube efficiency was low for very high strength concrete.

As part of his study on FRP confined concrete specimens, Li [69] in 2006 tested fifteen FRP tube encased concrete cylinders. The tubes had two wall thicknesses: 8.10 mm and 6.35 mm. The inner diameter of the tube was 101.6 mm. Each composite specimen was 304.8 mm in height. Four batches of concrete with normal to high strength were used. It was found that insufficiently confined cylinders behave similar to unconfined cylinders. FRP cannot confine the concrete core until the concrete was damaged (cracked or crushed) due to the larger transverse Poisson's ratio and lower axial stiffness of FRP. The rate of increase in confinement effectiveness decreased nonlinearly as confinement ratio increases.

Mohamed and Masmoudi [70] in 2009 investigated the performance of concrete-filled FRP tube columns (CFFT) under concentric and eccentric loads. The experimental program was conducted on ten unconfined cylinders and eight CFFT columns. The results were compared to steel spiral reinforcement which have the same confinement pressure of the FRP tubes. The diameter of the FRP tubes was 152 mm and the fibers orientation were mainly in the hoop direction. The test results indicated that by increasing the thickness of the GFRP tubes a significant improvement is achieved in the confinement efficiency. The confinement provided by the GFRP tubes improved both the load-carrying

capacity and the ductility of the concrete columns under concentric load. The stress-strain curve of the CFFT tube columns was bilinear and nonlinear for the concentric and eccentric loading, respectively. Increasing the eccentricity values decreased the ultimate load capacity and increased the horizontal and axial deformation of the CFFT columns.

2.3 Behavior of Concrete under Cyclic Loadings

Sinha et al. [71] in 1964 carried out an experimental investigation on the behavior of plain concrete under cyclic compression loading. A series of forty-eight tests were performed on concrete cylinders to obtain information about the properties of the envelope curve and the unloading and reloading curves, and analytical stress-strain relations for cyclic loading were derived. They assumed the property of uniqueness of the stress-strain relations (i.e. if the envelope of the unloading and the reloading curve passing through any point in the stress-strain plane remain independent of the previous load history, then the stress-strain relationship is unique) to predict behavior of concrete subjected to an arbitrary compression load history. This hypothesis was refuted by subsequent experimental evidence.

Karsan and Jirsa [72] in 1969 developed an experimental study of the strength and behavior of plain concrete subjected to repetitions of compressive stress to multiple levels. A total of 46 short rectangular columns were tested under cyclically varying axial loads. This was carried out in order to determine the stress-strain envelope and the unloading and reloading curves. The test results indicated that the stress-strain paths under cyclic loading generally do not exceed the envelope curve; furthermore, this curve can be modeled as the stress-strain curve obtained under monotonic loading to failure. The authors reported that the loading and unloading curves starting from a point within the stress-strain domain were not unique and that the value of stress and strain at the peak of the previous loading cycle had to be known to estimate the response. They considered the residual plastic strain as principal parameter to determine the unloading curve equation and proposed an empirical formula to correlate the

residual plastic strain with the point on the envelope from which unloading starts. When reloading started from zero stress to meet the envelope curve, it was found that the reloading curve becomes rather flat in most of its range and may be represented by a simple straight line.

Lam [13] in 1980 presented an experimental study on plain concrete cylinder specimens subjected to various uniaxial cyclic compressive loading. The experimental results were compared with the available data previously obtained by other investigators. Behavioral trends were studied and considerations for predictive model were given. The results obtained from this study indicated agreement with the previous findings on the behavior of concrete under uniaxial cyclic compressive loadings. Based on the results from this study, modifications were made to the predictive stress-strain equations of concrete proposed by previous investigators.

Maher and Darwin [73] in 1982 studied the behavior of the mortar constituent of concrete under monotonic and cyclic uniaxial compression. Two mixes were used. Forty four groups of three specimens each were tested. Complete monotonic and cyclic envelopes were obtained using six different loading regimes. Major emphasis was placed on tests using relatively high stress cycles. These different loading regimes were: monotonic loading, cyclic loading to the envelope, cyclic loading with a constant strain increment between successive cycles, cyclic loading between fixed maximum and minimum stresses, cyclic loading to specific strain and cyclic loading to common points. According to the tests results, they concluded that using the accumulation of residual strain and changes in the initial modulus of elasticity must be used to evaluate the damage and structural change. The maximum strain appeared to be the major factor controlling damage in mortar, but the total cyclic strain range and/or the number of load cycles also played significant roles. The behavior of concrete and mortar was highly similar, indicating that the mortar constituent may control the primary stress-strain behavior of concrete.

Buyukozturk and Tseng [74] in 1984 conducted an experimental program

to study the behavior of concrete under low-cycle high amplitude biaxial cyclic compression. Biaxial loading was achieved by subjecting square concrete plates to in-plane loading where compressive stress was applied in one direction while confining the deformation of the specimen in the orthogonal direction. Three main types of tests were performed: monotonic loading to failure, cycling of compressive stresses to a limiting envelop curve, and cycling of compressive stresses to prescribed values. In each category, tests were performed on specimens under different levels of strain confinement, and for comparison, on unconfined specimens. Complete stress-strain histories were recorded and analyzed to assess the effect of confinement on concrete behavior under different non proportional load conditions. A simple predictive model for the constitutive behavior of concrete in biaxial cyclic compression was proposed. Predicted behavior from the model which does not require any a priori information from experiments was found to be in good agreement with the measured response.

Perry et al. [75] in 1986 tested prisms concrete having the same 138 mm cross section and an overall length of 414 mm. Prisms were cast in the upright position and a rectangular arrangement of 54 ducts was formed in each, to accommodate the bolts. Prisms were confined by high-tensile steel bolts inserted horizontally in two orthogonal directions through pre-formed ducts, and the annular space between ducts and bolts was grouted with high strength epoxy resin. The specimens were subjected to monotonic and cyclic loading. The effects of cyclic loading, energy absorption and dissipation characteristics of concrete prisms at variable strain rates were studied. Significant enhancement of the strength and ductility of the concrete was obtained. Specimens displayed large energy absorption and dissipation capacity under cyclic loading. The validity of an envelope curve to describe cyclic behavior was discussed.

An experimental investigation of the behavior of steel fiber reinforced concrete under cyclic compressive loading was presented by Otter and Naaman [76] in 1988. Cylindrical specimens (100 × 200 mm) were cast using normal

and high strength concrete mixes with four types of steel fiber and three different volume fractions. Stress-strain responses were obtained for three cyclic loading regimes as well as for monotonic loading. Based on the tests results the envelope curve was shown to govern cyclic response. Toughness under cyclic loading was found to be at least as great as that under monotonic loading. The behavior of fiber reinforced concrete under cyclic loading, when normalized by its monotonic behavior, was very similar to that of plain concrete or concrete confined by steel spirals, indicating that the fibers primarily influence the envelope curve.

Bahn and Hsu [77] in 1998 developed a parametric study and an experimental investigation on the behavior of concrete under random cyclic compressive loading. They studied in a semi empirical way a set of parameters that control the overall shape of cyclic stress-strain curve. This was carried out by combining the theoretical simulation and a series of experimental results. A power type equation was proposed for the unloading curve and a linear relationship for the reloading curve.

Lam et al. [6] in 2006 presented the results of an experimental study on the behavior of FRP-confined concrete under cyclic compression. A total of 18 concrete cylinders of 152 mm in diameter and 305 mm in height were prepared and tested in two series. Each series consisted of six cylinders confined by carbon FRP (CFRP) jackets, plus three unconfined cylinders as control specimens. The six confined cylinders in Series I were wrapped with one ply of CFRP, and those in Series II were wrapped with two plies of CFRP. Test results obtained from CFRP-wrapped concrete cylinders were presented and examined, which allows a number of significant conclusions to be drawn, including the existence of an envelope curve and the cumulative effect of loading cycles. The results were also compared with two existing stress-strain models for FRP-confined concrete, one for monotonic loading and another one for cyclic loading. The monotonic stress-strain model of Lam and Teng was shown to be

able to provide accurate predictions of the envelope curve, but the only existing cyclic stress-strain model was shown to require improvement.

Shao et al. [78] in 2006 studied the behavior of FRP plain concrete stub under cyclic loading. A total of 24 FRP-confined concrete stub specimens were tested in uniaxial compression under different levels of loading and unloading. The stubs were 152mm in diameter and 305 mm in height. Test parameters included fiber type (GFRP and CFRP), thickness of the wrap, and loading patterns. A new model for FRP-confined concrete under uniaxial cyclic compression was proposed using regression analysis of test results. An existing bi-linear confinement model under uniaxial monotonic loading was employed to serve as the unique envelope curve. The proposed model included cyclic rules for loading and unloading, plastic strains, and stiffness and strength degradations. Good agreement was obtained between the analytical predictions of the model with the experimental results of an independent test series, confirming the ability of the model to predict the cyclic behavior of FRP-confined concrete.

A constitutive model for concrete subjected to cyclic loadings in both compression and tension was presented by Sima et al. [79] in 2008. The proposed model was intended to provide improvements on modeling the cyclic behavior of concrete structures in the context of computational programs based on a smeared crack approach. Particular emphasis has been paid to the description of the strength and stiffness degradation produced by the load cycling in both tension and compression, the shape of unloading and reloading curves and the transition between opening and closing of cracks. Two independent damage parameters in compression and in tension have been introduced to model the concrete degradation due to increasing loads. In the case of cyclic compressive loading, the model has been derived from experimental results obtained by other authors by considering the dependency of the cyclic variables with the damage level attained by the concrete. In the case of cyclic tension a simple model was adopted based on experimental observations. The

main novelty of the proposed constitutive model lays in the fact that all the required input data can be obtained through the conventional monotonic compression and tension tests.

A constitutive model to predict the cyclic axial compressive behavior of reinforced concrete columns confined with CFRP was proposed by Varama et al. [80] in 2008. The proposed model was implemented in a FEM-based computer program, able to simulate the material nonlinear behavior of reinforced concrete structures. The performance of the developed model was assessed using results obtained from experimental tests.

Thayalan et al. [81] in 2009 presented the results of static loading (SL) and variable repeated loading (VRL) tests on concrete filled steel tubular (CFST) columns. Assessment of the columns was based on its length, concrete strength and load eccentricity. The column behavior (with and without filling) from the tests was studied. The ultimate strength of the columns subjected to VRL reduced by up to 16% after undergoing a number of load cycles. The incremental collapse (IC) limit was found to lie between 70% and 88% of the static collapse load for CFST columns. The deformations at IC limit were significant and could affect practical designs. The theoretical strengths of the stub and long columns tested are determined on the basis of building code 318 of the American Concrete Institute, and compared with the test results. The squash load equation of the code was found to underestimate the nominal strength of short composite columns.

A new stress-strain formulation for confined concrete under cyclic loading was proposed by Sadeghi and Nouban [82] in 2010. This law can be used in numerical simulations to describe the stress-strain relationship for fibers or layers within the sections of reinforced concrete elements. In order to eliminate the problem of scale effect, a finite element model was generated and the simulated and experimental results of tests on the prototype reinforced concrete column models subjected to cyclic loading were compared. In this way, the

proposed stress-strain law for confined concrete under cyclic loading was accordingly modified and then validated.

An experimental program to study the cyclic behavior of steel fiber reinforced concrete was presented by Shukla [83] in 2011. Two types of cylindrical specimens, containing steel fibers in different proportions, one percent and two percent by volume of concrete, were subjected to cyclic uni-axial compressive loads. Unloading-reloading curves were obtained from these tests. Analytical expressions to predict the reloading and unloading stress-strain curves at various values of residual strain were proposed. It has been observed that simple parabola and an exponential expression were suitable to model the unloading and reloading curves respectively. The proposed models take in to account the potential effects of residual strain on these curves. Comparison of test results with the proposed analytical expressions showed good agreement.

2.4Summary

This chapter has reviewed many experimental and theoretical studies concerning the behavior of concrete columns confined with different techniques and the behavior of concrete columns subjected to axial compressive loadings.

It is apparent that a small amount of applications of ferrocement in strengthening concrete columns exists in comparison with the other techniques of confinement. Also, there is no application concerning the use of this technique to determine the ultimate strength of concrete columns subjected to axial compressive cyclic loading.

The available structural engineering softwares are not utilized for theoretically model concrete column strengthened with ferrocement, so that their behavior could be predicted.

However, all of the previous works described provide significant insight into the development of a confinement by ferrocement for current investigation.

CHAPTER THREE
Experimental Program

3.1 General

The experimental work was carried-out in the Construction Materials Laboratory of the College of Engineering at University of Basrah.

The primary aim of this experimental program is to study the structural behavior of concrete columns strengthened with ferrocement jackets. The experimental program included testing of forty eight circular columns subjected to monotonically increasing and cyclic concentric axial compression.

Details of the test specimens, their construction, material properties, test set-up, instrumentation, and test procedure are presented in this chapter.

The parameters studied included compressive strength of the mortar, specimen size, volume fraction of mesh reinforcements (number of wire mesh layers), and loading types. The column specimens were instrumented to evaluate the behavior in terms of the load-axial displacement response.

3.2 The Objectives of Experimental Work

The main objectives of experimental work were:

1. To study the influence of varying the number of mesh layers (volume fraction of mesh reinforcement) on the ultimate strength of strengthened columns.
2. To study the influence of varying compressive strength of mortar on the ultimate strength of strengthened columns.
3. To investigate the effect of specimens size.
4. To study the influence of loading type (monotonic and cyclic load) on behavior of concrete columns strengthened with ferrocement.

3.3 Materials Used to Fabricate the Specimens

The materials used in this investigation were commercially available materials, which include cement, natural gravel, natural silica sand, water, welded wire mesh (WWM) and superplasticizer.

3.3.1 Cement

Iraqi cement designed as ordinary Portland cement was used throughout this investigation. The whole quantity required was brought to the laboratory and stored in a dry place. The physical properties of cement used throughout this work are presented in Table (3.1).The setting time test is conducted according to ASTM C191 [84]. The compressive strength test is accomplished according to ASTM C109 [85]. The chemical compositions of it are presented in Table (3.2). Results indicate that the cement conforms to the Iraqi standard No. 5/1984 [86].

Table (3.1) Physical properties of ordinary Portland cement

Physical and Mechanical Properties	**Test Result**	**Limits of Iraqi specification No.5/1984**
Compressive strength, N/mm²		
3 – day	18	≥ 15.00
7 – day	25	≥ 23.00
Setting time, h:minutes		
Initial setting	02:31	≥ 00: 45
Final setting	03:19	≤ 10: 00
Standard consistency, %	27.92	
Fineness Specific surface area (by Blaine method), cm²/gm	3011	≥ 2300

Table (3.2) Chemical composition of cement

Components		Results	Requirement according to Iraqi specification No.5/1984	
			Minimum	Maximum
Silicon Dioxide	SIO2	21.14%		
Aluminum Trioxide	AL2O3	4.00%		
Ferric Oxide	Fe2O3	3.05%		
Calcium Oxide	CaO	62.69%		
Magnesium oxide	MgO	2.11%		5%
Sulphate	SO3	2.32%		3%
potassum oxide	K2O	0.66%		
Sodium Oxide	Na2O	0.18%		
Insoluble Residue	Ins.Res.	1.14%		1.50%
Loss on Ignition	LOI	3.38%		4%
Freelime	FL	0.84%		
Lime Saturation Factor	LSF	91.2	66	102
Silicon Ratio	SM	2.66%		
Alumina Ratio	AM	1.61%		
Tricalcium Silicate	C3S	50.59%		
Dicalcium Silicatr	C2S	22.44%		
Tricalcium Aluminates	C3A	7.82%		
Tetracalcium Aluminoferrate	C4AF	9.27%		

3.3.2 Aggregate

1. ***Fine aggregate (Sand)****:* Natural silica sand brought from Al-Zubair area was used as a fine aggregate in this research. The sieve analysis test was conducted according to ASTM C-136 [87]. Table (3.3) shows the grading of sand used for making concrete in this work. Results indicate that the sand conforms to Iraqi specification No. 45/1984 [88]. Same natural silica sand passing through sieve No. (1.18) was used for ferrocement shell as shown in Table (3.4).

Table (3.3) Sieve analysis of sand (for concrete core)

Sieve size mm	Percent Passing	
	Sand used	Limits of Iraqi Specification No. 45/1984
4.75	100	90-100
2.36	93	85-100
1.18	77	75-100
0.60	48	60-79
0.30	22	12-40
0.15	3	0-10
Sulfate content	0.09 %	< 0.5%

Table (3.4) Sieve analysis of sand (for ferrocement shell)

Sieve size mm	Percent Passing	
	Sand used	Limits of Iraqi Specification No. 45/1984
4.75	100	90-100
2.36	100	85-100
1.18	100	75-100
0.60	69.2	60-79
0.30	34.5	12-40
0.15	7.3	0-10

2. ***Coarse aggregate (Gravel)***: Crushed natural gravel obtained from Zubair area was used in making concrete. Its grading satisfied the limits of Iraqi standard No.45/1984 [88] for graded gravel with maximum size of 14 mm as shown in Table (3.5). The sieve analysis test was conducted according to ASTM C136 [87].

   Some properties of the aggregate are presented in Table (3.6).

Table (3.5) Grading of gravel

Sieve size (mm)	% Passing	% Passing of the overall limit of Iraqi Standards No. 45 /1984
20	100	100
14	96.5	90 – 100
10	68.9	50 – 85
5	6.6	0 – 10

Table (3.6) Properties of aggregate

Property	Sand	Gravel
Absorption (%)	1.10	0.54
Bulk specific gravity		
- Oven dry	2.60	2.63
- S.S.D.	2.45	2.65
Unit weight (kg/m^3)		
- Loose	1628	1470
- Tamped	1775	1584

3.3.3 Water

Ordinary potable water was used in making and curing concrete core and ferrocement shell.

3.3.4 Superplasticizer

The superplasticizer used was highly effective in the production of free flowing concrete and also as a substantial water reducing agent to enhance the

early and ultimate strength of concrete. KUT PLAST MF (ADM-07-0104) was used for the present study. Its specific gravity was 1.10. Different dosages of superplasticizer were used for finding the target strength of the mixes. KUT PLAST MF complies with BS-5075, 1982 and ASTM-C494, Type F.

3.3.5 Steel Mesh Reinforcement

Steel welded wire meshes (WWM) of 12.5 mm square opening with average wire diameter of (1 mm) has been used in this investigation. Figure (3.1) shows the geometry and dimensions of the mesh type used throughout this work.

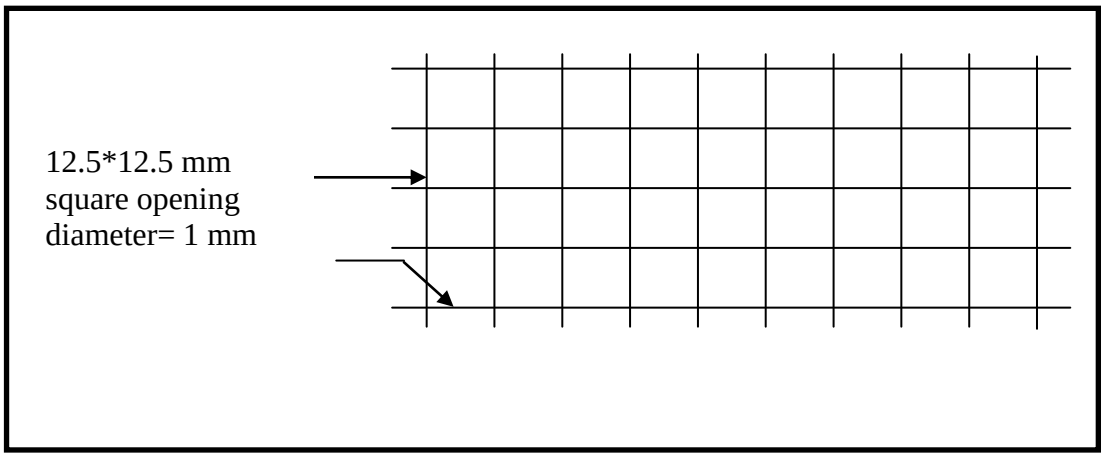

Figure (3.1): Typical square welded wire mesh

3.3.5.1 Mechanical Properties of WWM

Locally available it was decided to determine the mechanical properties of the WWM, by conducting a tensile test on three coupon specimen using the guidelines presented by ACI committee 549, 1999 [9].The tested specimen was prepared by embedding both ends of a rectangular coupon of mesh in mortar over a length equal to the width of the specimen, that should not be less than six times the mesh opening or wire spacing measured normally to the loading direction (11 mm). The width of the specimen was taken 80 mm, and it was embedded in mortar with a length of 100 mm. The length of the tested specimen should not be less than three times its width or 150 mm whichever is larger. The

length of the tested specimen was taken 240 mm. Wooden Molds were prepared to cast mortar blocks at the end of the WWM coupon. The dimension of the molds was in accordance with the ACI committee 549 [9] recommendations. It was 100 mm length, 80 mm width, 20 mm thick to be sufficiently attached to the testing machine clamper, and the length of the tested sample was 240 mm. Plate (3.1) shows the tested WWM coupon inserted in the wooden mold before applying the mortar at ends.

The wooden molds were filled with mortar (1: 2 cement to sand with water cement ratio of 0.45) and pressed well to fill all voids. The final shape of the tested specimen with its final dimensions after removing the wooden forms is shown in plate (3.2).

Plate (3.1) Tested WWM Coupon inserted in the wooden mold before applying mortar at ends

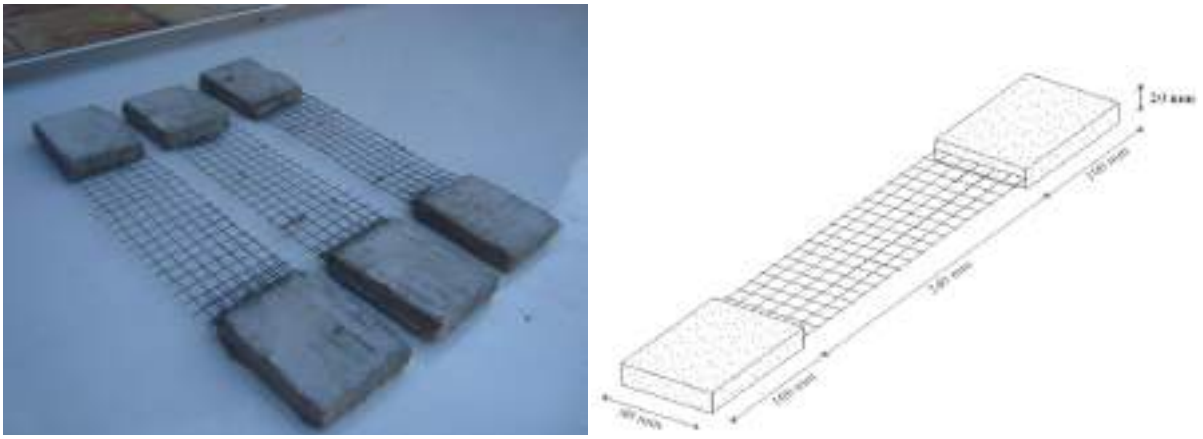

(a) (b)

Plate (3.2)Testeed specimens and their dimensions

3.3.5.2 Test Setup for Tensile Test of WWM

A 5 kN tensile test machine (Bench-Top) model BT-1000 as shown in plate (3.3) was used to perform the tensile test on three specimens of WWM coupons. Plate (3.3) shows the setup of tension test. The tensile stress was determined by dividing the tensile load by the total cross section area of the mesh coupon (cross section area of 7 wires = $7 * \pi/4 * (1)^2$ = 5.498 mm^2) while the tensile strains were determined by dividing the axial elongation by the coupon length (240mm).The resulted stress-strain curves were plotted for all tested WWM specimens. The yield stress was determined as recommended by ACI committee 549, 1988 [9], as the stress at the yield strain (ϵ_y). ϵ_y is taken as the strain at the intersection of the best straight line fits the initial portion of the stress-strain curve and the best straight line fits the yielded portion of the stress-strain curve, as shown in Fig. (3.2).

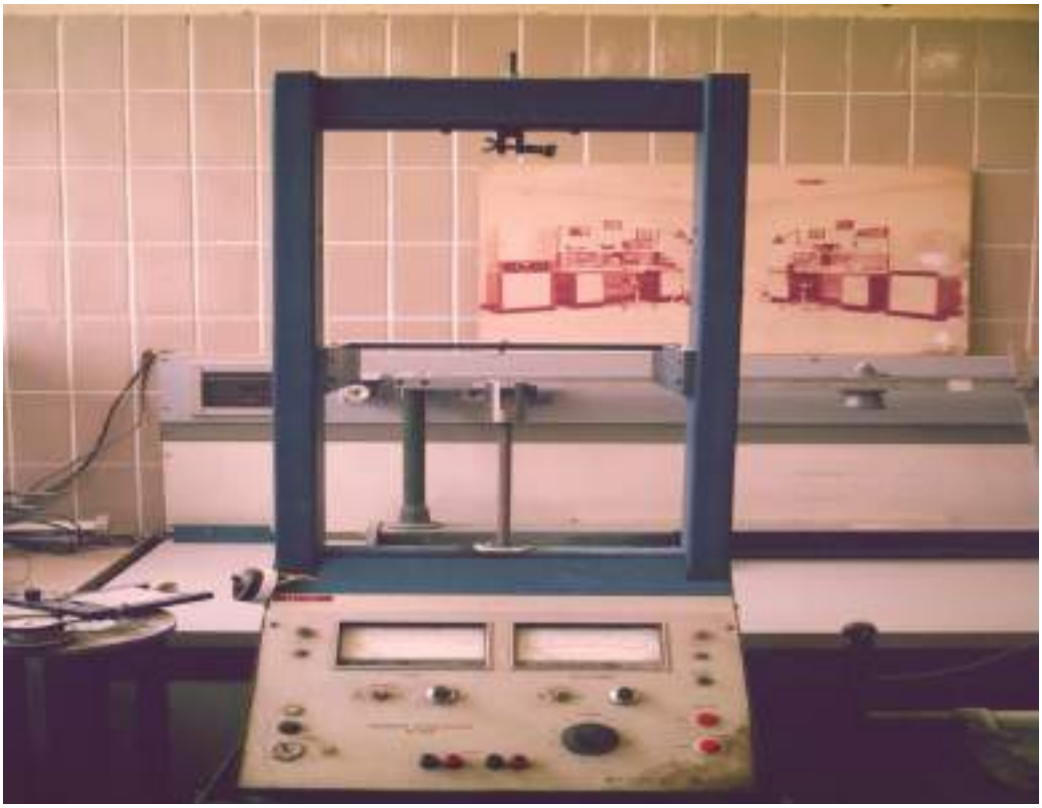

Plate (3.3) Tension testing machine for wire mesh

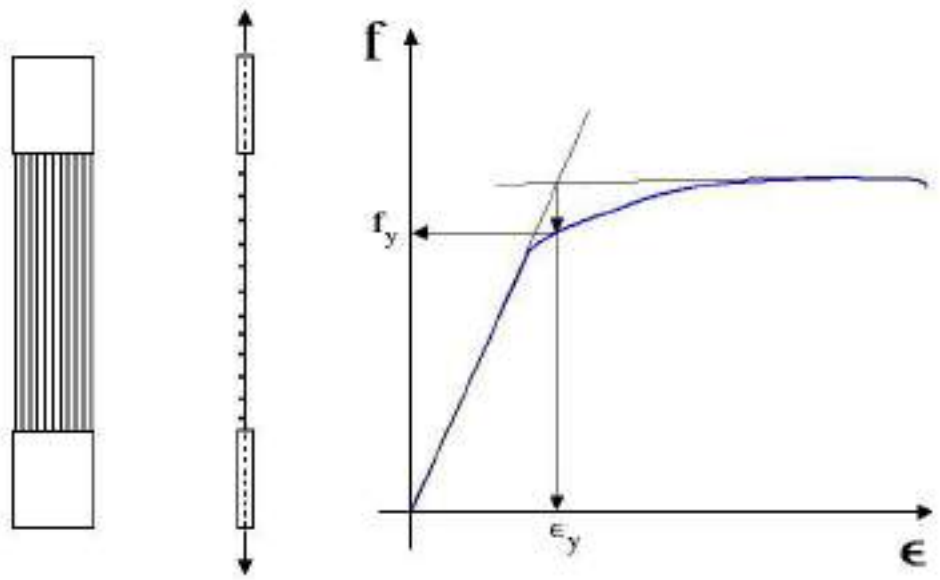

Figure (3.2) Schematic description of mesh tensile yield stress and corresponding strain.

3.3.5.3 WWM Coupon Test Results

The stress-strain curves of the three tested WWM specimens were obtained and plotted as shown in Fig. (3.3). All specimens failed by wire cutting at ultimate loads as shown in plate (3.4). The yield strength, ultimate strength and the modulus of elasticity of the three tested specimen were obtained from the resulted stress-strain curves and are given in Table (3.7).

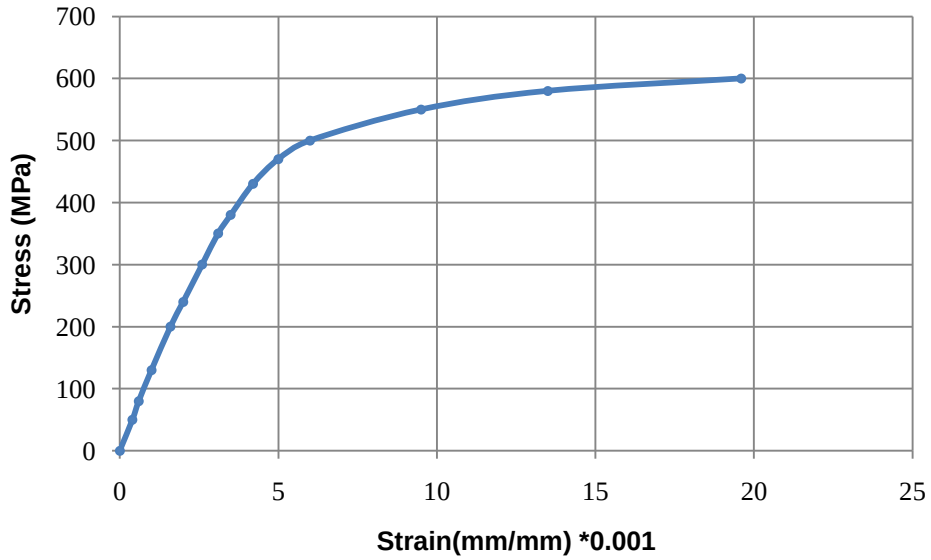

Figure (3.3) Stress-strain curve for the tested WWM specimens

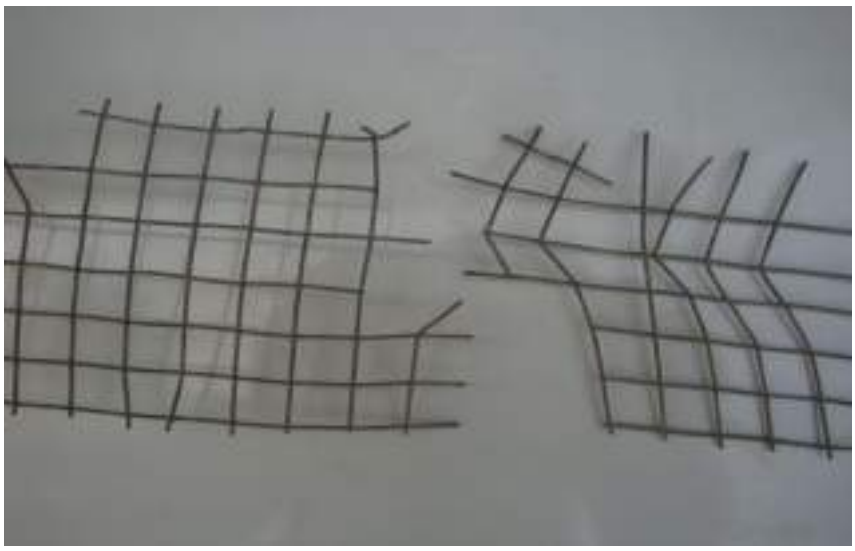

Plate (3.4) Failure mode of tested WWM specimens

Table (3.7) Tensile test results of WWM specimens

Specimens	**Wire diameter (mm)**	f_y **(MPa)**	f_u **(MPa)**	**Modulus of Elasticity (MPa)**
Coupon 1	1	406	588	89400
Coupon 2	1	410	602	89500
Coupon 3	1	394	583	88910
Average	1	403.33	591	89270

3.4 Concrete and Ferrocement Mixes

3.4.1 Concrete Core

The same concrete mix was used through the whole investigation. The mix proportions of the ingredients by dry weights were [1 cement : 1.5 sand : 3 gravel], and the water cement ratio (w/c) was 60%, to give a cube compressive strength of about 30 N/mm^2 at age of 28 days and slump of about 100 mm.

Mixing was carried out according to BS1881 [89]. Drum mixer was used. The interior surface of the drum mixer was cleaned and moistened before use. The dry ingredients were added in the following order, about one half of the coarse aggregate, all the fine aggregate, all the cement, and finally the remaining part of coarse aggregate. Then water was added and mixing was started. The

period of mixing ranged from two to three minutes so that a homogenous mix was obtained.

3.4.2 Ferrocement Shell

Two mortar mixes were used to investigate the influence of the mortar strength on the behavior of concrete columns confined with ferrocement. The mix proportions of the ingredients of the first mix, Mix 1, by dry weights were [1 cement: 2 sand], and the water cement ratio (w/c) was 40%. To improve workability a superplasticizer was added at 0.02% by weight of cement. The target 50 mm cube compressive strength of this mix was 35 MPa at age of 28 days. For the second mix, Mix 2, the mix proportions of the ingredients by dry weights were [1 cement: 1.5 sand], and the water cement ratio (w/c) was 35%. Also 0.025 % superplasticizer was added. The average compressive strength of 50mm mortar cube samples was 45MPa at age of 28 days.

The mixing was carried out in a Tilting pan type mixer. The mixing procure was according to ASTM specification C305-65 [90] of mixing mortars. The water with superplasticizer and cement was first mixed for 30 second. Then sand was added while mixing continued for another 30 seconds. Mixing was continued for a further 30 second, after which the mixer was stopped for 90 seconds for the mixture to settle. During that time, any lumps on the blades were quickly removed. The mixing was resumed for a further 60 seconds, after which the mortar was ready for casting.

3.5 Mould Preparation

Three circular steel moulds were used in this work. The dimensions of these moulds are (150*300mm),(150*450mm) and (200*750mm). They were cleaned with a scraper and a steel hair brush and were lubricated to ensure an easy demolding.

3.6 Fabrication of the Column Specimens

The preparation of specimens involves several steps as follows.

A PVC-tube of external diameter equal to the inner diameter of ferrocement shell, 151.5 mm diameter for (200*750 mm) specimens and 101mm diameter for both (150*300mm) and (150*450mm) specimens, was fastened on a wood base.

The wire mesh was cut from the roll (1.2*25m) to the required width and length. An overlap of 100 mm was provided in lateral direction for the wire mesh. The required number of wire mesh layers was properly wrapped around the PVC-tube. The steel mould was then fastened to cover the PVC-tube.

Casting was carried out on a vibrating table. The specimen mould with the ferrocement packed in was placed on the vibrating table. Mortar was filled in between the mesh layers while the vibration table was in operation. After about 15 minutes of casting the PVC-tube was drawn from the mould leaving hollow cylindrical shape of ferrocement as shown in plate (3.5).

Plate (3.5) Hollow cylindericl ferrocement shell after drawing of PVC-tube.

Then this hollow cylinder was filled with concrete in approximately 10 cm layers and each layer was compacted by steel rod. After the mold was filled the top surface was flattened carefully. After 24 hours the specimens were removed from the molds and stored in a water tank till the time of testing (28 days). Finally the specimens were taken out from the tank and kept in the natural temperature of laboratory room before testing. The specimens were prepared for testing by capping its top surface with grout cement paste to ensure parallel

surfaces, and to distribute the load uniformly in order to reduce any eccentricities. All specimens were painted white before testing so that cracks would be easily noticed and clearly photographed.

3.7 Strength of Concrete and Mortar

During casting, three 150 x 150 x 150 mm cubes and two 150 x 300 mm cylinders for concrete were made. The control specimens were compacted by a steel rod as the original columns, and were cured under the same conditions.

The cube compressive strength of concrete was obtained by testing three cubes according to BS1881 [89], and the cylinder compressive strength was evaluated by testing two cylinders according to ASTM C39 [91].The properties of concrete are shown in Table (3.8).

The mortar specimens were prepared for both mixes according to ASTM C 109 [85] specifications. For each mortar mix, six standard cubes for compressive tests and three standard briquettes for tensile tests were prepared, as shown in plate (3.6). All specimens were moist cured for one day and water cured for 28 days before testing.

The compressive strength and tensile strength of tested specimen for both mortar mixes are summarized in Table (3.9).

Plate (3.6) Control mortar specimens

Table (3.8) Properties of concrete

Group No.	Compressive Strength (MPa)	
	Cube	Cylinder
J	28.4	22.4
J1	27.3	23
J2	28.5	24
J3	29.5	22.7
J4	27.0	21.8
J5	30.1	24.5
J6	29.0	22.6
J7	28.3	23.1
J8	30.0	24.3
J9	28.2	23
J10	27.4	22.8
J11	28.8	24.2
J12	29.1	23.6
J13	28.2	21.8
J14	29.0	23.1
J15	27.3	24.5
J16	29.2	24.1
J17	27.6	21.5
Average	28.5	23.2

Table (3.9) Compressive and tensile strength of tested mortar specimens

Group No.	Compressive Strength (MPa)	Tensile Strength (MPa)
J	36.2	3.73
J1	35.8	3.93
J2	34.9	3.14
J3	35.3	3.35
J4	34.4	3.1
J5	46.1	4.6
J6	44.6	4.14
J7	45.2	4.33
J8	45.4	4.32
J9	44.7	4.38
J10	46	4.58
J11	45.8	4.32

3.8 Calculation of Volume Fraction of WWM Layers

The volume fraction of the mesh reinforcement used was calculated as given by the ACI committee 549, 1988 [9]. The volume fraction of mesh in a ferrocement section may be readily calculated if the density of the mesh material and the weight of mesh per unit area were known [9]. By using a micrometer six random readings were taken and the average diameter (Db) was found to be 1 mm. Using a caliper, twenty readings on both inner longitudinal and transverse spacings at different locations were taken and the average reading was found to be 11.5 mm. For ferrocement reinforced with square or rectangular mesh, the

volume fraction of mesh reinforcement may be calculated from the Equation below [10]. Table (3.10) gives the volume fraction for 2, 3, 4, 5 and 7 layers of mesh reinforcement.

$$V_f = \frac{N\pi {D_b}^2}{4h}\left[\frac{1}{D_l} + \frac{1}{D_t}\right] \quad (3.1)$$

where;

N = number of layers of mesh reinforcement

D_b = diameter of mesh wire = 1 mm

h = thickness of ferrocement

D_l=center-to-center spacing of wires aligned longitudinally in reinforcing mesh

D_t = center-to-center spacing of wires aligned transversely in reinforcing mesh

$D_l = D_t$ = 11.5 + (2) (1/2) (1) = 12.5 mm.

Table (3.10) Volume fraction for each number of layers

No. of Layers	Thickness(h) (mm)	Volume Fraction (V_f)
2	23	1.09%
3	23	1.64%
4	23	2.18%
5	23	2.73%
7	23	3.82%

3.9 Details of Test Specimens

A total of forty eight circular short concrete columns were prepared for test. Forty-two columns out of 48 circular columns were strengthened with ferrocement jackets. The jacket thickness was constant and equal to 23 mm for all strengthened specimens. The strengthened columns were divided into twelve groups (J-J11). Group J and J9 has one specimen only and remaining groups, four specimens were prepared one of them was tested under monotonically increasing axial compressive loading condition and the three others were tested under cyclic axial load. All groups were casted without steel reinforcement in

concrete core and the same concrete mix was used through the investigation. Two mortar mixes were used, Mix 1 was used for groups (J- J4) and Mix 2 was used for groups (J5-J11)). The variables of these specimens were the column height (300, 450 and 750 mm), number of wire mesh layers (2, 3, 4, 5, and 7), mortar cube compressive strength (35 and 45 N/mm^2), and type of loading history imposed on the specimen (monotonic and cyclic load conditions). Specimen diameter was constant. Six columns were remained of 48 plain concrete without ferrocement jacket group (J12-J17). Specimens J12 to J17 were tested under monotonically increased axial compressive loading and they were used as control specimens. Table (3.11) gives the details of the columns including their designation. For the strengthened specimens (J-J11) on the specimen designation, shown in the second column of Table (3.11) is as follows: the first number in the designation refers to the number of layers of wire mesh in. The first letter A, B or D indicates the height of the column. The second letter pertains to the loading type, M for monotonic load, E for cyclic to envelope, L for cyclic between maximum stress level (90% f'_c) and zero stress level and S for cyclic between maximum stress level (90% f'_c) and minimum stress level (40% f'_c). The last numbers 1 and 2 in the designation refer to the mortar compressive strength (35 and 45 MPa) respectively. For plain concrete specimens (J13-J18), the first number 100, 150 or 200 indicates the diameter of the column in mm. The first letter A, B or D indicates the height of the column. The second letter pertains to the loading type (monotonic load).

For example specimen 7DM2 is a strengthened circular concrete column with 7 layers of wire mesh, height of 750 mm, under monotonic load and 45 MPa compressive strength of mortar. Specimen 150BM is a plain concrete column with150 mm diameter of cross section, height of 450 mm and under monotonic load. Figure (3.4) shows cross section dimensions for plain concrete columns and strengthened columns with ferrocement.

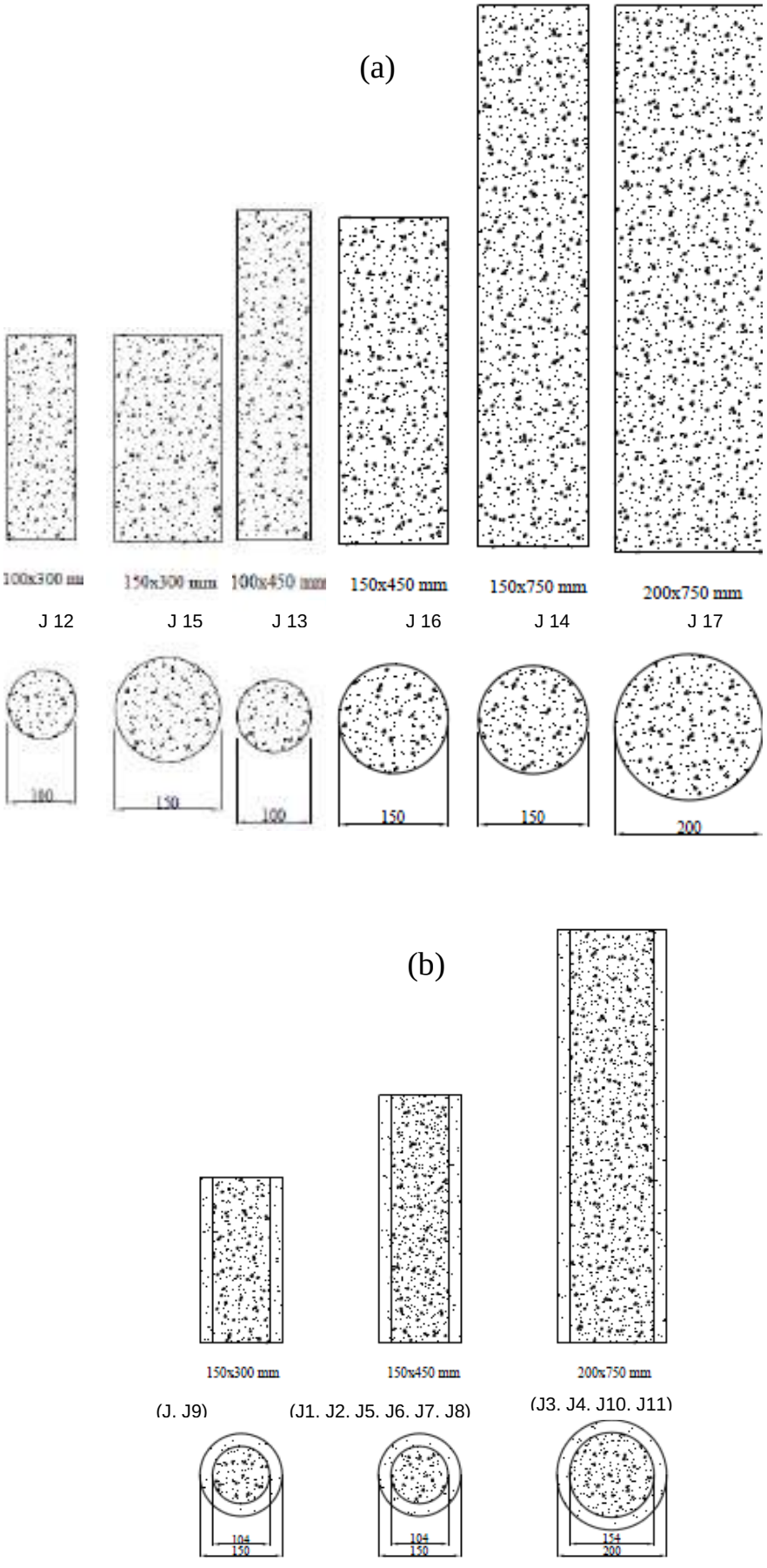

Figure (3.4) (a) Cross section dimensions for plain concrete specimens (b) cross section dimensions for strengthened specimens with ferrocement

Table (3.11) Details of columns

Group No.	Column designation	No. of welded wire mesh	Nominal mortar strength (MPa)	External diameter *(D)* (mm)	Jacket thickness (*h*) (mm)	Height of specimen *(L)* (mm)
J	**4AM1**	4	35	150	23	300
J1	**2BM1**	2	35	150	23	450
	2BE1	2	35	150	23	450
	2BL1	2	35	150	23	450
	2BS1	2	35	150	23	450
J2	**4BM1**	4	35	150	23	450
	4BE1	4	35	150	23	450
	4BL1	4	35	150	23	450
	4BS1	4	35	150	23	450
J3	**4DM1**	4	35	200	23	750
	4DE1	4	35	200	23	750
	4DL1	4	35	200	23	750
	4DS1	4	35	200	23	750
J4	**7DM1**	7	35	200	23	750
	7DE1	7	35	200	23	750
	7DL1	7	35	200	23	750
	7DS1	7	35	200	23	750
J5	**2BM2**	2	45	150	23	450
	2BE2	2	45	150	23	450
	2BL2	2	45	150	23	450
	2BS2	2	45	150	23	450
J6	**3BM2**	3	45	150	23	450
	3BE2	3	45	150	23	450
	3BL2	3	45	150	23	450
	3BS2	3	45	150	23	450
J7	**4BM2**	4	45	150	23	450
	4BE2	4	45	150	23	450
	4BL2	4	45	150	23	450
	4BS2	4	45	150	23	450
J8	**5BM2**	5	45	150	23	450
	5BE2	5	45	150	23	450
	5BL2	5	45	150	23	450
	5BS2	5	45	150	23	450
J9	**4AM2**	4	45	150	23	300
J10	**4DM2**	4	45	200	23	750
	4DE2	4	45	200	23	750

Table (3.11) Continued

J10	**4DL2**	4	45	200	23	750
	4DS2	4	45	200	23	750
J11	**7DM2**	7	45	200	23	750
	7DE2	7	45	200	23	750
	7DL2	7	45	200	23	750
	7DS2	7	45	200	23	750
J12	**100AM**	---	---	100	---	300
J13	**100BM**	---	---	100	---	450
J14	**150DM**	---	---	150	---	750
J15	**150AM**	---	---	150	---	300
J16	**150BM**	---	---	150	---	450
J17	**200DM**	---	---	200	---	750

3.10 Instrumentation and Test Setup

All specimens were tested under axial compression using a Torsee's universal testing machine with a capacity of 1000 kN at the laboratory of construction materials at the University of Basrah. The column specimen was centered in the testing machine to ensure that the compressive axial load was applied without any eccentricity. The top and bottom faces of specimen were grinded and made smooth and leveled to remove surface imperfections and maintain uniformity of loading on the surface. The vertical displacement of the lower movable head of the testing machine was measured in relation to the upper head of the testing machine by a dial gauge with magnetic base. This measured displacement was assumed to be equal to the vertical shortening of the test specimen. Two dial gauges, one at the right and the other at the left of the specimen were used. The accuracy of the dial gauge was 0.01 mm. The test setup along with specimen is shown in plate (3.7).

Tests performed in four different series. These test series are classified according to the type of loading history imposed on the specimen. They are:

1. Monotonic loading to failure: unconfined and confined specimens were tested by monotonically increasing the axial strain until the failure of column.
2. Cyclic to envelop curve: confined specimens were loaded axially up to a given value of axial strain, unloaded to zero axial stress, and then reloaded to a new stress level. The specimen was again unloaded to zero axial stress and the procedure was repeated in the same fashion until failure occurred.
3. Cyclic between two fixed value of stress: this series can be subdivided into two groups;
    a. Confined specimens were loaded monotonically up to 90% of ultimate strength, unloaded to zero axial stress and then reloaded until the stress attained the same previous point (90% of ultimate strength). This procedure was repeated until failure occurred or 70 cycles of loading were applied. If the failure did not occur then the load was increased monotonically to failure.
    b. Specimens were loaded as in the above case except that in this case the minimum stress level was 40% of ultimate strength instead of zero stress level.

Plate (3.7) Test setup and instrumentation of tested columns

CHAPTER FOUR
Finite Element Method

4.1 Introduction

The finite element method is now firmly accepted as a powerful general technique for the numerical solution of a variety of problems encountered in engineering. One of the principal advantages of the finite element method is the unifying approach; it offers the solution of diverse engineering problems [92]. The basic steps of the finite element process can be listed as follows [93].

1- The structure is divided into distinct non-overlapping regions known as elements over which the main variables are interpolated.

2- These elements are connected at a discrete number of points along their periphery known as nodal points.

3- For each element the stiffness matrix and the applied load vector are calculated.

4- The stiffness matrices and the load vectors of all elements are assembled to give respectively, the global stiffness matrix and the global load vector for the complete structure.

5- The resulting system of simultaneous equations is solved for the unknown nodal variables; which for structural problems are the displacement components.

6- Finally subsidiary quantities such as stress components are evaluated for each element.

In the present work, ANSYS computer program (**AN**alysis **SYS**tem) is used to create the finite element model.

4.2 Finite Element Formulation

4.2.1 Basic Finite Element Relationships

The basic step in any finite element analysis is the derivation of the element stiffness matrix, which relates the nodal displacement vector, {a}, to the nodal force vector, {f}. To derive this relation, three conditions must be satisfied [94]:

1. Compatibility of strains and displacements (kinematic condition).
2. Equations of equilibrium (equilibrium condition).
3. Stress-strain relations (constitutive relations).

The element stiffness matrix can be determined by using the principle of virtual displacement, which states that, if the work done by the external forces on a structural system is equal to the increase in strain energy of the system for any set of admissible virtual displacements, then the system is in equilibrium [95].

When a body is subjected to a set of external forces, the displacement vector at any point within the element, $\{U\}_e$, is given by,

$$\{U\}_e = [N].\{a\}_e \tag{4.1}$$

where, [N] is the matrix of shape functions, and $\{a\}_e$ is the column vector of nodal displacements. The strain at any point can be determined by differentiating Eq. (4.1),

$$\{\varepsilon\}_e = [L].\{U\}_e \tag{4.2}$$

where, [L] is the matrix of differential operator. In expanded form, the strain vector can be expressed as,

$$\{\varepsilon\}_e = \begin{Bmatrix} \varepsilon_x \\ \varepsilon_y \\ \varepsilon_z \\ \gamma_{xy} \\ \gamma_{yz} \\ \gamma_{xz} \end{Bmatrix} = \begin{Bmatrix} \frac{\partial u}{\partial x} \\ \frac{\partial v}{\partial y} \\ \frac{\partial w}{\partial z} \\ \frac{\partial u}{\partial y} + \frac{\partial v}{\partial x} \\ \frac{\partial v}{\partial z} + \frac{\partial w}{\partial y} \\ \frac{\partial w}{\partial x} + \frac{\partial u}{\partial z} \end{Bmatrix} \tag{4.3}$$

Substitution of Eq. (4.1) into Eq. (4.2) gives,

$$\{\varepsilon\}_e = [B].\{a\}_e \tag{4.4}$$

where [B] is strain-nodal displacement matrix given by,

$$[B] = [L].[N] \tag{4.5}$$

With the strains within the element are known, the stress vector can be determined by using the appropriate stress-strain relationship as:

$$\{\sigma\}_e = [D].\{\varepsilon\}_e \tag{4.6}$$

where [D] is the constitutive matrix and $\{\sigma\}_e$ is:

$$\{\sigma\}_e = [\sigma_x\ \sigma_y\ \sigma_z\ \tau_{xy}\ \tau_{yz}\ \tau_{xz}]^T \tag{4.7}$$

From Eqs. (4.4) and (4.6), the stress-nodal displacement relationship can be expressed as,

$$\{\sigma\}_e = [D].[B].\{a\}_e \tag{4.8}$$

For writing the force-displacement relationship, the principle of virtual displacement is used. If an arbitrary virtual nodal displacement, $\{a^*\}_e$, is imposed, the external work, W_{ext}, will be equal to the internal work, W_{int} ,

$$W_{ext} = W_{int} \tag{4.9}$$

in which

$$W_{ext} = \{a^*\}_e^T . \{f\}_e \tag{4.10}$$

and

$$W_{int} = \int_e \{\varepsilon^*\}_e^T . \{\sigma\}_e . dv \tag{4.11}$$

where $\{f\}_e$ is the nodal force vector. Substitution of Eq. (4.4) into Eq. (4.11), yields,

$$W_{int} = \{a^*\}_e^T . \int_v [B]^T . \{\sigma\}_e . dv \tag{4.12}$$

From Eqs. (4.8) and (4.12),

$$W_{int} = \{a^*\}_e^T . \int_v [B]^T . [D].[B].dv.\{a\}_e \tag{4.13}$$

Then Eq. (4-9) can be written as,

$$\{a^*\}_e^T . \{f\}_e = \{a^*\}_e^T . \int_v [B]^T . [D].[B].dv.\{a\}_e \tag{4.14}$$

or,

$$\{f\}_e = \int_v [B]^T . [D].[B].dv.\{a\}_e \tag{4.15}$$

Letting:

$$[K]_e = \int_v [B]^T . [D].[B].dv. \tag{4.16}$$

then

$$\{f\}_e = [K]_e . \{a\}_e \tag{4.17}$$

where, $[K]_e$ is the element stiffness matrix.

The overall stiffness matrix, [K], can be obtained by direct addition of the elements stiffness matrices after transforming from the local to the global coordinates, therefore,

$$[K]= \sum_{n}\int_{v}[B]^{T}.[D].[B].dv \tag{4.18}$$

The total external force vector {f} is then,

$$\{f\}= [K].\{a\} \tag{4.19}$$

where, {a} is the unknown nodal point displacement vector.

4.2.2 Strain-Displacement Matrix

The strain vector at any point within the brick element (8 nodes) is related to the nodal displacements vector by Eq. (4.3) which may be written in expanded

form as [94]:

$$\begin{Bmatrix}\varepsilon_x\\ \varepsilon_y\\ \varepsilon_z\\ \gamma_{xy}\\ \gamma_{yz}\\ \gamma_{zx}\end{Bmatrix} = \sum_{i=1}^{8}\begin{bmatrix}\frac{\partial N_i}{\partial x} & 0 & 0\\ 0 & \frac{\partial N_i}{\partial y} & 0\\ 0 & 0 & \frac{\partial N_i}{\partial z}\\ \frac{\partial N_i}{\partial y} & \frac{\partial N_i}{\partial x} & 0\\ 0 & \frac{\partial N_i}{\partial z} & \frac{\partial N_i}{\partial y}\\ \frac{\partial N_i}{\partial z} & 0 & \frac{\partial N_i}{\partial x}\end{bmatrix}\begin{Bmatrix}u_i\\ v_i\\ w_i\end{Bmatrix} \tag{4.20}$$

where, the 6x3 matrix is the strain-displacement [B], which contains the global derivatives of the shape functions, N_i.

Since the shape functions are defined in terms of the local coordinates, then a relationship between the derivatives of the shape functions in the two coordinate systems must be defined. This relationship can be found by using the chain rule as follows [94]:

$$\begin{aligned}\frac{\partial N_i}{\partial s} &= \frac{\partial N_i}{\partial x}\cdot\frac{\partial x}{\partial s}+\frac{\partial N_i}{\partial y}\cdot\frac{\partial y}{\partial s}+\frac{\partial N_i}{\partial z}\cdot\frac{\partial z}{\partial s}\\ \frac{\partial N_i}{\partial t} &= \frac{\partial N_i}{\partial x}\cdot\frac{\partial x}{\partial t}+\frac{\partial N_i}{\partial y}\cdot\frac{\partial y}{\partial t}+\frac{\partial N_i}{\partial z}\cdot\frac{\partial z}{\partial t}\\ \frac{\partial N_i}{\partial r} &= \frac{\partial N_i}{\partial x}\cdot\frac{\partial x}{\partial r}+\frac{\partial N_i}{\partial y}\cdot\frac{\partial y}{\partial r}+\frac{\partial N_i}{\partial z}\cdot\frac{\partial z}{\partial r}\end{aligned} \tag{4.21}$$

In matrix form, Eq. (4.21) can be written as,

$$\begin{Bmatrix} \frac{\partial N_i}{\partial s} \\ \frac{\partial N_i}{\partial t} \\ \frac{\partial N_i}{\partial r} \end{Bmatrix} = \begin{bmatrix} \frac{\partial x}{\partial s} & \frac{\partial y}{\partial s} & \frac{\partial z}{\partial s} \\ \frac{\partial x}{\partial t} & \frac{\partial y}{\partial t} & \frac{\partial z}{\partial t} \\ \frac{\partial x}{\partial r} & \frac{\partial y}{\partial r} & \frac{\partial z}{\partial r} \end{bmatrix} \begin{Bmatrix} \frac{\partial N_i}{\partial x} \\ \frac{\partial N_i}{\partial y} \\ \frac{\partial N_i}{\partial z} \end{Bmatrix} \tag{4.22}$$

The 3x3 matrix is called the Jacobian matrix [J], therefore,

$$\begin{Bmatrix} \frac{\partial N_i}{\partial s} \\ \frac{\partial N_i}{\partial t} \\ \frac{\partial N_i}{\partial r} \end{Bmatrix} = [J] \begin{Bmatrix} \frac{\partial N_i}{\partial x} \\ \frac{\partial N_i}{\partial y} \\ \frac{\partial N_i}{\partial z} \end{Bmatrix} \tag{4.23}$$

For the isoparametric element, the shape functions are also used to define the geometry of the element. Therefore, the Cartesian coordinates of any point within the element are given by [94],

$$\begin{aligned} x(s,t,r) &= \sum_{i=1}^{8} N_i(s,t,r) \cdot x_i \\ y(s,t,r) &= \sum_{i=1}^{8} N_i(s,t,r) \cdot y_i \\ z(s,t,r) &= \sum_{i=1}^{8} N_i(s,t,r) \cdot z_i \end{aligned} \tag{4.24}$$

Making use of Eq. (4.24), the Jacobian matrix can be written as,

$$[J] = \begin{bmatrix} \sum_{i=1}^{8} \frac{\partial N_i}{\partial s} \partial x_i & \sum_{i=1}^{8} \frac{\partial N_i}{\partial s} \partial y_i & \sum_{i=1}^{8} \frac{\partial N_i}{\partial s} \partial z_i \\ \sum_{i=1}^{8} \frac{\partial N_i}{\partial t} \partial x_i & \sum_{i=1}^{8} \frac{\partial N_i}{\partial t} \partial y_i & \sum_{i=1}^{8} \frac{\partial N_i}{\partial t} \partial z_i \\ \sum_{i=1}^{8} \frac{\partial N_i}{\partial r} \partial x_i & \sum_{i=1}^{8} \frac{\partial N_i}{\partial r} \partial y_i & \sum_{i=1}^{8} \frac{\partial N_i}{\partial r} \partial z_i \end{bmatrix} \tag{4.25}$$

The global derivatives of the shape functions can be obtained by inverting the Jacobian matrix.

$$\begin{Bmatrix} \frac{\partial N_i}{\partial x} \\ \frac{\partial N_i}{\partial y} \\ \frac{\partial N_i}{\partial z} \end{Bmatrix} = [J]^{-1} \begin{Bmatrix} \frac{\partial N_i}{\partial s} \\ \frac{\partial N_i}{\partial t} \\ \frac{\partial N_i}{\partial r} \end{Bmatrix} \tag{4.26}$$

4.2.3Element Stiffness Matrix

The stiffness matrix for an element as given in Eq. (4.16) can be written as [94]:

$$[K]_e = \iiint_v [B]^T.[D].[B].dv \tag{4.27}$$

in which dv represents the volume of the element in the global coordinates and can be expressed as:

$$dv = dx.dy.dz \tag{4.28}$$

In local coordinates it can be written as:

$$dv = |J|.ds.dt.dr \tag{4.29}$$

where, $|J|$ is the determinate of the Jacobian matrix.

Substituting Eq. (4.28) into equation (4.29), the element stiffness matrix is then given by,

$$[K]_e = \int_{-1}^{+1}\int_{-1}^{+1}\int_{-1}^{+1} [B]^T.[D].[B].|J|.ds.dt.dr \tag{4.30}$$

4.3 Material Constitutive Relationships

The performance of any structure under load depends to a large degree on stress-strain relationship of the material from which it is made.

The problem of short concrete columns strengthened with ferrocement jacket deals with different materials (concrete, welded wire mesh and mortar)

which are brought together to work as a composite system. That system is made to exploit the material relationship of each constituent material according to its designated position so as to form a composite relationship describing the behavior of the whole configuration under loading conditions [96].

In the following sections and as required within the frame of this study, a description of the constitutive relationships for the materials comprising concrete column strengthened with ferrocement shell are given.

4.3.1 Concrete

Concrete exhibits a large number of microcracks, especially, at the interface between coarse aggregate and mortar, even before subjected to any load. The presence of these microcracks has a great effect on the mechanical behavior of concrete, since their propagation during loading contributes to the nonlinear behavior at low stress levels and causes volume expansion near failure. Many of these microcracks are caused by segregation, shrinkage or thermal expansion of the mortar. Some microcracks may develop during loading because of the difference in stiffness between aggregates and mortar. Since the aggregate-mortar interface has a significantly lower tensile strength than mortar, it constitutes the weakest link in the composite system. This is the primary reason for the low tensile strength of concrete. The response of a structure under load depends to a large extent on the stress-strain relation of the constituent materials and the magnitude of stress [97].

Concrete exhibits varying deformation characteristics under different loading conditions and load levels. The uniaxial stress-strain response is essentially linear elastic up to about (30%) of the uniaxial strength (f_c') [98]. Above this stress level, non-linearity in response is obtained. An increase in non-linearity is evidenced in the stress range of approximately (0.75 f_c') to (0.90 f_c'). From this point onward the curve bends sharply until the peak stress f_c' is reached. Beyond the peak stress, concrete exhibits strain softening characterized by the descending portion of the curve as shown in Fig. (4.1-a). Concrete

Poisson's ratio, ν, has been observed to remain approximately constant and ranging in value from about 0.15 to 0.22 up to stress level of about (0.8 f_c'), at which stress the Poisson's ratio begins to increase suddenly [99].

As shown in Fig. (4.1-b)When the volumetric strain ($\varepsilon_v = \varepsilon_1 + \varepsilon_2 + \varepsilon_3$) is found initially to be almost linear up to about $0.75f_c'$ to $0.90f_c'$ (here1, 2, 3 are subscripts representing direction of principal stresses and strains). At this point, the direction (or sign) of the volumetric strain is reversed, resulting in a volumetric expansion near or at (f_c'). The stress corresponding to the minimal value of volumetric strain beyond which no further reduction in volume occur is termed critical stress [100].

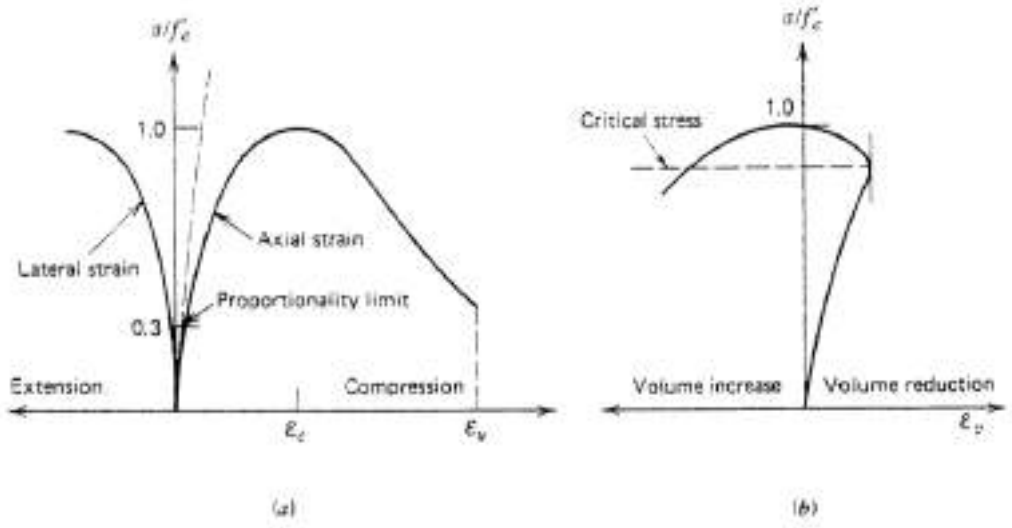

Figure (4.1) Typical stress-strain curves for concrete in uniaxial compression test. (a) Axial and lateral strains. (b) Volumetric strain ($\varepsilon_v = \varepsilon_1 + \varepsilon_2 + \varepsilon_3$) [3].

Figure (4.2) shows the response of concrete to uniaxial loading and unloading. If the unloading is performed in the stress range between 50 and 75 percent of f_c', the unloading curve exhibits some nonlinearity. If reloading takes place, the small characteristics hysteresis loop is formed, the unloading-reloading curve is fairly parallel to initial tangent of the original curve. However, for unloading from stresses at about 75 percent of f_c' the unloading-reloading curves exhibit strong nonlinearities, and a significant degradation of

stiffness can be also observed. A reloading shows that the materials-stiffness properties have changed drastically [99].

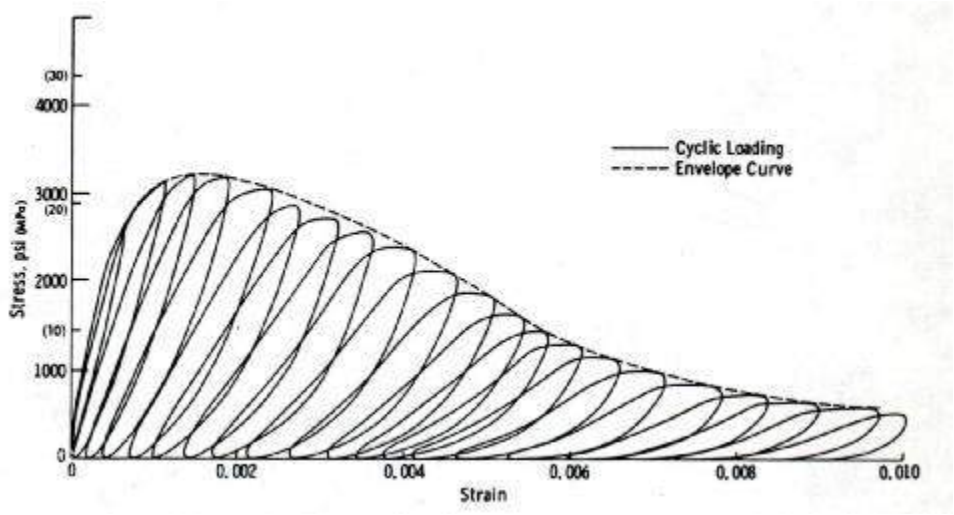

Figure (4.2) Response of concrete to uniaxial cyclic loading [72].

In Fig. (4.3) different uniaxial stress-strain curves are given for concrete with various values of compressive strength, f_c'. The shape of the stress-strain curve is similar for concrete of low, normal, and high strength concrete. High-strength concrete behaves in a linear fashion to a relatively higher stress level than the low-strength concrete, but all peak points are located close to the strain value of 0.002 (although high-strength concretes have somewhat a little higher strain at peak stresses). On the descending portion of the stress strain curve, higher strength concretes tend to behave in a more brittle manner, with the stress dropping off more sharply than it does for concrete with lower strength [101].

According to ACI-318M Code [102], ultimate compressive strength occurs at a strain (ε_o) of approximately (0.002). Also, the code specifies that the ultimate strain (ε_u) be taken as (0.003).

Under different combinations of proportional biaxial loading, concrete exhibits strength and stress-strain relation somewhat different from that under uniaxial conditions. For equal biaxial compression a strength increase of about

(16%) over f_c' is achieved; this increase is about (25%) at a stress ratio of (σ_2/σ_1 = 0.5) [103].

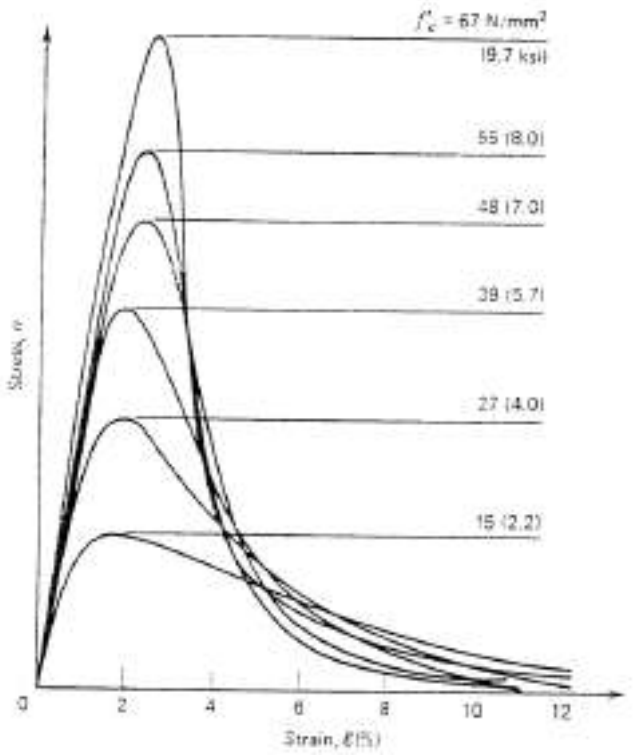

Figure (4.3) Uniaxial compressive stress-strain curves for concrete with different strengths [100].

In the vicinity of peak stresses concrete under compression exhibits inelastic volume increase. This phenomenon, termed as volume dilatancy, is usually attributed to the progressive microcracking in concrete during loading, Fig. (4.4).Under biaxial compression-tension, the compressive strength decreases almost linearly as the applied tensile stress is increased. Under biaxial tension, the strength is almost the same as that of uniaxial tensile strength.

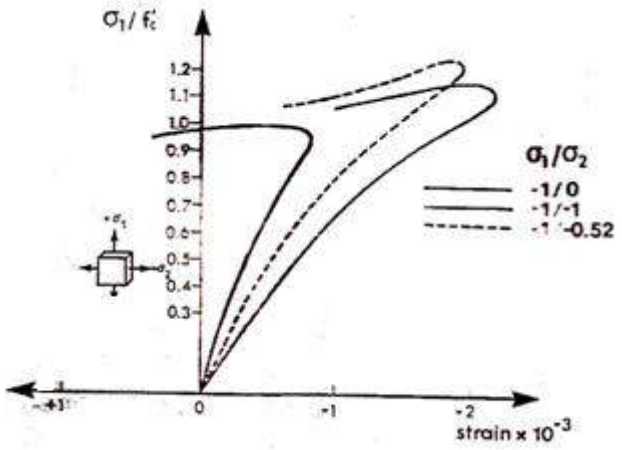

Figure (4.4) Stress-volumetric strain curves [96].

A typical biaxial strength envelope obtained by Kupfer et al. [103] is presented in Fig. (4.5).

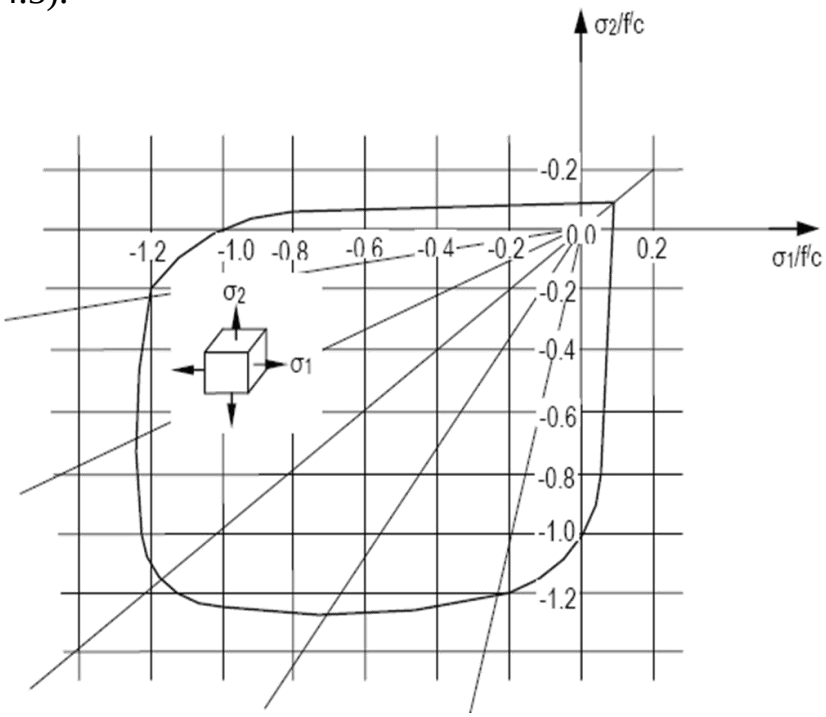

Figure (4.5) Failure envelope of plain concrete in biaxial stress space [96].

Concrete under triaxial compression shows a fairly consistent failure surface, Fig. (4.6) which is a function of the three principal stresses [104]. Experimental results indicate that the failure surface of concrete is a function of the three principal stresses. For increasing hydrostatic compression (along $\sigma_1=\sigma_2=\sigma_3$) the deviatoric section (planes perpendicular to the axis $\sigma_1=\sigma_2=\sigma_3$) of the failure surface becomes increasingly bulged (Mohr's circle) indicating that the failure in the region is independent of the third stress invariant. For small hydrostatic pressure, this deviatoric cross section is convex and noncircular [99].

In the present study, concrete behavior is simulated by using:

- Nonlinear-inelastic-isotropic material (multilinear stress-strain relationship).
- Failure criterion to simulate cracking and crushing types of fractures.
- Cracking modeling.
- Crushing modeling.

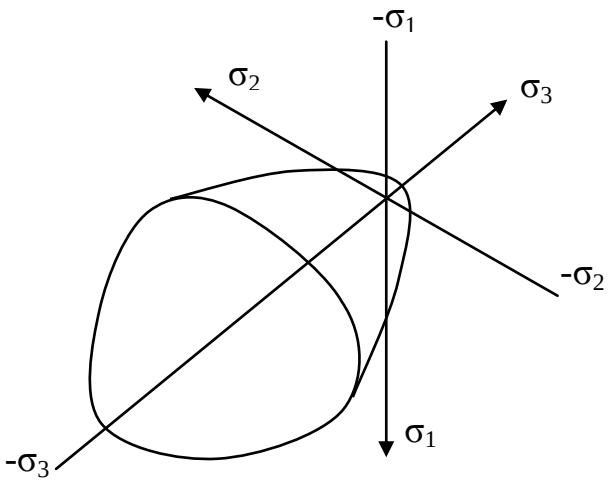

Figure (4.6) 3-D Failure surface in principal stress space [96].

4.3.1.1 Multilinear Stress-Strain Relationship

The uniaxial behavior is described by a piece-wise linear total stress-total strain curve. The slope of the first segment of the curve must correspond to the elastic modulus of the material and no segment slope should be larger. No segment can have a slope less than zero. The slope of the stress-strain curve is assumed to be zero beyond the last defined stress-strain data point [105].

ANSYS program requires the uniaxial stress-strain relationship for concrete in compression. Experimental results of the columns that tested in this study are used to construct the uniaxial compressive stress-strain curve for concrete in the present study.

The modulus of elasticity (E_c) is calculated with reasonable accuracy from the following empirical formula suggested by ACI Committee 318M-2008 [102],

$$E_c=4700\sqrt{f_c'} \quad \text{(MPa)} \qquad (4.31)$$

The shape of the uniaxial tensile stress-strain curves is similar to the uniaxial compression curves. The tensile strength of concrete f_t' is lower than

its compressive strength. The limit of elasticity in tension may be taken to about (60%) of the uniaxial tensile strength f_t' [106].

The ratio between uniaxial tensile and compressive strength may vary considerably but usually ranges from 0.05 to 0.10. The modulus of elasticity under uniaxial tension is somewhat higher and the Poisson's ratio somewhat lower than in uniaxial compression [107].

Based on the above information, the stress-strain curve of concrete in tension is drawn by using the same modulus of elasticity, and f_t' is used instead of f_c'. In this study the magnitude of tensile strength in (MPa) is taken as [108],

$$f_t' = (0.31\sqrt{f_c'}) \quad \text{(MPa)} \tag{4.32}$$

4.3.1.2 Failure Criteria for Concrete

In general, the actual behavior and strength of concrete materials are quite complicated because they depend on many factors such as the physical and mechanical properties of the aggregate, cement paste and the nature of loading. No single mathematical model can describe the strength of real concrete materials completely under all conditions, so, simpler models or criteria are used to represent the properties that are essential to the problem being considered [105].

Willam and Warnke in 1975[109], developed a mathematical model capable of predicting failure for concrete materials under multiaxial stress state. Both cracking and crushing failure modes are accounted for this model is represented by the following Eq.:

$$\frac{F}{f_c'} - S \geq 0 \tag{4.33}$$

Where

F = function of principal stress state ($\sigma_{xp}, \sigma_{yp}, \sigma_{zp}$).

S = failure surface expressed in terms of principal stresses and five

input parameters (f_t, $f_c^{'}$, f_{cb}, f_1 *and* f_2).

σ_{xp} , σ_{yp}, σ_{zp}= principal stresses in principal directions

If Eq. (4.33) is satisfied, the material cracks or crushes.

A total of five input strength parameters are needed to define the failure surface as well as an ambient hydrostatic stress state (σ_h^a). These are:

f_t = ultimate uniaxial tensile strength.

$f_c^{'}$ = ultimate uniaxial compressive strength.

f_{cb} = ultimate biaxial compressive strength

f_1 =ultimate compressive strength for a state of biaxial compression superimposed on hydrostatic stress state (σ_h^a)

f_2 = ultimate compressive strength for a state of uniaxial compression superimposed on hydrostatic stress state (σ_h^a)

σ_h^a = ambient hydrostatic stress state.

The failure surface can be specified with a minimum of two constants, f_t and f'_c. The other three constants can be determined from Willam and Warnke [109]:

$$f_{cb} = 1.2\, f'_c \tag{4.34}$$

$$f_1 = 1.45\, f'_c \tag{4.35}$$

$$f_2 = 1.725\, f'_c \tag{4.36}$$

However, these values are valid only for stress states where the condition stated below is satisfied:

$$|\sigma_h| \le \sqrt{3}\ f'_c \tag{4.37}$$

where:

σ_h = hydrostatic stress state = $\frac{1}{3}(\sigma_{xp} + \sigma_{yp} + \sigma_{zp})$ (4.38)

When the crushing capability is suppressed with f'_c =-1.0, the material cracks whenever a principal stress component exceeds f_t.

Both function *F* and failure surface S are expressed in terms of principal stresses denoted as σ_1, σ_2, and σ_3 where:

$\sigma_1 = \max(\sigma_{xp}, \sigma_{yp}, \sigma_{zp})$

$\sigma 3 = \min(\sigma_{xp}, \sigma_{yp}, \sigma_{zp})$

and $\sigma_1 \geq \sigma_2 \geq \sigma_3$.

The failure of concrete is categorized into four domains [96]:

1- $0 \geq \sigma_1 \geq \sigma_2 \geq \sigma_3$ (compression – compression – compression)

2- $\sigma_1 \geq 0 \geq \sigma_2 \geq \sigma_3$ (tensile – compression – compression)

3- $\sigma_1 \geq \sigma_2 \geq 0 \geq \sigma_3$ (tensile – tensile – compression)

4- $\sigma_1 \geq \sigma_2 \geq \sigma_3 \geq 0$ (tensile – tensile – tensile).

Concrete cracks if any principal stress is a tensile stress, while crushing will occur if all principal stresses are compressive [96].

Figure (4.7) shows the failure surface for states of stress that are biaxial or nearly biaxial. If the most significant nonzero principal stresses are in the x and y directions, represented by σ_{xp} and σ_{yp}, the three surfaces presented are for σ_{zp} slightly greater than zero, σ_{zp} equal to zero, and σ_{zp} slightly less than zero. Although the three surfaces, shown as projections on the σ_{xp} - σ_{yp} plane, are nearly equivalent and the three-dimensional failure surface is continuous, the mode of material failure is a function of the sign of σ_{zp} [96].

In a concrete element, cracking occurs when the principal tensile stress in any direction lies outside the failure surface.

After cracking, the elastic modulus of the concrete element is set to zero in the direction parallel to the principal tensile stress direction. Crushing occurs when all principal stresses are compressive and lies outside the failure surface;

subsequently, the elastic modulus is set to zero in all directions at that Gauss point and its stiffness, and the element effectively disappears [96].

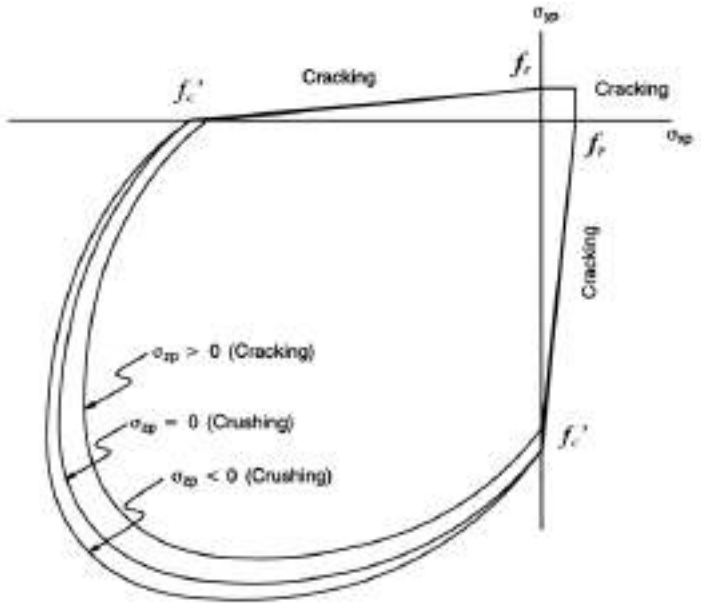

Figure (4.7) Failure surface in principal stress space with nearly biaxial stress states (ANSYS).

4.3.1.3 Modeling of Cracking

The internal stresses and deflections of reinforced concrete structures are affected by cracking. This phenomenon can be modeled in finite element schemes either as discrete cracking approach, or as smeared cracking approach.

- In the discrete cracking approach, the disconnecting or separating of the concrete element nodes through which the cracking is passing, requires additional nodes to occupy the same location, and connected by linkage elements [110]. This physically appealing representation has computational difficulties in that it requires node renumbering after the development of the cracks and there is restriction on the crack propagation direction depending on the mesh layout [111].
- The smeared crack model introduced by Rashid [112], who represents cracks as a change in the material property of the element over which the

cracks are assumed to be smeared and offer an automatic generation of cracks without the redefinition of the finite element topology. It assumes that the concrete becomes orthotropic after the cracking has occurred with zero modulus of elasticity in the direction normal to the crack. Poisson's effect is neglected due to lack of interaction between the two orthogonal directions after cracking.

ANSYS adapts smeared cracking model to simulate the cracking of concrete. The shear transfer coefficient β represents conditions of the crack face. The value of β ranges from (0.0 - 1.0). β= 0.0 represents a smooth crack (complete loss of shear transfer) and 1.0 represents a rough crack (no loss of shear transfer) [113]. Therefore, the shear transfer coefficient used in this study is 0.3 for a smooth crack and 0.9 for a rough crack.

4.3.1.4 Modeling of Crushing

If the material at an integration point fails in uniaxial, biaxial, or triaxial compression, the material is assumed to crush at that point. Under this condition, material strength is assumed to have degraded to an extent such that the contribution to the stiffness of an element at the integration point in equation can be ignored [105].

4.3.1.5 Nonlinear Behavior-Concrete

In solid mechanics problems, there are two sources of nonlinearity. The first is due to non-linear material behavior and is usually referred to as material nonlinearity. The second is geometric nonlinearity due to the change in solid geometry.

In the present study, material nonlinearity due to nonlinear stress-strain relationship is considered.

4.3.2 Ferrocement Matrix

There are numerous similarities between ferrocement and reinforcement concrete. In addition to fact that both use similar matrix and reinforcement

material, they obey the same principles of mechanic and can be modeled according to the same theories.

They can be analyzed using similar techniques and they can be designed according to the same philosophy. So, the ferrocement can be considered as an extreme boundary of reinforced concrete and scale effect may be significant enough to differentiate them [10].

In the present study, the adopted stress-strain relation for ferrocement matrix is based on work done by Desayi and Krishnan [114], Fig. (4.8).

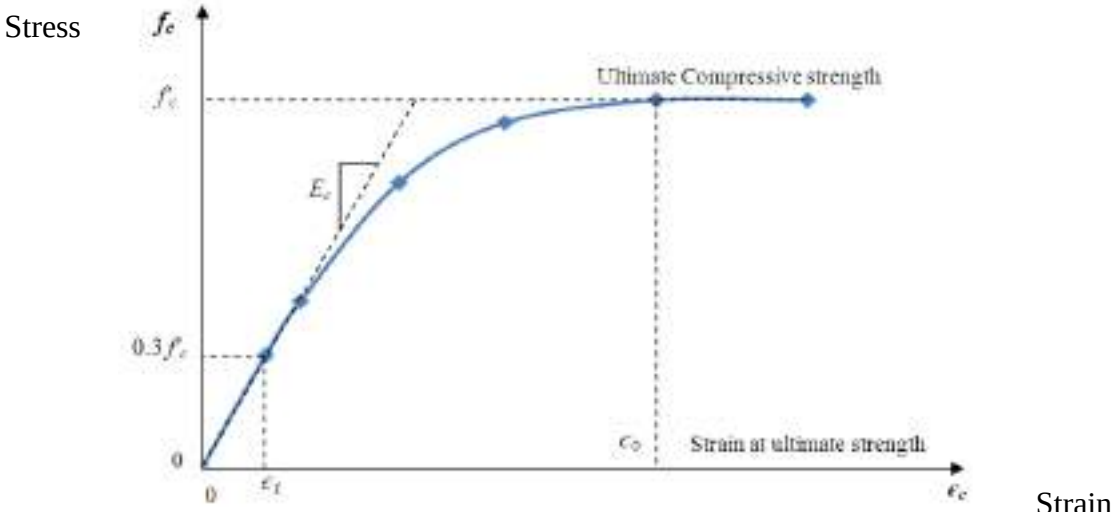

Figure (4.8) Idealized uniaxial stress-strain curve for ferrocement matrix [114].

The compressive uniaxial stress-strain relationship for ferrocement model was obtained by using the following equations to compute the multilinear isotropic stress-strain curve for the ferrocement.

$$f_c = \varepsilon\ E_c \qquad for \qquad 0 \le \varepsilon \le \varepsilon_1 \tag{4.39}$$

$$f_c = \frac{\varepsilon E_c}{1 + \left(\frac{\varepsilon}{\varepsilon_\circ}\right)^2} \qquad for \qquad \varepsilon_1 \le \varepsilon \le \varepsilon_\circ \tag{4.40}$$

$$f_c = f_c^{'} \qquad for \qquad \varepsilon_\circ \le \varepsilon \le \varepsilon_{cu} \tag{4.41}$$

and

$$\varepsilon_1 = \frac{0.3 f_c^{'}}{E_c} \quad \text{(Hooke's law)} \tag{4.42}$$

$$\varepsilon_\circ = \frac{2 f_c^{'}}{E_c} \tag{4.43}$$

where

f_c = stress at any strain ε, MPa

ε = strain at stress f

ε_o =strain at ultimate compressive stress f_c' and

E_c = concrete elastic modulus, MPa

The multilinear curves were used to conduct the nonlinear solution algorithm [115].

4.3.3 Steel Wire Mesh

In the current work, an elastic linear work hardening model is adopted to simulate the uniaxial stress-strain behavior of reinforcing steel wire mesh. The initial slope of the curve is taken as the elastic modulus of the material. At the specified yield stress (fy=C1), the curve continues along the second slope defined by the tangent modulus C2 (having the same units as the elastic modulus). The tangent modulus cannot be less than zero nor greater than the elastic modulus.

An idealized uniaxial stress-strain curve for steel wire mesh is shown in Fig. (4.9).

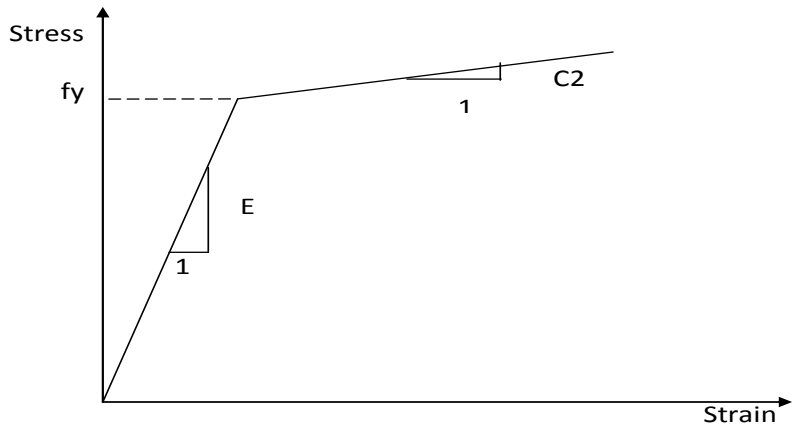

Figure (4.8) Idealized uniaxial stress-strain curve for steel wire mesh.

4.4 ANSYS Computer Program

The computer program **ANSYS (ANalysis SYStem version 11)** is a powerful and impressive engineering finite element package that may be used to solve a variety of problems. Over the years, finite element method has become the most commonly used method for studying the stress, deformation, and other engineering parameters. Finite element method uses complicated mathematical equations to accurately approximate how a complex structure reacts to a certain load or condition. Finite element packages such as **ANSYS** solve thousands or millions of these equations to find a solution for a model. Handling all these equations as a whole be difficult and mostly impossible to solve manually. **ANSYS** is a comprehensive general-purpose finite element computer program that contains different elements implemented in the program. **ANSYS** has the capacity of solving linear and nonlinear problems including the effect of cracking, crushing, yielding of reinforcement, creep….. etc. In order to use **ANSYS** or any other finite element analysis computer program intelligently, it is imperative that one first fully understands the underlying basic concepts and limitation of the finite element method.

4.4.1. Nonlinear Solution Techniques

In general, applying the finite element method for any problem leads to a set of algebraic equations of the following form:

$$[K]\{a\}=\{f\} \tag{4.44}$$

where

$\{a\}$ is the unknown nodal displacement vector.

$\{f\}$ is the nodal applied force vector.

[K] is the stiffness matrix $\left(\int [B]^T [D][B]dv\right)$ (4.45)

The solution for these equations for linear elastic structural problems can be obtained directly. In nonlinear problems, a direct solution is no longer

possible since the stiffness matrix [K] depends on the displacement level ([K] = [K (a)]), and therefore, it cannot be exactly calculated before the determination of the unknown nodal displacement {a}. For nonlinear solution, the state of equilibrium of structural system corresponding to the applied load must be found. These equilibrium equations can be derived by applying the equilibrium to the structural system. The equilibrium equations can be expressed as [103]:

$$\{r\} = \{p\} - \{f\} \tag{4.46}$$

where $\{r\}$ the out of balance force vector, and $\{p\}$ represents the vector of the nodal forces equivalent to the stress level, which is given by:

$$(\{p\} = \{p\}(\{a\})) \tag{4.47}$$

and have to be approximated in successive steps until equation (4.46) is satisfied. The solution of nonlinear problems by finite element method is usually attempted by one of the following three basic techniques [116]:

4.4.1.1 Incremental Method

In this method, the load $\{R^j\}$ is divided into a number of small increments $\{\Delta R^j\}$. The response {d} is obtained by the summation of the incremental displacement {Δd} calculated from a series of incremental equilibrium Eqs.

$$\{\Delta d\}_i = [K_t]_{i-1}^{-1} \{R^j\}_i \tag{4.48}$$

$$\{d\}_i = \{d\}_{i-1} + \{\Delta d\}_i \tag{4.49}$$

where, i represents the ith loading step, and $[K_t]_{i-1}$ is the tangent stiffness matrix at the end of the pervious increment.

The solution tends to drift away from the true path unless $\{\Delta R^j\}_i$ is chosen to be very small as shown in Fig.(4.10-a).

A more accurate solution can be obtained when the unbalanced force $\{R^u\}_{i-1}$ from the previous step are added to the current load increment $\{\Delta R^j\}_i$ from the solution of $\{\Delta d\}_i$. Mathematically this can be represented as

$$\{\Delta d\}_i = [K_t]_{i-1}^{-1} \left(\{\Delta R^j\}_i + \{R^u\}_{i-1} \right) \tag{4.50}$$

$$\{d\}_i = \{d\}_{i-1} + \{\Delta d\}_i \tag{4.51}$$

Unbalanced forces at any stage $\{R^u\}_i$ is the difference between the applied external loads $\{R^j\}$ and the internal resisting loads $\{R^i\}$, Fig.(4.10-b).

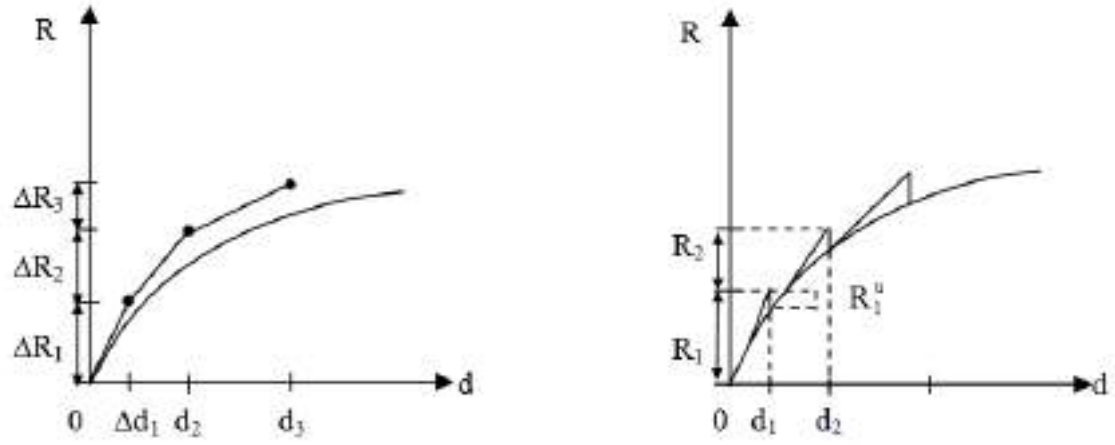

a. Pure incremental b. Incremental with residual corrections

Figure (4.10) Scheme of the solution procedure in a non-linear problem

4.4.1.2 Newton-Raphson Iterative Method

In this iterative method, the total value of $\{R^j\}$ is applied only once and the values of the tangent stiffness matrix, $[K_t]$, and displacement vector, $\{d\}$, are continuously updated by successive application of unbalanced forces through an iterative fashion, until convergence is achieved, as shown in Fig.(4.10-c).

More than one Newton-Raphson iteration is needed to obtain a converging solution. The general algorithm proceeds as follows:

1- At the ith iteration, the unbalanced forces $\{R^u\}_i$ can be evaluated from the difference between the total joint loads $\{R^j\}$ and the internal resisting loads $\{R^i\}$

$$\{R^u\}_i = \{R^j\} - \{R^i\}_{i-1} \quad (4.52)$$

2- The unbalanced force vector is then applied to obtain the incremental displacements $\{\Delta d\}_i$

$$\{\Delta d\}_i = [K_t]_{i-1}^{-1} \{R^u\}_i \quad (4.53)$$

then,

$$\{d\}_i = \{d\}_{i-1} + \{\Delta d\}_i \quad (4.54)$$

where, the tangent stiffness matrix $[K^t]_{i-1}$ is a function of the total displacements $\{d\}_{i-1.}$

To avoid the processes of formulating the tangent stiffness $[K^t]$ at each iteration a modified Newton-Raphson method may be employed, as shown in Fig. (4.10-d). In this method the initial tangent stiffness $[K^t]_0$ is used for the successive iterations such that Eq. (4.53) becomes,

$$\{\Delta d\}_i = [K^t]_0^{-1} \{R^u\}_i \quad (4.55)$$

Savings in the computation time in each iteration due to this modification may compensate the increased number of iterations, especially for elements with high degrees of freedom.

The modified initial Newton-Raphson procedures converge slower than the full Newton-Raphson procedure, but they require fewer matrix reformulation and inversion.

4.4.1.3 Step-Iterative Method (Mixed Procedure)

In order to overcome the defects of the so far described methods, a combination of the incremental and iterative schemes has been used. In this

procedure the load is applied incrementally and within each increment successive iterations are performed to obtain more accurate results, as shown in Fig. (4.10-e). It is not necessary that the values of the increments of the load are equal. This method has been widely used in the non-linear analysis of reinforced concrete structures, and it is adopted in the present investigation.

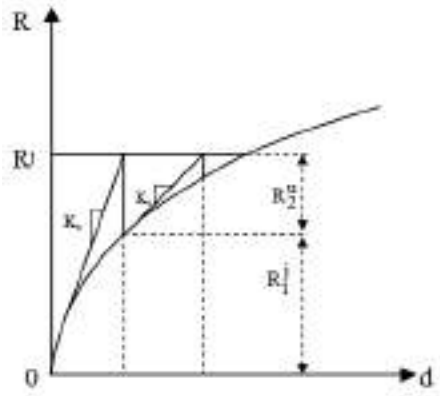

c. Newton- Raphson method

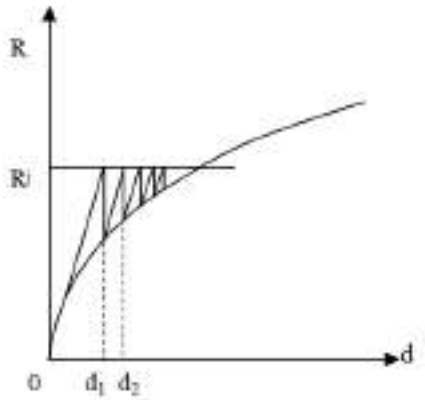

d. Modified Newton- Raphson method

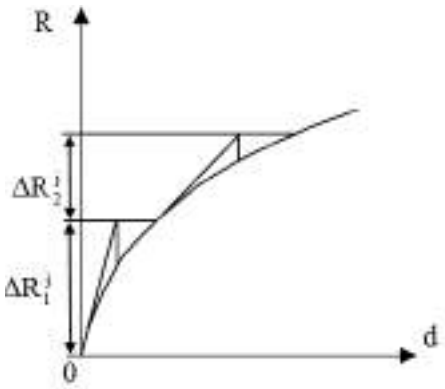

e. Combined incremental and iterative

Figure (4.10) continued

4.4.2Convergence Criteria

The problem associated with iterative techniques is the decision as to whether the current iteration is sufficiently close to the root without knowing the

true solution. The convergence criterion for non-linear structural problems can usually be classified as:

i- Force criterion, ii- Displacement criterion, iii- Stress criterion

In the present study the force criterion is used.

In the ANSYS software convergence is assumed when,

$$\|\{R\}\| < \varepsilon_R \; R_{ref} \quad \text{(out of balance convergence)} \tag{4.56}$$

where, {R} is the residual vector, given by

$$\{R\} = \{F^a\} - \{F^{nr}\} \tag{4.57}$$

$\varepsilon_R$is tolerance and R_{ref} is reference values. $\|\bullet\|$ is a vector norm; that is, a scalar measure of the magnitude of the vector. F^a is vector of applied loads. F^{nr} is vector of restoring loads corresponding to the element internal loads.

Convergence, therefore, is obtained when the size of the residual (disequilibrium) is less than a tolerance times a reference value. The default tolerance is 0.001.

The default out-of-balance reference value R_{ref} is $\|\{F^a\}\|$. For DOFs with imposed displacement constraints, $\{F^{nr}\}$ at those DOFs are used in the computation of R_{ref}. For structural DOFs, if $\|\{F^a\}\|$ falls below 1.0, then R_{ref} uses 1.0 as its value.

4.4.3 Analysis Termination Criteria

In the physical test under force control, collapse of a structure takes place when no further loading can be sustained. This is usually indicated in the numerical tests by successively increasing iterative displacements and a continuous growth in the dissipated energy. Hence, the convergence of the iterative process cannot be achieved. A maximum number of iterations for each increment are specified to stop the nonlinear solution if the convergence limit has not been achieved for this study. This maximum number of iterations depends on the type of the problem, extent of nonlinearities, and on the specified

tolerance. In this study the maximum number of iteration is equal to 100 are adopted for load control problems.

4.5 Material Modeling of Confined Concrete Column

To create the finite element model in **ANSYS** there are multiple tasks that have to be completed for the model to run properly. Models can be created using command prompt line input or Graphical User Interface (GUI). To create this model both the command prompt line input and GUI are utilized. Due to symmetry in the cross section of the tested column as well as their loading, symmetry was utilized in the finite element analysis; only one quarter of the column was modeled. This section described the different tasks and entries used to create the finite element analysis.

4.5.1 Representation of Concrete Core and Mortar

The choice of the proper element is very important in the finite element formulation. For a reinforced concrete idealization, the element type depends upon the geometry of the structure and the number of independent space coordinates necessary to describe the problem. In the present study, SOLID65 three-dimensional reinforced concrete brick element, Fig. (4.11), is used to model the concrete core and ferrocement shell.

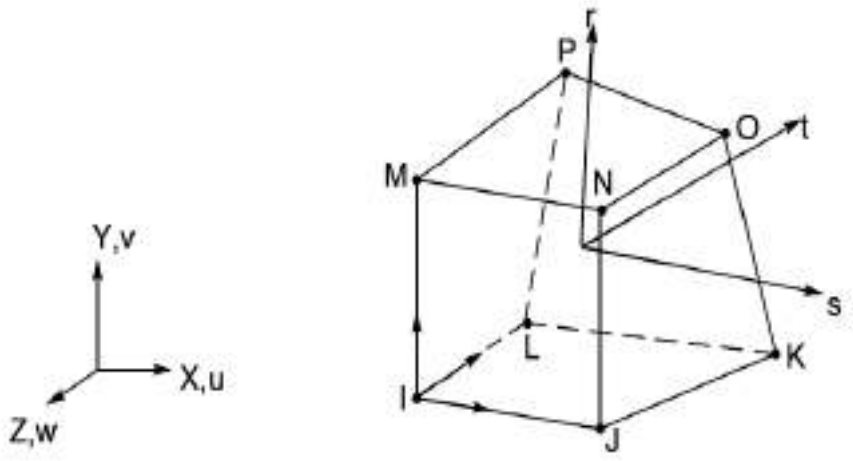

Figure (4.11) Geometry of the brick element SOLID 65 (ANSYS)

SOLID65 can be used for the three-dimensional modeling of solids with or without reinforcing bars (rebars). The element is defined by eight nodes having three degrees of freedom at each node, translation in the x, y, and z directions. The element is capable of cracking in tension, in three orthogonal directions, crushing in compression, and plastic deformation. The rebars are capable to resist tension and compression, but not shear. They are also capable to reveal plastic deformation. The most important aspect of this element is the treatment of nonlinear material properties [105].

SOLID65 allows the presence of four different materials within each element; one matrix material and a maximum of three independent reinforcing materials. The matrix material is capable of directional integration point cracking and crushing besides incorporating plastic and creep behavior [105]

The shape functions of the SOLID65 element are interpolation functions used to express the displacements at any point within the element in terms of nodal displacements.

Using the shape functions, the displacement components (u, v, and w) at a particular point can be found as follows [105],

$$u = 1/8\,[u_I(1-s)(1-t)(1-r) + u_J(1+s)(1-t)(1-r) + u_K(1+s)(1+t)(1-r) + u_L(1-s)(1+t)(1-r) + u_M(1-s)(1-t)(1+r) + u_N(1+s)(1-t)(1+r) + u_O(1+s)(1+t)(1+r) + u_P(1-s)(1+t)(1+r)] + u_1(1-s^2) + u_2(1-t^2) + u_3(1-r^2) \quad (4.58)$$

$$v = 1/8\,[v_I(1-s) \ldots\ldots\ldots\ldots \text{(analogous to u)}] \quad (4.59)$$

$$w = 1/8\,[w_I(1-s) \ldots\ldots\ldots\ldots \text{(analogous to u)}] \quad (4.60)$$

where, (s, t, and r) are the local coordinates, and they are normalized, ranging from -1 to +1, and are not necessary orthogonal to one another.

4.5.2 Representation of Wire Mesh

In developing a finite element model of reinforced concrete member, at least three alternative representations of the reinforcement have been used [113], Fig. (4.12).

1- ***Distributed (smeared) representation***: the steel is assumed to be distributed over the concrete element, with a particular orientation angle θ, Fig. (4.13). A composite-reinforcement constitutive relation is used in this case. To derive such a relation, perfect bond must be assumed to occur between the concrete and the steel.

2- ***Embedded representation***: the reinforcing bar is considered as an axial member built into the concrete element such that its displacements are consistent with that of the element. Also perfect bond must be assumed to occur between the concrete and the steel.

3- ***Discrete representation***: one-dimensional bar element may be used in this approach to simulate the reinforcement, this element is connected to concrete mesh nodes at bar location. Therefore, the concrete and the reinforcement mesh share the same nodes and concrete occupies the same regions occupied by the reinforcement.

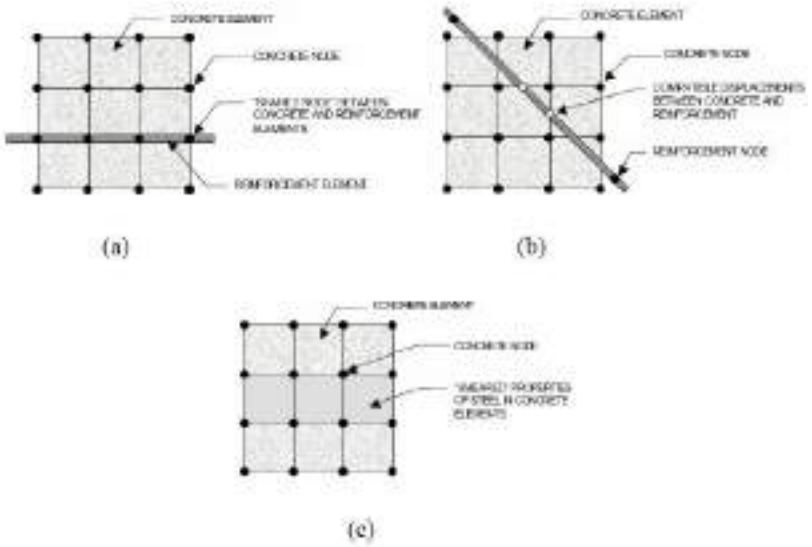

Figure (4.12) Models for reinforcement in reinforcement concrete; (a) discrete, (b) embedded and (c) smeared

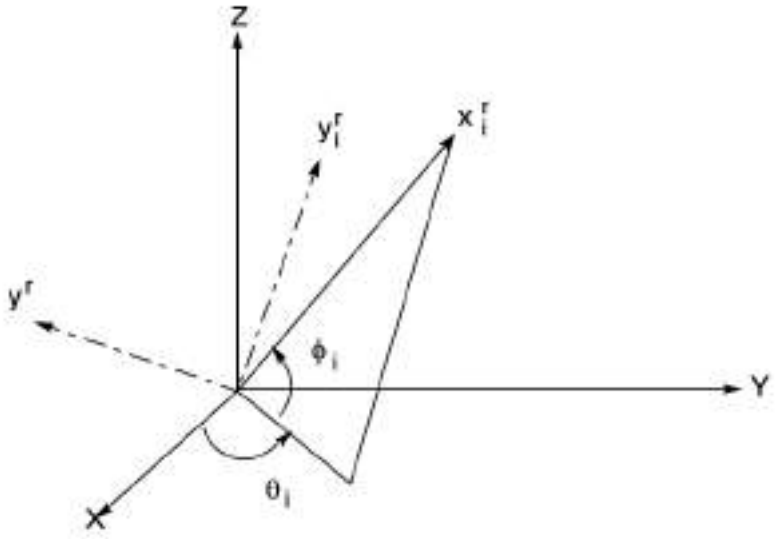

Figure (4.13) Reinforcement orientation for distributed model

In the present study the distributed representation of reinforcement is considered to model steel wire mesh within ferrocement matrix.

4.5.3 Representation of Steel Plate

In the present study, SOLID45 three-dimensional structural brick element, Fig. (4.14) is used to model steel plate. The element is defined by eight nodes having three degrees of freedom at each node, translation in the x, y, and z directions.

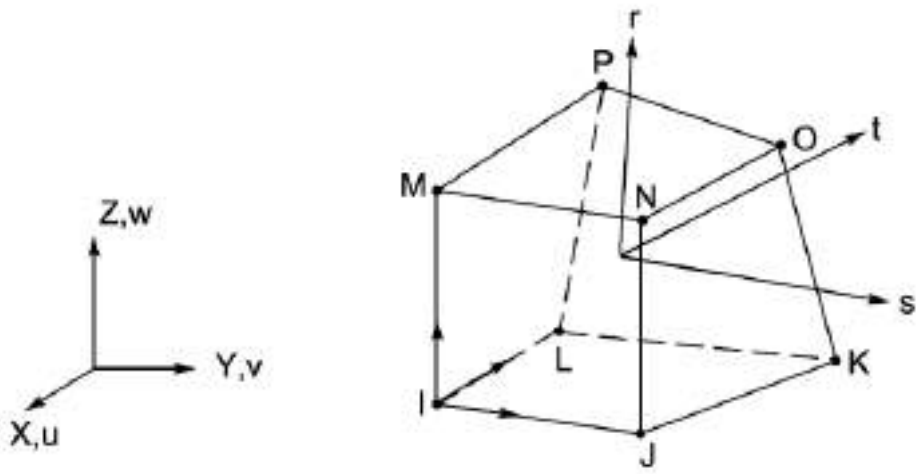

Figure (4.14) SOLID 45 3-D Structural Solid element (ANSYS)

The used material properties for this element include Young's modulus (of elasticity), density, and Poisson ratio, and they are taken into account.

This element was generated in the x-y plane, and then, extruded in the z direction, to complete the three dimensional model.

The element has plasticity, creep, swelling, stress stiffening, large deflection, and large strain capabilities.

The used shape functions for this element are illustrated in section (4.5.1) and Eqs. (4.58), (4.59), and (4.60).

4.5.4 Modeling and Meshing

A three dimension model of the concrete structure was built using ANSYS. For modeling circular columns a cylindrical coordinate system was created in the active work plane. The cylindrical model was built by first modeling 1/36th radial sector (10°) of the concrete cylinder. This first sector was used so that a regular radial symmetric mesh can be generated. Once the radial sector was meshed and due to symmetric geometry and loading only a quarter of the column of given radius and height was created. The cylindrical column was generated by repetition of this first sector. The ferrocement jacket was also modeled in the same way and was incorporated onto the initial sector. The concrete column was modeled using a special concrete element SOLID 65. It enables to define up to three different rebar materials within the concrete. A rebar material is defined by specifying the rebar material properties including volume fraction with respect to the concrete, and the orientation of the rebar with respect to element coordinate system. The welded wire mesh in ferrocement shell was represented by smeared model. Reinforcement has uniaxial stiffness only and is assumed to be smeared throughout the element [105]. The interfacial bonding between the concrete core and ferrocement shell was controlled by the number of nodes merged at the interface of the two materials assuming a perfect bonding between them. For the validation of the model, the dimensions used were of those specimens used in the experiments

program of this study which presented in chapter three. Refinement of the mesh increases accuracy of the simulation and also increases the analysis time. The number and size of elements in the models was vary depend on the size of the specimen. The properties of element materials were defined using the experimental results. The both concrete core and ferrocement jacket were meshed with Solid65 and the steel plate was meshed with Solid45 elements. The coordinate axes of all the element of the model are oriented to the cylindrical coordinate system. In the model, Z-axis of the coordinate system coincides with the axis of the column. The X and Y axis represent the radial and hoop directions of the column respectively. Figure (4.15) shows the finite element model of the circular concrete column strengthened with ferrocement.

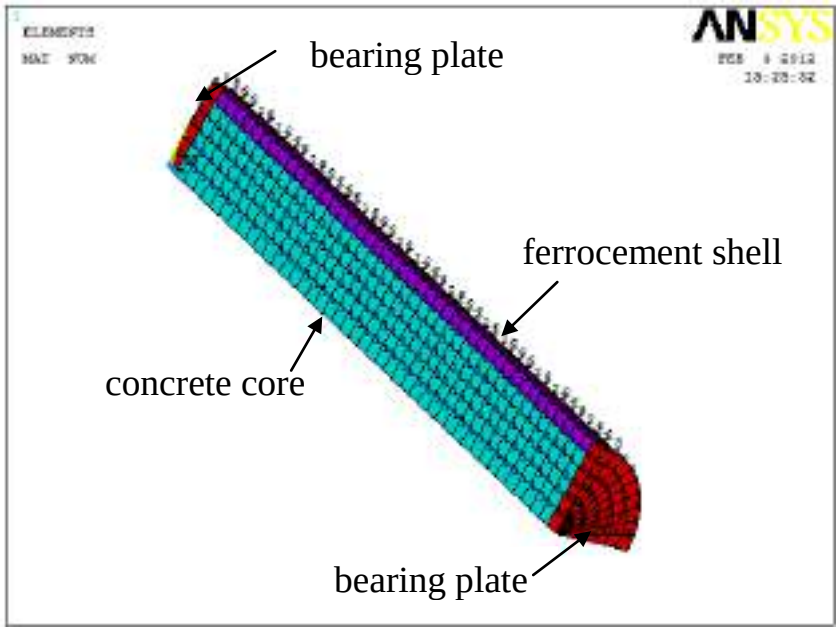

Figure (4.15) Finite element model of concrete column strengthened with ferrocement jacket (ANSYS)

4.5.5 Boundary Conditions and Loading

It has been found that the simulation of the applied load and the supports has significant effect on the results of the finite element analysis. In the experimental work of the present investigation bearing plates were used at the loading and supporting points. Displacement boundary conditions are needed to

constrain the model to get a unique solution. To ensure that the model acts the same way as the experimental column, the boundary conditions needed to be applied at points of symmetry and where the supports exist. The boundary conditions are:

1. The concrete column was considered fixed at the bottom end with no vertical displacement of the nodes in the z direction.
2. The model being used is symmetry about two planes. The symmetric boundary conditions are applied at the two cut planes XZ and YZ parallel to axis of the column and all nodes on each plane of symmetry were fixed only in the direction normal to that plane but were free to move within that plane.
3. An axial compressive pressure load was applied onto the surface of a steel plate which was placed on the column top cross-section.

The axial pressure load is increased gradually until the ferrocement jacket fails. Figure (4.16) demonstrate the loading and boundary conditions for a concrete column strengthened with ferrocement jacket.

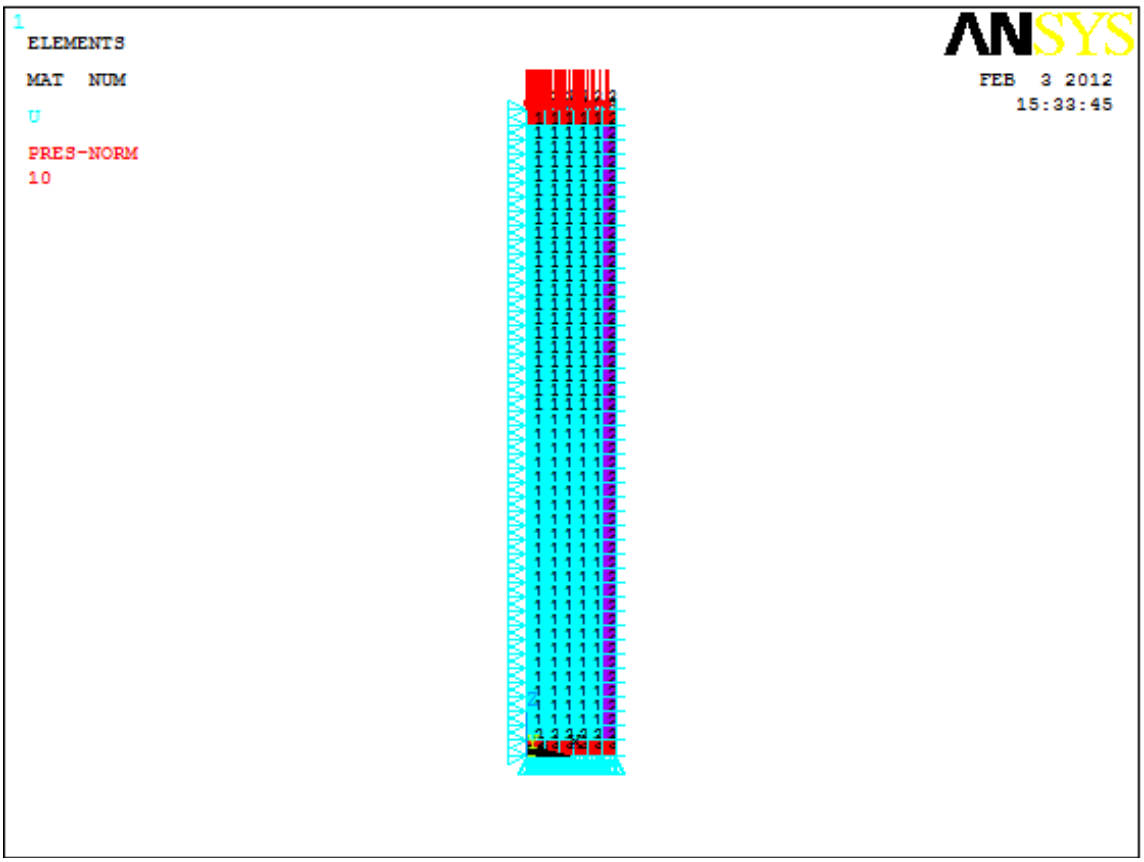

Figure (4.16) Boundary conditions and loading on quarter model (ANSYS)

CHAPTER FIVE
Results and Discussion

5.1 Introduction

This chapter describes the results of the experimental work conducted on 48 concrete columns strengthened with ferrocement jackets and tested under concentrated monotonic and cyclic loads. Concrete columns behavior under various loading history and failure modes of strengthened columns are discussed. The behavior of the strengthened columns is compared with that of the plain concrete. A study is carried out to explore the affect the various parameters which are expected to affect the behavior of such columns. The parameters include:

1. Volume fraction of wire mesh reinforcement.
2. Size of the concrete columns.
3. Strength of mortar compressive strength.
4. Type of loading (monotonic and cyclic).

The three dimensional finite element model described in the previous chapters was used to analyze the tested columns in order to examine the ability of the model to predict the overall behavior of the columns and to obtain more information about the stresses and strains developed in the columns. Parameters, which affect the analysis such as compressive strength of concrete core, stiffness of ferrocement shell, and loading applied on the ferrocement shell, which give best fit to the experimental results, are selected.

5.2 Results of the Experimental Program and Discussion

5.2.1 Testing Program and Procedure

A total of 48 test specimens described in the previous chapters were tested to investigate the behavior of strengthened concrete columns with ferrocement

jackets under varied axial compressive load histories. Characteristics of specimens and the loading histories are described below.

5.2.1.1 Monotonically Increasing Axial Load Tests

Monotonically increasing axial load tests were conducted to obtain the ultimate strength of specimens and to determine the strain at ultimate strength. These testes were also used in investigating the existence of an envelope curve. The envelope is defined as the locus of limiting stress values in stress-strain domain which will not be exceeded by any loading curve. The existence of the envelope curve was examined by comparing the results of specimens subjected to monotonic loading to failure with the results of specimens subjected to various stress and strain histories.

Axial load tests were conducted on groups of specimens in which one specimen was tested under monotonic load. In this way, the maximum capacity and the strain at the maximum stress were determined for each specimens tested under various load histories.

5.2.1.2 Axial Compressive Load Cycles to the Envelope Curve

In these tests the stress-strain envelope was reached during each load cycle. By comparing the stress- strain curve obtained from the tests with monotonic load and the curves in these tests existence of the envelope curve was examined. This test was also used to investigate the common points limit.

The confined specimens were loaded axially up to a given value of axial strain, unloaded to zero axial stress, and then reloaded until the stress follows the previous loading point. The specimen was again unloaded to zero axial stress and the procedure was repeated in the same fashion until failure occurred. The histories were controlled by the incremental strain in each cycle. The incremental strain was chosen so that the loading curve, in each cycle attained the envelope curve.

5.2.1.3 Repeated Loads Between Specified Maximum and Minimum Stress Levels

Repeated axial loading between specified stress levels were carried out to examine the mechanism of failure under stress levels below ultimate. This series was subdivided into two groups:

a. Confined specimens were loaded under monotonically increasing axial compression up to 90% of ultimate strength, unloaded to zero axial stress and then reloaded until the stress approaches the same previous point. This procedure was repeated until failure occurred or 70 cycles were applied. The specimens in which a large number of cycles would have been needed to reach failure were loaded monotonically from the minimum stress level to ultimate after a finite number of cycles had been applied.

b. Confined specimens were loaded as in the above case except that in this case the minimum stress level was 40% of ultimate strength.

5.2.2 Evaluation of the Tests Results

5.2.2.1 Confinement Effect on Concrete

A. Behavior under a Monotonic Axial Loading up to Failure

In order to evaluate the beneficial effect of confinement on the total load carrying capacity of concrete column strengthened with ferrocement jacket, the measured axial load-axial strain behavior of column 5BM2 is given in Fig. (5.1). On the same figure the behavior of plain concrete column is also shown. The axial load-axial strain behavior of the plain concrete core was obtained using the measured axial load-axial strain curve of column 150BM. The figure clearly indicates that the capacity of the strengthened column significantly exceeds the load capacity of the plain concrete columns.

For the concrete column confined with the ferrocement shell, the initial axial load-axial strain behavior was similar to that of unconfined concrete, since the lateral expansion of the core was insignificant and confinement causes very little change in the initial slope of the stress-strain curves. Hence, the initial stiffness is not affected by confinement. At this stage, the circumferential strain is low and hence there is no confining pressure from wire mesh. After that, the ferrocement shell was activated and the axial load-axial strain curve of confined concrete showed nonlinear behavior until the final rupture of the ferrocement jacket. From that stage the concrete is under triaxial compression due to restraint by the ferrocement shell, which is under vertical compression and transverse tension. Due to the confinement of the concrete the triaxial stress state causes a reduction of the axial compressive strength of the ferrocement shell while there is an increase in the longitudinal compressive strength of the concrete core. The interaction between the ferrocement shell and the concrete core works beneficially and leads to an ultimate load exceeding the uniaxial compression loads of plain concrete.

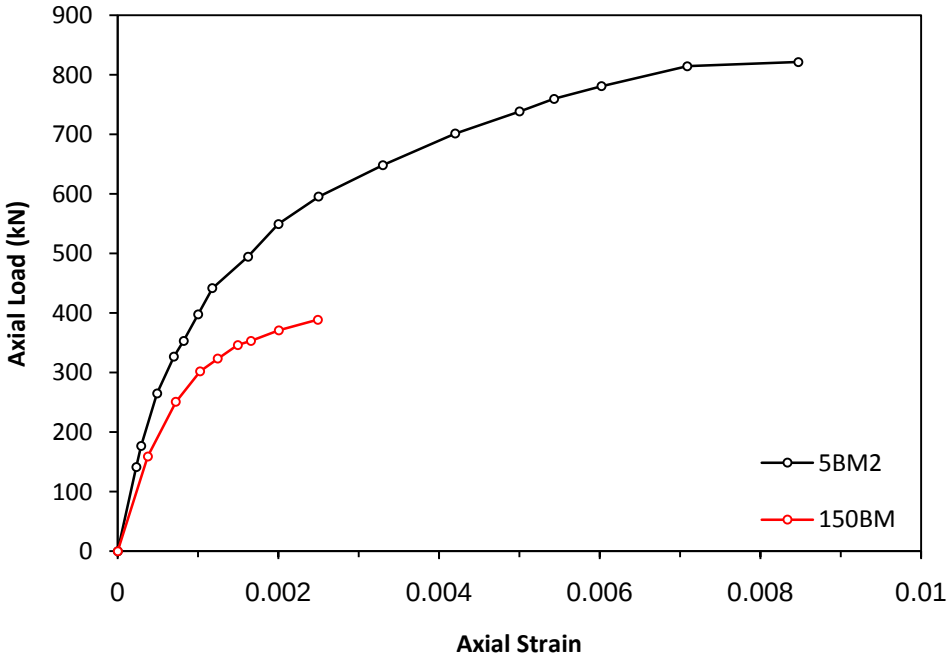

Figure (5.1) Effect of ferrocement jacket on ultimate load of strengthened concrete columns

B. A Cyclic Axial Loading to Failure (Existence of Envelope Curve)

The envelope is defined as the locus of limiting stress values in stress-strain domain which will not be exceeded by any loading curve without having an apparent failure. In the following discussion the existence and validity of the envelope curve will be examine. The existence of an envelope curve for strengthened concrete columns with ferrocement jackets can be investigated by comparing with test results of the monotonically increased axial load tests.

A basic hypothesis in studies on the cyclic stress-strain behavior of unconfined and steel-confined concrete is that an envelope curve exists and this envelope curve is approximately the same as the stress-strain curve for the same concrete under monotonic loading [6]. Such an envelope curve can be considered as the upper boundary of the response of the concrete subjected to different loading histories in the stress-strain domain.

To compare the monotonic and cyclic stress-strain curves of concrete confined with ferrocement jackets in present study, Figs. (5.2) to (5.11) show envelope curves for the axial stress-axial strain, which were obtained by connecting the initial unloading points on the stress-strain curve for the cyclic loading. The envelope curve is approximately coincident with the stress-strain curve for corresponding monotonic loaded specimens, as the two almost coincide. This observation indicates that the basic hypothesis of envelope curves is valid for concrete confined with ferrocement jackets.

This observation supports the concept that the monotonic curve (or envelope curve) serves as a limiting curve below which lie all the stress-strain paths under cyclic loading.

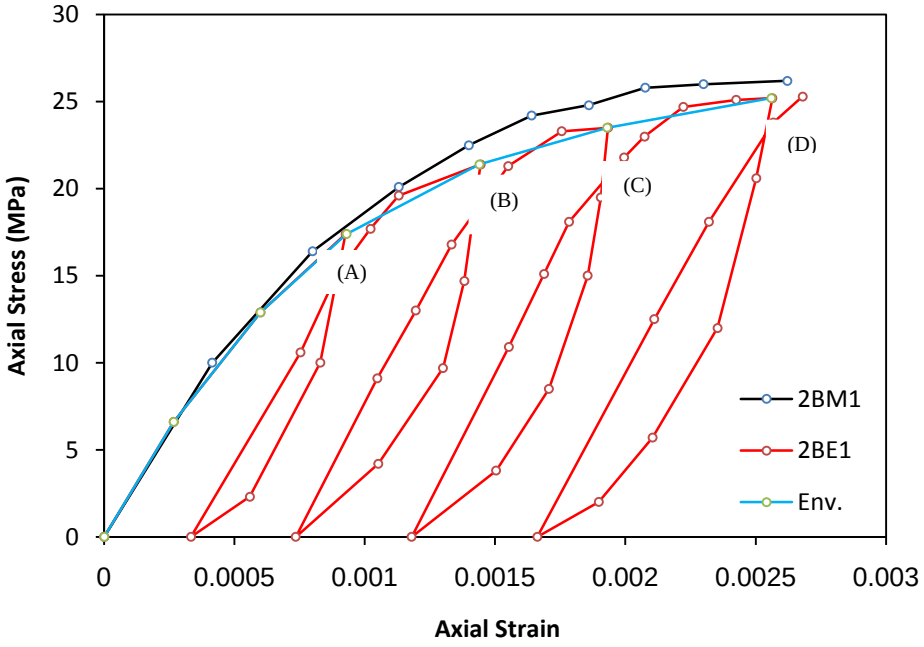

Figure (5.2) Comparison of monotonic axial load with cyclic to envelope for J1

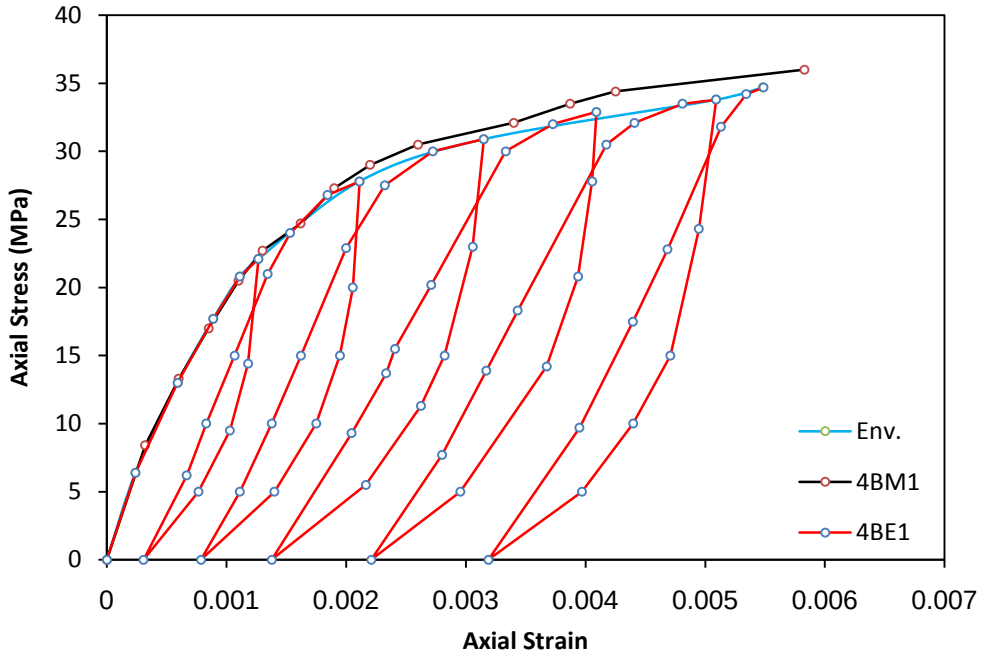

Figure (5.3) Comparison of monotonic axial load with cyclic to envelope for J2

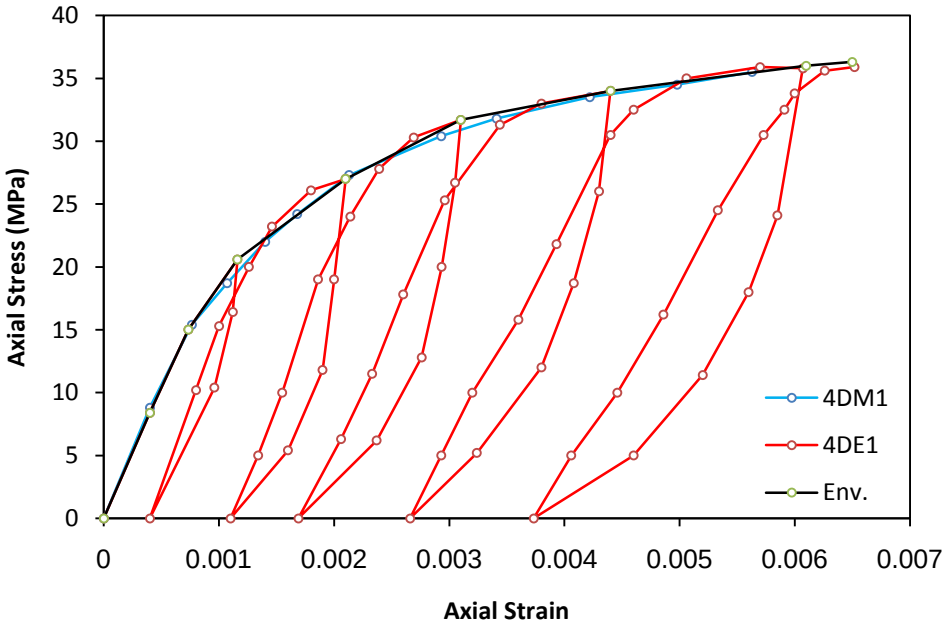

Figure (5.4) Comparison of monotonic axial load with cyclic to envelope for J3

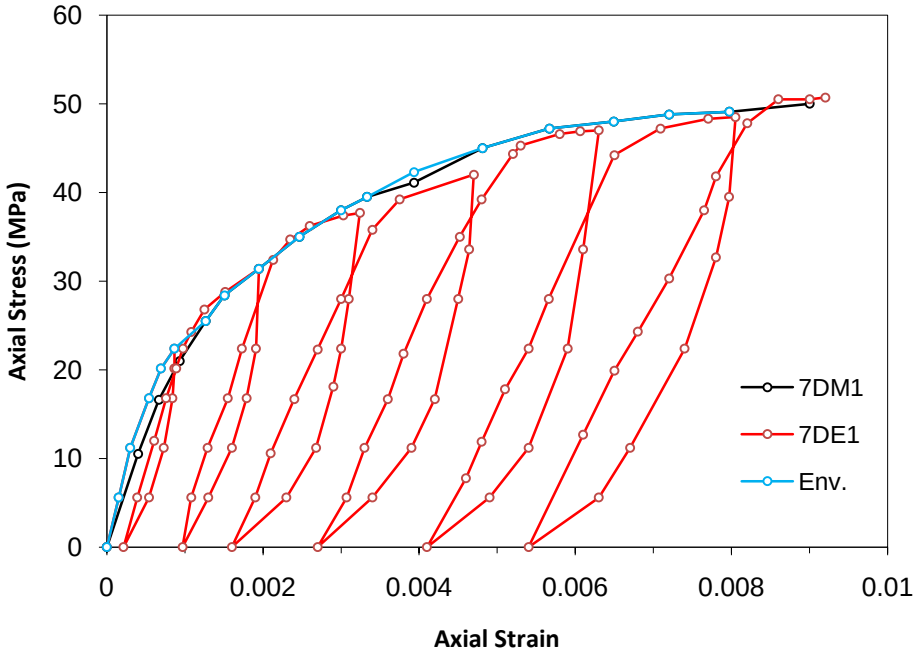

Figure (5.5) Comparison of monotonic axial load with cyclic to envelope for J4

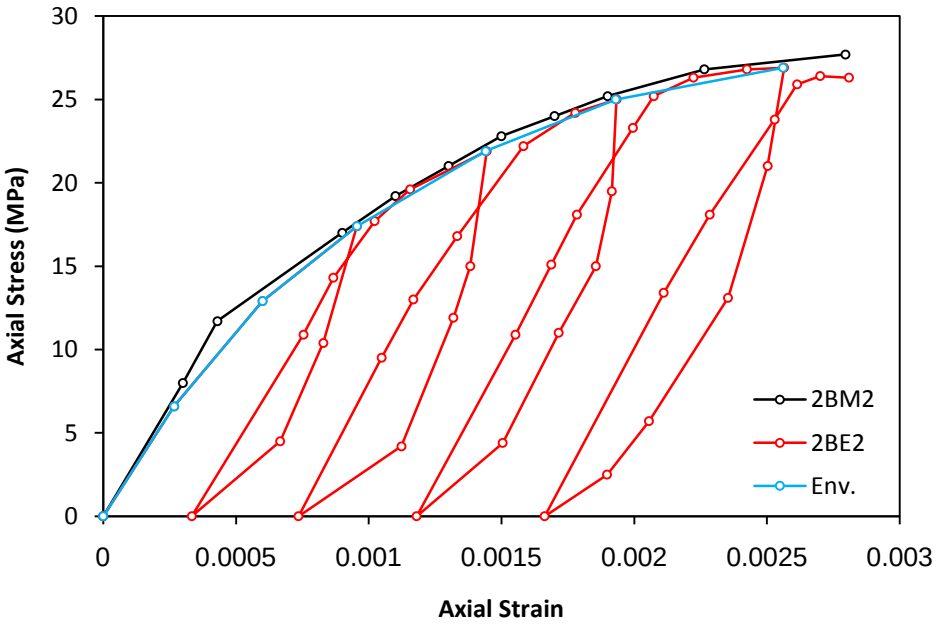

Figure (5.6) Comparison of monotonic axial load with cyclic to envelope for J5

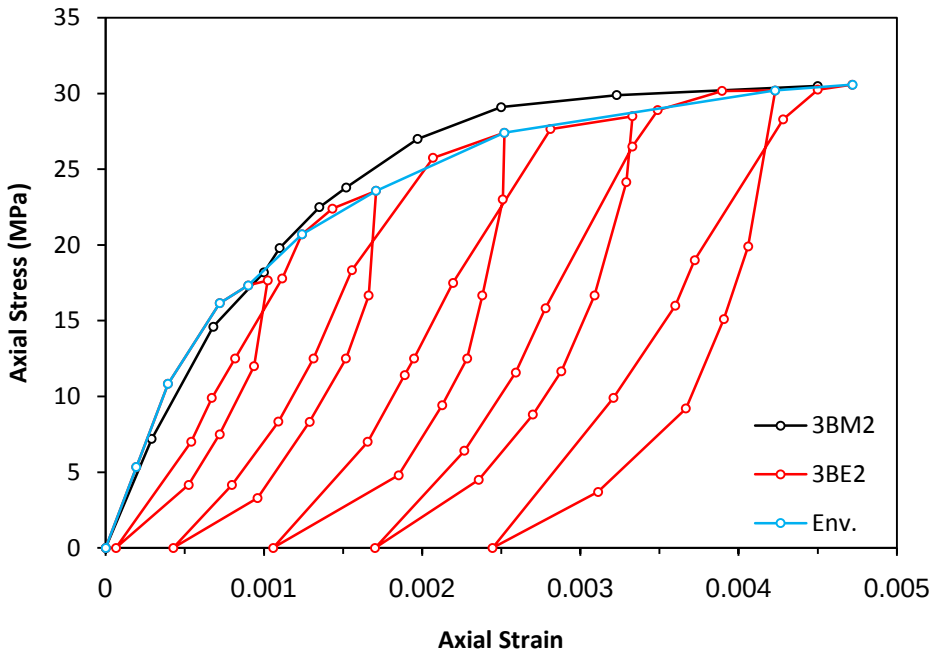

Figure (5.7) Comparison of monotonic axial load with cyclic to envelope for J6

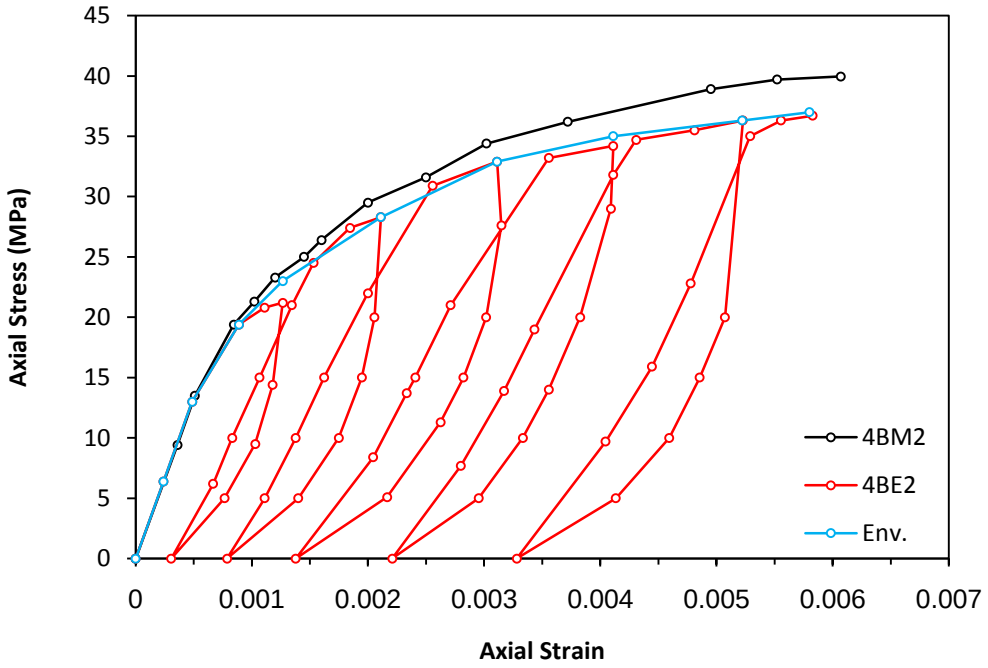

Figure (5.8) Comparison of monotonic axial load with cyclic to envelope for J7

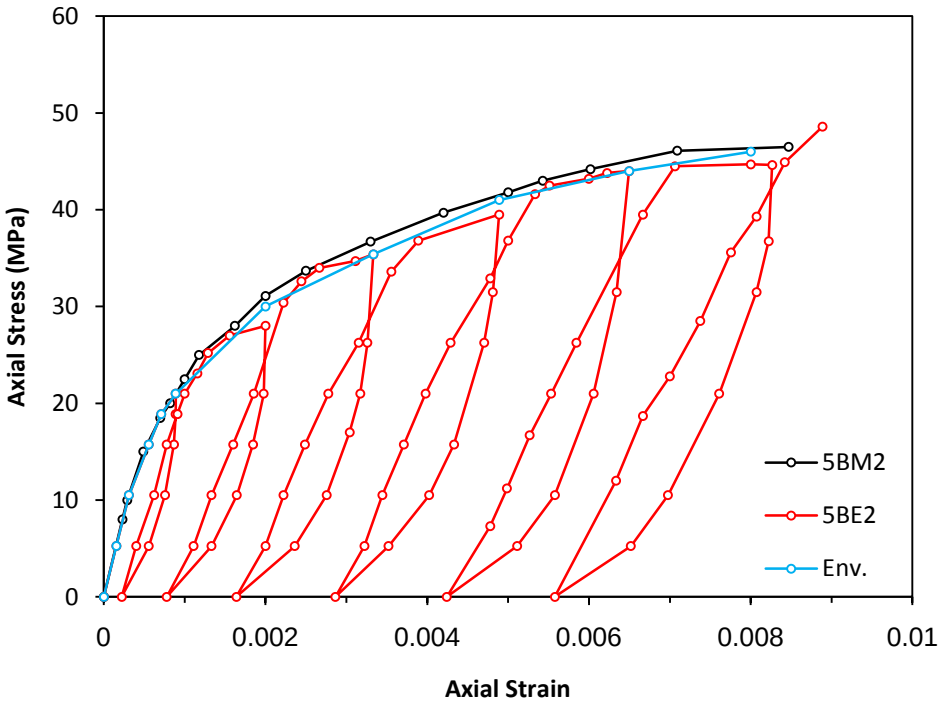

Figure (5.9) Comparison of monotonic axial load with cyclic to envelope for J8

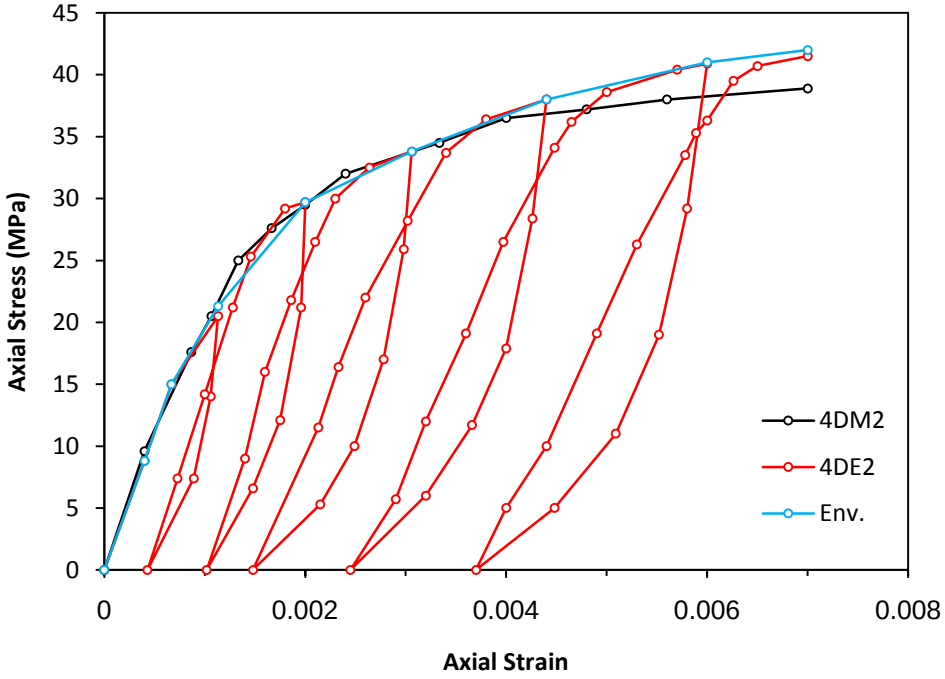

Figure (5.10) Comparison of monotonic axial load with cyclic to envelope for J10

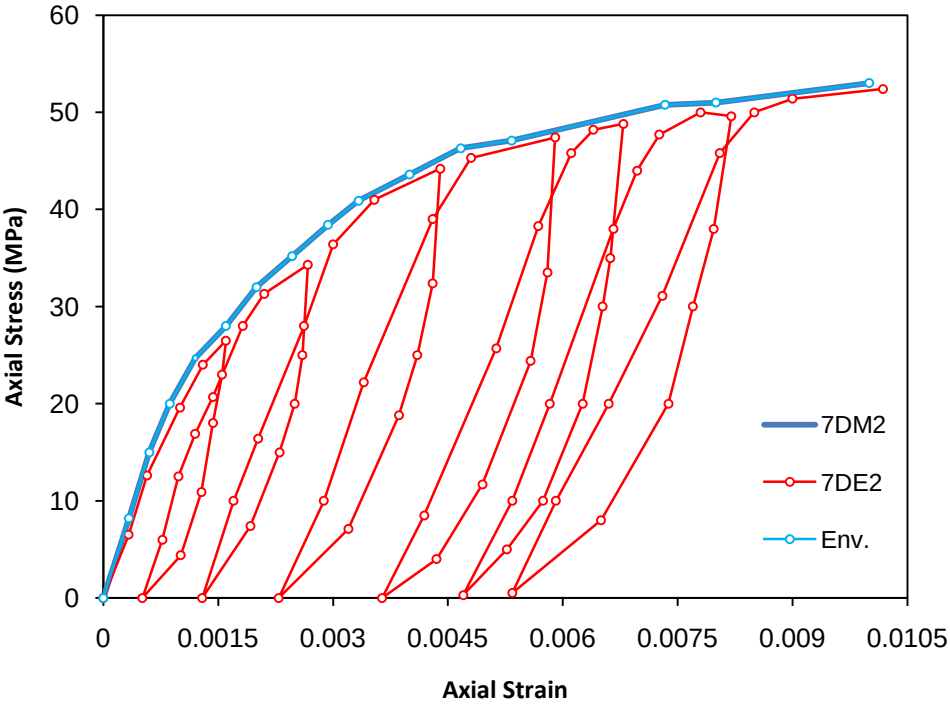

Figure (5.11) Comparison of monotonic axial load with cyclic to envelope for J11

5.2.2.2 Strength of Concrete Columns Strengthened with Ferrocement

The ultimate load and the corresponding strain for all specimens are summarized in Tables (5.1), (5.2) and (5.3). From these tables, it can be seen that the use of ferrocement jackets enhances the load carrying capacity of concrete columns. For all the specimens strengthened with ferrocement jacket, the load ratio P_{cc}/P_{coi} is always larger than one. The P_{cc}/P_{co1} varies between (2.481 and 4.116) and P_{cc}/P_{co2} between (1.132 and 2.291) for columns with 35 MPa mortar compressive strength. However, P_{cc}/P_{co1} varies between (2.571 and 4.873) and P_{cc}/P_{co2} between (1.173 and 2.367) for columns made with 45 MPa mortar compressive strength. This increase in strength is due to the ferrocement materials which have mesh reinforcement providing confinement to the core concrete. Large confining pressure was also exerted on the core contents and the redistribution of crack propagation resulted in less lateral expansion of the core. Thus, the strength increased in the confined specimens as compared to the control specimens (unconfined columns).

TABLE (5.1) Test results of plain concrete columns

Group No.	Column designation	P_{co1} (kN)	Displacement (mm)	ε_{co1}
J12	**100AM**	180.5	0.870	0.00290
J13	**100BM**	177.3	1.156	0.00257
J14	**150DM**	405.5	1.897	0.00253

TABLE (5.2) Test results of plain concrete columns

Group No.	Column designation	P_{co2} (kN)	Displacement (mm)	ε_{co2}
J15	**150AM**	390.0	0.759	0.00253
J16	**150BM**	388.7	1.121	0.00249
J17	**200DM**	703.4	1.995	0.00266

Table (5.3) Test results of strengthened concrete columns with ferrocement shell

Group No.	Column designation	P_{cc} (kN)	Displacement (mm)	ε_{cc}	$\frac{P_{cc}}{P_{co1}}$	$\frac{P_{cc}}{P_{co2}}$	$\frac{\varepsilon_{cc}}{\varepsilon_{co1}}$	$\frac{\varepsilon_{cc}}{\varepsilon_{co2}}$
J	**4AM1**	743.0	2.010	0.00670	4.116	1.905	2.310	2.648
J1	**2BM1**	463.0	1.179	0.002621	2.611	1.191	1.019	1.053
	2BE1	447.1	1.206	0.00268	2.521	1.150	1.043	1.076
	2BL1	455.9	1.165	0.00259	2.571	1.173	1.007	1.040
	2BS1	439.9	1.170	0.00260	2.481	1.132	1.012	1.044
J2	**4BM1**	636.1	2.623	0.00583	3.587	1.636	2.143	2.341
	4BE1	613.2	2.466	0.00548	3.458	1.577	2.015	2.201
	4BL1	583.1	2.560	0.00569	3.288	1.500	2.092	2.285
	4BS1	636.1	2.412	0.00536	3.587	1.637	1.971	2.153
J3	**4DM1**	1115.3	4.222	0.00563	2.750	1.586	2.225	2.117
	4DE1	1127.8	4.890	0.00652	2.781	1.603	2.577	2.451
	4DL1	1171.8	4.912	0.00655	2.890	1.666	2.589	2.462
	4DS1	1090.1	4.800	0.00640	2.688	1.550	2.530	2.406
J4	**7DM1**	1570.8	6.750	0.00900	3.874	2.233	3.557	3.383
	7DE1	1592.8	6.900	0.00920	3.928	2.264	3.636	3.459
	7DL1	1611.6	6.885	0.00918	3.974	2.291	3.628	3.451
	7DS1	1577.1	6.675	0.00890	3.889	2.242	3.518	3.346
J5	**2BM2**	489.5	1.260	0.00280	2.760	1.259	1.029	1.124
	2BE2	464.7	1.264	0.00281	2.621	1.196	1.033	1.129
	2BL2	455.9	1.327	0.00295	2.571	1.173	1.085	1.185
	2BS2	459.4	1.381	0.00307	2.591	1.182	1.129	1.233
J6	**3BM2**	538.9	2.025	0.00450	3.039	1.386	1.654	1.807
	3BE2	540.3	2.123	0.004718	3.047	1.390	1.735	1.895
	3BL2	530.1	2.340	0.00520	2.989	1.364	1.912	2.088
	3BS2	556.6	2.218	0.00493	3.139	1.432	1.813	1.980
J7	**4BM2**	705.9	2.731	0.00607	3.981	1.816	2.232	2.438
	4BE2	648.5	2.623	0.00583	3.657	1.668	2.143	2.341
	4BL2	671.5	2.709	0.00602	3.787	1.728	2.213	2.418
	4BS2	676.8	2.561	0.00569	3.817	1.741	2.092	2.285

Table (5.3) Continued

J8	**5BM2**	821.7	3.812	0.00847	4.634	2.114	3.114	3.402
	5BE2	858.8	4.001	0.00889	4.843	2.209	3.268	3.570
	5BL2	759.8	3.668	0.00815	4.285	1.955	2.996	3.273
	5BS2	812.8	3.668	0.00815	4.584	2.091	2.996	3.273
J9	**4AM2**	749.2	1.980	0.00660	4.151	1.921	2.276	2.609
J10	**4DM2**	1222.1	5.250	0.00700	3.014	1.737	2.767	2.632
	4DE2	1303.8	5.250	0.00700	3.215	1.854	2.767	2.632
	4DL2	1288.1	5.483	0.00731	3.177	1.831	2.889	2.748
	4DS2	1193.8	4.800	0.00640	2.944	1.697	2.530	2.406
J11	**7DM2**	1665.05	7.500	0.01000	4.106	2.367	3.953	3.759
	7DE2	1646.2	7.635	0.01018	4.060	2.340	4.024	3.827
	7DL2	1269.2	6.698	0.00893	3.130	1.804	3.530	3.357
	7DS2	1319.5	6.998	0.00933	3.254	1.876	3.688	3.508

5.2.2.3 Strain behavior of concrete columns strengthened with ferrocement

From Tables (5.1), (5.2) and (5.3), it can be seen that the use of ferrocement jackets enhances the extrapolated axial strain at ultimate load of concrete columns. For all the specimens strengthened with ferrocement jacket, the strain ratio $\varepsilon_{cc}/\varepsilon_{coi}$ is always larger than one. The $\varepsilon_{cc}/\varepsilon_{co1}$ varies between (1.007 and 3.636) and $\varepsilon_{cc}/\varepsilon_{co2}$ between (1.04 and 3.459) for mortar compressive strength of f'_c=35 MPa. However, $\varepsilon_{cc}/\varepsilon_{co1}$ varies between (1.029 and 4.024) and $\varepsilon_{cc}/\varepsilon_{co2}$ between (1.124 and 3.827) for specimens having mortar compressive strength of f'_c=45 MPa. This increase in strain could be attributed to the containment of concrete inside the ferrocement shell and the restrained lateral expansion of concrete during loading. Because of confinement, the crack growth and crack network formations occurred at a much controlled rate, leading to these higher strains as compared to the control specimens. A typical combined axial stress-strain is shown in Fig. (5.12). From this curve, it is observed that the

confined concrete specimens have high ultimate strengths and strains as compared to the conventional specimens.

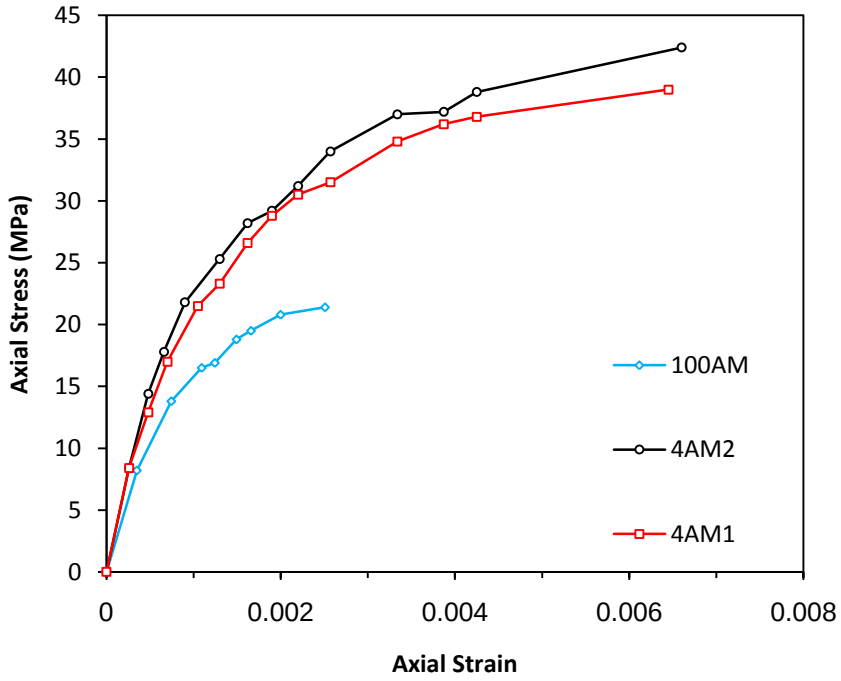

Figure (5.12) Stress-Strain curve for concrete confined with ferrocement and control specimen for (150*300) mm specimens

5.2.2.4 Load-Axial Displacement Response

The axial load plotted as a function of axial displacement for strengthened concrete columns and plain concrete columns are shown in Figs. (5.13 to 5.18). Together, these figures and Table (5.3) clearly show that confinement with ferrocement jackets can considerably enhance the structural performance of concrete columns, both its strength and ductility, under axial load.

In strengthening concrete columns, at low levels of axial stress the transverse strain are so small that the ferrocement jacket induces little

confinement, if any. At higher axial stress levels, the dramatic increase in transverse strains activates the ferrocement jacket and confining pressure becomes more significant. The general confining pressure induces a triaxial state of stress in the confined concrete. That concrete under triaxial stress exhibits superior behavior, in both strength and ductility as compared to plain concrete.

The load-displacement relationships of all strengthened concrete columns with ferrocement jackets are generally nonlinear in nature. The behavior of strengthened columns under axial loading can be divided into two regions. In the first region, the behavior of confined column is similar to that of plain concrete column: this is due to the fact that the confining effect of ferrocement shell is still not activated by the lateral expansion of the concrete core. In the vicinity of the peak load of plain concrete columns, the confined concrete reaches a state of unstable volumetric growth caused by excessive cracking. At this point, the ferrocement shell is activated and starts to gradually restrain the rapid growth of the lateral strains. This region of response is characterized by a transition curve at approximately the ultimate load of the plain concrete column. And, this region is recognized in which the ferrocement jacket shell is fully activated and the load-displacement relationship continued as a nonlinear line up to the failure at ultimate load.

Observations, after peak loads, showed that the failure of the strengthened columns happens step by step and a complete collapse of the column by a sudden explosive mode does not occur until large deformations are introduced. This indicates that the energy absorption capacity or the ductility of the confined concrete columns with ferrocement shell is much greater. However, the presence of the ferrocement shell significantly enhanced the axial plastic strain before collapse. This would provide warning to progressive failure rather than brittle failure of plain concrete columns.

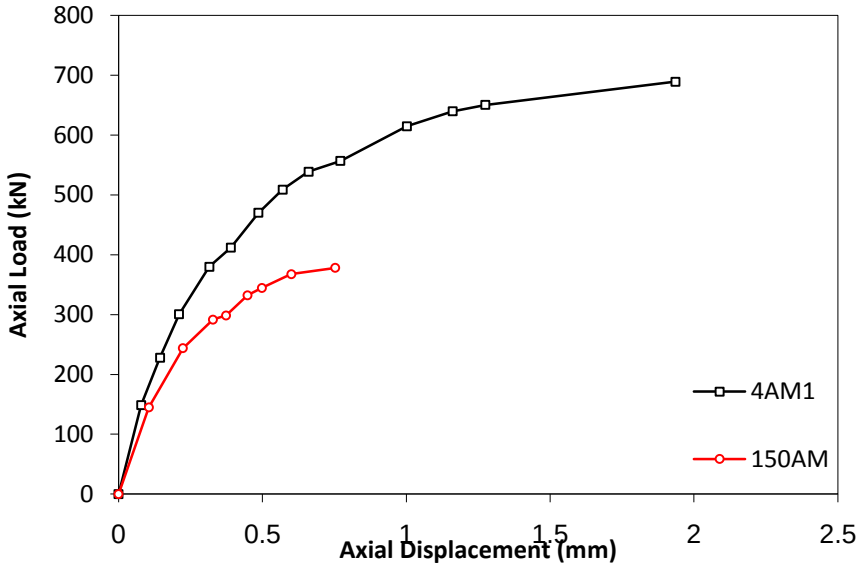

Figure (5.13) Load-displacement relation of (150*300)mm specimens and f'cm=35 MPa

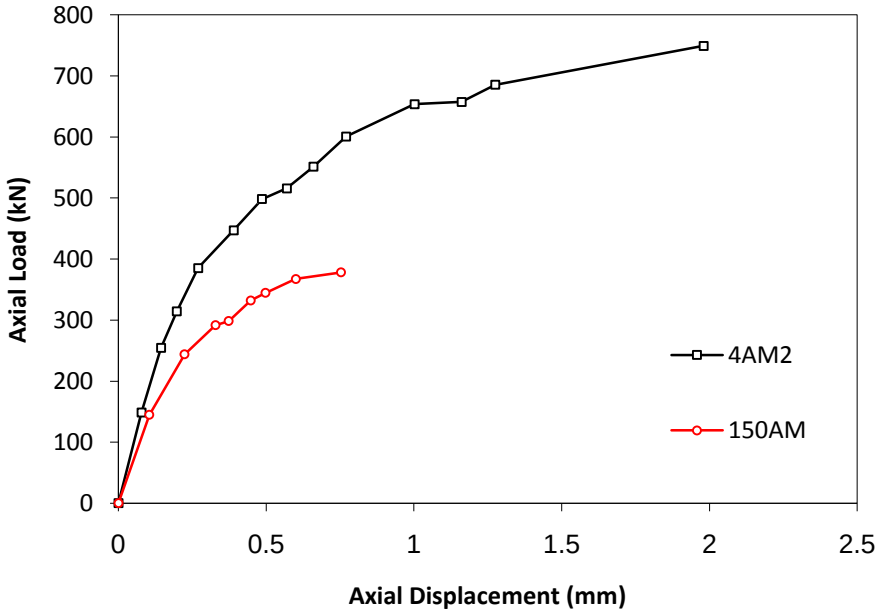

Figure (5.14) Load-displacement relation of (150*300) mm specimens and f'cm=45 MPa

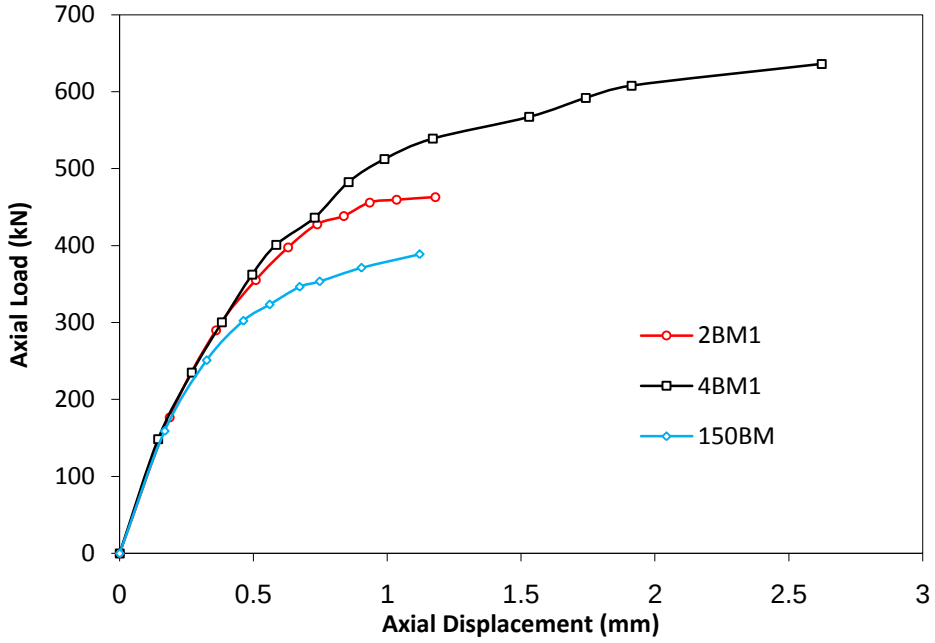

Figure (5.15) Load-displacement relation of (150*450) mm specimens and f'cm=35 MPa

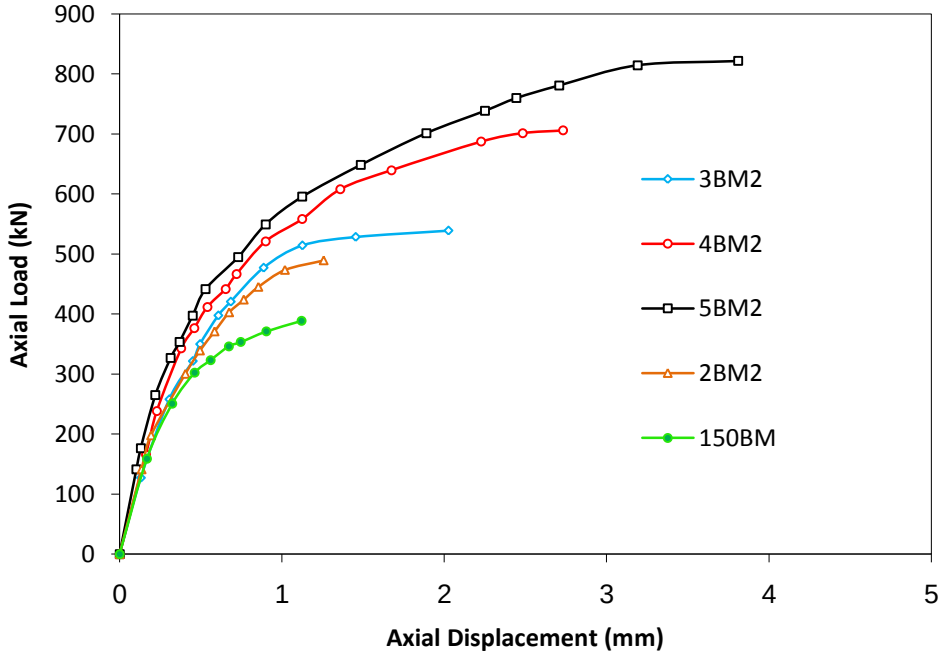

Figure (5.16) Load-displacement relation of (150*450) mm specimens and f'cm=45 MPa

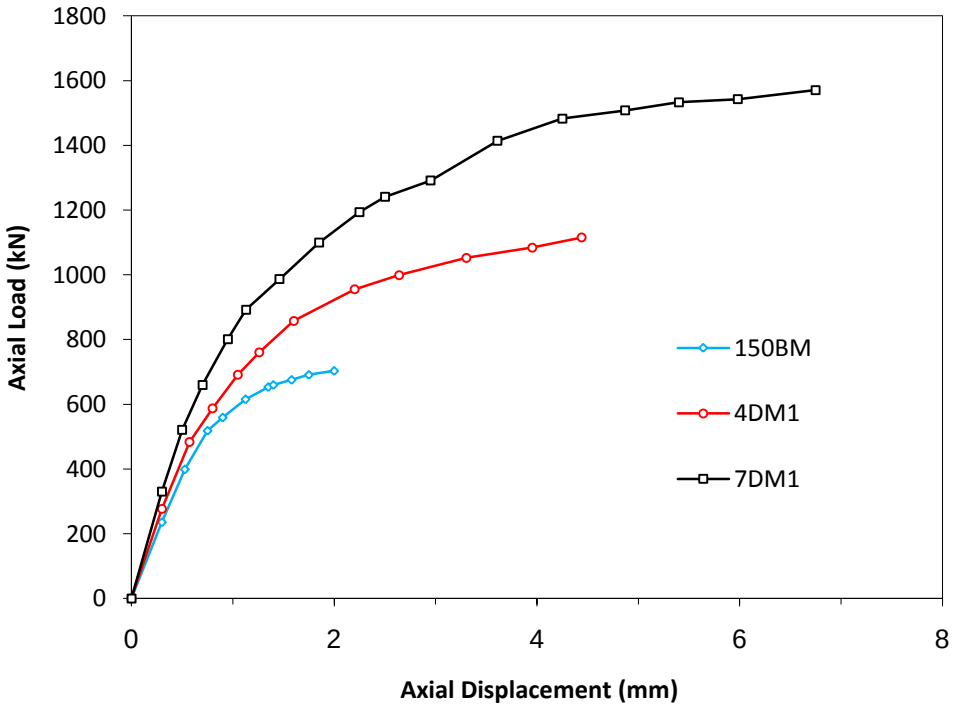

Figure (5.17) Load-displacement relation of (200*750) mm specimens and f'cm=35 MPa

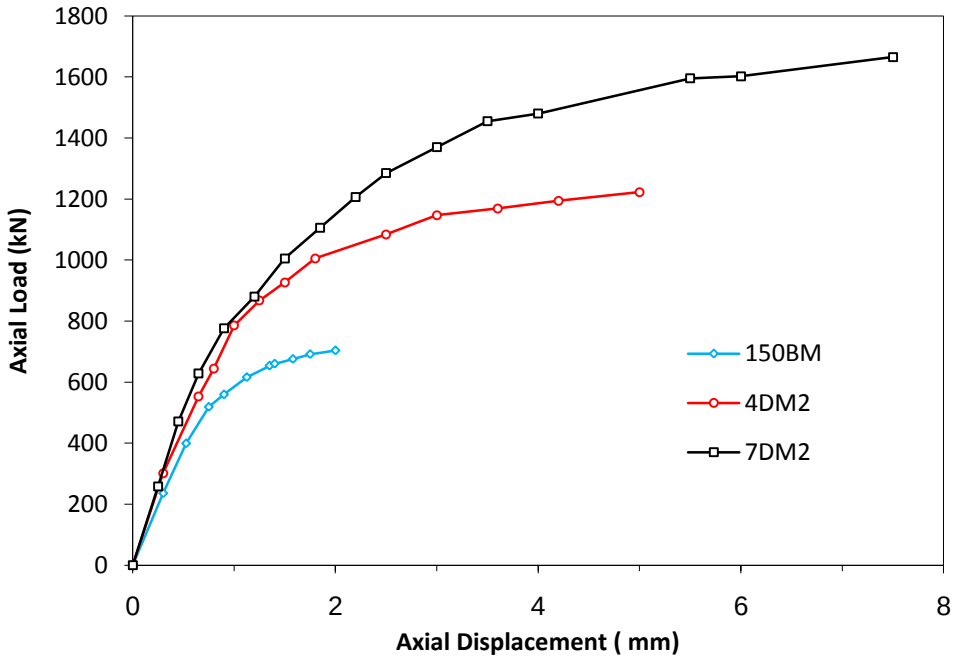

Figure (5.18) Load-displacement relation of (200*750) mm specimens and f'cm=45 MPa

5.2.2.5 Effect of Number of Wire Mesh Layers

In this section, the effect of number of wire mesh layers is investigated. The number of layers is changed from 2 to 5 for the specimens having (150*450mm) dimensions, (4 and 7 layers) for specimens with (200*750 mm) dimensions and 4 layers for specimen with (150*300 mm) dimensions. The designation of specimens is used such that the first number indicates the number of wire mesh layers.

Table (5.3) shows the effect of increasing the number of wire mesh layers (volume fraction of mesh reinforcement) on the behavior of strengthened concrete columns with ferrocement jackets. It can be seen from this table, when all other parameters are the same, the increase of number of wire mesh layers leads to greater increase in ultimate strength and the corresponding strain of the strengthened columns with ferrocement jackets. This could be attributed to the different ratios of the volume fraction reinforcement. The volume fraction of reinforcement (v_f) in this study is defined by the ratio of the volume of reinforcement to the volume of composite [10]. It is noted that when increasing the number of layers from 2 to 7 a considerable increase in the strength of specimens is obtained.

Figures (5.19) and (5.20) show the effect on ultimate strength and strain, respectively, of the volume fraction (v_f) of wire mesh of strengthened specimens. From Fig. (5.19), it can be seen that the ultimate strength increases as the volume fraction is increased. It is clear that increasing v_f leads to increase of axial strength capacity and show that increasing v_f from 1.09% to 2.73% in specimen having size of (150*450 mm) gives an increase of axial strength in the ratio of 1.952.

Also Figs. (5.13) to (5.18) show that as the number of mesh layers increases, the axial displacement at ultimate load increases and the specimens become more ductile. The same figures depict that the number of layers has an insignificant effect on load displacement relationships at the first loading stage,

until approaching the strength of unconfined columns, and strongly influences the behavior after this point. The higher volume fraction, the stiffer the response of the second region of axial load-displacement curves. This stiffer response is due to the higher stiffness of these specimens. The ultimate load of specimens with ferrocement jackets was reached at axial displacement which is higher than that of plain concrete specimens.

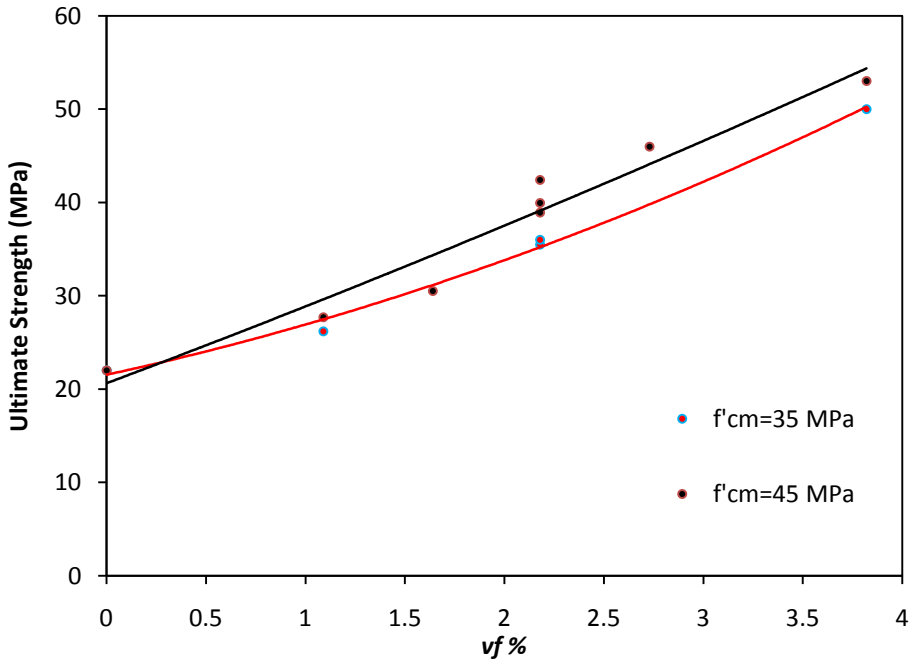

Figure (5.19) Effect of volume fraction on ultimate strength

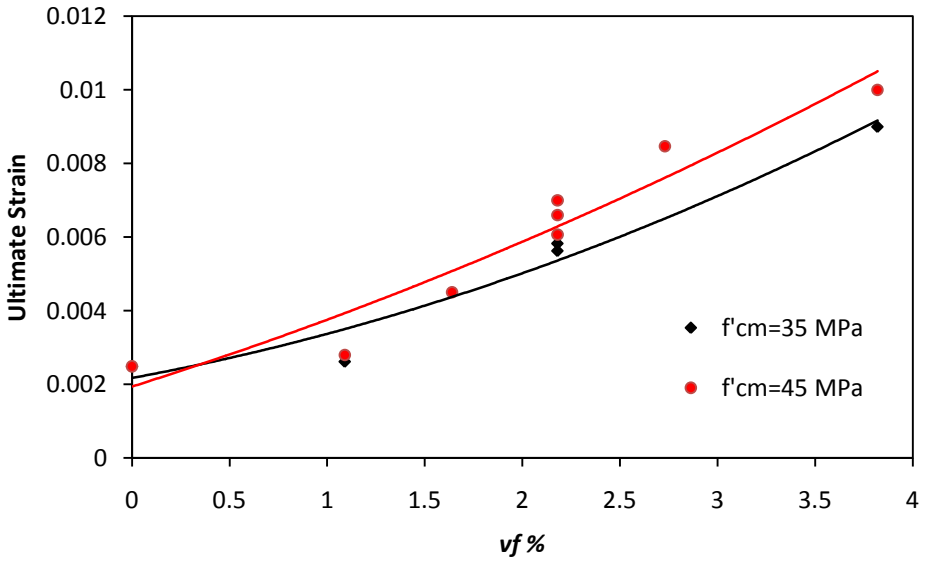

Figure (5.20) Effect of volume fraction on ultimate strain

5.2.2.6 Effect of Mortar Compressive Strength

Table (5.4) shows the ultimate load of the strengthened columns with ferrocement jackets for the two different used mortar strengths. From this table, it can be seen that the strength of the strengthened columns slightly increases as the mortar strength increases.

The extrapolated axial strain at ultimate load of the strengthened columns is plotted against the mortar strengths as shown in Fig. (5.21). From this figure and Table (5.5), it can be seen that the ultimate axial strain of the strengthened columns slightly increases as the concrete strength increases.

The load–displacement relationships for specimens 4AM1 and 4AM2 have been drawn in Fig. (5.12) to examine the effect of mortar strength on this relationship. As shown in this figure, the ultimate strength slightly increases as the mortar strength increases, and also the strain at ultimate load increases as the mortar strength increases.

Table (5.4) Ultimate load of specimens with different mortar compressive strength

Layer No.		Ultimate load (kN)		$\frac{P_{45}}{P_{35}}$
		f'_{cm}=35 MPa	f'_{cm}=45 MPa	
Monotonic load	2	463.0	489.5	1.057
	4	636.1	705.9	1.110
	4	1115.3	1222.1	1.096
	7	1570.8	1665.1	1.060
Cyclic to envelope curve	2	447.1	464.7	1.040
	4	613.2	648.5	1.058
	4	1127.8	1303.8	1.156
	7	1592.8	1646.2	1.034
			average	1.076
			Standard deviation	0.0415

Table (5.5) Ultimate strain of specimens with different mortar compressive strength

Layer No.		Ultimate strain		$\frac{\varepsilon_{45}}{\varepsilon_{35}}$
		f'_{cm}=35 MPa	f'_{cm}=45 MPa	
Monotonic load	2	0.00262	0.00280	1.068
	4	0.00583	0.00607	1.041
	4	0.00563	0.00700	1.243
	7	0.00900	0.01000	1.111
Cyclic to envelope curve	2	0.00268	0.00281	1.049
	4	0.00548	0.00583	1.064
	4	0.00652	0.00700	1.074
	7	0.00920	0.01020	1.109
			average	1.095
			Standard deviation	0.065

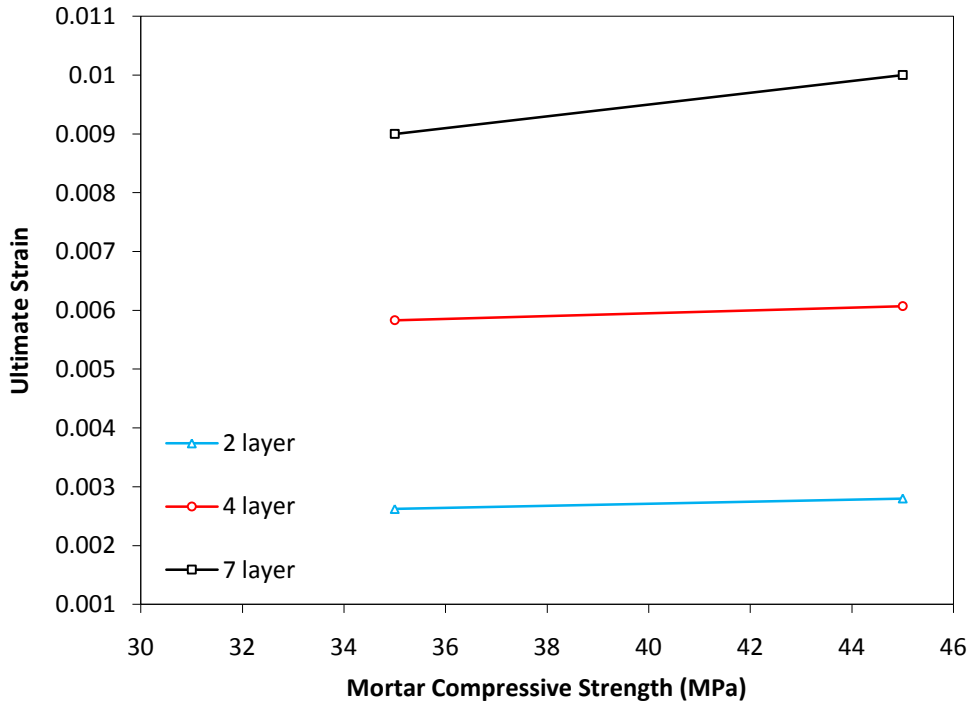

Figure (5.21) Effect of mortar compressive strength on ultimate strain of specimens

5.2.2.7 Effect of Column Size

Table (5.6) demonstrates the effect of the column size on the ultimate strength of concrete columns strengthened with ferrocement jacket. As it is evident from this table, the increase of the column size led to decrease ultimate strengths.

Figure (5.22) also shows the effect of the column size on the strength of concrete column strengthened with ferrocement jacket. As shown in this figure, the increase of size causes a reduction in the ultimate compression stress of the column. This reduction in ultimate strength is not significant and could be attributed to that with an increase in the column height, the effect of the friction between the machine loading plates and the ends of the column is decreased providing a region at the midheight of the column far from the ends which are subjected to combined stresses. The region at the midheight of column will be free to expand laterally and this will cause excessive cracking of concrete which leads to failure of columns.

Table (5.6) Effect of slenderness ratio on ultimate stress of specimen

Compressive Strength (MPa)	No. of Layer	Dimension* (mm)	Slenderness ratio	Ultimate strength (MPa) (Monotonic load)
35	4	450*150	12	36.0
	4	750*200	15	35.5
45	4	300*150	8	42.4
	4	450*150	12	39.9
	4	750*200	15	38.9

***Height×Diameter**

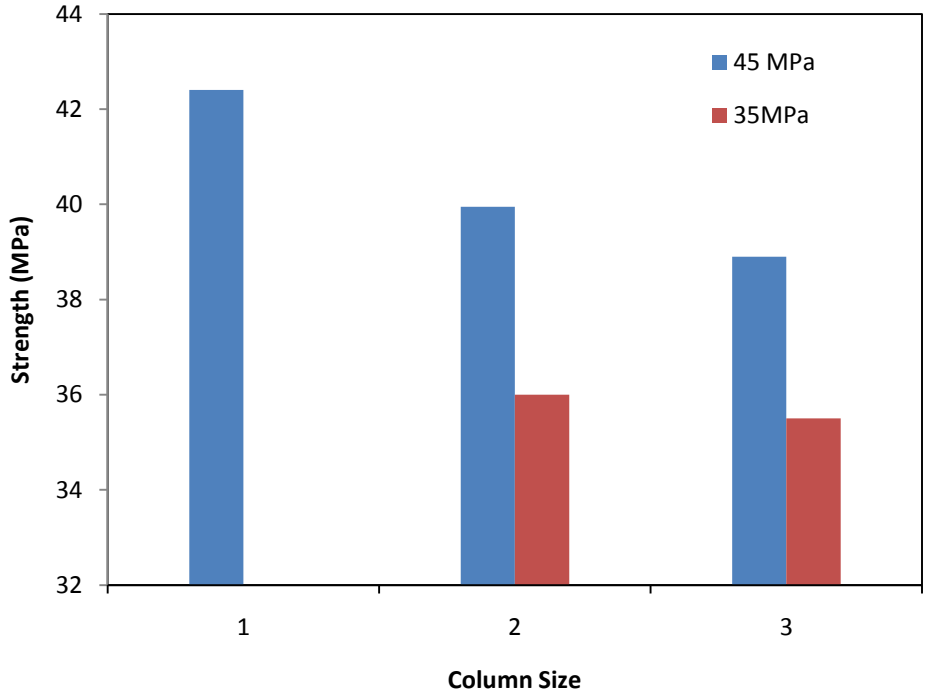

1 :(300*150), 2 :(450*150), 3 :(750*200)

Figure (5.22) Histogram of the column size effect

5.2.2.8 Investigation of the Common Points Limit

The common point limit has been defined as "the locus of the points where the reloading portion of any cycle crosses the unloading portion of previous cycle. Stresses above this limit will lead to additional strains, while the stresses below this limit give no strain increments, and the stress-strain curves will go into a closed hysteresis loop" (as cited in Ref. [13])

Figures (5.2) to (5.11) show the common point limit for cycles with zero minimum stress levels applied to specimens loaded to or very close to the envelope curve before they are unloaded. At points (A through D) in Fig. (5.2), the reloading portion of the cycles starting from stress equals zero intersects the unloading curves of the previous cycle given the locus of points which constitute the common point limit for the applied load history.

The effect of the level of minimum stress is illustrated in Figs. 5.23) to (5.32). In these figures, two tests on specimens made of the same concrete were

conducted and the specimens were loaded to same maximum stress level (90 percent of ultimate strength) but the minimum stress level was different. First test specimen was subjected to cyclic loading between $0.9\,f'_c$ and zero minimum stress level. Failure occurred after a certain number of cycles when accumulated strain reached the envelope curve. The second test specimen was subjected to cycles with the same maximum stress level but with a minimum stress level of $0.4\,f'_c$. Although the minimum stresses were different, the common point limit was the same for both tests. The figures show that the minimum stress in a cyclic loading does not have a significant effect on the location of the common point limit. Therefore, it can be assumed that the common point limit is unique and identical with the common point limit corresponding to a cycle with zero minimum stress level.

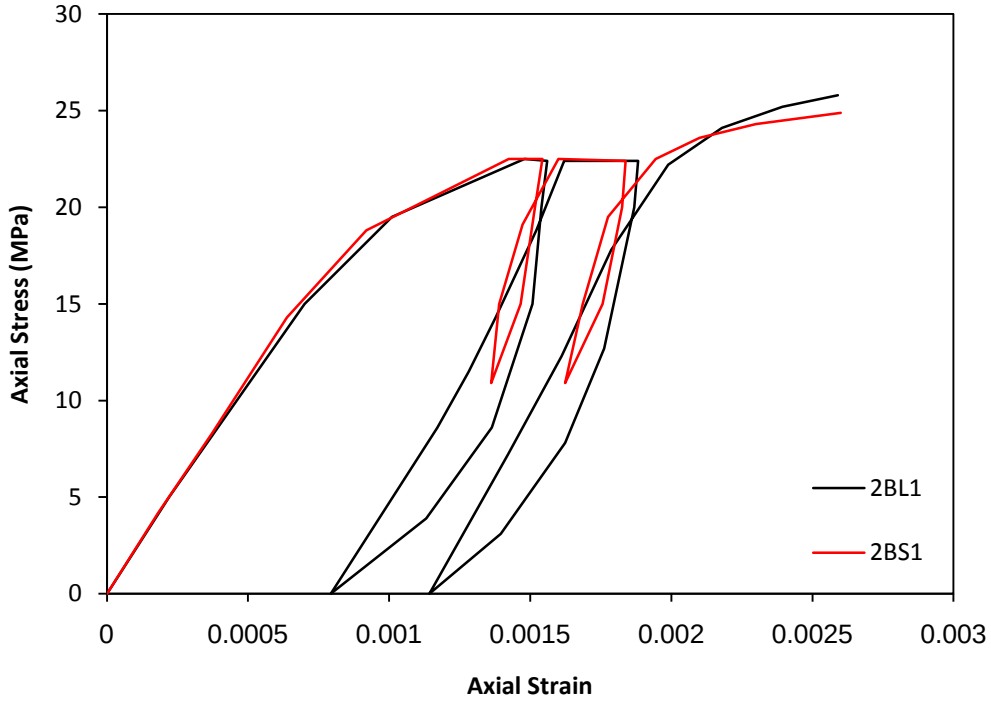

Figure (5.23) Effect of minimum stress level on common point limit J1

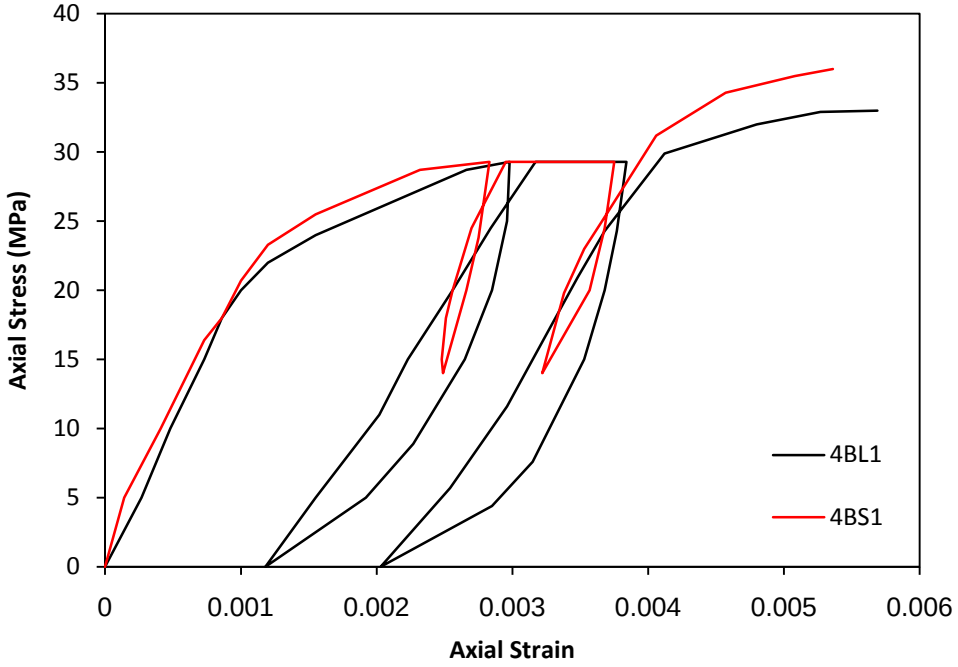

Figure (5.24) Effect of minimum stress level on common point limit J2

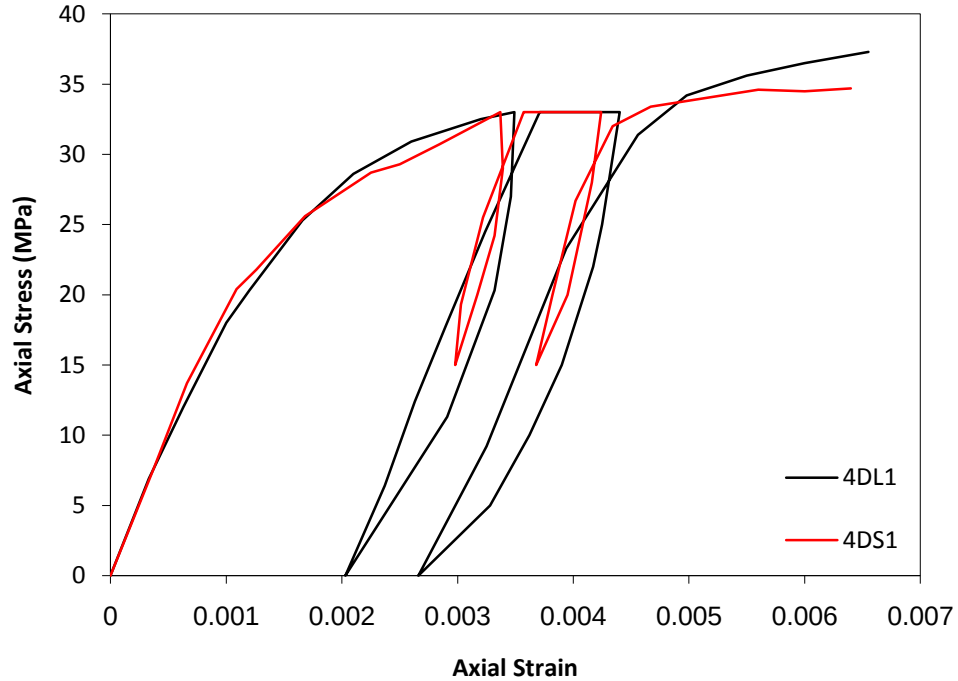

Figure (5.25) Effect of minimum stress level on common point limit J3

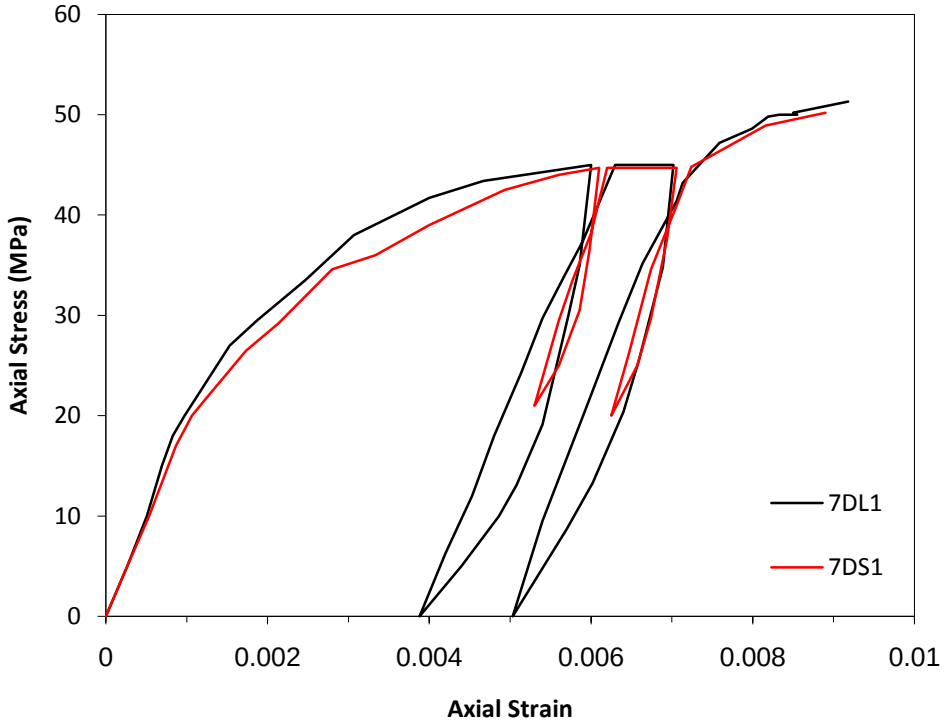

Figure (5.26) Effect of minimum stress level on common point limit J4

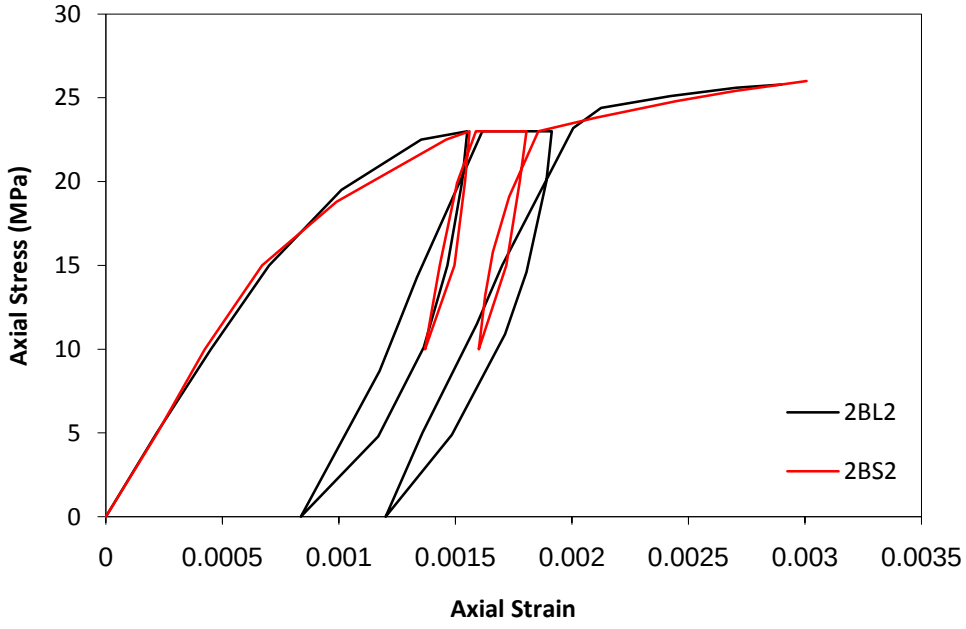

Figure (5.27) Effect of minimum stress level on common point limit J5

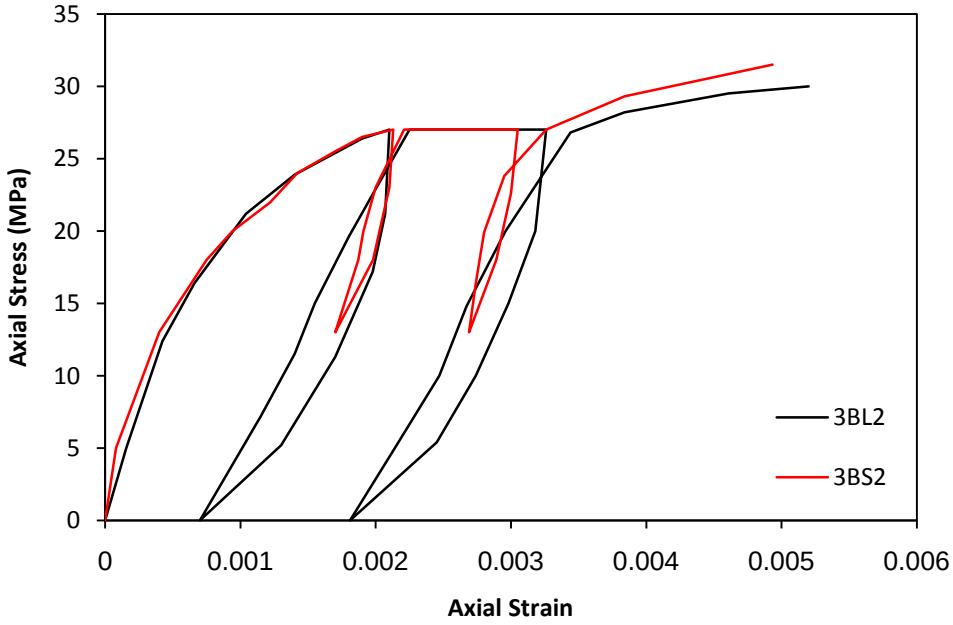

Figure (5.28) Effect of minimum stress level on common point limit J6

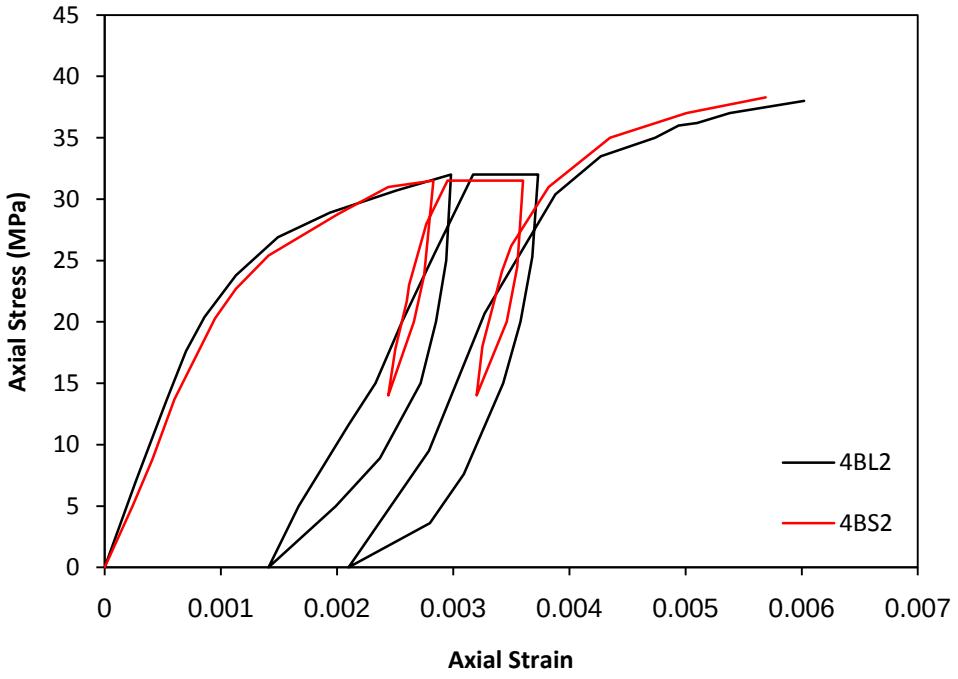

Figure (5.29) Effect of minimum stress level on common point limit J7

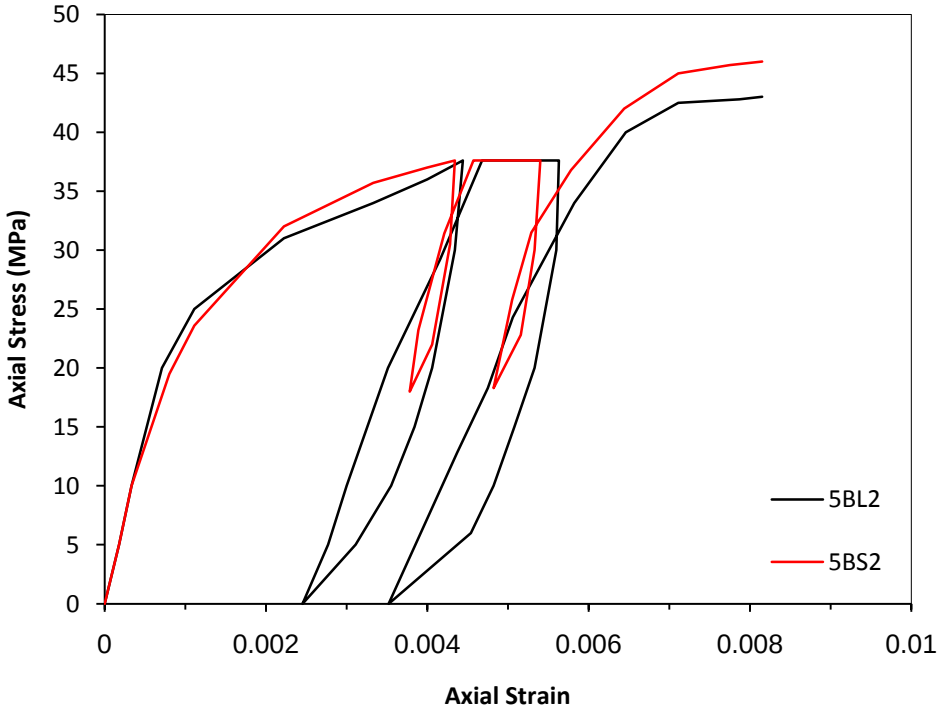

Figure (5.30) Effect of minimum stress level on common point limit J8

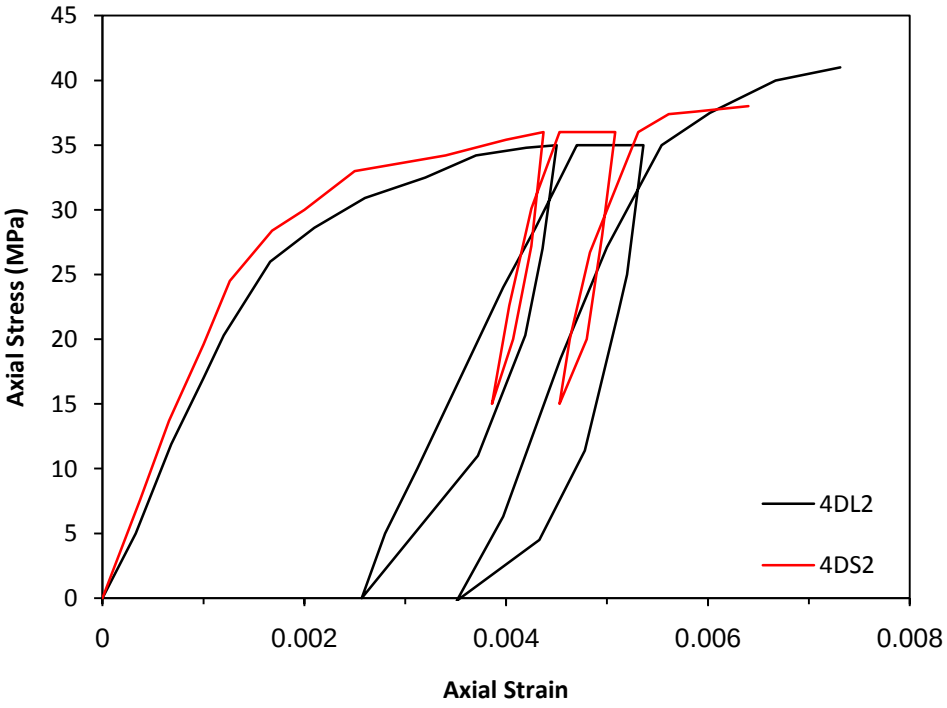

Figure (5.31) Effect of minimum stress level on common point limit J10

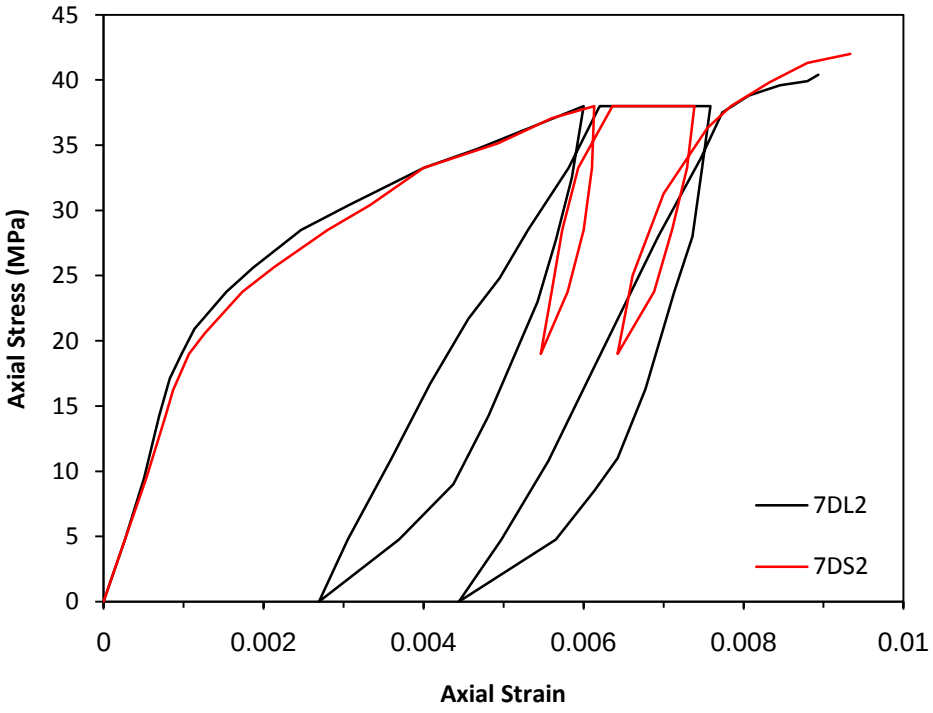

Figure (5.32) Effect of minimum stress level on common point limit J11

5.2.2.9 Effect of Nonrecoverable Strain on Behavior

The nonrecoverable or plastic strain of concrete is defined as the residual axial strain corresponding to a zero stress level on the loading or unloading stress-strain curve. In the present study, all the unloading curves were terminated when reaching the zero stress. In a number of existing studies [78, 117], the plastic strain of unconfined or steel-confined concrete was related to the axial strain at the starting point of unloading. Sakai and Kawashima [117] suggested that the plastic strain of steel-confined concrete is a linear function of the unloading strain. It should be noted that unloading can be initiated from the envelope curve, or from a reloading path. Only the plastic strain for unloading from the envelope curve can be directly related to the unloading strain, as shown in Fig. (5.33). This unloading strain is referred to as the envelope unloading strain. In this figure, a linear relationship between the plastic strain and the envelope unloading strain is also observed for ferrocement confined concrete. Figure (5.33) shows that all series of specimens confined with (2, 3, 4, 5 and 7)

layers of wire mesh have approximately the same line trend. This appears to indicate that the plastic strain of confined concrete with ferrocement jacket is independent of the amount of confinement for the range considered. As all series of specimens had almost the same unconfined concrete strength, it is not clear whether the unconfined concrete strength has an effect on the plastic strain.

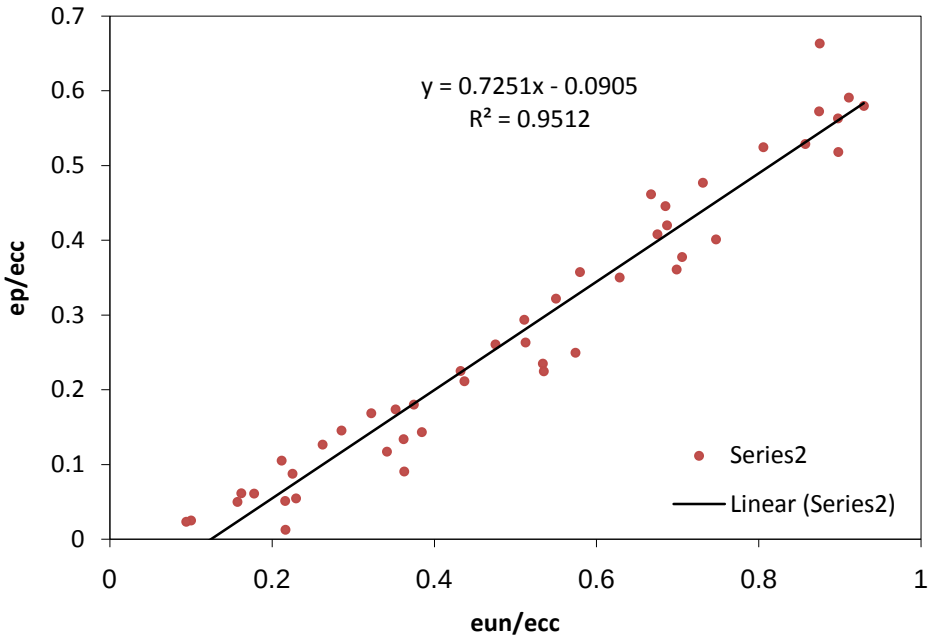

Figure (5.33) plastic strain vs. envelope unloading strain

5.2.2.10 Effect of Loading History

Sinha et al. [71] suggested a uniqueness concept which means that the locus of common points, where the reloading path of an unloading/reloading cycle crosses the unloading path, can be considered as a stability limit. Stresses at or below this limit will lead to stress–strain responses following the same path without causing further permanent strains. According to this uniqueness concept, the effect of loading history is negligible in predicting the unloading and reloading paths of concrete. However, this uniqueness concept was not supported by subsequent tests by Karson and Jirsa [72]. This non-uniqueness

concept has been verified by other studies on unconfined concrete and steel confined concrete [78, 117].

The results of the present tests show that the uniqueness concept is also invalid for confined concrete with ferrocement jackets. Figures (5.23) to (5.32) show that when subjected to repeated cycles at each prescribed axial displacement level, the axial stress-axial strain response of a subsequent unloading/ reloading cycle does not coincide with that of the previous cycle and instead shifts to the higher axial strain side. This shift of the unloading/reloading curve indicates a cumulative effect of the loading history on the permanent strain (plastic strain) and stress deterioration of confined concrete with ferrocement jackets.

5.2.2.11 Failure Modes

The failure modes of all the test specimens are shown in Plates (5.1) and (5.2).

The unconfined (plain concrete) columns, as shown in Plates (5.1), suffers from excessive lateral expansion due to unstable propagation of the internal micro-cracks, which causes the strain softening behavior and eventually the concrete mass loses its integrity and fails in splitting manner. The complete collapse of the column usually occurred suddenly at strains between 0.00249 and 0.00290.

For the concrete columns confined with ferrocement jacket, the typical failure mode for columns was as follows. The first crack started at the top of the specimen and the number of cracks started increasing gradually on all the sides of the specimens. The cracks were widened at approximately 1/3rd height from top or bottom of the specimen and ultimately the specimen reached the failure. It was observed that there was no failure between the core and ferrocement laminate. But the specimen failure was due to the network of cracks in the concrete core and the yielding of transverse wires. The failure modes clearly demonstrated that the transverse wires were subjected to hoop tension and

thereby produced passive confinement pressure. The domination of vertical cracks indicates that the failure was initiated by the development of vertical cracks which led to the ultimate failure through the yielding of transverse wires. Some of the meshes retrieved from crushed specimens showed broken horizontal wire, indicating that the yielding of these wires is due to hoop tension. The failure modes of confined concrete specimens are shown in plate (5.2).

(a) (b)

Group J 12 plain concrete (100*300) mm **Group J 15 plain concrete (150*300) mm**

(c)

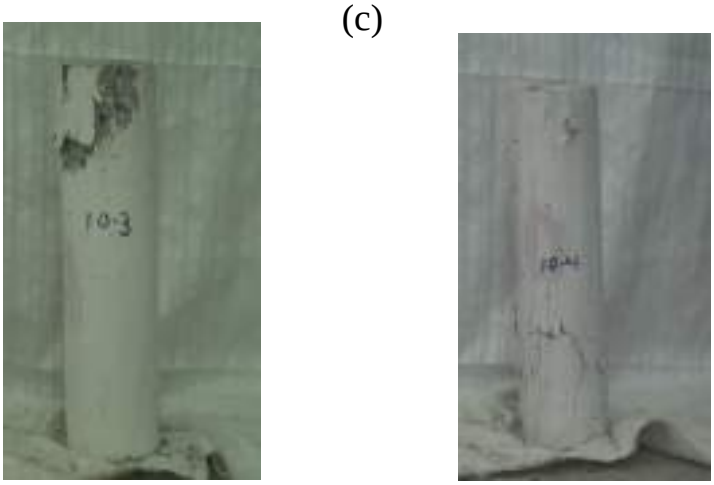

Group J 13 plain concrete (100*450) mm

Plate (5.1) Failure mode of plain concrete columns

(d)

Group J 16 plain concrete (150*450) mm

(e)

Group J 14 plain concrete (150*750) mm

(f)

Group J 17 plain concrete (200*750) mm

Plate (5.1) Continued

(a)

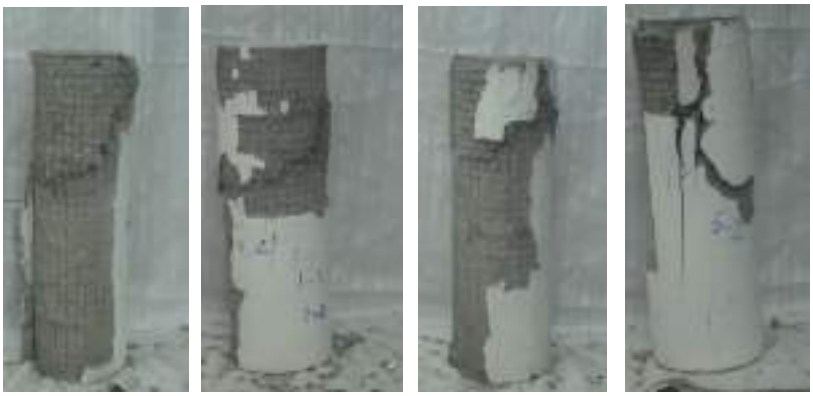

Group J 1 Strengthen Column with 2wwm and f'cm=35 MPa (150*450) mm

(b)

Group J 5 Strengthen Column with 2wwm and f'cm=45 MPa (150*450) mm

(c)

Group J 6 Strengthen Column with 3wwm and f'cm=45 MPa (150*450) mm

Plate (5.2) Failure mode of strengthened concrete column with ferrocement jacket

(d)

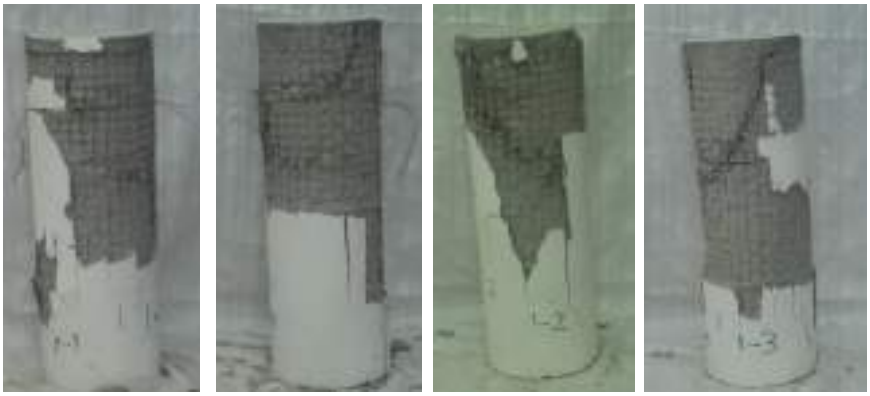

Group J 2 Strengthen Column with 4wwm and f'cm=35 MPa (150*450) mm

(e)

Group J 7 Strengthen Column with 4wwm and f'cm=45 MPa (150*450) mm

(f)

Group J 8 Strengthen Column with 5wwm and f'cm=45 MPa (150*450) mm

Plate (5.2) Continued

(g)

Group J 3 Strengthen Column with 4wwm and f'cm=35 MPa (200*750) mm

(h)

Group J 10 Strengthen Column with 4wwm and f'cm=45 MPa (200*750) mm

(i)

Group J 4 Strengthen Column with 7wwm and f'cm=35 MPa (200*750) mm

Plate (5.2) Continued

(k)

Group J 11 Strengthen Column with 7wwm and f'cm=45 MPa (200*750) mm

(l)

Group J 9 Strengthen Column with 4wwm and f'cm=45 MPa (150*300) mm

(m)

Group J Strengthened Column with 4wwm and f'cm=35 MPa (150*300) mm

Plate (5.2) Continued

5.3 Finite Element Analysis

In the present section, the tested concrete columns strengthened with ferrocement jackets have been analyzed using three dimensional finite element models. The main objectives of the analysis are to check the validity of the adopted finite element models in predicting the overall behavior of the tested columns, and to get more information about stresses and strains developed in the specimens.

It has been found that the simulation of the applied load has a significant effect on the results of the finite element analysis. In the experimental work of the present investigation, and to insure uniform distributed load on the top of specimens, loading plates are used. Therefore in the present study the load is distributed on the nodes under the loading plate in such a manner that each node takes a load equal to the uniform applied pressure times the related area to the node.

The analysis is made by using ANSYS 11.0 computer program. The three dimensional 8-noded brick element (SOLID65) is selected to represent the concrete column core and ferrocement jacket, while (SOLID45) is used for the loading steel plate. The contact between concrete core and ferrocement jacket is assumed perfect bonded.

5.3.1 Stress-Strain Relationship

Figures (5.34) and (5.35) illustrate the contours for axial displacement obtained from the finite element model for one loading step. The hidden lines represent the undeformed (original) edge of the column while the solid lines represent the deformed shape of the column. Fig. (5.36) shows the cracking and crushing of concrete specimen at ultimate load.

Figures (5.37) to (5.66) illustrate the stress-strain relationships for the tested columns. The theoretical relationships alongside the experimental ones are collected for each column. These figures show that the predicted behavior

concerning the stress-strain curve is almost similar to the experimental results. Good agreement between the experimental and theoretical results is achieved.

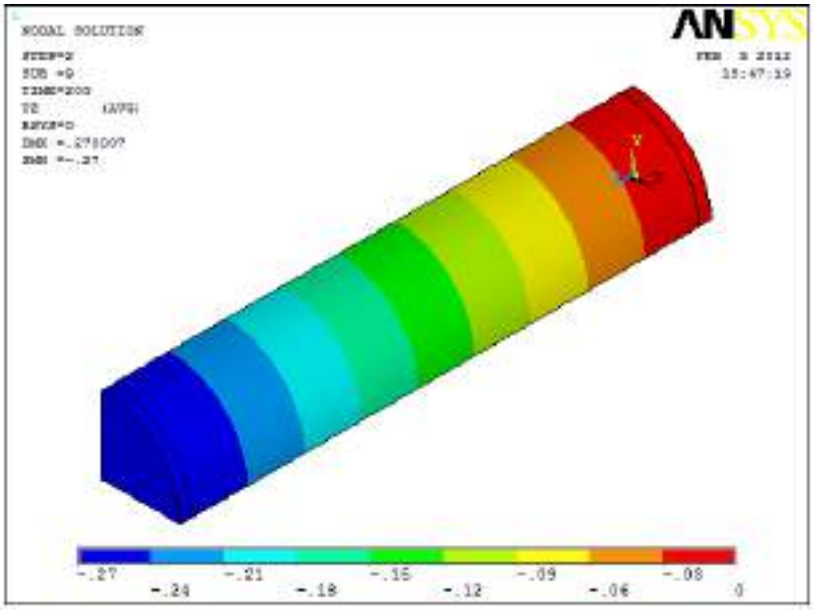

Figure (5.34) contour plot of axial displacement for specimen (150*450) mm

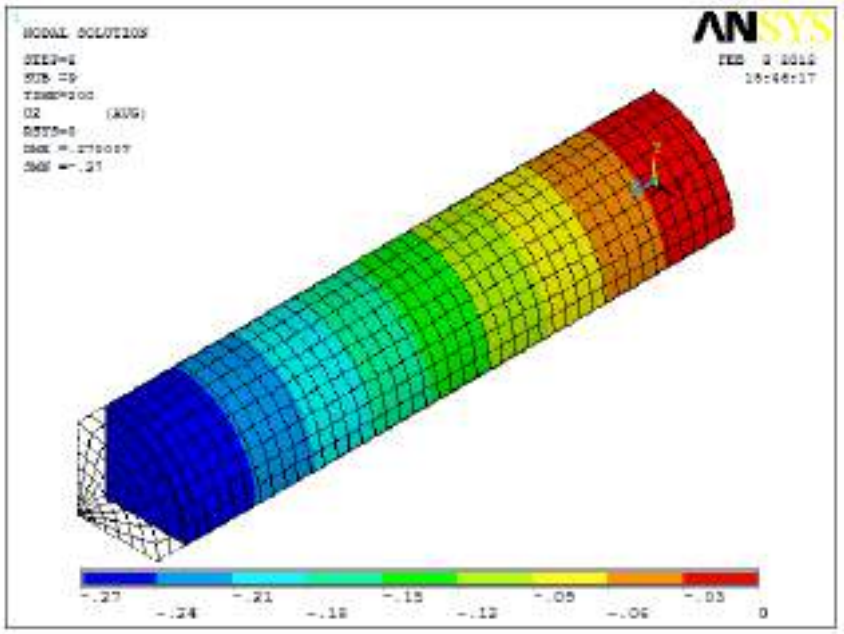

Figure (5.35) Deformed shape of axial displacement for specimen (150*450) mm

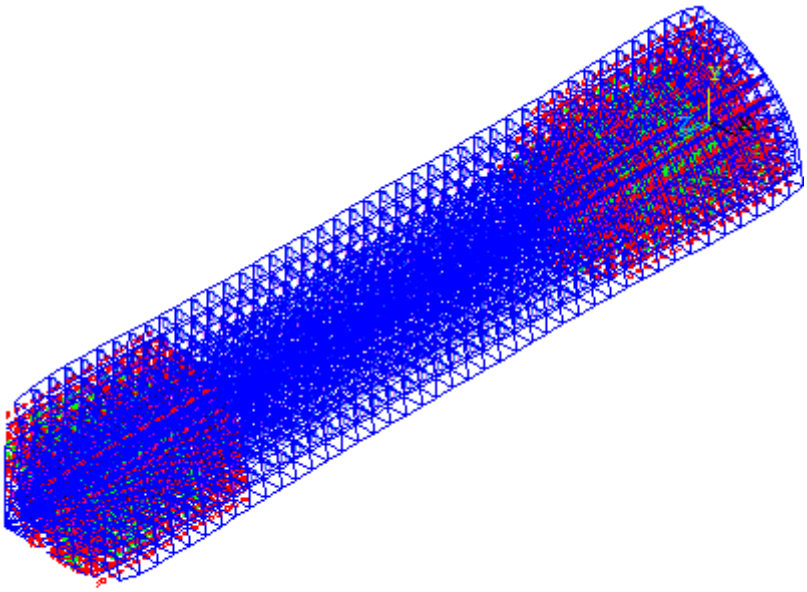

Figure (5.36) Concrete cracking and crushing of concrete specimen with two layers of wire mesh reinforcement

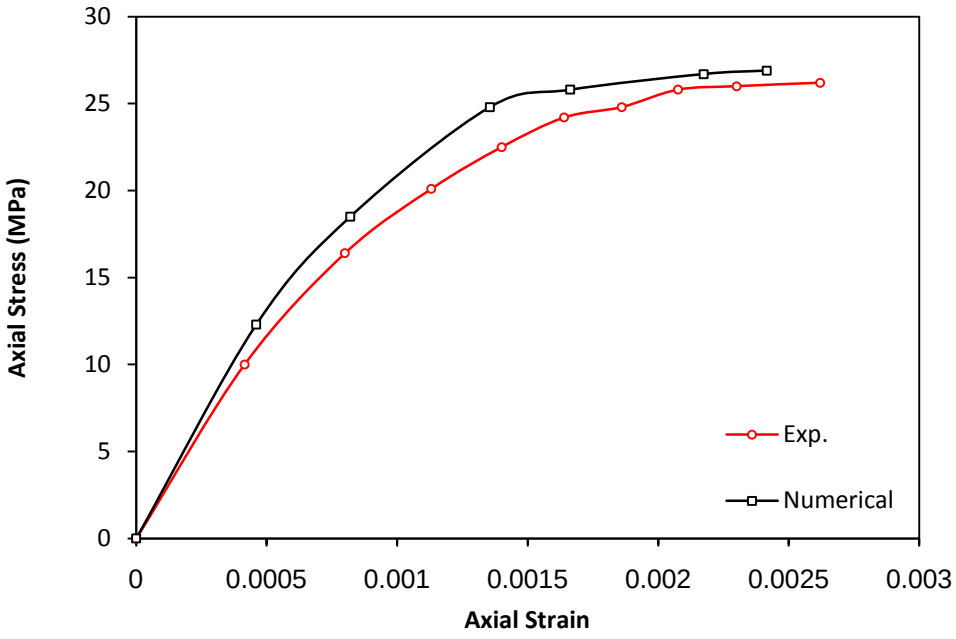

Figure (5.37) Stress-strain relation of monotonic load for 2BM1

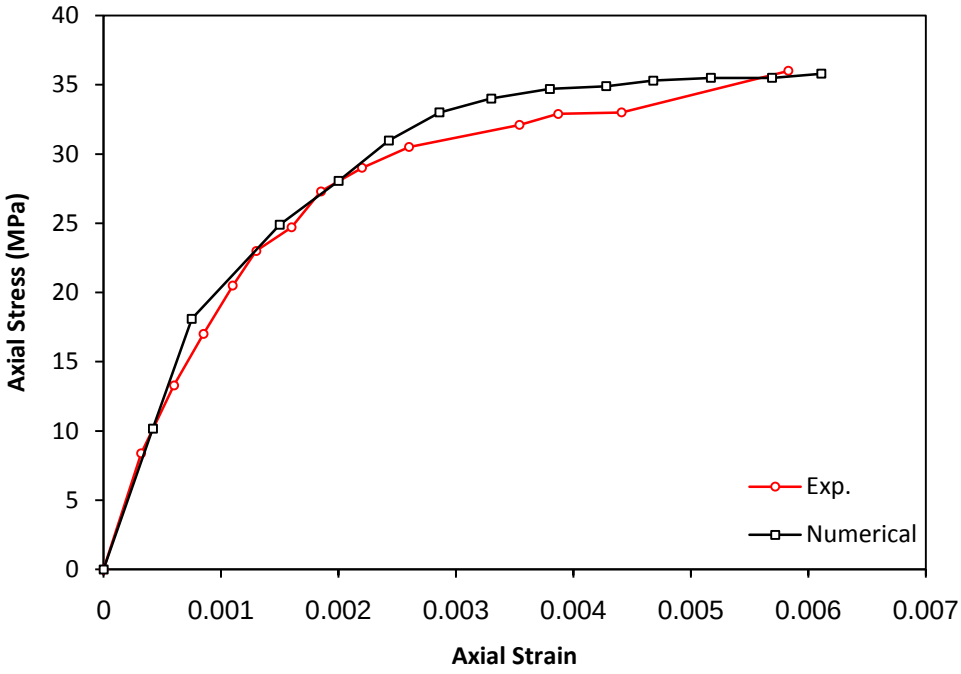

Figure (5.38) Stress-strain relation of monotonic load for 4BM1

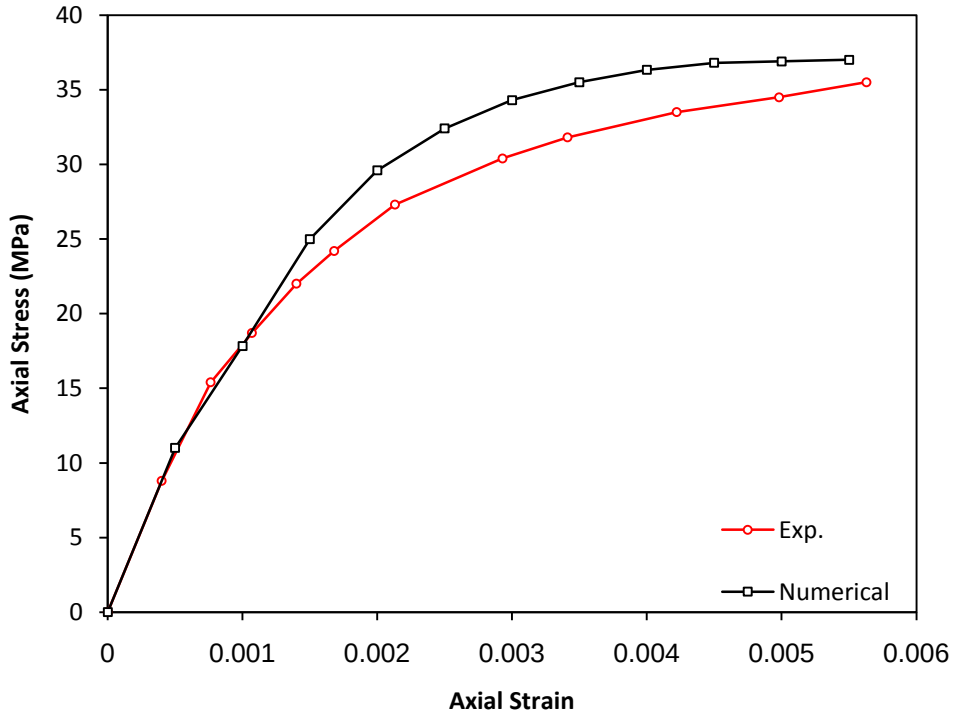

Figure (5.39) Stress-strain relation of monotonic load for 4DM1

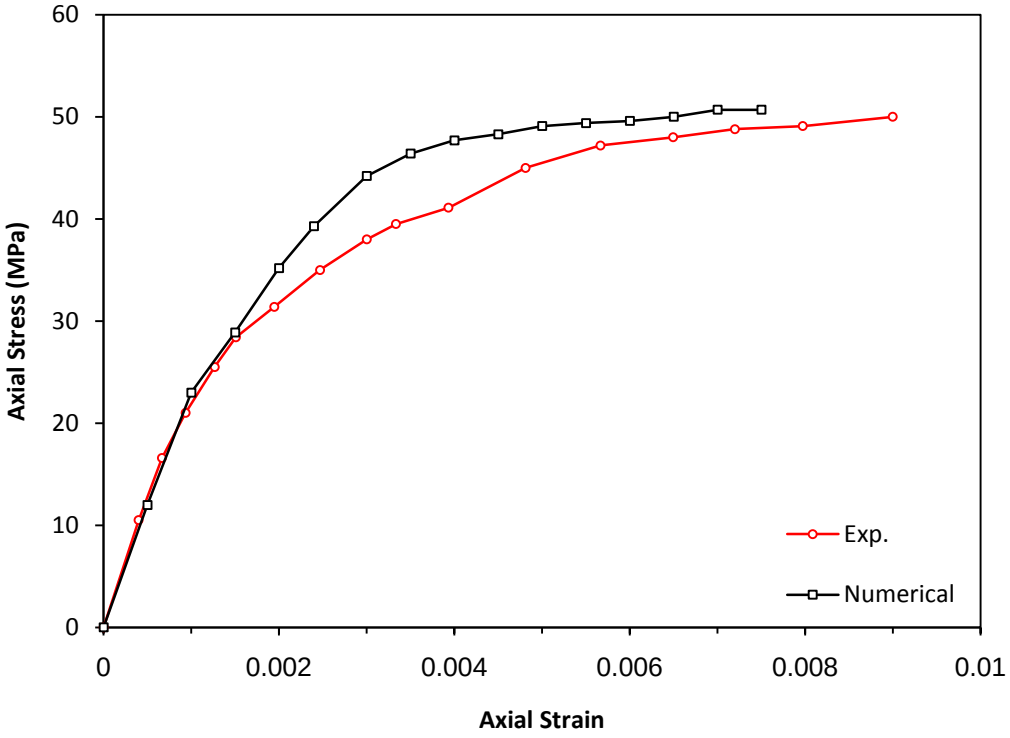

Figure (5.40) Stress-strain relation of monotonic load for 7DM1

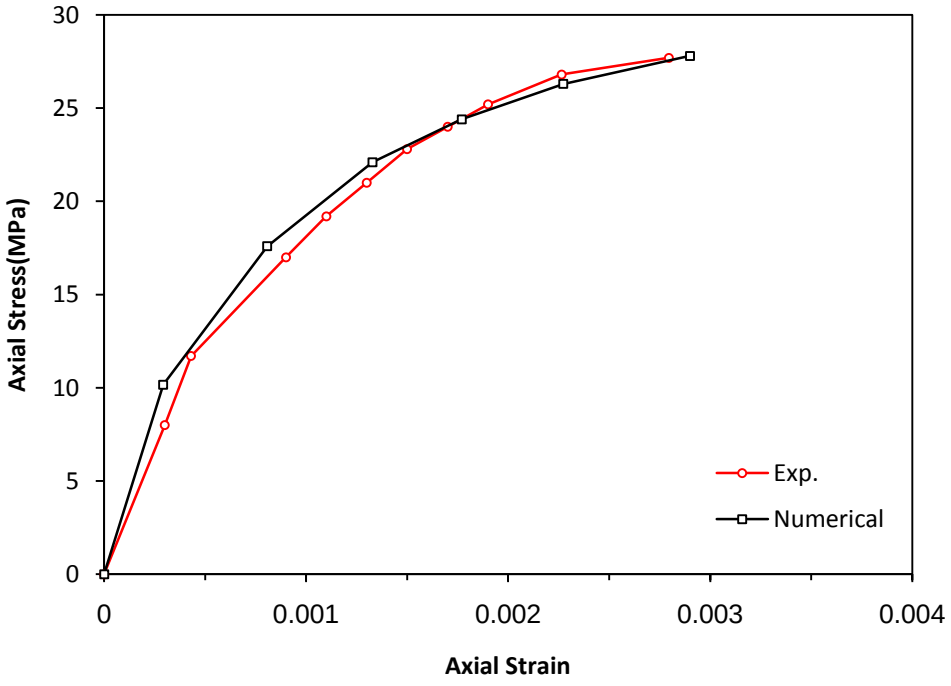

Figure (5.41) Stress-strain relation of monotonic load for 2BM2

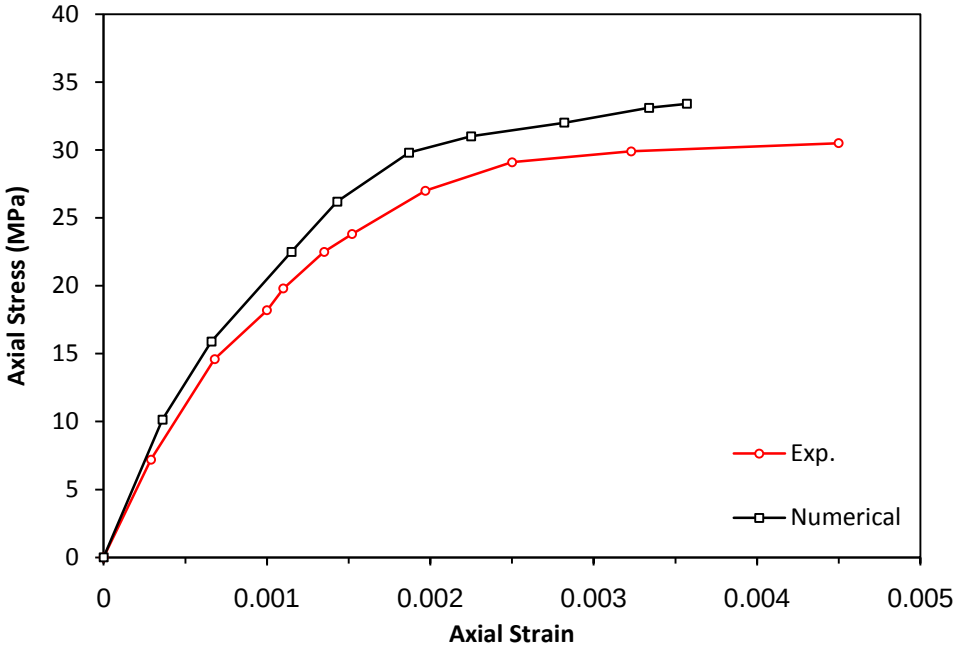

Figure (5.42) Stress-strain relation of monotonic load for 3BM2

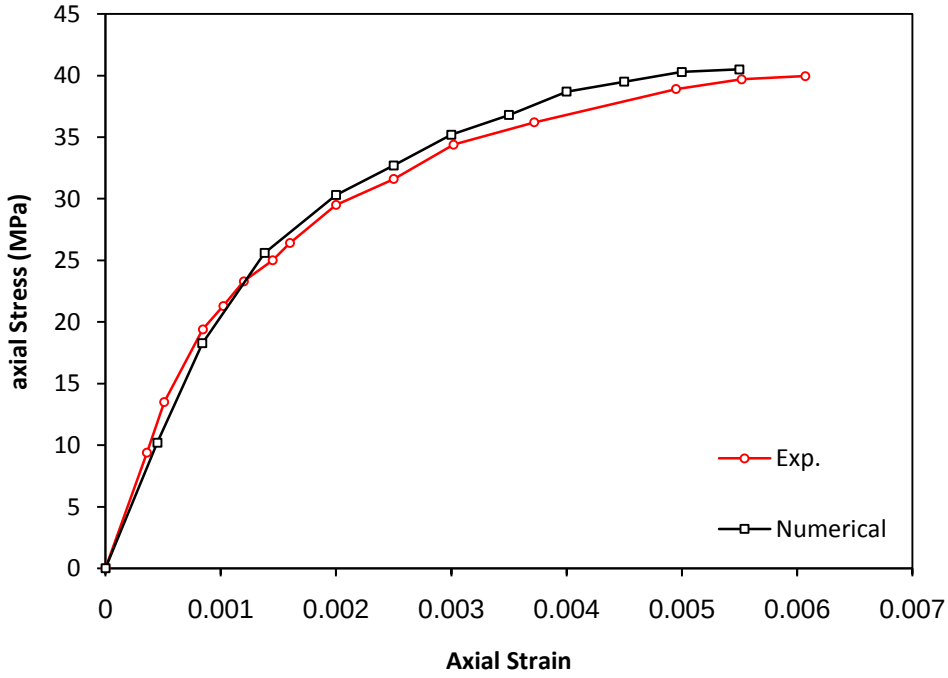

Figure (5.43) Stress-strain relation of monotonic load for 4BM2

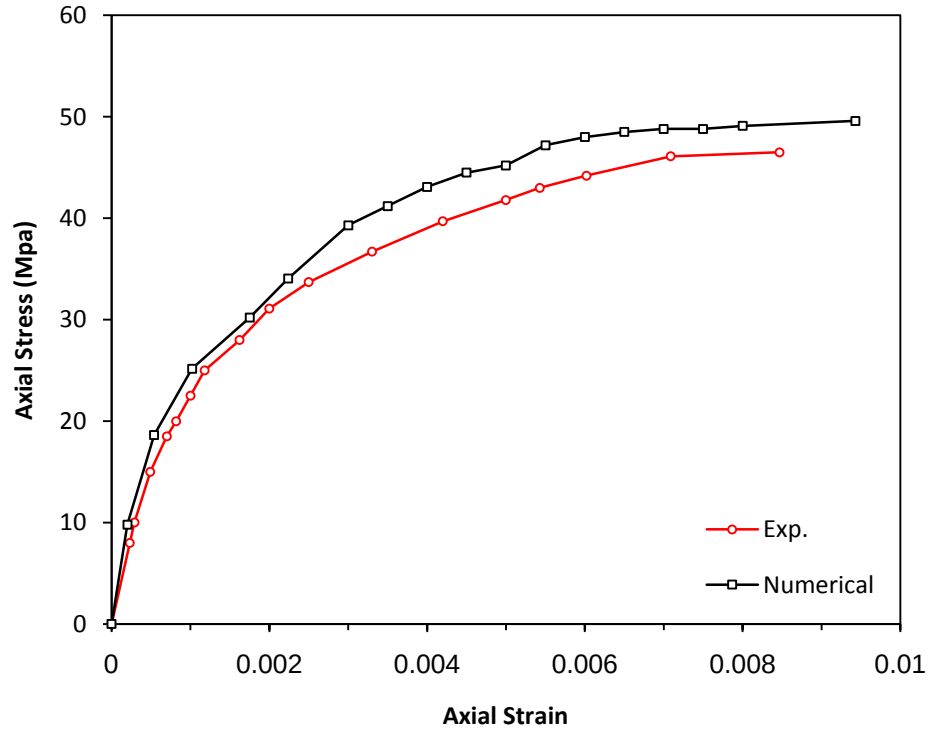

Figure (5.44) Stress-strain relation of monotonic load for 5BM2

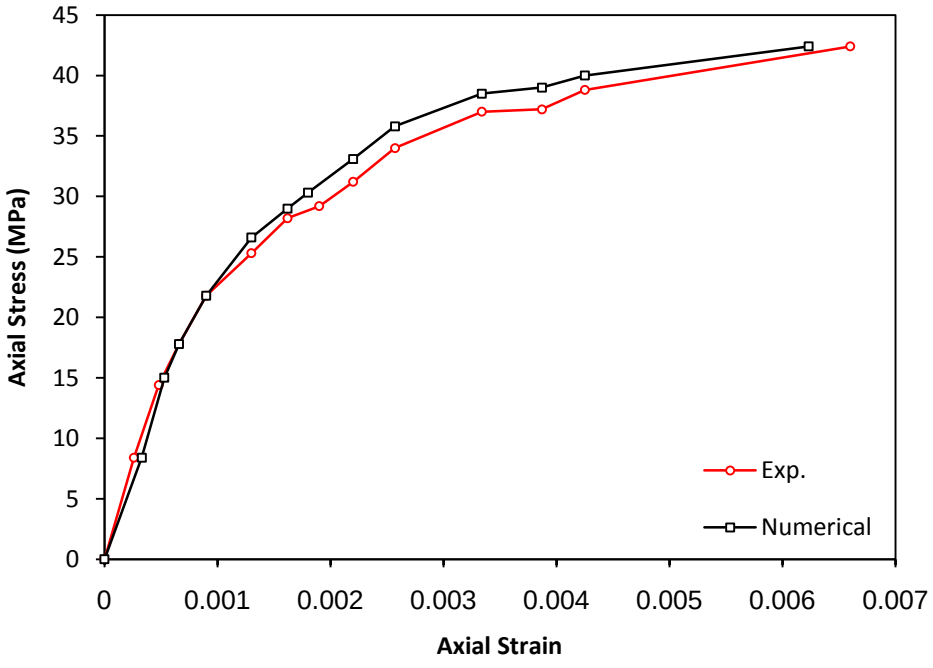

Figure (5.45) Stress-strain relation of monotonic load for 4AM2

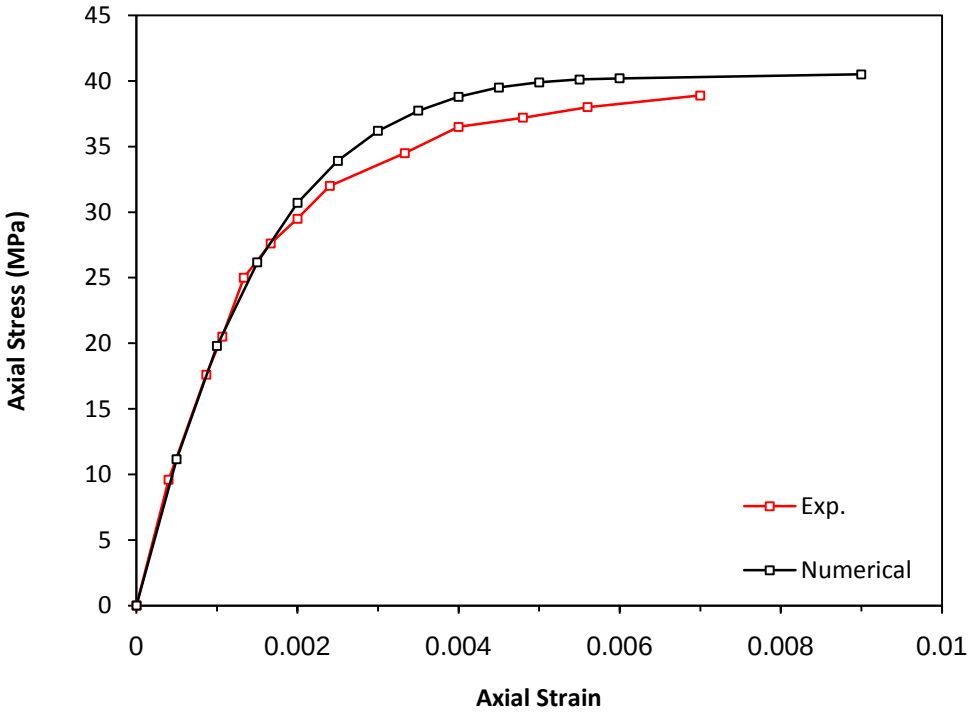

Figure (5.46) Stress-strain relation of monotonic load for 4DM2

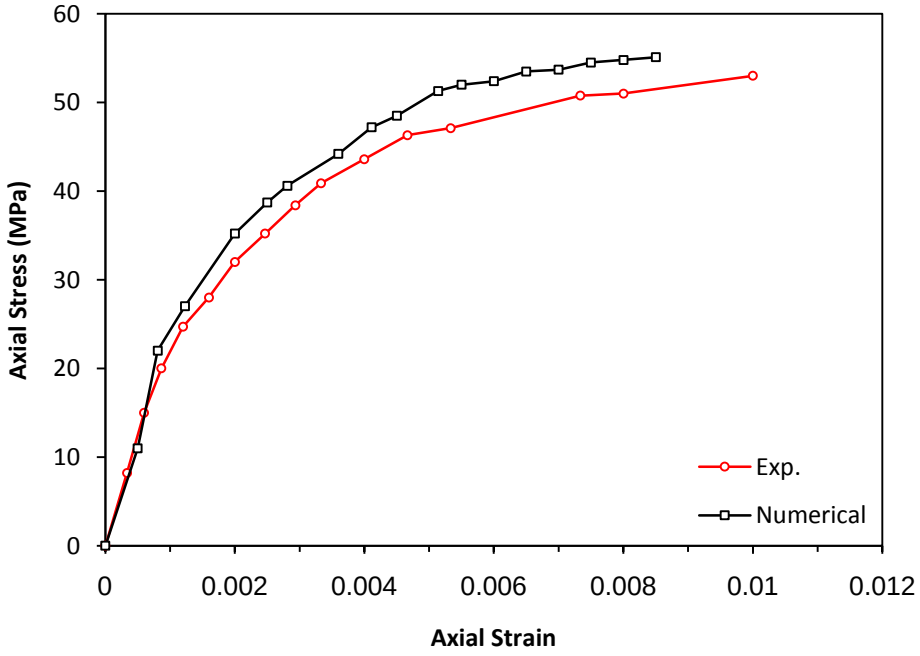

Figure (5.47) Stress-strain relation of monotonic load for 7DM2

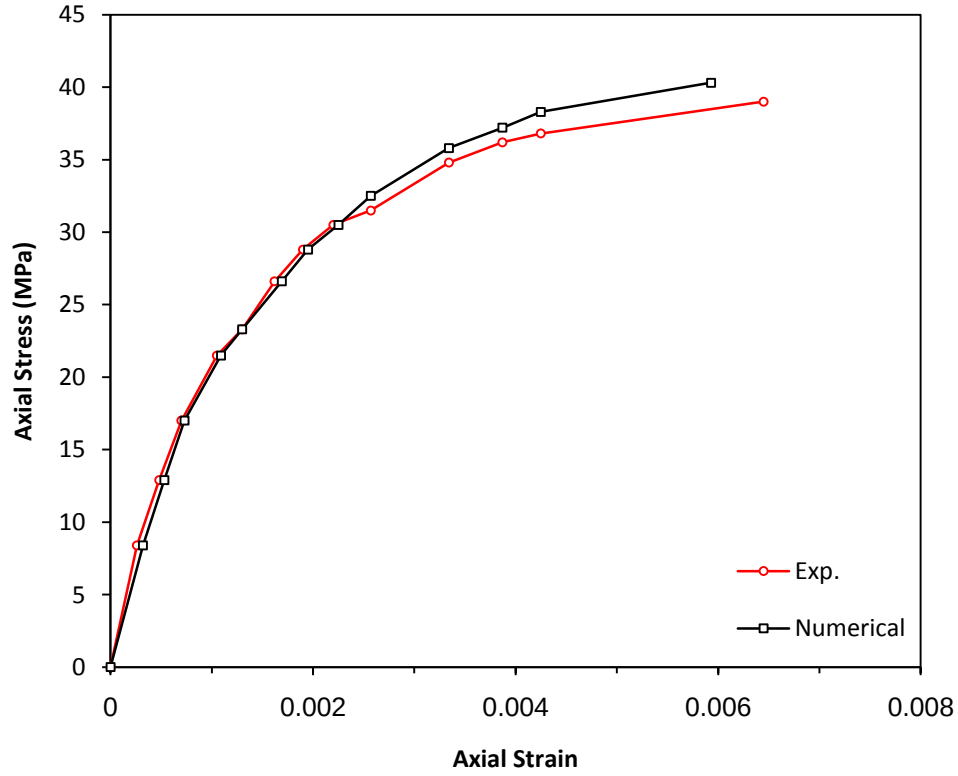

Figure (5.48) Stress-strain relation of monotonic load for 4AM1

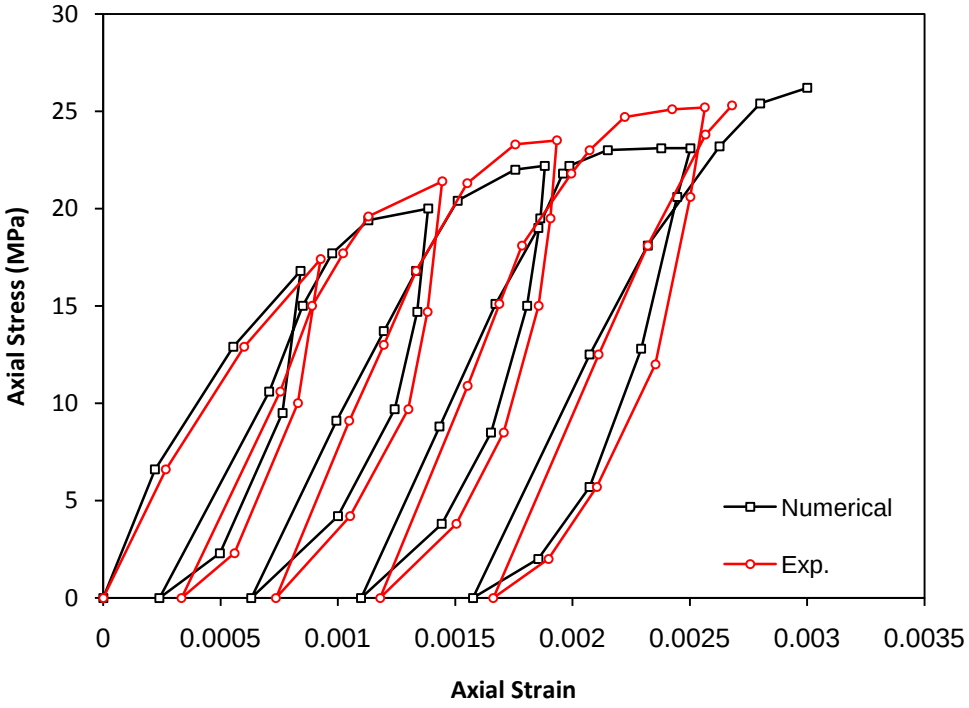

Figure (5.49) Stress-strain relation of cyclic load to envelope for 2BE1

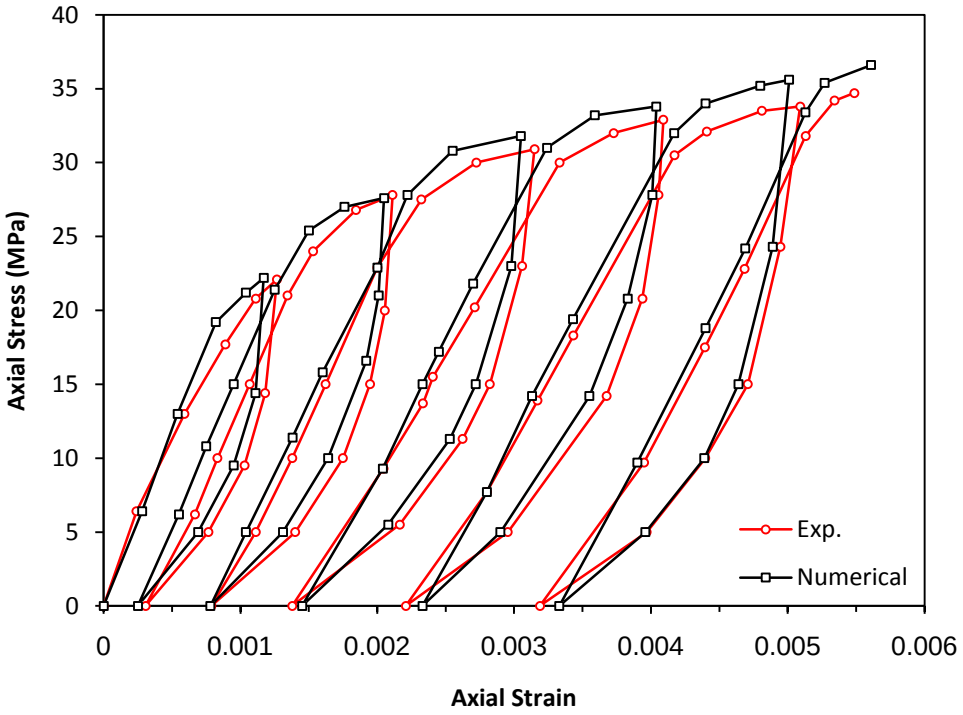

Figure (5.50) Stress-strain relation of cyclic load to envelope for 4BE1

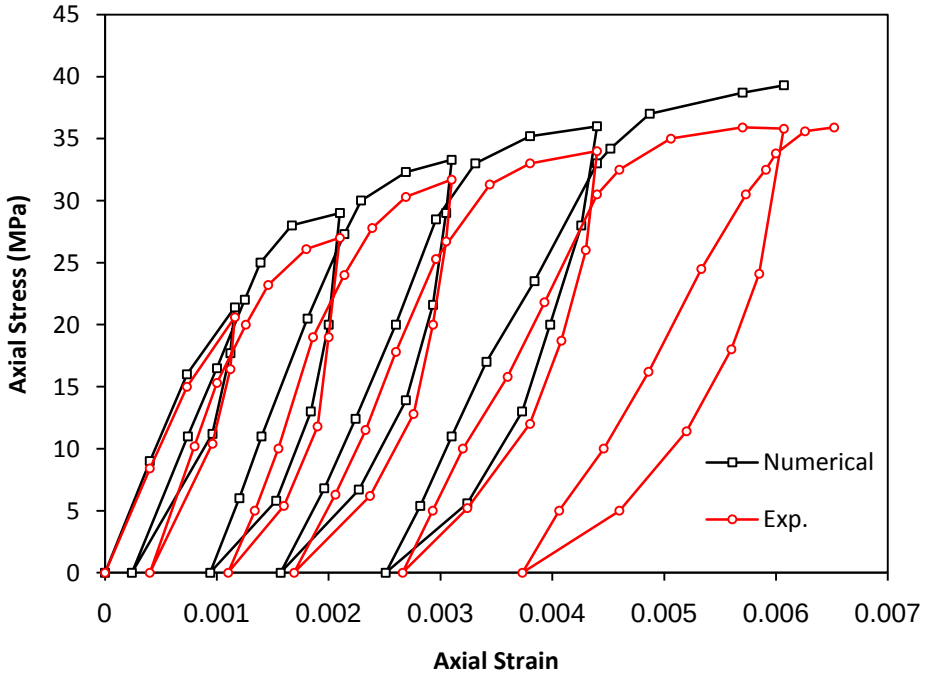

Figure (5.51) Stress-strain relation of cyclic load to envelope for 4DE1

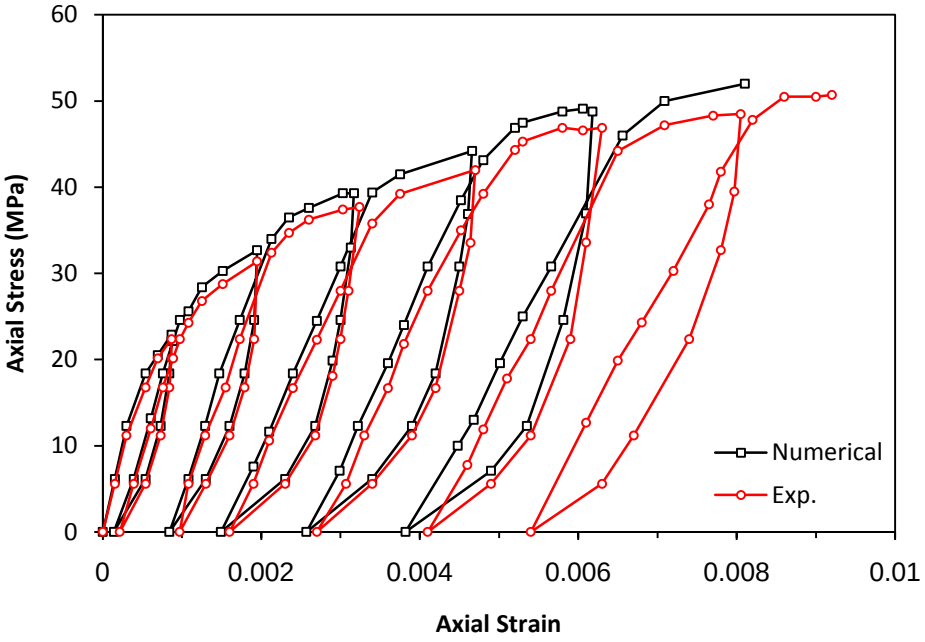

Figure (5.52) Stress-strain relation of cyclic load to envelope for 7DE1

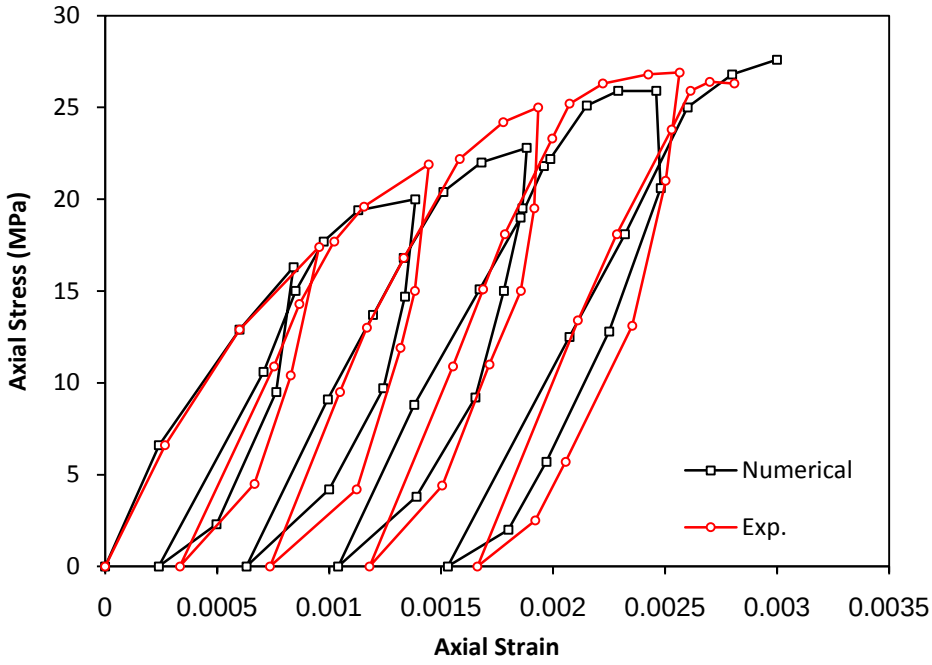

Figure (5.53) Stress-strain relation of cyclic load to envelope for 2BE2

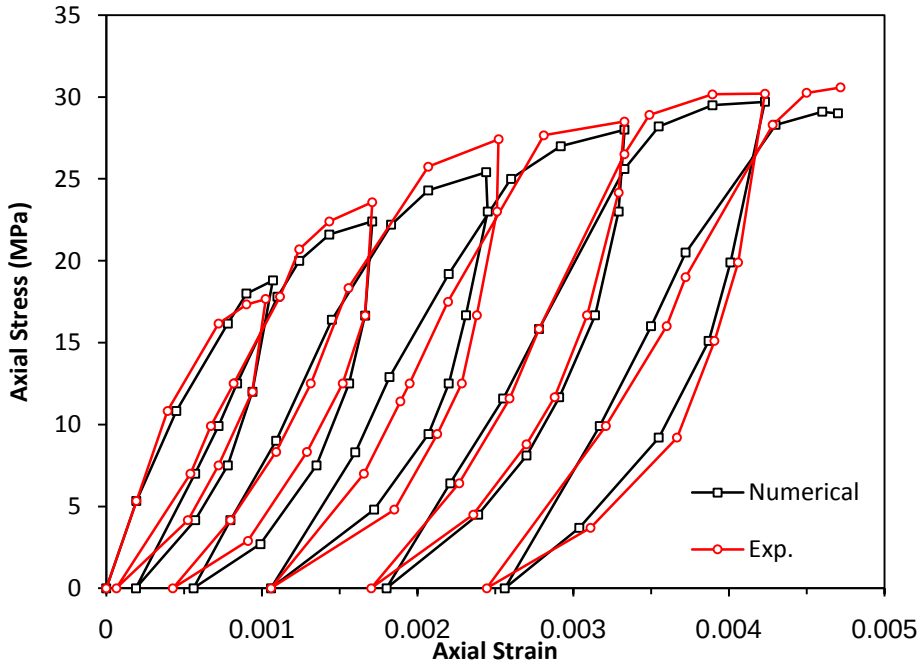

Figure (5.54) Stress-strain relation of cyclic load to envelope for 3BE2

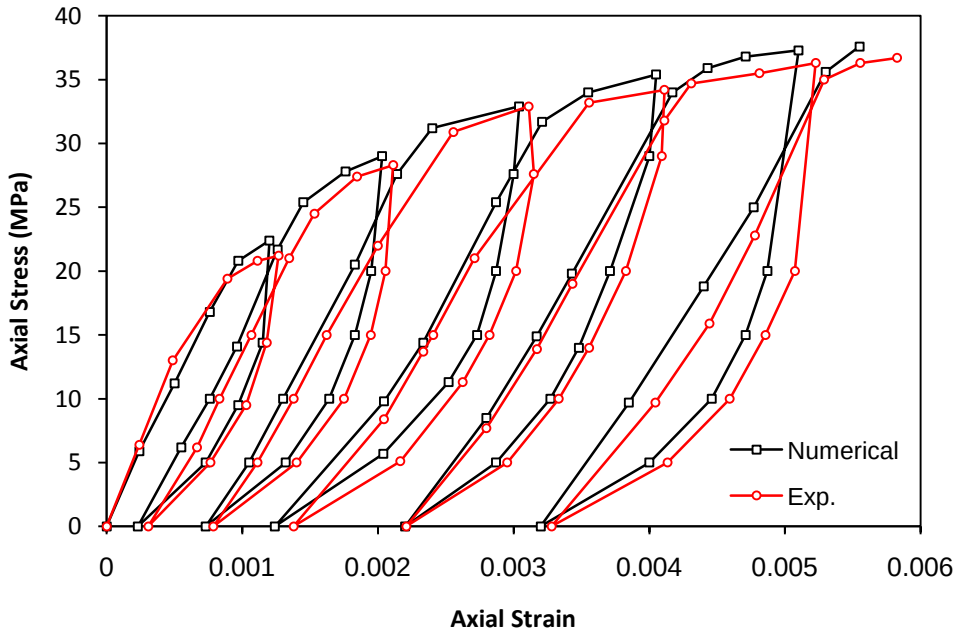

Figure (5.55) Stress-strain relation of cyclic load to envelope for 4BE2

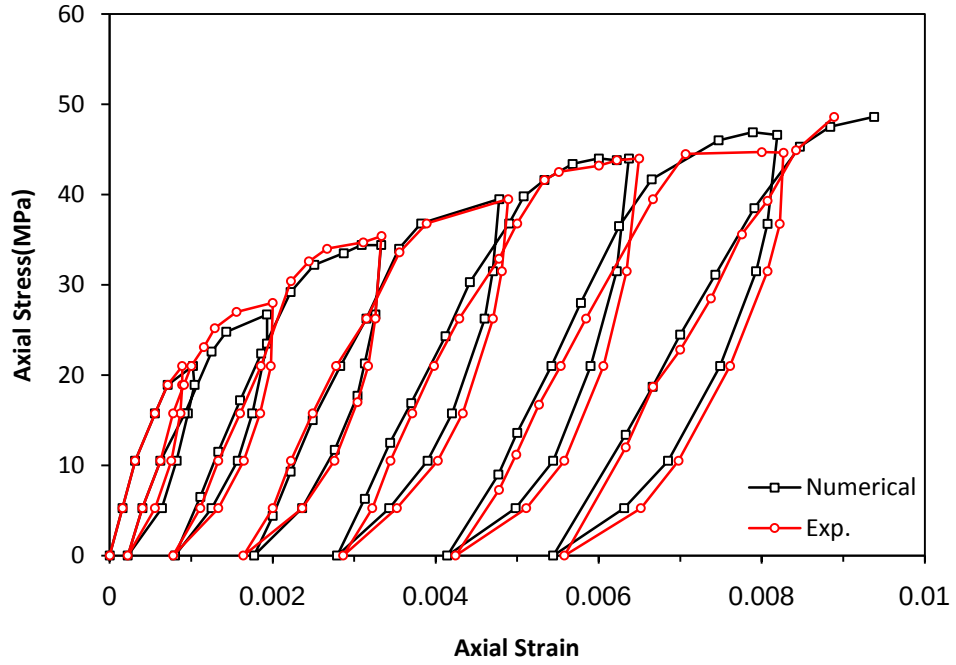

Figure (5.56) Stress-strain relation of cyclic load to envelope for 5BE2

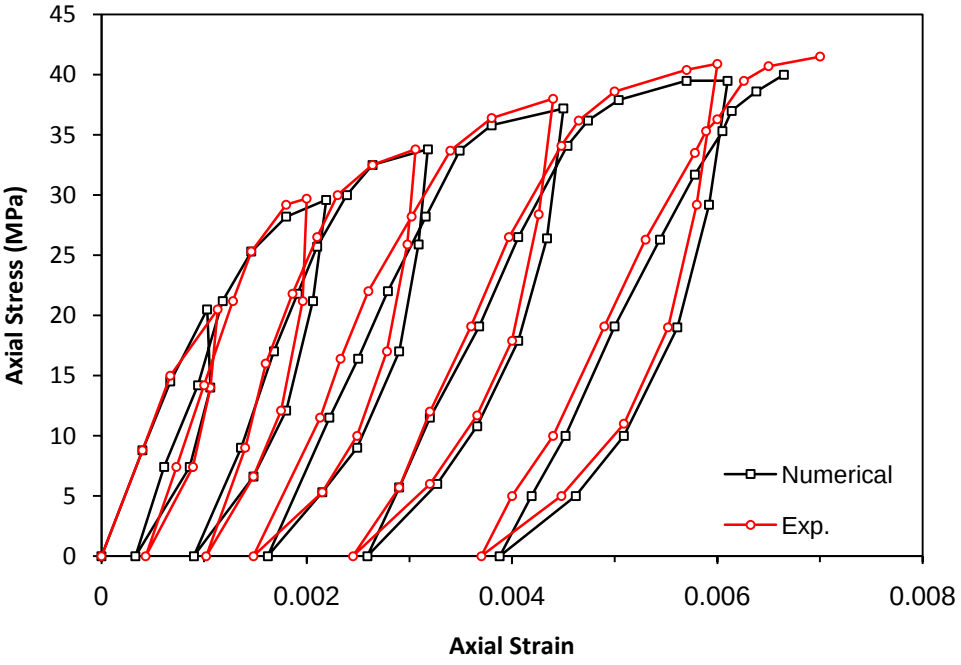

Figure (5.57) Stress-strain relation of cyclic load to envelope for 4DE2

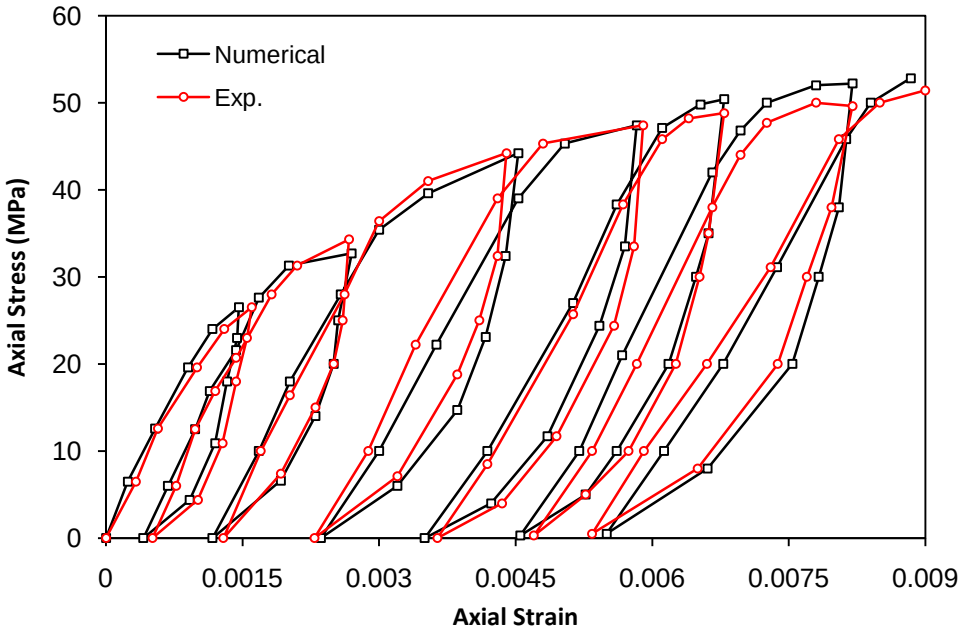

Figure (5.58) Stress-strain relation of cyclic load to envelope for 7DE2

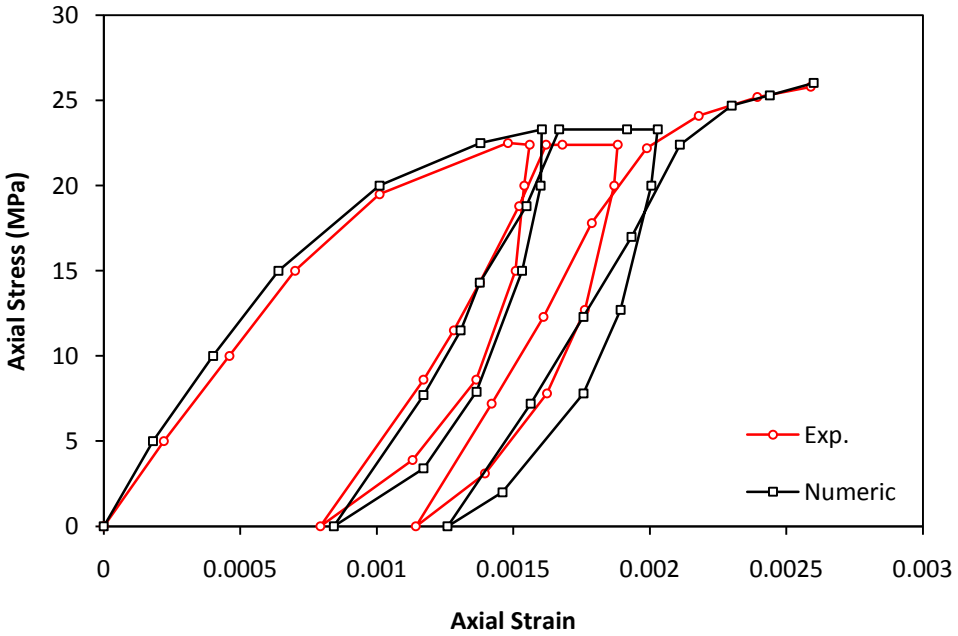

Figure (5.59) Stress - strain relation of cyclic load to 90% of ultimate strength and zero stress level for 2BL1

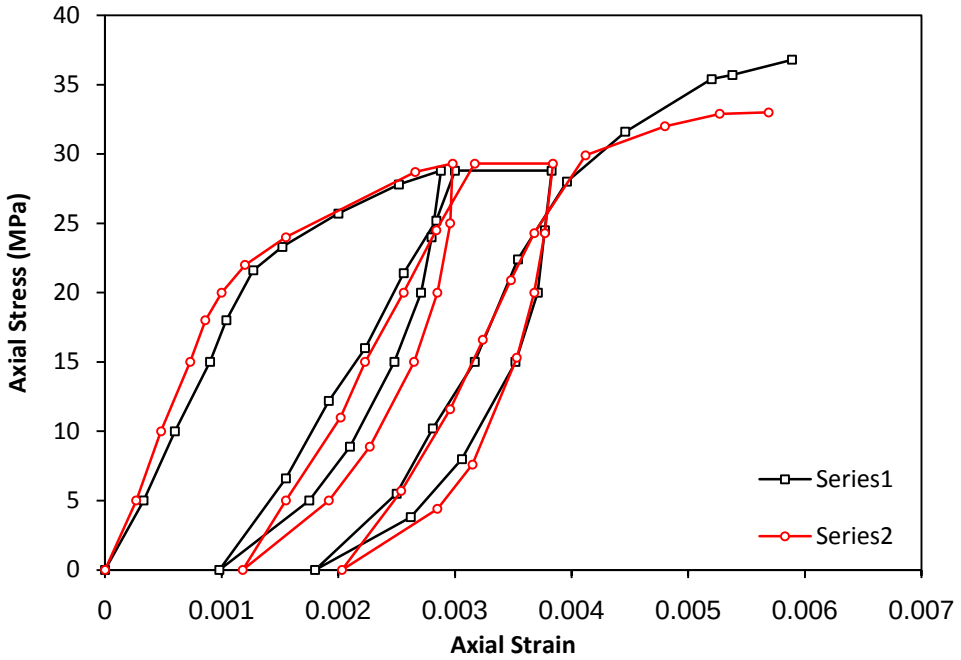

Figure (5.60) Stress - strain relation of cyclic load to 90% of ultimate strength and zero stress level for 4BL1

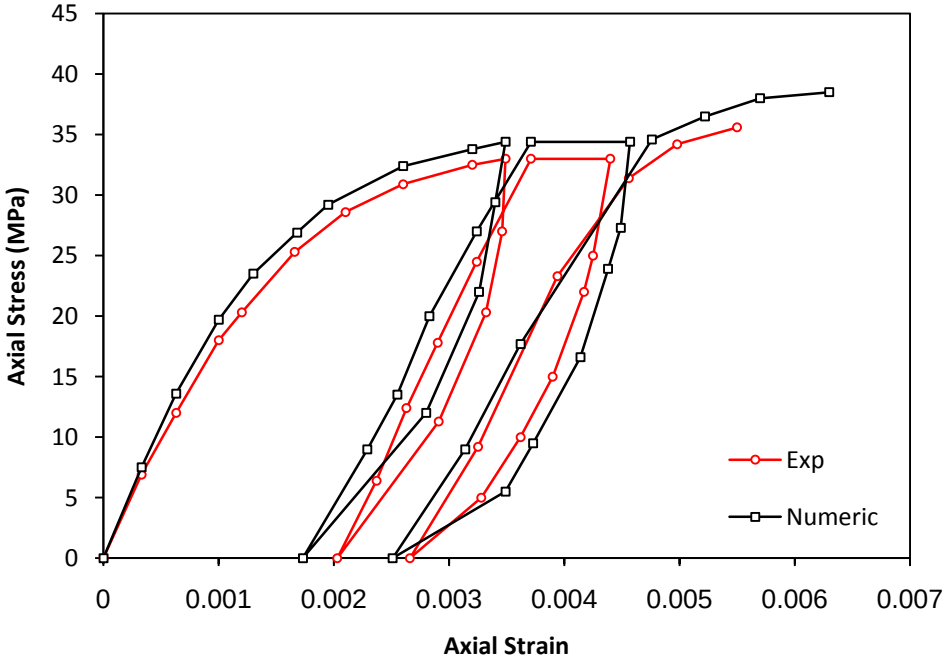

Figure (5.61) Stress - strain relation of cyclic load to 90% of ultimate strength and zero stress level for 4DL1

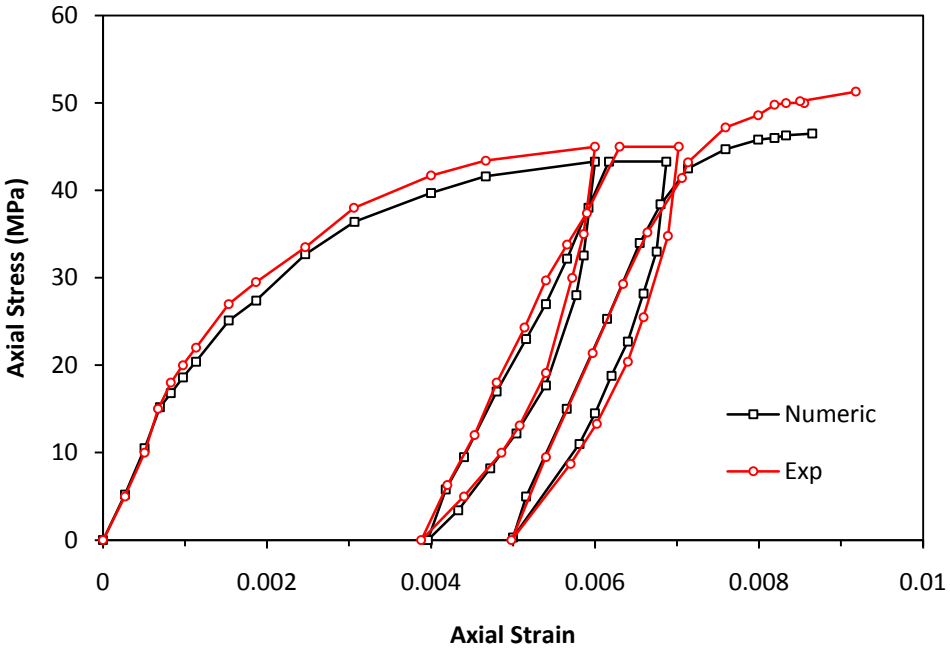

Figure (5.62) Stress - strain relation of cyclic load to 90% of ultimate strength and zero stress level for 7DL1

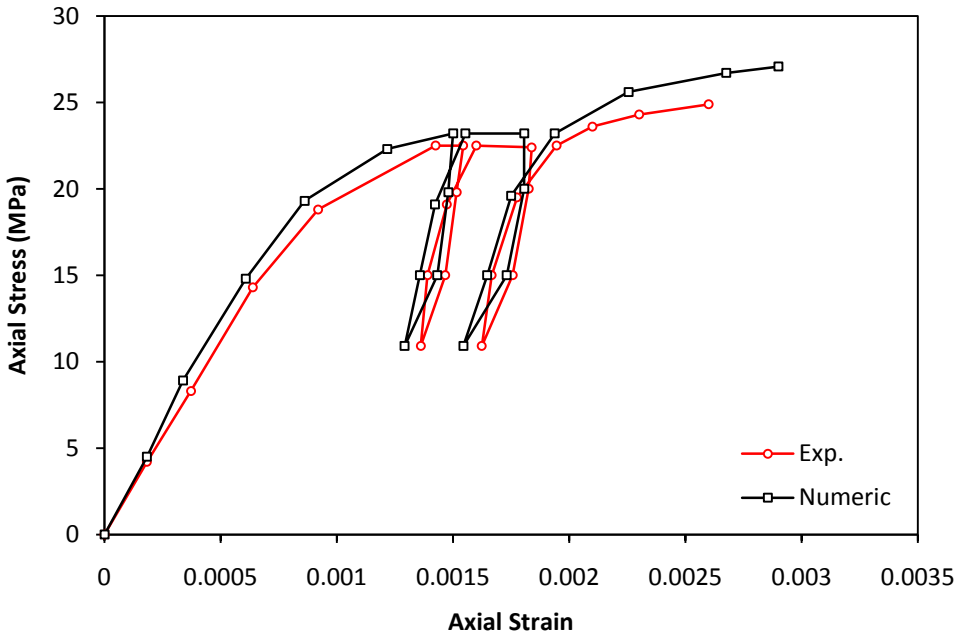

Figure (5.63) Stress - strain relation of cyclic load between (90% - 40%) of ultimate strength for 2BS1

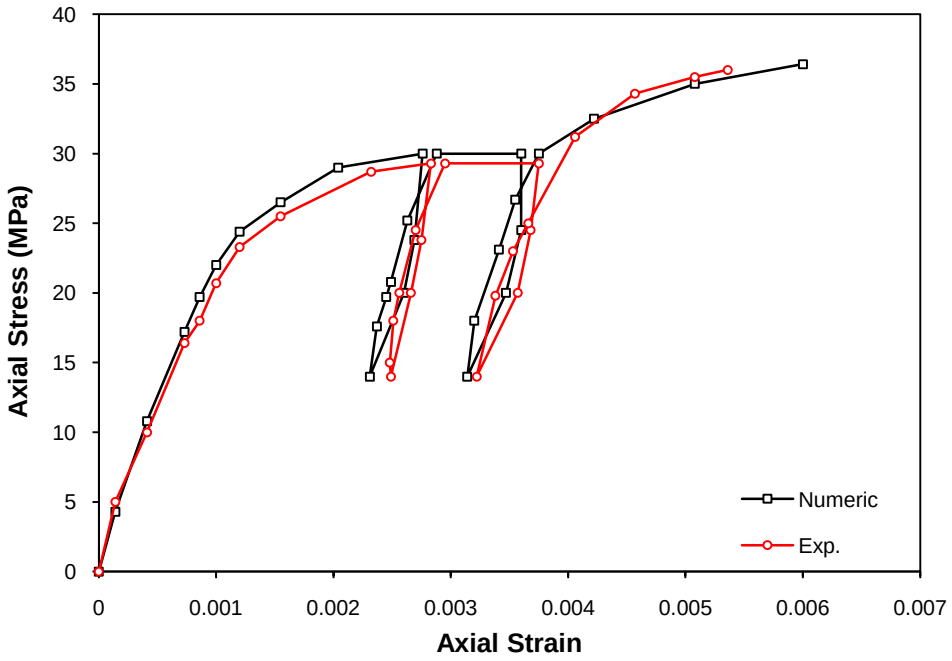

Figure (5.64) Stress - strain relation of cyclic load between (90% - 40%) of ultimate strength for 4BS1

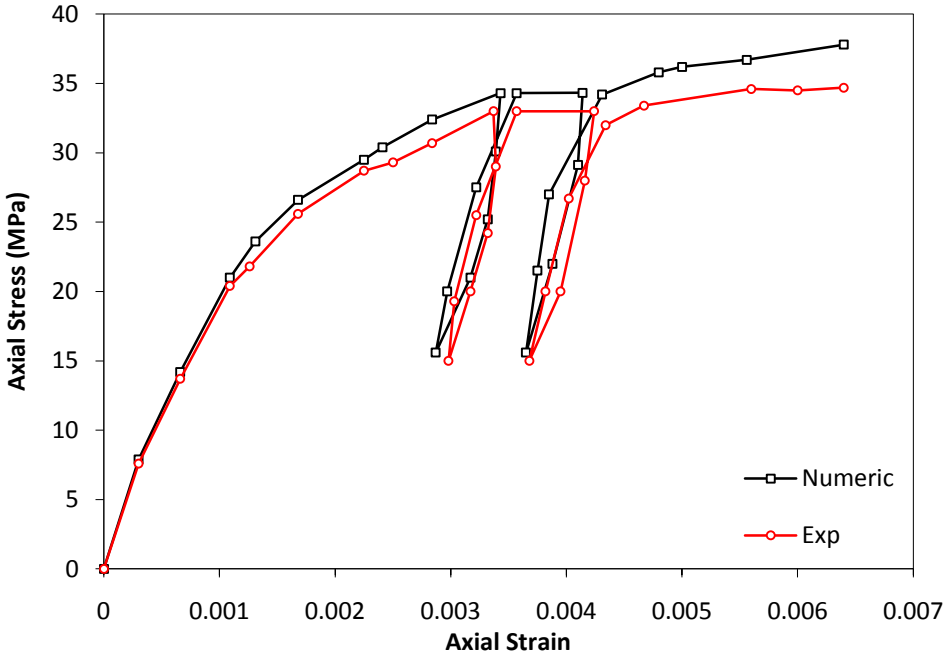

Figure (5.65) Stress - strain relation of cyclic load between (90% - 40%) of ultimate strength for 4DS1

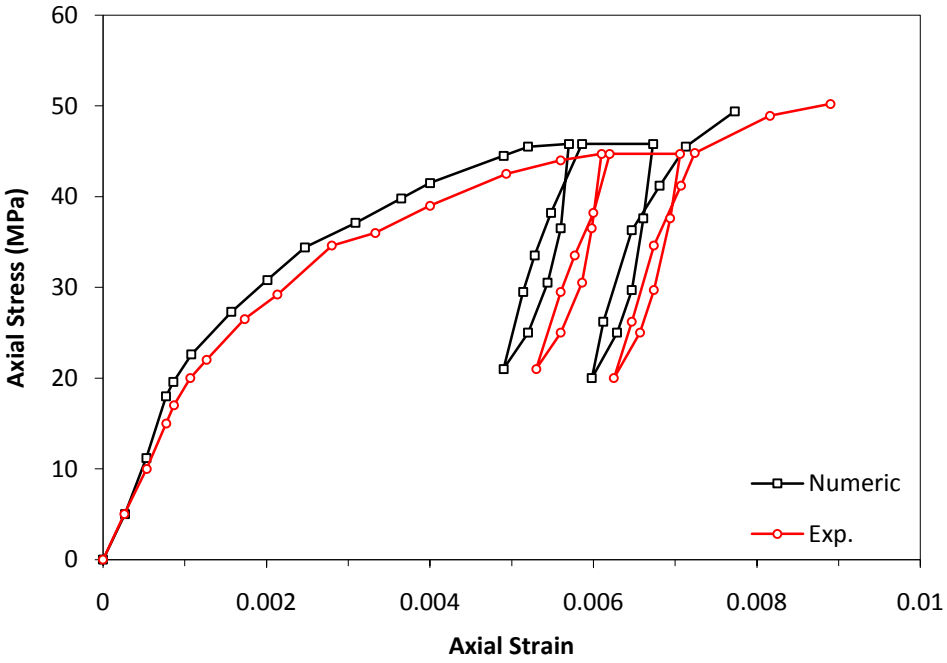

Figure (5.66) Stress - strain relation of cyclic load between (90% - 40%) of ultimate strength for 7DS1

5.3.2 Ultimate Load

The values of ultimate load and ultimate strain for all columns are shown in Table (5.7). It can be seen that the ratios of values of experimental to theoretical ultimate loads are between 0.88 to 1.094 with average value of 0.983 for strengthened concrete columns with ferrocement jackets.

Table (5.7) also gives the experimental (extrapolated) and theoretical values of strain at ultimate loads. The ratios of experimental to theoretical values of strain are between 0.858 to 1.261 with average value of 1.04.

Table (5.7) Ultimate load of tested columns

Group No.	Column designation	P_{Exp} (kN)	ε_{Exp}	P_{Num} (kN)	ε_{Num}	$\frac{P_{Exp}}{P_{Num}}$	$\frac{\varepsilon_{Exp}}{\varepsilon_{Num}}$
J	**4AM1**	743.0	0.00670	715.6	0.00607	1.038	1.104
J1	**2BM1**	463.0	0.002621	475.3	0.00242	0.974	1.083
	2BE1	447.1	0.00268	462.9	0.003	0.966	0.893

Table (5.7) Continued

	2BL1	455. 9	0.00259	460.3	0.0026	0.990	0.996
	2BS1	439.9	0.00260	478.4	0.0029	0.920	0.897
J2	**4BM1**	636.1	0.00583	632.6	0.00611	1.006	0.954
	4BE1	613.2	0.00548	646.7	0.00561	0.948	0.977
	4BL1	583.1	0.00569	650.3	0.00589	0.897	0.966
	4BS1	636.1	0.00536	644.7	0.0061	0.987	0.879
J3	**4DM1**	1115.3	0.00563	1162.4	0.0055	0.959	1.024
	4DE1	1127.8	0.00652	1234.6	0.0061	0.914	1.069
	4DL1	1171.8	0.00655	1162.5	0.00587	1.008	1.116
	4DS1	1090.1	0.00640	1187.4	0.0064	0.918	1.000
J4	**7DM1**	1570.8	0.00900	1592.8	0.0075	0.986	1.200
	7DE1	1592.8	0.00920	1633.6	0.0081	0.975	1.136
	7DL1	1611.6	0.00918	1473.4	0.00865	1.094	1.061
	7DS1	1577.1	0.00890	1552.2	0.00789	1.016	1.128
J5	**2BM2**	489.5	0.00280	475.7	0.00248	1.029	1.124
	2BE2	464.7	0.00281	450.0	0.00249	1.033	1.129
	2BL2	455.9	0.00295	420.2	0.00249	1.085	1.185
	2BS2	459.4	0.00307	406.9	0.00248	1.129	1.233
J6	**3BM2**	538.9	0.00450	590.2	0.00357	0.913	1.261
	3BE2	540.3	0.004718	512.4	0.0047	1.054	1.004
	3BL2	530.1	0.00520	546.3	0.00415	0.970	1.253
	3BS2	556.6	0.00493	533.9	0.00392	1.043	1.258
J7	**4BM2**	705.9	0.00607	715.6	0.00550	0.986	1.104
	4BE2	648.5	0.00583	664.4	0.00555	0.976	1.050
	4BL2	671.5	0.00602	687.3	0.00522	0.977	1.153
	4BS2	676.8	0.00569	691.8	0.00581	0.978	0.979
J8	**5BM2**	821.7	0.00847	876.4	0.00943	0.938	0.898
	5BE2	858.8	0.00889	858.8	0.00938	1.000	0.948
	5BL2	759.8	0.00815	863.4	0.00894	0.880	0.912
	5BS2	812.8	0.00815	875.6	0.00950	0.928	0.858
J9	**4AM2**	749.2	0.00660	749.2	0.00623	1.000	1.059

TABLE (5.7) Continued

J10	**4DM2**	1222.1	0.007	1272.4	0.009	0.920	0.897
	4DE2	1303.8	0.007	1303.7	0.007	1.006	0.954
	4DL2	1288.1	0.00731	1288.2	0.0085	0.948	0.977
	4DS2	1193.8	0.0064	1293.6	0.0088	0.897	0.966
J11	**7DM2**	1665.05	0.01	1731.1	0.0085	0.987	0.879
	7DE2	1646.2	0.01018	1658.8	0.00885	0.959	1.024
	7DL2	1269.2	0.00893	1715.3	0.0086	0.914	1.069
	7DS2	1319.5	0.00933	1679.9	0.0092	1.008	1.116
J12	**100AM**	180.5	0.00290	189.7	0.00285	0.952	1.017
J13	**100BM**	177.33	0.00257	166.7	0.00266	1.064	0.966
J14	**150DM**	405.5	0.00253	387.4	0.00243	1.047	1.041
J15	**150AM**	390.3	0.00253	388.6	0.00255	1.004	0.992
J16	**150BM**	388.7	0.00249	398.2	0.00237	0.976	1.050
J17	**200DM**	703.4	0.00266	712.6	0.00257	0.987	1.035
mean						0.983	1.04
Standard deviation						0.054	0.107

5.3.3 Parametric Study

To investigate the effect of some material and solution parameters on the nonlinear finite element analysis of concrete columns strengthened with ferrocement jackets, column J1 for small size and column J2 for large size have been chosen to carry out this study. The parameters considered are the concrete compressive strength, applied load on ferrocement jackets and modulus of elasticity of ferrocement jackets. In each numerical test, one parameter has been considered to vary while the other parameters being held constants in order to isolate the effects of the parameters considered. In the following sections, the effect of each parameter considered in this study is described.

5.3.3.1 Effect of Concrete Compressive Strength

In order to study the effect of using different values of compressive strength of concrete f_c' on the overall behavior of the concrete columns strengthened with ferrocement jackets, the concrete column J1 and J3 have been analyzed for different values of f_c'. The values considered are 30, 35 and 40 MPa. Figures (5.67) and (5.68) show the effect of this parameter on the response of strengthened concrete column represented by the stress-strain relationships.

It is obvious from these figures that the ultimate capacity of the concrete column increases with the increase of the compressive strength f_c'.

Figure (5.69) shows a plot of the confinement effectiveness f'_{cc}/f'_{co} versus the unconfined concrete strength f'_{co} for specimens with two and four layers of wire mesh reinforcement. It is evident that as the unconfined concrete strength increase, the confinement effectiveness decreases. The strengthened specimens with ferrocement jacket having the least f'_{co} show the maximum increase in confined stress.

Table (5.8) shows the ultimate loads obtained for different values of concrete compressive strength. The increase of the concrete compressive strength leads to higher ultimate loads. The increase in axial strength in term of confinement effectiveness f'_{cc}/f'_{co} decreases from a maximum of 83.2% and 26.8% for the specimen having unconfined compressive strength of 22 MPa to 37.5% and 14.3% for the specimen having unconfined compressive strength of 40MPa for specimens strengthened with two and four layers of wire mesh reinforcement respectively. Maximum confined concrete strength is observed in the case of specimen having 22 MPa grade of concrete.

Table (5.8) Ultimate load of specimens with different concrete strength

No. of Layer	f'_{cc} (MPa)	f'_{co}(MPa)	f'_{cc}/f'_{co}
2	36.2	30.0	1.21
	41.0	35.0	1.17
	45.7	40.0	1.14
4	48.0	30.0	1.60
	52.5	35.0	1.50
	55.0	40.0	1.38

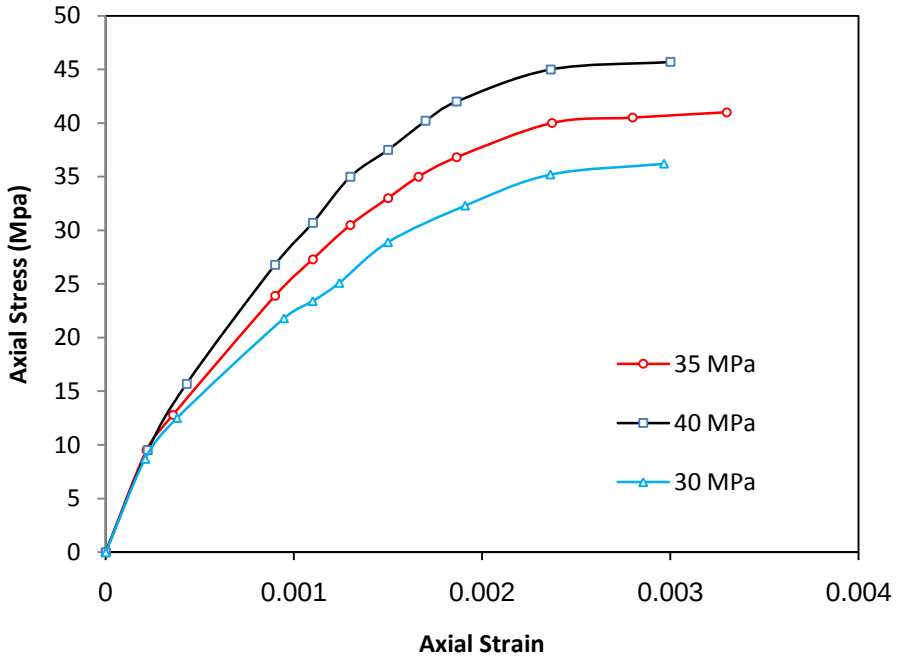

Figure (5.67) Effect of concrete compressive strength for column with 2 layers of wire mesh

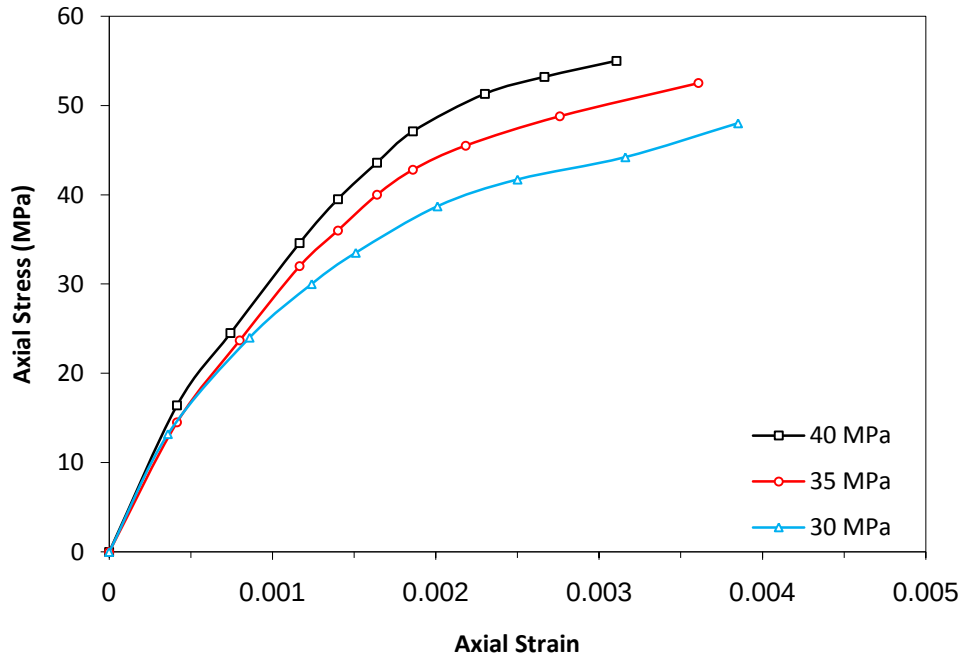

Figure (5.68) Effect of concrete compressive strength column with 4 layers of wire mesh

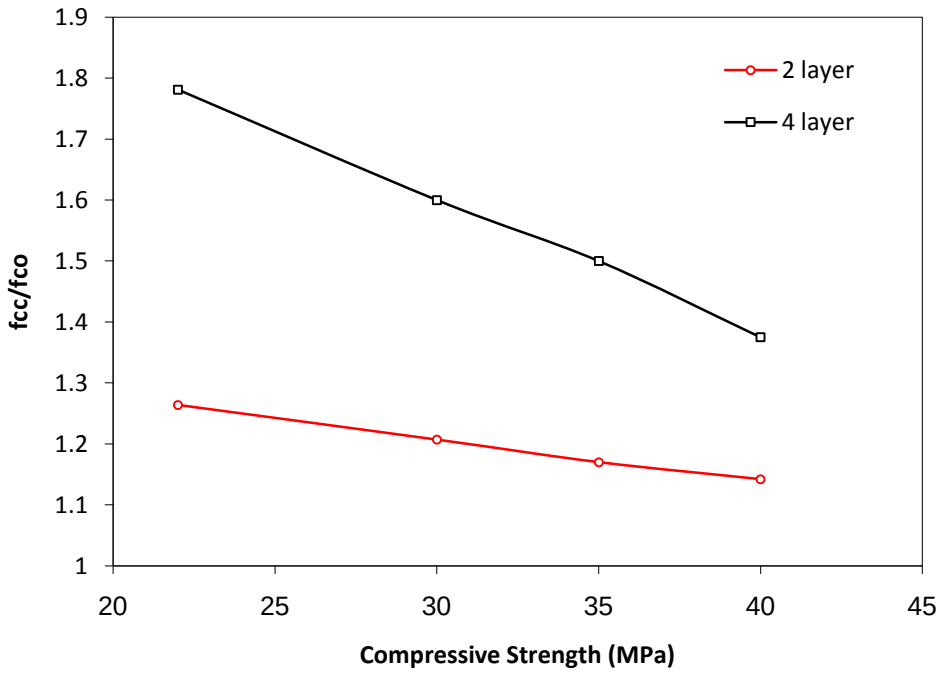

Figure (5.69) Effect of concrete compressive strength on confinement (2 layer of wire mesh)

5.3.3.2 Effect of Loading the Ferrocement Shell in the Axial Direction

The effect of loading the shell in the axial direction simultaneously with the concrete core can be illustrated by comparing results of experimentally tested columns (2BM2, 3BM2, 4BM2, and 5BM2) with another group of columns for which concrete cores only were axially loaded. The results of this effect are shown in Table (5.9) for comparison. From Table (5.9), it is clearly shown that the specimens loaded through both core and shell showed less strength under the same other parameters. This is mainly attributed to the fact that the ferrocement jackets were axially loaded, therefore, they expanded outward due to Poisson's ratio effect under their own share of axial load, which results in less confinement pressure on concrete. Another factor is that the shells are also axially loaded and lateral tension reduces their tensile strength in the hoop direction. On the other hand, the ferrocement shells in the second group are fully utilized in the hoop direction only, under uniaxial tensile stresses which allow the development of their tensile strengths.

Table (5.9) Effect of Loading of ferrocement shell on ultimate strength

No. of Layer	f'_{cc} (MPa) Exp.	f'_{cc} (MPa) Num.	f'_{cc}/f'_{co} Exp.	f'_{cc}/f'_{co} Num.
2	27.70	29.26	1.26	1.33
3	30.50	36.52	1.39	1.66
4	39.90	43.34	1.82	1.97
5	46.00	48.18	2.10	2.19

5.3.3.3 Effect of Modulus of Elasticity of Ferrocement Shell

In order to study the effect of modulus of elasticity of ferrocement shell (E_s) on the behavior of strengthened concrete columns, different values of (E_s)

have been considered. The selected values for this parameter are $35x10^3$, $38x10^3$, $41x10^3$ and $44x10^3$MPa. Figure (5.70) shows the stress-strain relationships obtained from the finite element model for the selected values of (E_s). The ultimate loads obtained from this study are listed in Table (5.10). The table shows that the increase of the modulus of elasticity of ferrocement jacket from $35x10^3$MPa to $44x10^3$MPa leads to an increase in the ultimate load of 24.5%. From the figures, it can be seen that the effect of the stiffness of the ferrocement jacket on the stress-strain relation is insignificant in the first region and the ferrocement shells are activated gradually in region two. Once the ferrocement shells are fully activated, the effect of the stiffness of the ferrocement layers on the stress-strain is substantial.

Table (5.10) Ultimate Loads for Different Values of Modulus of Elasticity of ferrocement shell

Specimen No.	Modulus of Elasticity (MPa)	Load (kN)	Displacement (mm)
1	35 000	777.04	2.619
2	38000	842.38	2.750
3	41000	900.66	2.439
4	44000	967.77	2.327

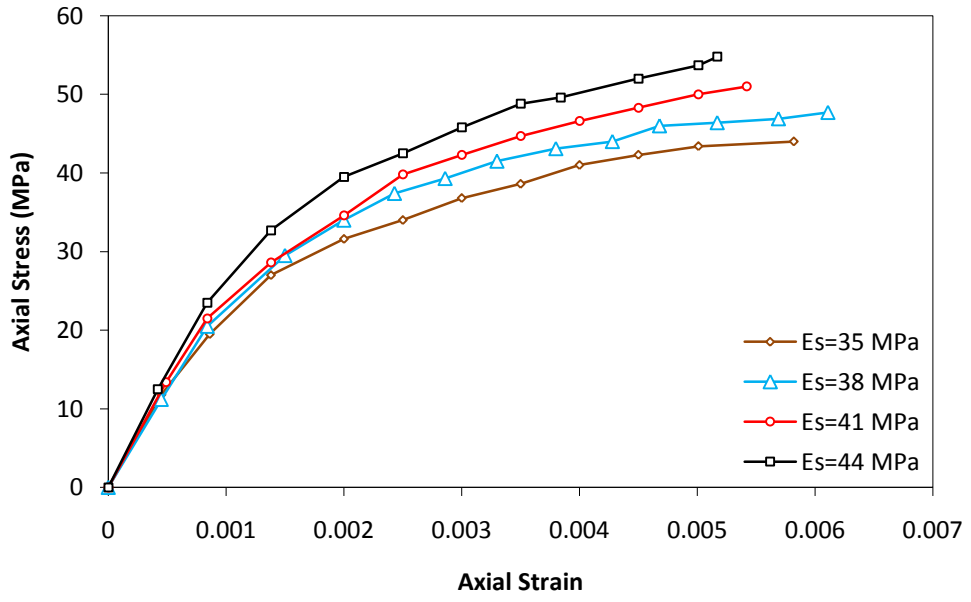

Figure (5.70) Effect of modulus of elasticity of ferrocement jacket on column strength

5.4 Proposed Stress-Strain Relationship of Confined Concrete by Ferrocement Jacket

The results shown in the previous section clearly indicated that confinement produced by ferrocement jackets leads to enhancement of concrete strength under axial loading. In addition, use of ferrocement jacket in columns improves ductility of concrete. The strength and ductility enhancement of concrete by confinement gives a considerable influence on stress strain relationship of concrete. Therefore, stress-strain relationship of confined concrete is quite different from that of unconfined concrete. The stress-strain relationship of confined concrete provides a better understanding of the behavior of the strengthened columns with ferrocement jacket. Also the stress-strain relationship of confined concrete is essential in predicting the response of the strengthened concrete column members.

5.4.1 Stress-Strain Relation for Confined Concrete under Monotonic Loading

Based on the test results, a new model for stress-strain relation of confined concrete by ferrocement under compression monotonic loading is described below. This curve is also used as the envelope curve for the cyclic loading case. The proposed analytic equation for the stress-strain relationship is a parabola. An expression originally proposed by Popovics in1973 [118], and later used by Cusson and Paultre in1995 [119] for high-strength concrete, was adopted for the proposed stress strain relationship of the confined concrete with ferrocement jacket. The mathematical expression for the curve is represented as

$$f_c = f'_{cc}\left[\frac{r(\frac{\varepsilon_c}{\varepsilon_{cc}})}{r-1+(\frac{\varepsilon_c}{\varepsilon_{cc}})^r}\right] \quad (5.1)$$

$$r = \frac{E_c}{E_c - E_{sec}} \quad (5.2)$$

where;

f_c : axial compressive stress of concrete.

f'_{cc} : axial compressive strength of confined concrete.

ε_c : concrete strain.

ε_{cc} : strain at maximum stress of confined concrete.

The parameter (r) above determines the initial slope and the curvature of the curve. In Eq. (5.2), E_{sec} is the secant modulus of elasticity of confined concrete and can be determined from

$$E_{sec} = \frac{f'_{cc}}{\varepsilon_{cc}} \tag{5.3}$$

The following equation, based on regression analysis of test results obtained from this study are used to determine the maximum stress of confined concrete with ferrocement jacket as shown in Fig. (5.71).

$$f'_{cc} = f'_{co} + (32 * K * f_y - 7) \tag{5.4}$$

where;

f'_{co} : strength of unconfined concrete.

$$K = V_f \frac{k_z}{L/r} \tag{5.5}$$

$$k_z = \sqrt[2]{\frac{f'_{cm}}{f'_{co}}} \tag{5.6}$$

V_f : volume fraction of wire mesh reinforcement.

f_y :yield strength of wire mesh reinforcement.

f'_{cm} : compressive strength of mortar.

L/r : slenderness ratio.

Table (5.11) shows a comparison between the experimental and predicted ultimate strength. As can be seen from this table, good agreement with the test data was obtained.

The strain gain was found based on the regression analysis of test results of this study as shown in Fig. (5.72). The strain gain is defined as difference between the strain at the maximum stress of confined concrete and strain at the maximum stress of unconfined concrete. The following equation is proposed for the strain at the maximum stress of confined concrete.

$$\varepsilon_{cc} = \varepsilon_{co} + 0.194 * (\frac{K*f_y}{f'_{co}}) - 0.0025 \quad (5.7)$$

where;

ε_{co} : strain at the maximum stress of unconfined concrete.

Figures (5.73) and (5.74) show the regression analysis of the results of the proposed maximum stress and strain from Eqs. (5.4) and (5.7), respectively. As shown in these figures, R^2 = 0.9604 and 0.9436 for stress and strain, respectively. These values indicate a well agreement between the predicted and the actual values.

The proposed model was verified by comparing the analytically generated stress-strain relation with those obtained from concrete columns tested in this study. Figures (5.75 to 5.88) show the comparison of the experimental and analytical results for the selected columns. The comparison indicates satisfactory correlation between the analytical and experimental results.

5.4.2 Stress-Strain Relation for Confined Concrete under Cyclic Loading

5.4.2.1 Unloading from Envelope Curve to Zero Stress

Test data sets were collected from present study, for full unloading from the envelop curve to a zero stress level. Figure (5.89) shows the obtained experimental values of the stress and strain. The stresses are expressed as ratios between the unloading stresses (f_c) and the residual stress(f_{un}). The strains are expressed in terms of $\left(\frac{1-\epsilon'}{1+\epsilon'}\right)$. The unloading curves in Figs. (5.2) to (5.11) show

that the strain is constant as the stress decrease from $f_c to\ 0.9f_c$. On the other hand, after the point (ε_{un} , $0.9f_c$) a shape of convex curve is not unique. The unloading curve starts from the unloading point (ε_{un}, f_{un}) to the point of plastic strain (ε_p, 0). Depending on Fig. (5.89) unloading branches may be represented by two equations, such as

$$\epsilon' = 1 \qquad \text{for} \quad 0.9f_{un} \le \epsilon' \le f_{un} \tag{5.8}$$

$$f_c = f_{un}\left[0.6 * \left(\frac{1-\epsilon'}{1+\epsilon'}\right)^2 + 0.3 * \left(\frac{1-\epsilon'}{1+\epsilon'}\right)\right] \quad \text{for} \quad 0 \le \epsilon' \le 1 \tag{5.9}$$

where;

ϵ' is the normalized strain of the unloading branch, as given by

$\epsilon' = \frac{\varepsilon-\varepsilon_{un}}{\varepsilon_p-\varepsilon_{un}} \qquad 0 \le \epsilon' \le 1$

Two boundary conditions are given, as follows:

1. $\epsilon' = 0$, lead to $f_c = 0.9f_{un}$
2. $\epsilon' = 1$, lead to $f_c = 0$ at the zero stress level.

To predict the plastic strain at the residual point, the relationship of the strain between the unloading point (ε_{un}, f_{un}) and the residual point (ε_p, 0) is plotted in Fig. (5.33). Both strains are divided by the peak strain (ε_{cc}). The relation in Fig. (5.33) is formulated according to the regression analysis of experimental results in this study as a linear function as follows:

$$\varepsilon_p = \varepsilon_{cc}\left[0.725\left(\frac{\varepsilon_{un}}{\varepsilon_{cc}}\right) - 0.09\right] \tag{5.10}$$

Figures (5.90) to (5.99) show comparison between analytic and experimental unloading curves obtained from tests. The curves are in very good agreement.

5.4.2.1 Reloading from Zero Stress to Envelope Curve

To determine the reloading path from zero stress to envelope curve, the new stress at the reference strain (the envelope unloading strain) f_{new} on a reloading path is a key value as shown in Fig.(5.100), which is determine by

$$f_{new} = 0.9 f_{un} \tag{5.11}$$

The reloading path can therefore, be constructed between the point of plastic strain $(\varepsilon_p, 0)$ and the new stress level $(\varepsilon_{un}, f_{new})$. For simplicity, the reloading branch is then extended using the same slope until its return to the envelope curve $(\varepsilon_{re}, f_{re})$ as

$$\frac{f_{re}}{\varepsilon_{re}} = \frac{f_{new}}{\varepsilon_{un} - \varepsilon_p} \tag{5.12}$$

where the return point $(\varepsilon_{re}, f_{re})$ can be computed in combination with Eq. (5.1) for the envelope curve.

Figures (5.101) to (5.110) show the comparison between analytic and experimental reloading curves obtained from tests. The curves are in very good agreement.

Table (5-11) Ultimate Loads for Columns

Group No.	Ultimate Load (kN)		
	Experimental ($P_{Exp.}$)	**Analytical ($P_{Anal.}$)**	$\frac{P_{Exp.}}{P_{Anal}}$.
J	689.1	689.1	1.000
J1	463.0	468.2	0.989
J2	636.1	642.3	0.990
J3	1115.3	1065.3	1.047
J4	1570.8	1517.1	1.035

J5	489.5	474.9	1.031
J6	538.9	585.2	0.921
J7	705.9	692.6	1.019
S8	821.7	800.9	1.026
J9	749.2	749.2	1.000
J10	1222.1	1118.9	1.092
J11	1665.05	1664.3	1.000
		mean	1.013
		Standard deviation	0.039

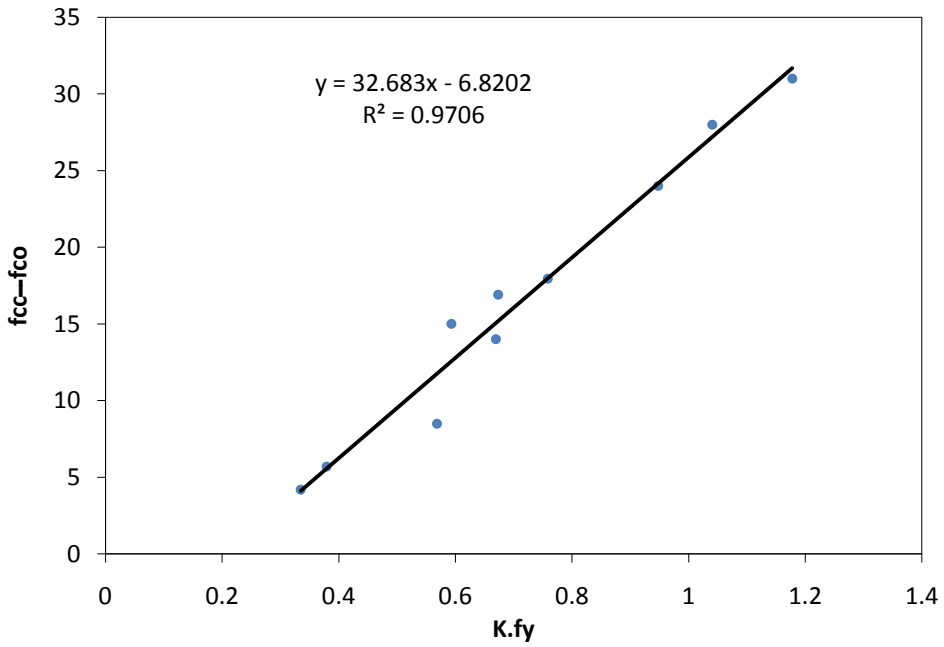

Figure (5.71) Comparison between $f'_{cc} - f'_{co}$ and K. f_y

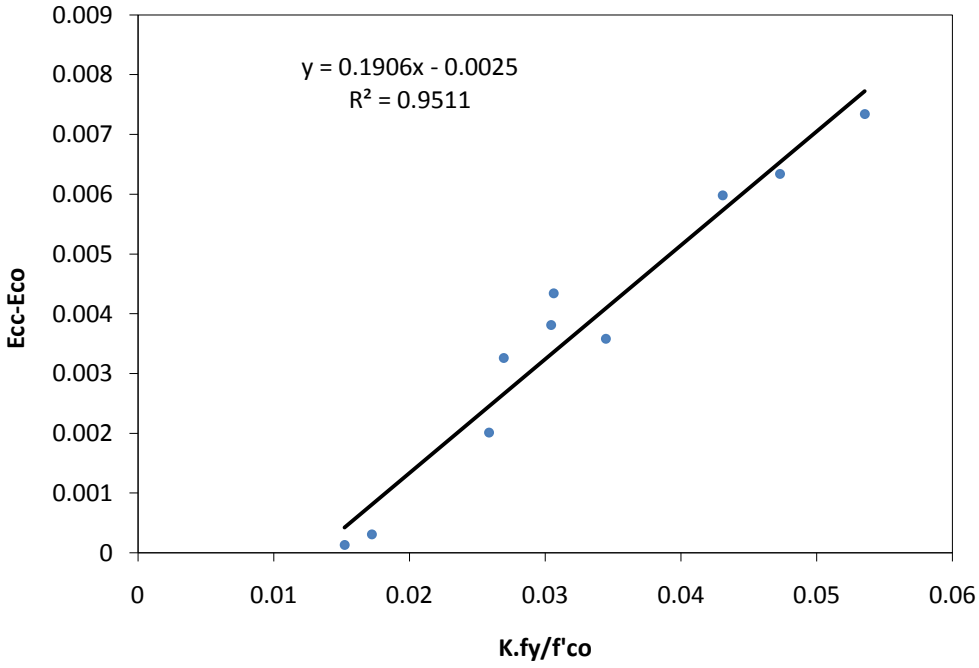

Figure (5.72) Comparison between $\varepsilon_{cc} - \varepsilon_{co}$ and K. f_y / f'_{co}

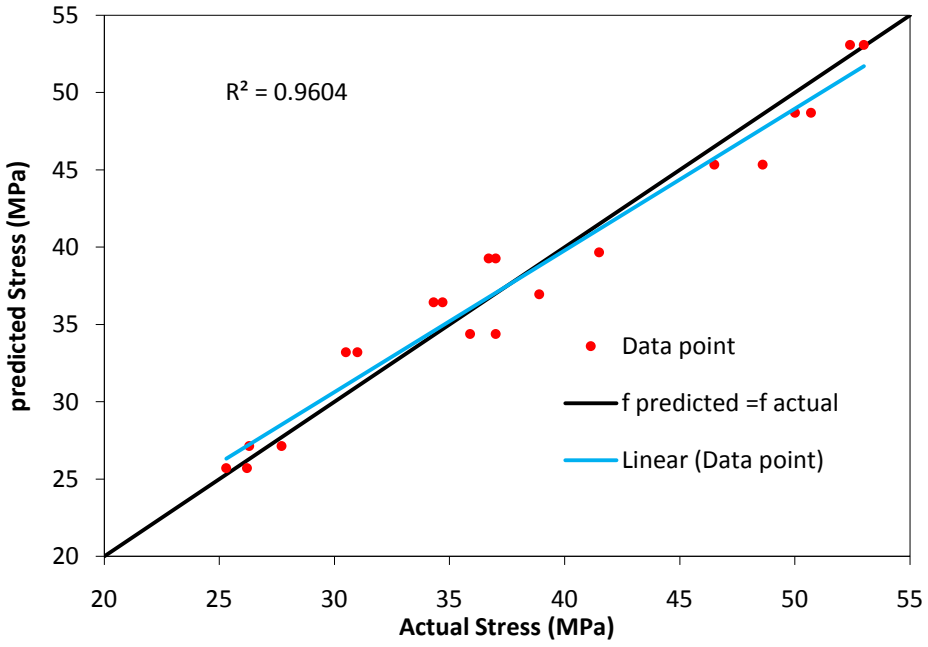

Figure (5.73) Regression analysis between predicted and actual values of ultimate strength

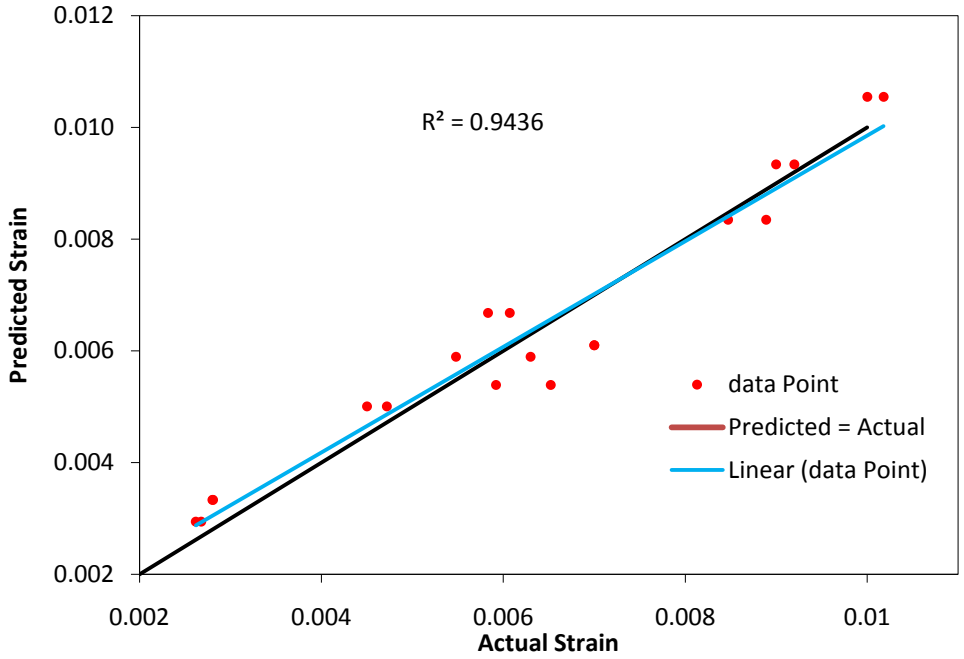

Figure (5.74) Regression analysis between predicted and actual values of ultimate strain

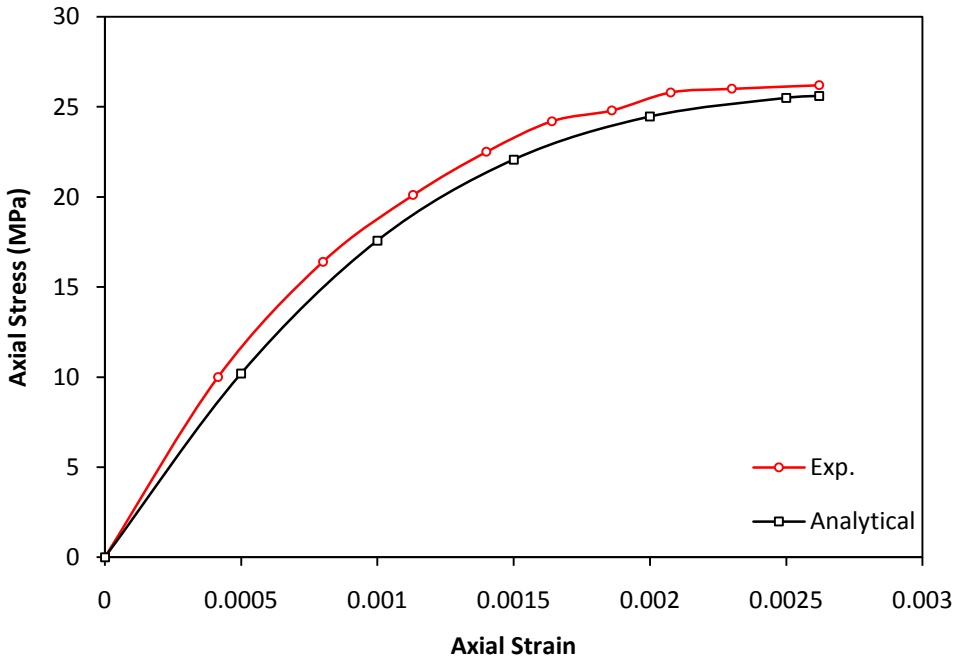

Figure (5.75) Variation of stress-strain with monotonic load for 2BM1

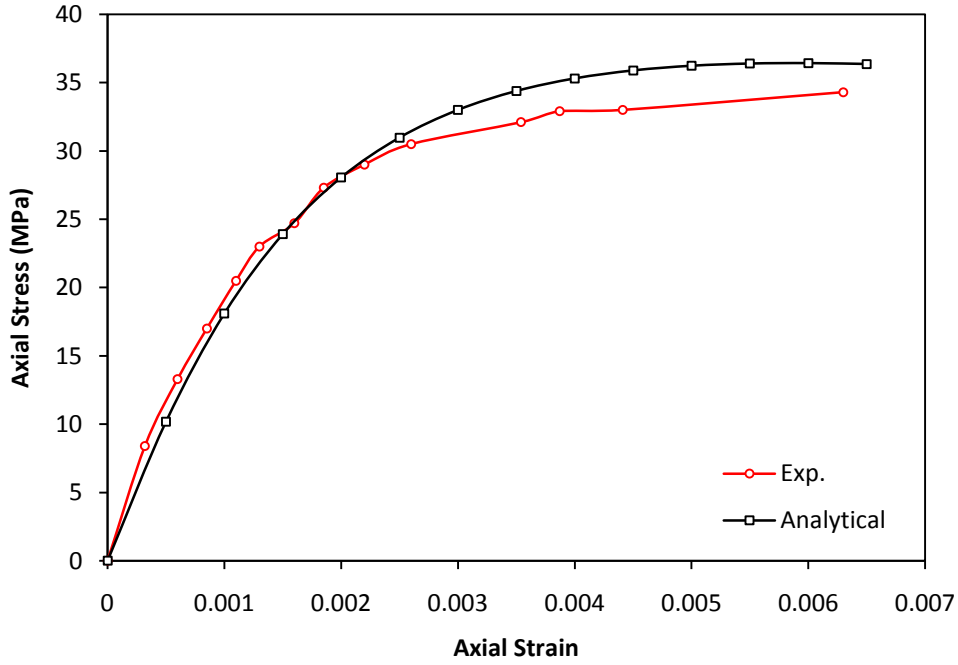

Figure (5.76) Variation of stress-strain with monotonic load for 4BM1

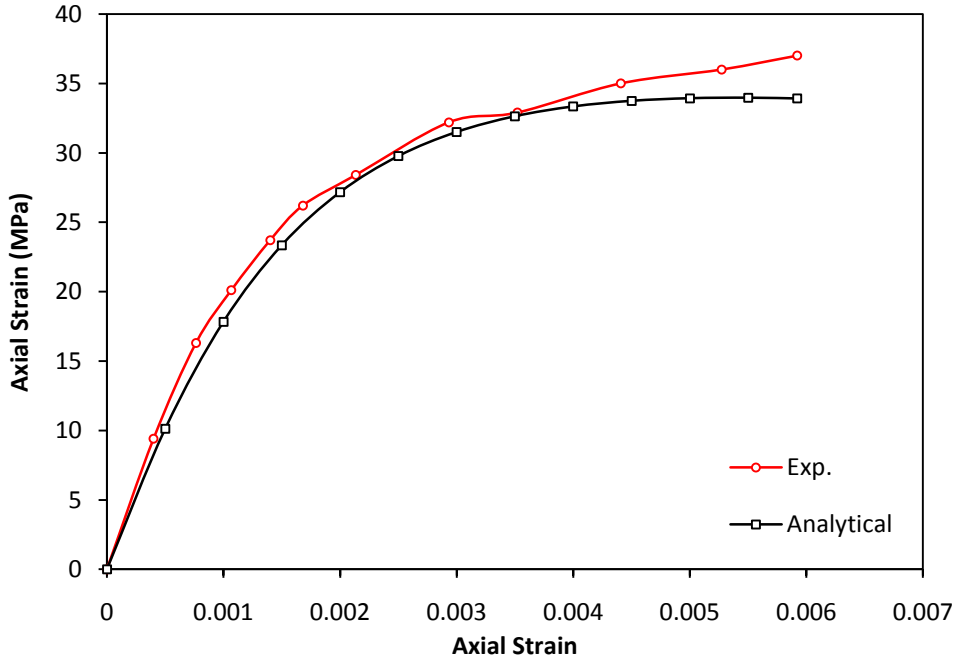

Figure (5.77) Variation of stress-strain with monotonic load for 4DM1

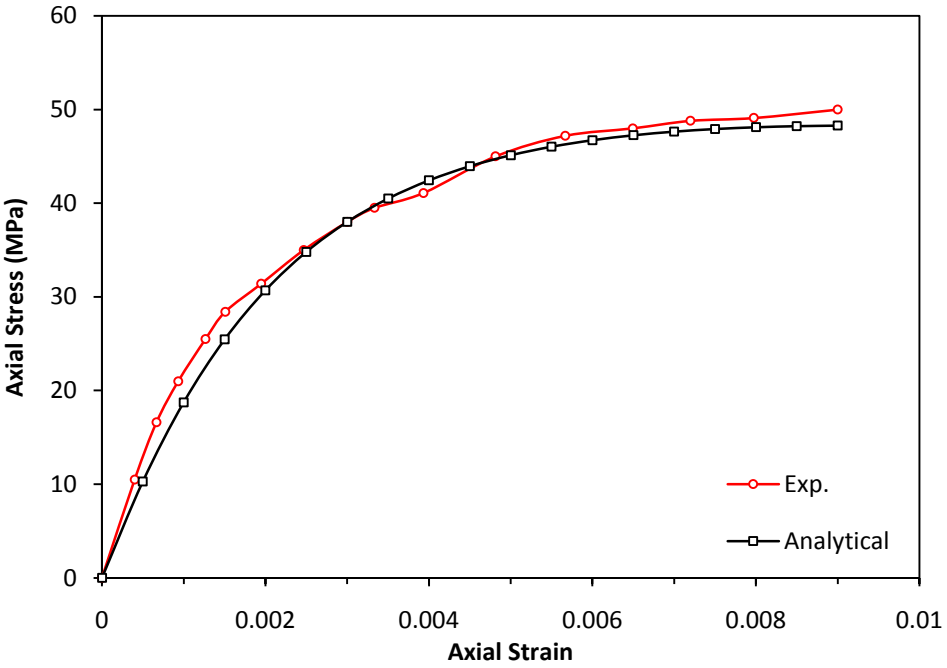

Figure (5.78) Variation of stress-strain with monotonic load for 7DM1

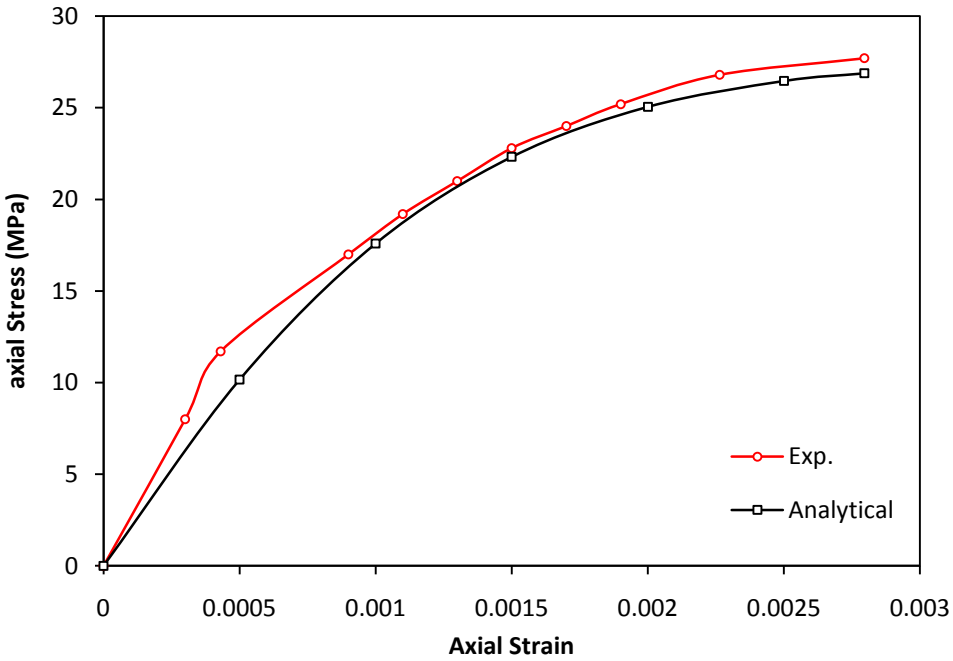

Figure (5.79) Variation of stress-strain with monotonic load for 2BM2

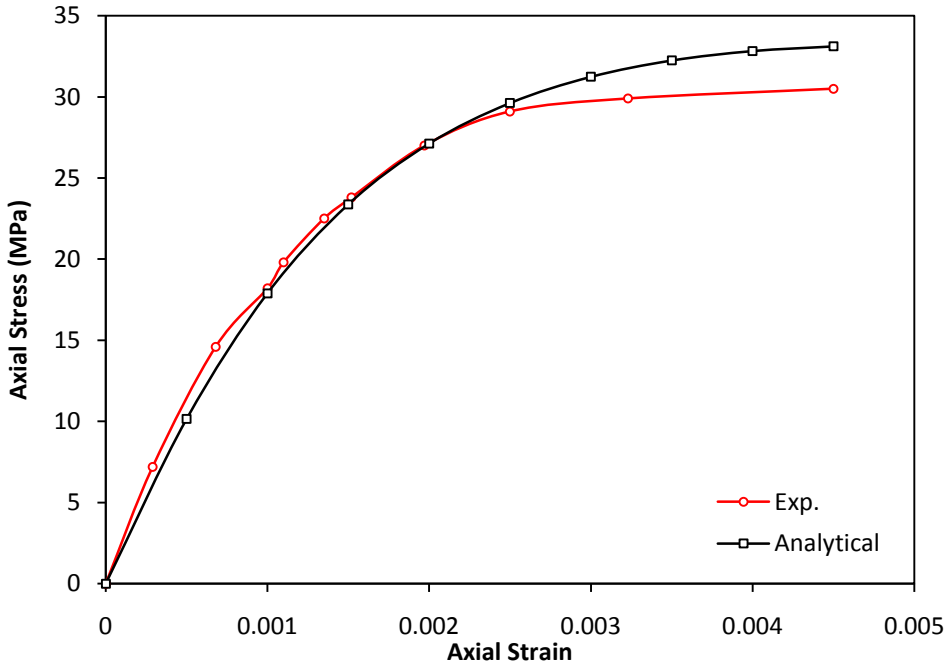

Figure (5.80) Variation of stress-strain with monotonic load for 3BM2

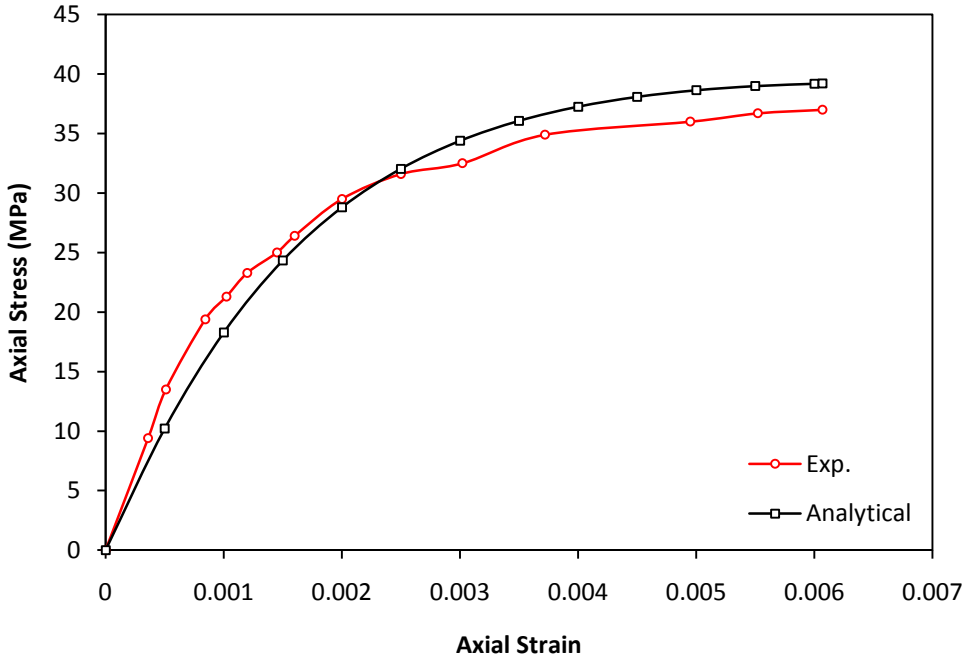

Figure (5.81) Variation of stress-strain with monotonic load for 4BM2

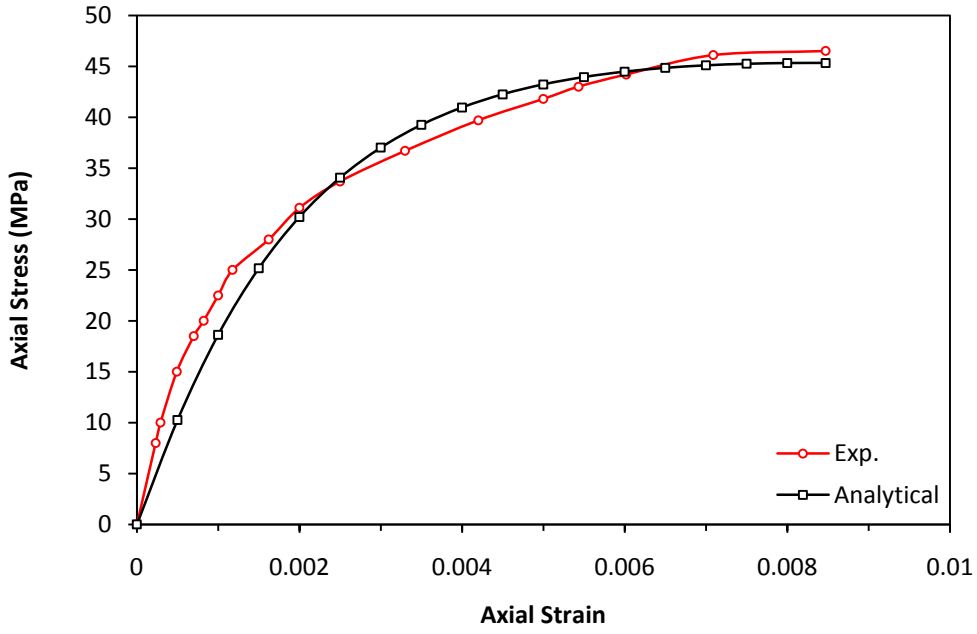

Figure (5.82) Variation of stress-strain with monotonic load for 5BM2

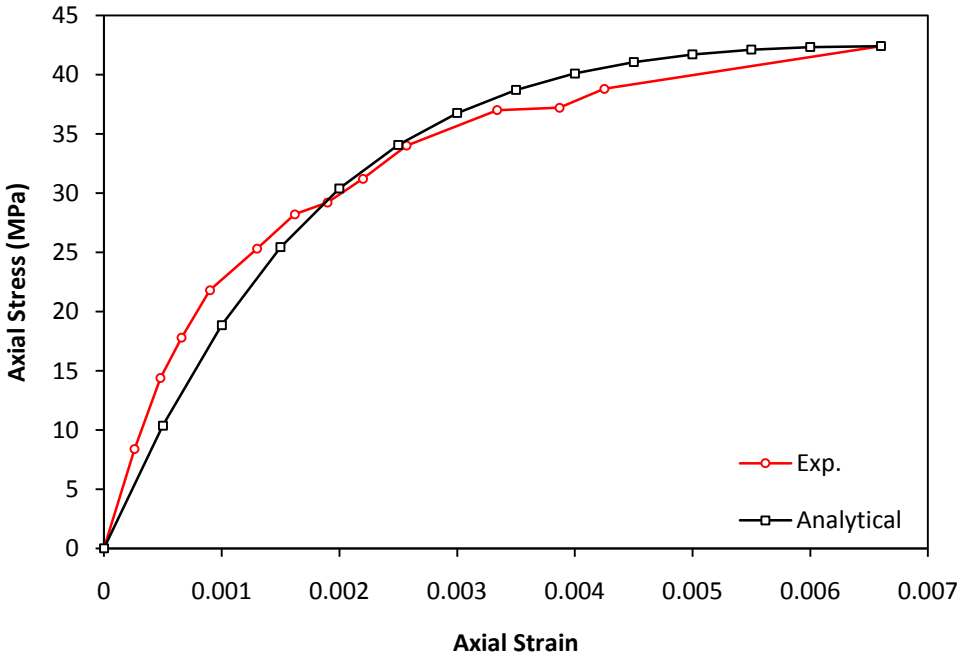

Figure (5.83) Variation of stress-strain with monotonic load for 4AM2

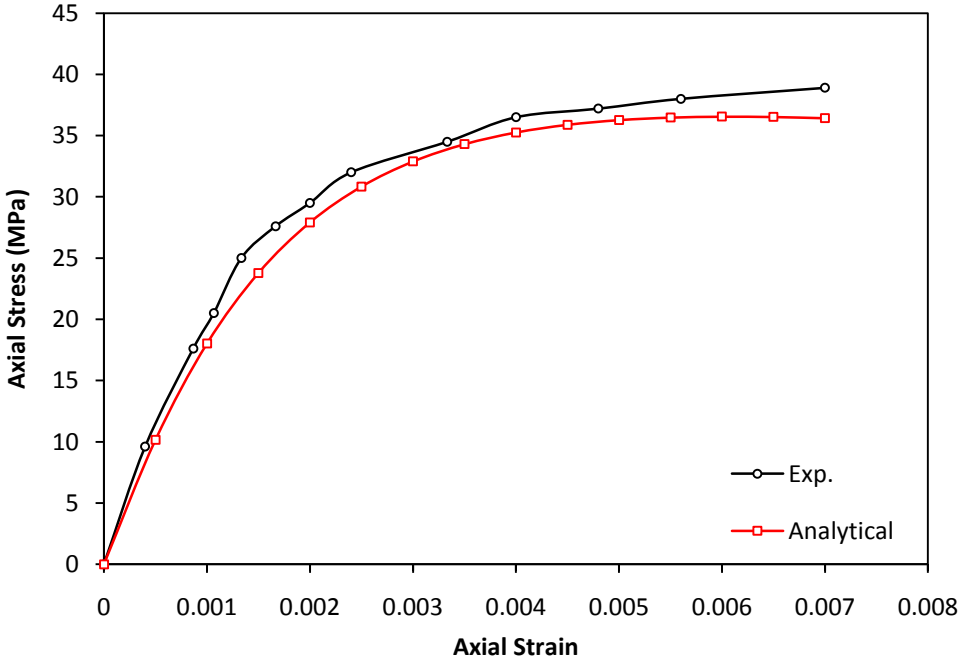

Figure (5.84) Variation of stress-strain with monotonic load for 4DM2

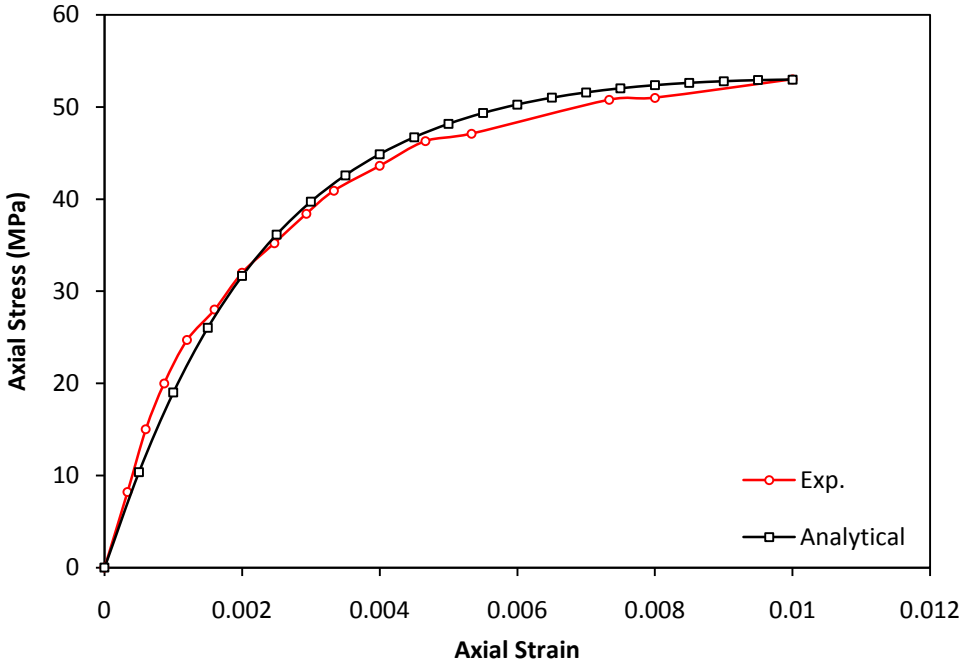

Figure (5.85) Variation of stress-strain with monotonic load for 7DM2

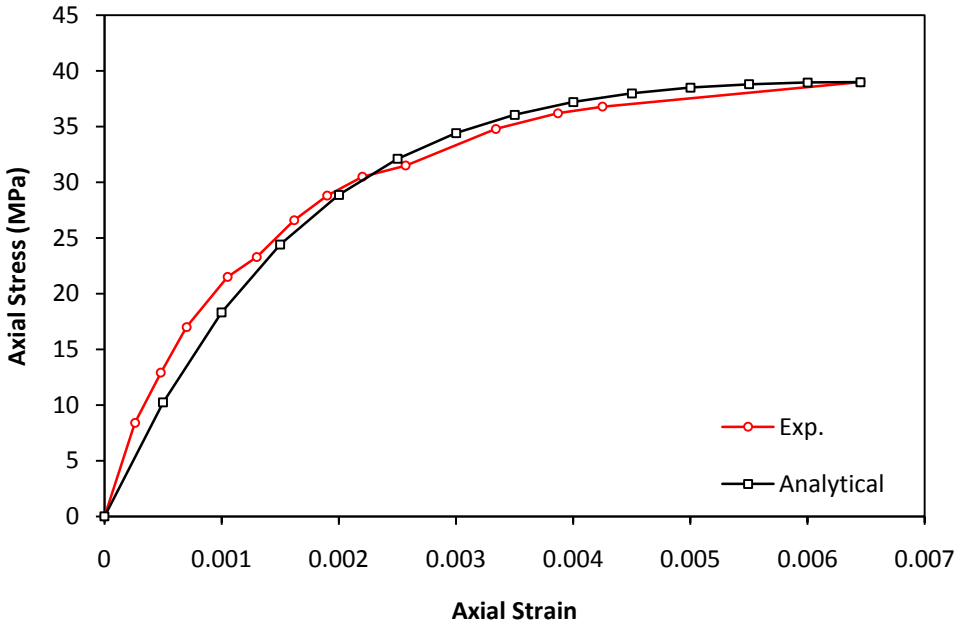

Figure (5.86) Variation of stress-strain with monotonic load for 4AM1

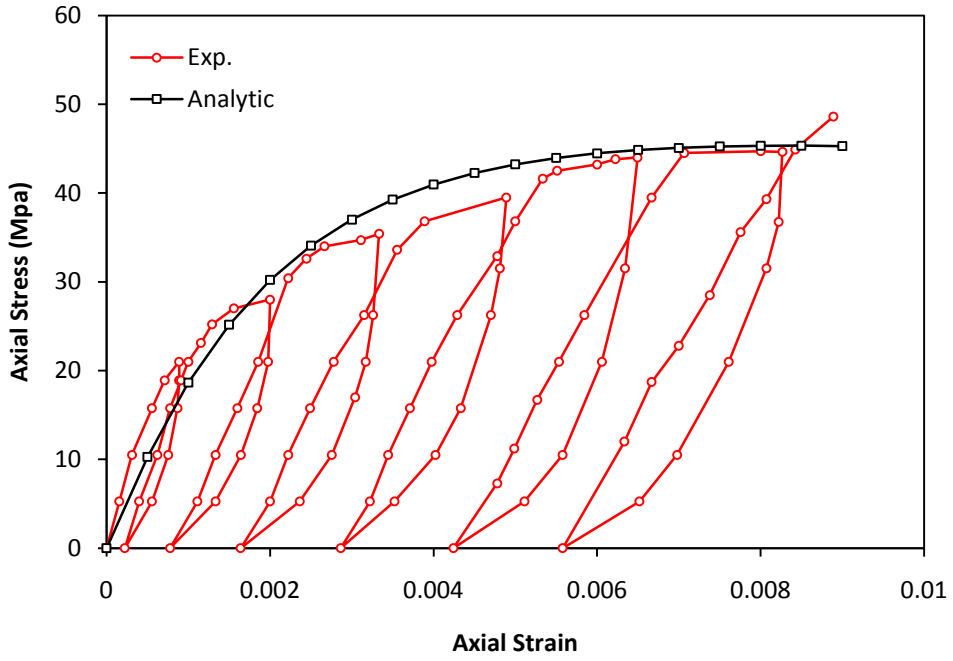

Figure (5.87) Variation of stress-strain with cyclic to envelope load for column J8

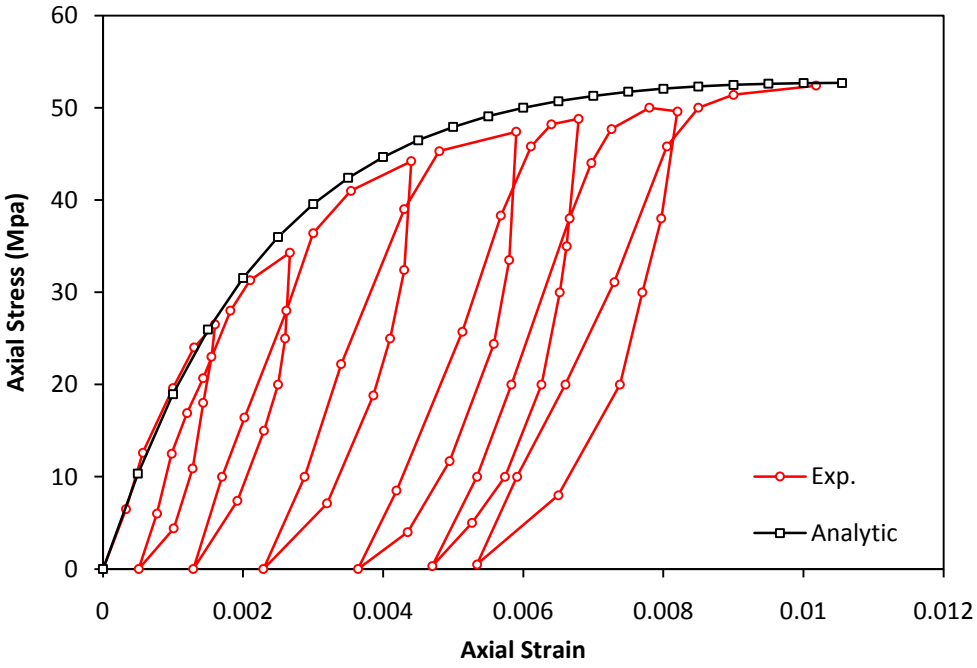

Figure (5.88) Variation of stress-strain with cyclic to envelope load for column J11

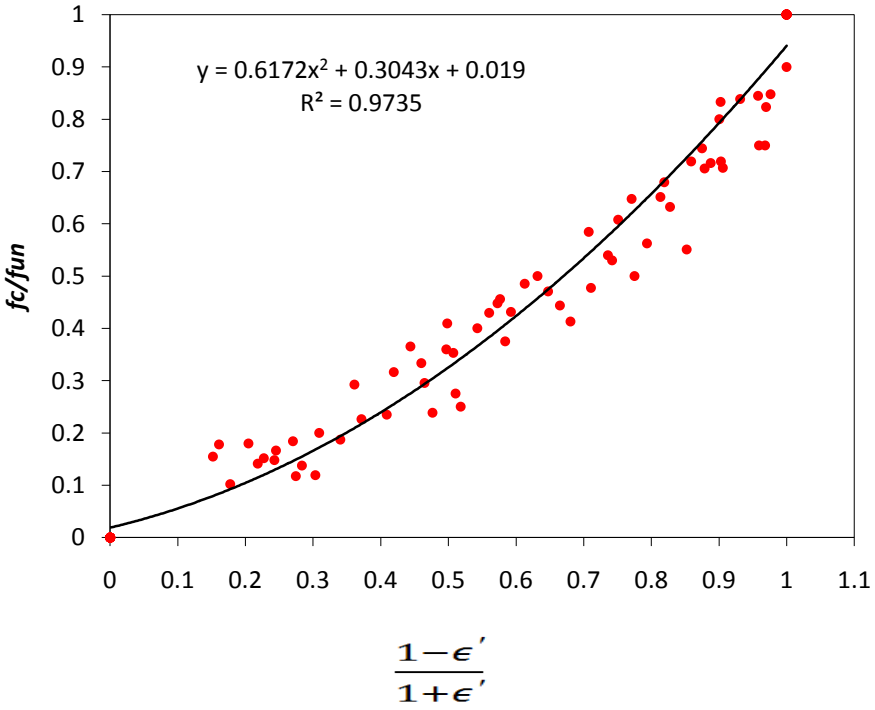

Figure (5.89) Relation between $\frac{fc}{f_{un}}$ and $\frac{1-\epsilon'}{1+\epsilon'}$

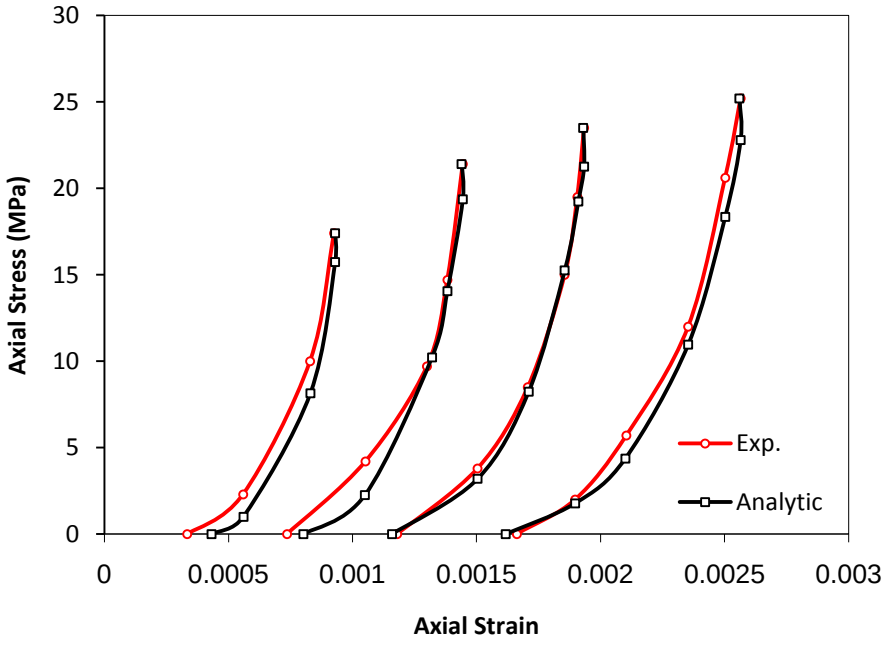

Figure (5.90) Variation of stress-strain with unloading path for column J1

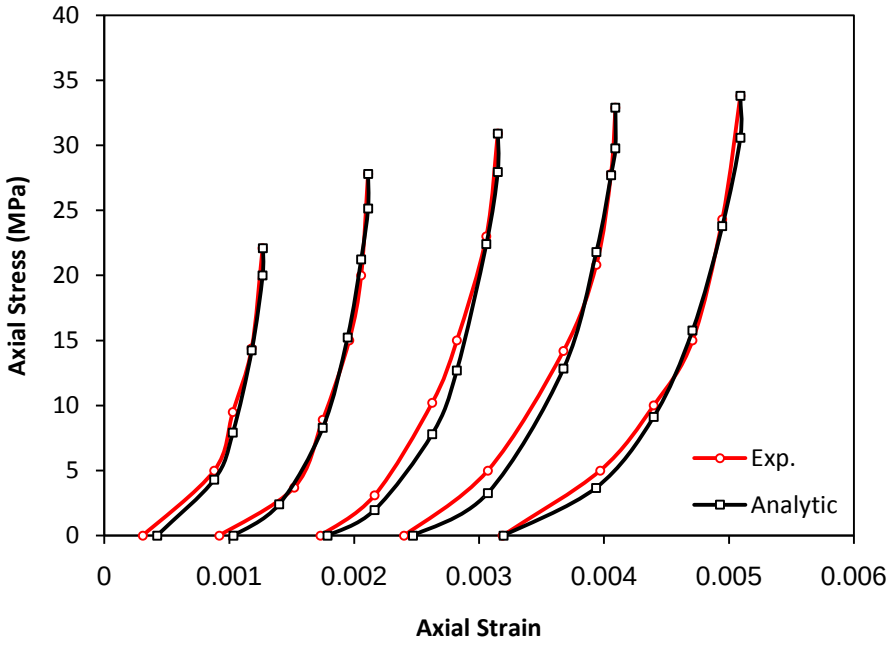

Figure (5.91) Variation of stress-strain with unloading path for column J2

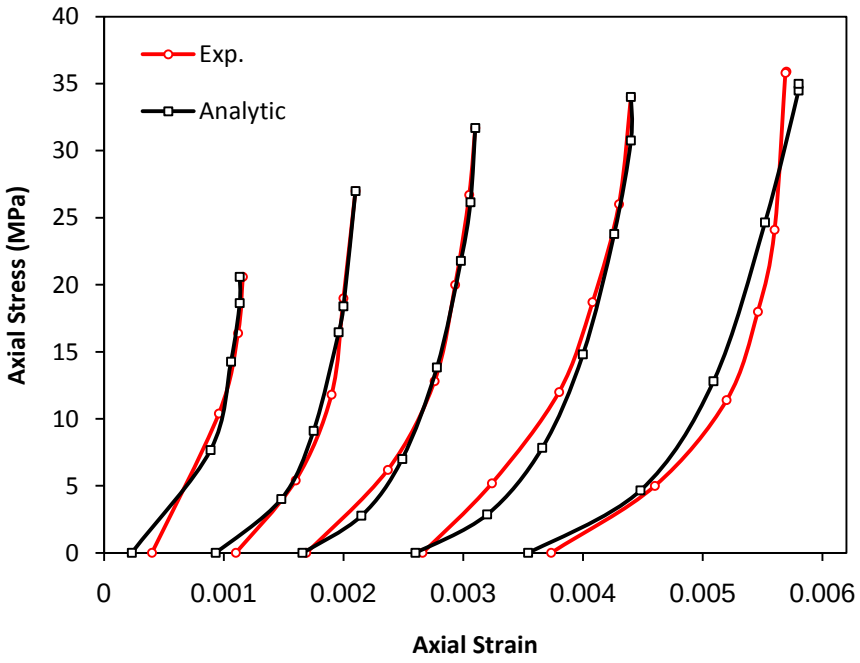

Figure (5.92) Variation of stress-strain with unloading path for column J3

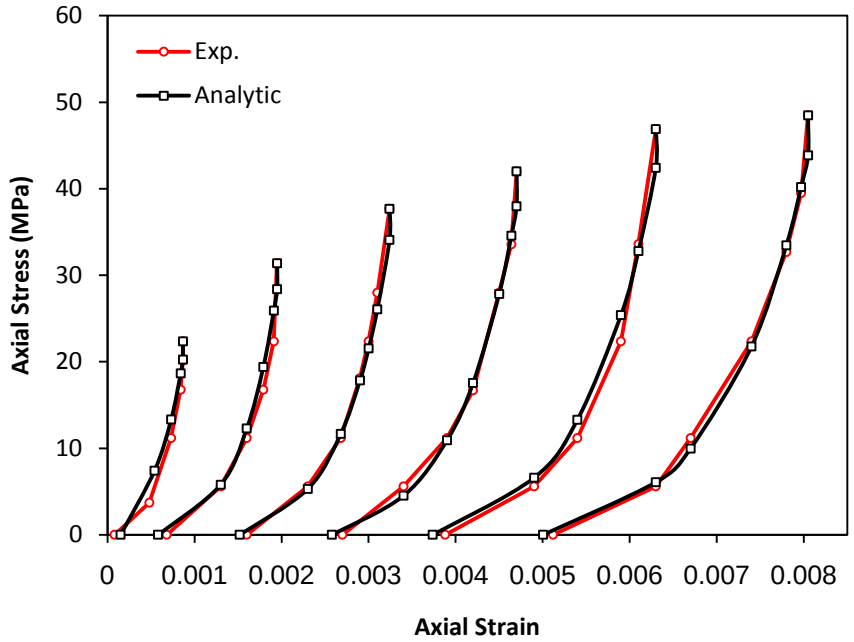

Figure (5.93) Variation of stress-strain with unloading path for column J4

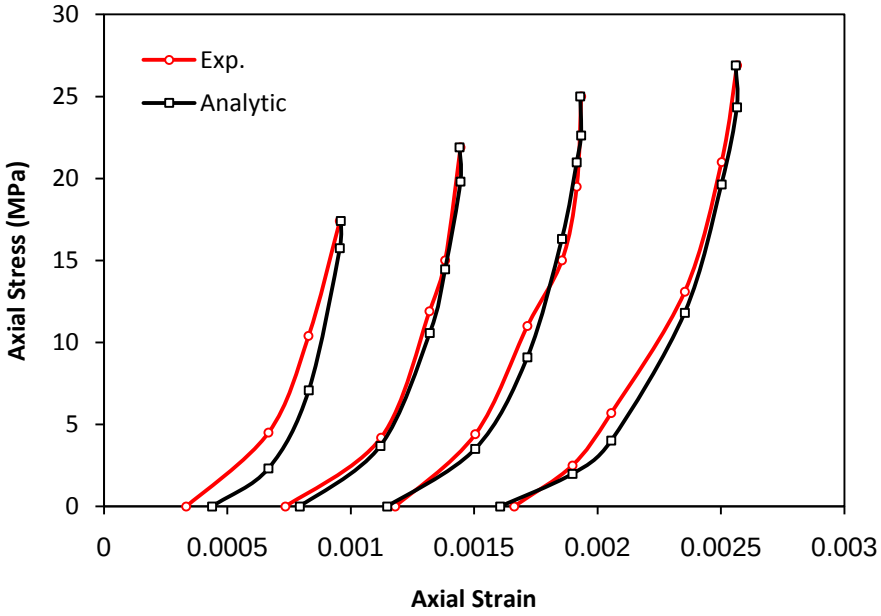

Figure (5.94) Variation of stress-strain with unloading path for column J5

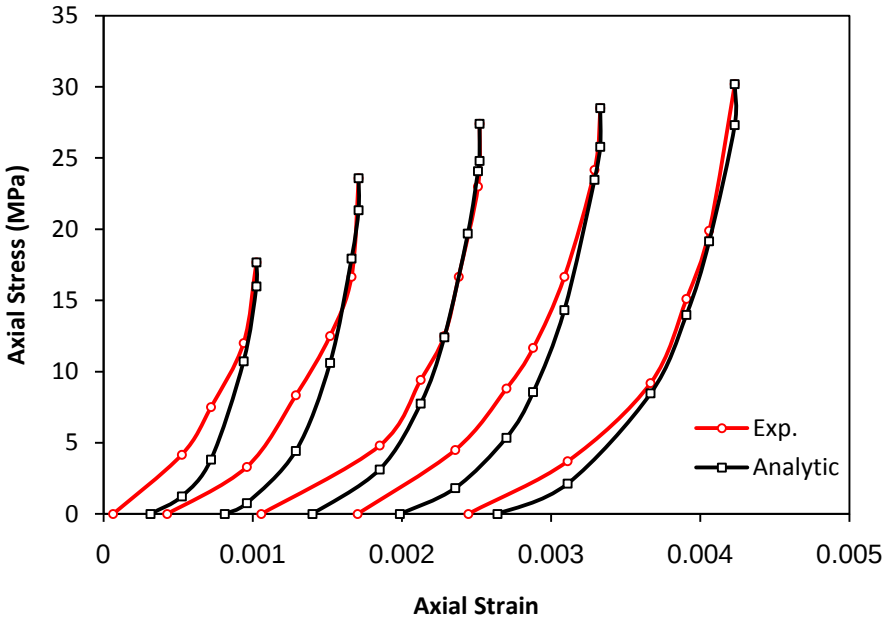

Figure (5.95) Variation of stress-strain with unloading path for column J6

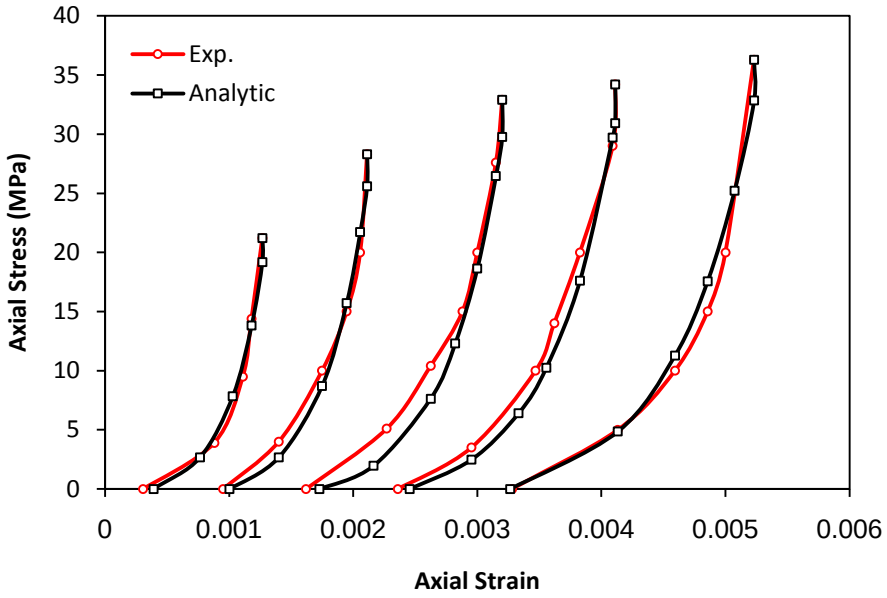

Figure (5.96) Variation of stress-strain with unloading path for column J7

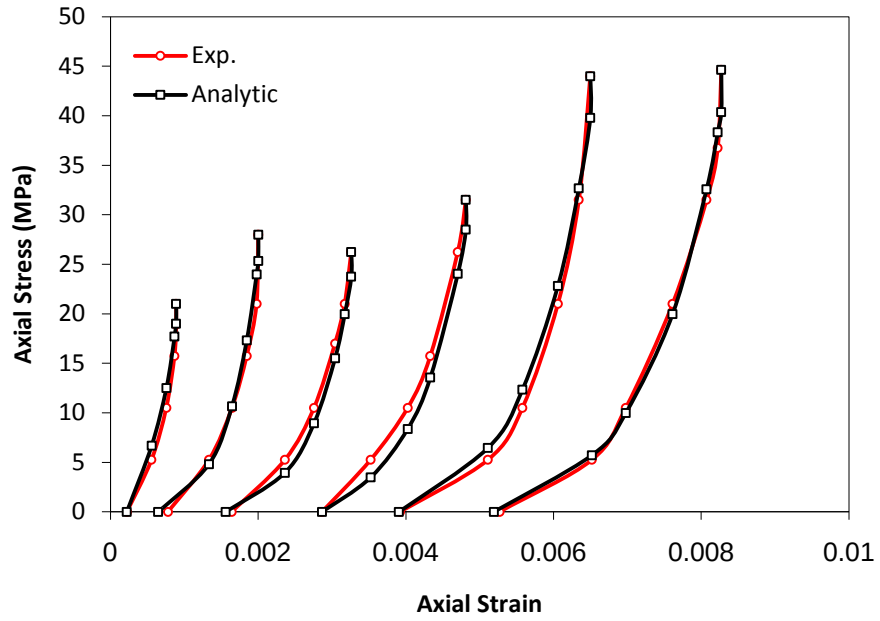

Figure (5.97) Variation of stress-strain with unloading path for column J8

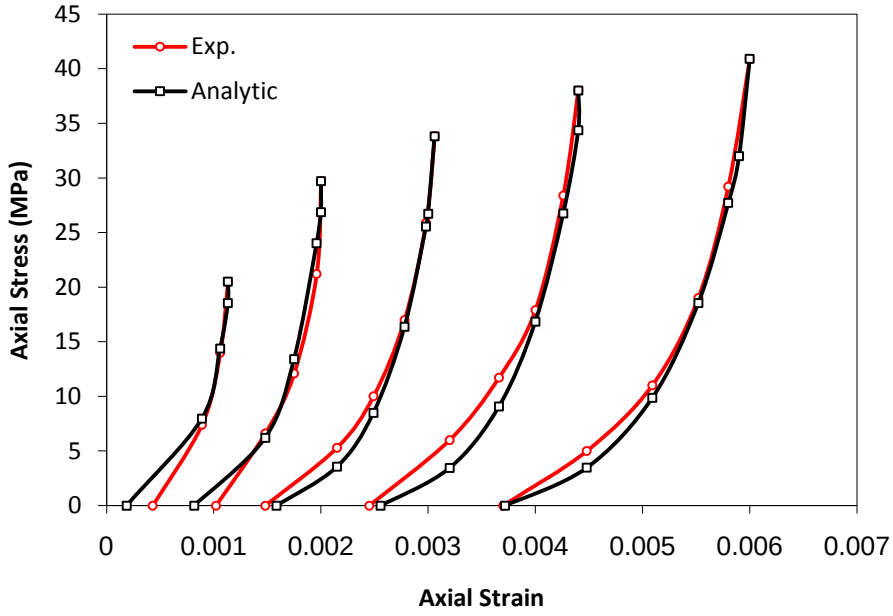

Figure (5.98) Variation of stress-strain with unloading path for column J10

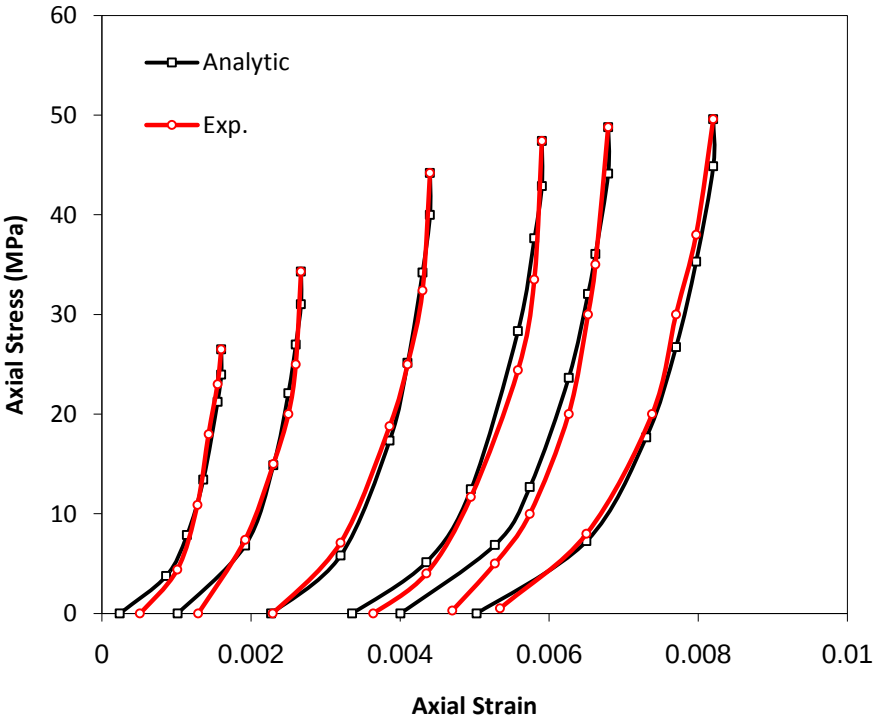

Figure (5.99) Variation of stress-strain with unloading path for column J11

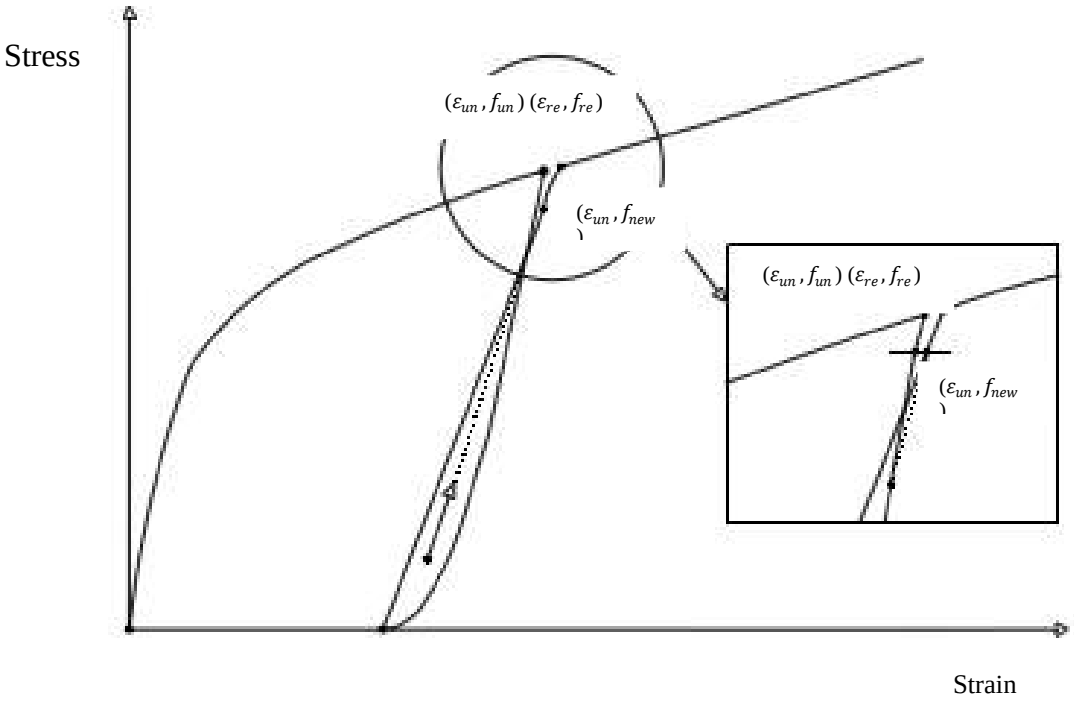

Figure (5.100) Illustrates the reloading point of stress

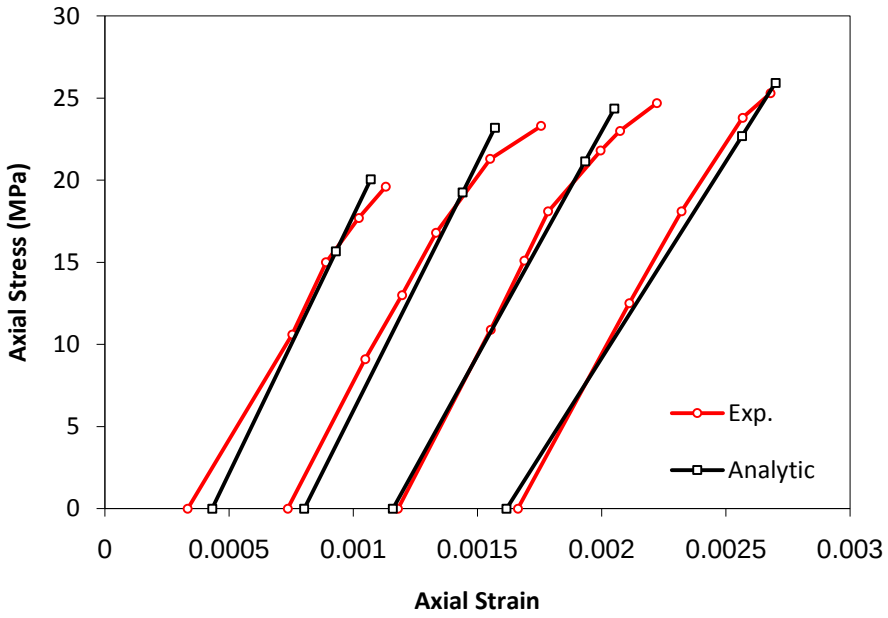

Figure (5.101) Variation of stress-strain with reloading path for column J1

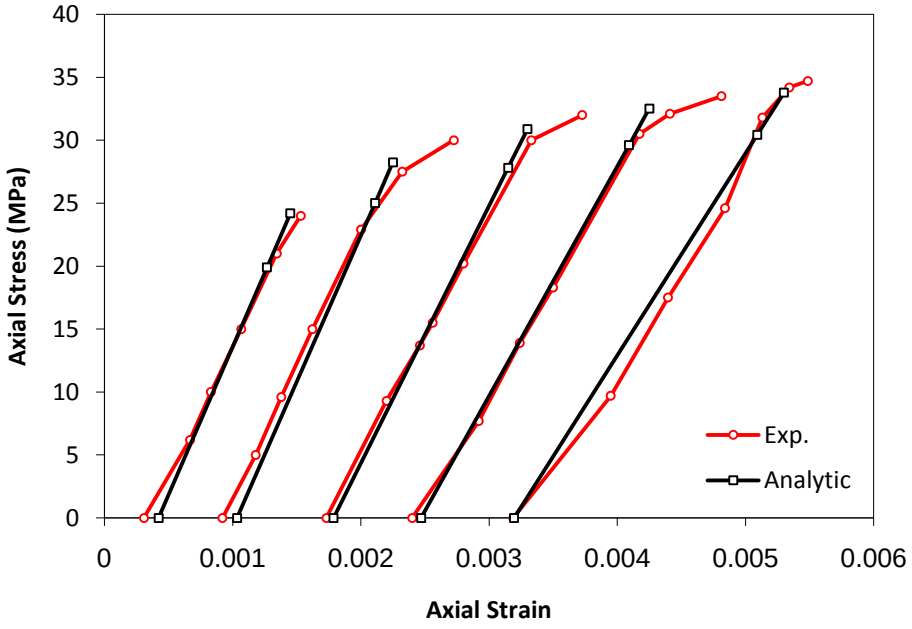

Figure (5.102) Variation of stress-strain with reloading path for column J2

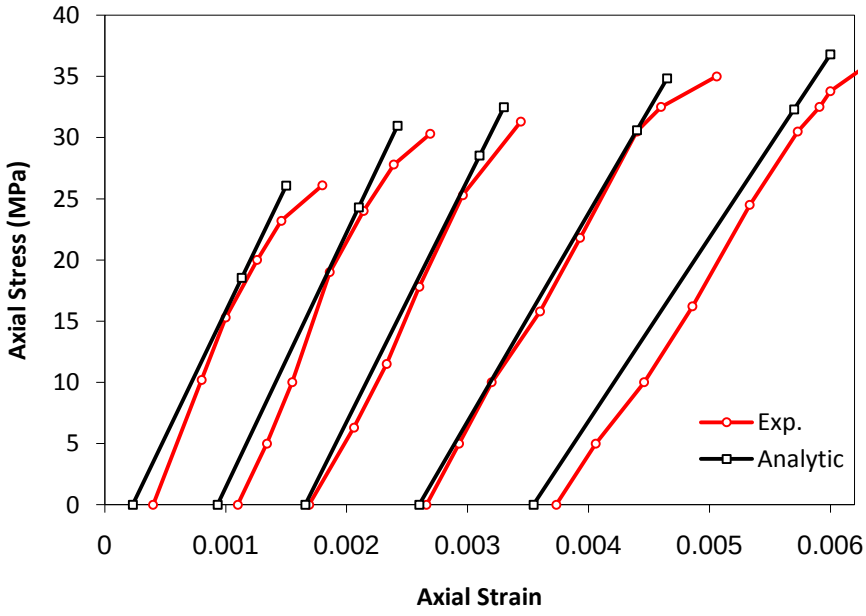

Figure (5.103) Variation of stress-strain with reloading path for column J3

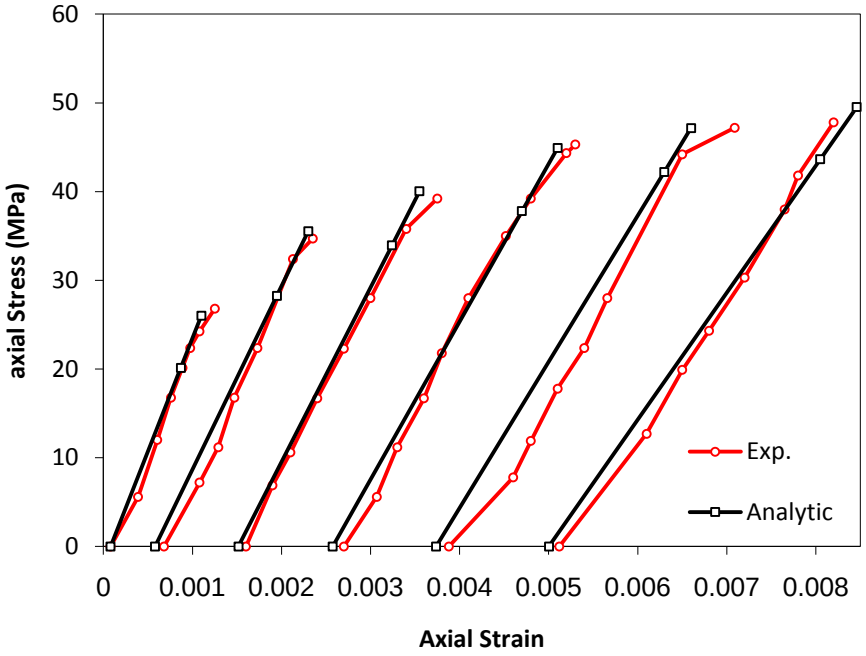

Figure (5.104) Variation of stress-strain with reloading path for column J4

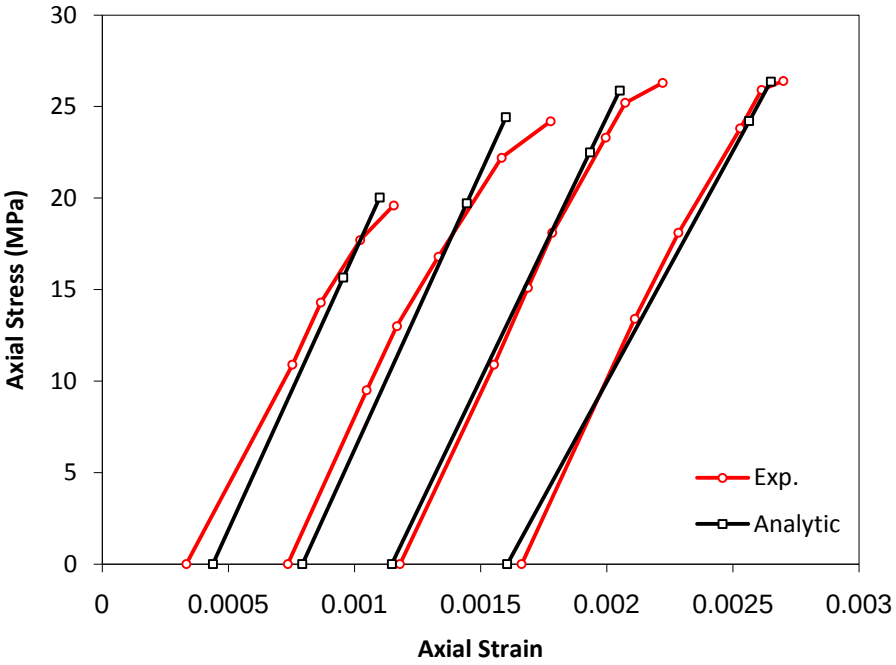

Figure (5.105) Variation of stress-strain with reloading path for column J5

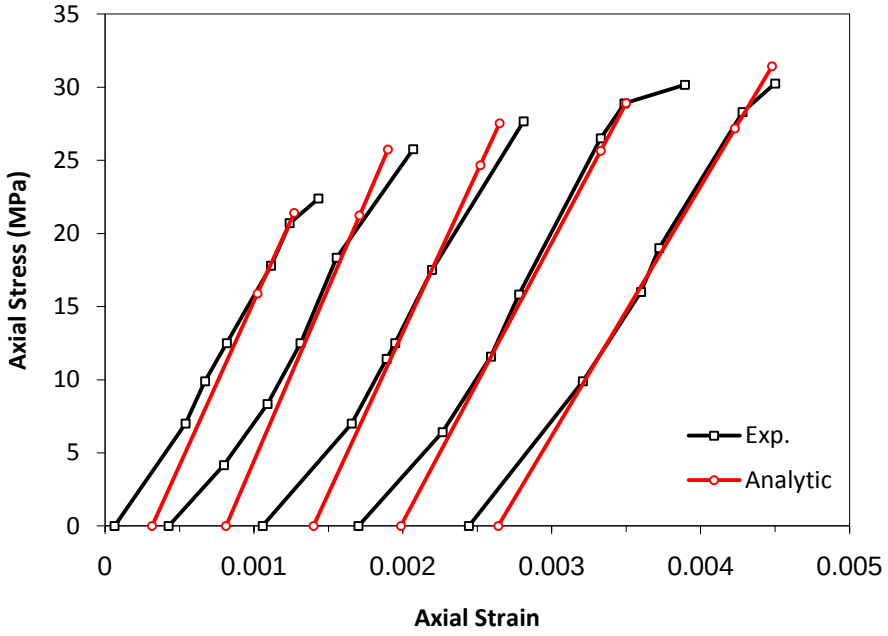

Figure (5.106) Variation of stress-strain with reloading path for column J6

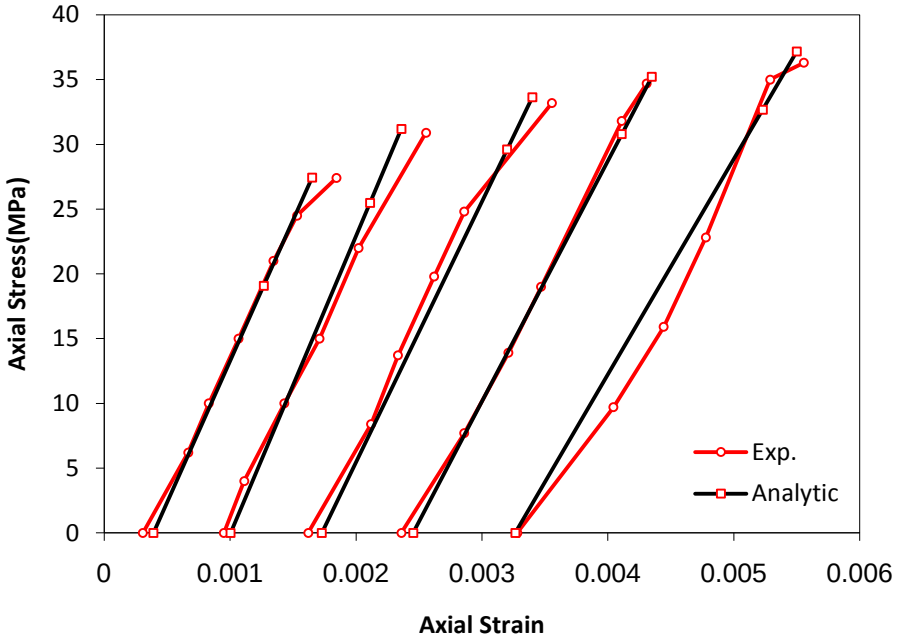

Figure (5.107) Variation of stress-strain with reloading path for column J7

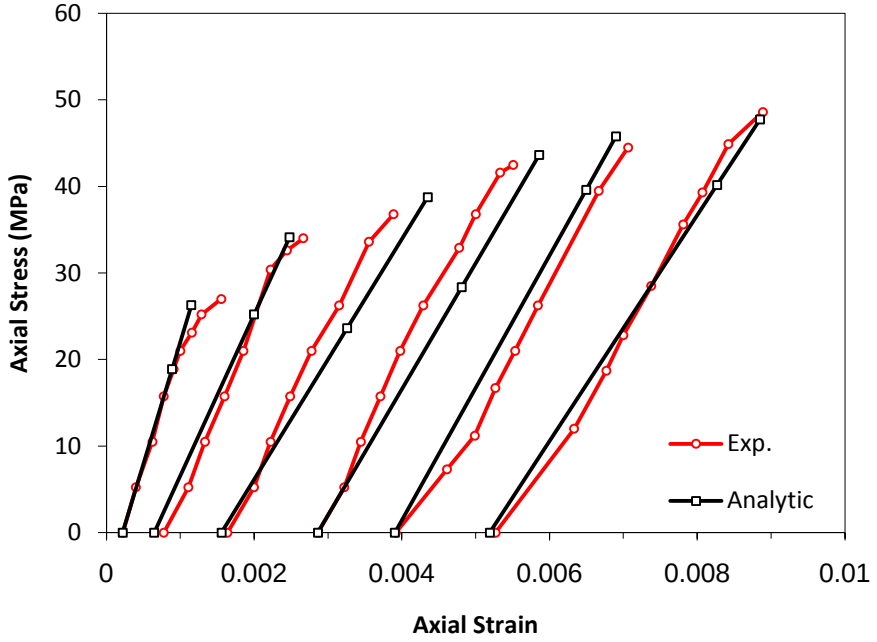

Figure (5.108) Variation of stress-strain with reloading path for column J8

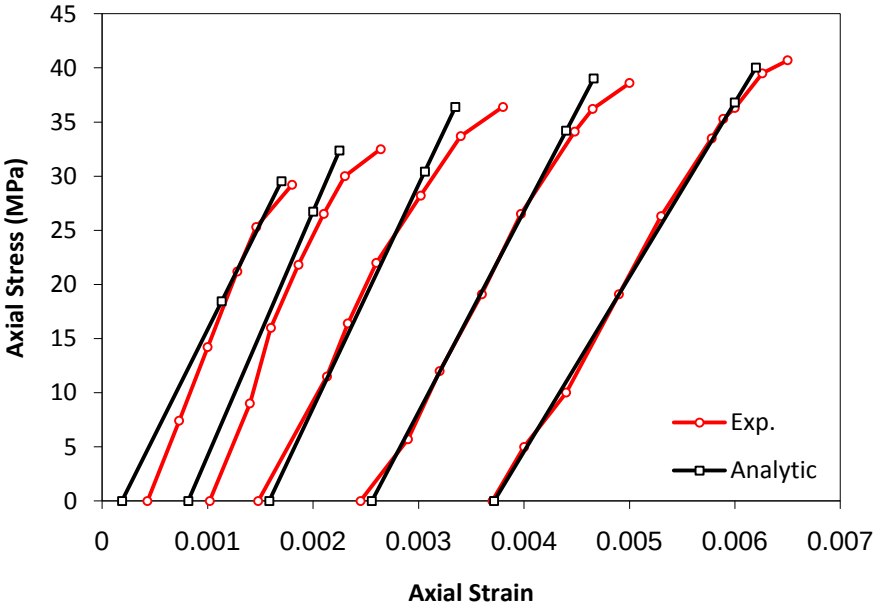

Figure (5.109) Variation of stress-strain with reloading path for column J10

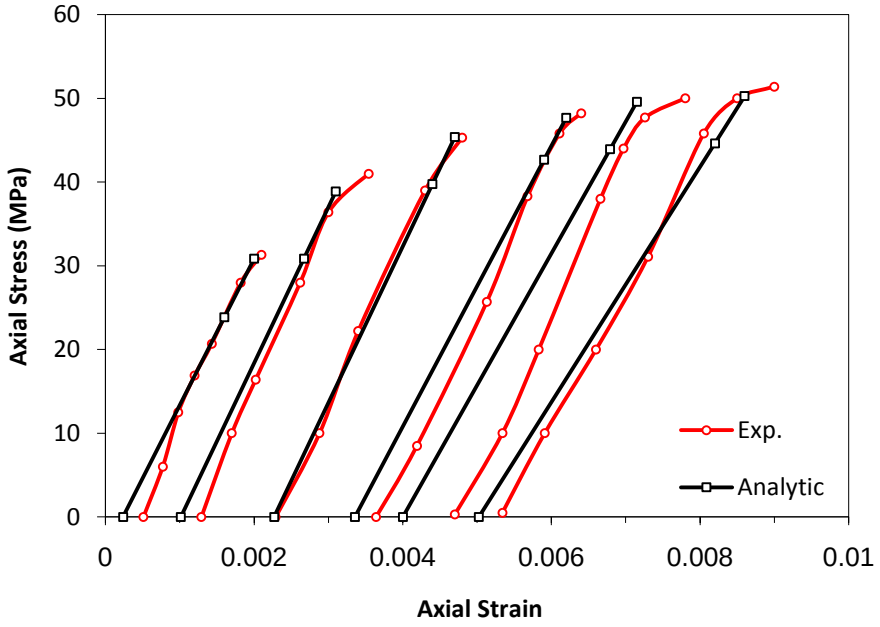

Figure (5.110) Variation of stress-strain with reloading path for column J11

CHAPTER SIX
Conclusions and Recommendations

6.1 Introduction

This study investigates the behavior of short concrete columns strengthened with ferrocement jacket subjected to various axial monotonic and cyclic compression loadings. Different volume fraction of wire mesh reinforcement, column size, mortar strengths and loading type are used in order to assess the effect of these variables on the strength of columns.

Moreover, a finite element model is presented to predict the behavior of short concrete columns strengthened with ferrocement jacket through the stages of the test program. As well as new analytical models are proposed for stress-strain relationship of confined concrete with ferrocement under monotonic load and for unloading and reloading under complete cyclic load.

6.2 Conclusions

The most important conclusions that can be drawn from the present study are the followings:

1. The external confinement with ferrocement jacket can provide sufficient lateral support to the concrete core and significantly increase the strength and ductility of the specimens under axial loading. The experimental results clearly demonstrate that jacket can enhance the structural performance of concrete columns under axial loading.
2. The ratio of strength of concrete column strengthened with ferrocement jacket to strength of plain concrete column ranged between 1.132 and 2.291 for columns with 35 MPa mortar compressive strength, whereas it

was between 1.364 and 2.34 for columns strengthened with 45 MPa mortar compressive strength.

3. The strain ratio of concrete column strengthened with ferrocement jacket to strain of plain concrete column ranged between 1.04 and 3.459 for columns with 35 MPa mortar compressive strength, whereas it was between 1.124 and 3.827 for columns strengthened with 45 MPa
4. The number of layers of wire mesh is the major parameter and has significant influence on the behavior of specimens. The test results proved that the benefit of confinement could be enhanced by multiple layers.
5. The stress-strain relationship of the concrete columns strengthened with ferrocement under monotonic load is generally parabola.
6. The failure of the tested specimens usually occurred near the top or bottom of the columns (within the upper or lower quarter or one third of the column height).
7. The results of experimental test showed that ferrocement jackets can produce a good lateral confinement pressure to column specimens. Then it can be used for strengthening and repairing structures.
8. The stress-strain relationship of concrete column under cyclic loadings possesses an "Envelope Curve". This envelope curve is constructed by joining the end of all the reloading curves. Moreover, this envelope curve approximately coincides with the stress-strain curve obtained from tests on specimens under monotonic loading.
9. In the stress-strain relationship of concrete column under axial cyclic loading, the reloading curves intersect the previous unloading curves at so-called "Common Points". The locations of common points are found to be independent of the minimum stress level.
10. The stress-strain curve of monotonic loading for strengthened specimens can employ to serve as the envelope curve of cyclic load.

11. The analysis of the test specimen indicates that the maximum of the common point limits is at a stress level of about 90% of the ultimate strength of concrete.
12. For the same concrete strength, the plastic strain of concrete column strengthened with ferrocement jacket is linearly related to the envelope unloading strain, but is independent of the amount of volume fraction of wire mesh of reinforcement.
13. Repeated unloading/reloading cycles have a cumulative effect on the permanent strain and stress deterioration.
14. Nonlinear finite element solution by ANSYS package program using three dimensional elements for modeling the concrete column strengthened with ferrocement jacket gives acceptable agreement with the experimental results for the stress-strain relationships.
15. The ratios of theoretical to experimental values of ultimate loads are between 0.88 to 1.094 for strengthened concrete columns with ferrocement jackets. The ratios of theoretical to experimental values of strain are between 0.858 to 1.261.
16. The finite element analysis shows that the increase in the modulus of elasticity of the ferrocement shell (E_s) causes an increase in the ultimate load.
17. The specimens loaded on both concrete core and ferrocement shell showed less strength than specimens loaded on the concrete core only under the same other parameter.

6.3 Recommendations for Future Work

The following is a list of problems on which further studies are recommended:

1. Experimental and theoretical studies for investigating the behavior of concrete columns strengthened with ferrocement jacket with longitudinal and transverse steel reinforcement are required.

2. Experimental and theoretical studies for investigating the behavior of concrete columns strengthened with ferrocement jacket under eccentric loads are recommended.
3. The effectiveness of using ferrocement jackets for columns with high strength concrete under cyclic load.
4. The effectiveness of using ferrocement jackets on concrete columns having square or rectangular cross sections.
5. Further testing is recommended on long concrete column strengthened with ferrocement under monotonic and cyclic loads.

References

1. Saadon, A. S., "Experimental and Theoretical Investigation of PVC-Concrete composite Columns", Ph.D. Thesis, University of Basrah, 2010.
2. Murat, S.and Cem, Y.," Retrofitting Existing Concrete Columns by External Prestressing", Unites States Patent, No. US6247279B1, Jun., 2001.
3. Balbool, A. N.A., "Prestressed Fiber Reinforced Polymer (FRP) for Strengthening of Concrete Members", Ph.D Thesis, University of Baghdad, Civil Engineering Department, July 2009.
4. Chapman, J.R. and Driver, R.G., "Behavior of Collared Concrete Columns under Concentric Loads" Structural Engineering Report No. 263, University of Alberta, January 2006.
5. Yau, G.,"Repair and Strengthening of Columns with Fiber Reinforced Composites", Master thesis, University of Toronto, Canada, 1998
6. Lam, L., Teng, J.G, Cheung, C.H. and Xiao, Y.," FRP-Confined Concrete under Axial Cyclic Compression", Cement & Concrete Composites 28, 2006, pp. 949-958.
7. Samaan, M.S., "An Analytical and Experimental Investigation of Concrete-Filled Fiber Reinforced Plastics (FRP) Tubes", Ph.D Thesis, University of Central Florida, Orlando, Florida, 1997.
8. Mourad, S. M. ,"Performance of Plain Concrete Specimens Externally Confined with Welded Wire Fabric", Final Research Report No. 47/426, King Saud University, College of Engineering, 2006.
9. ACI Committee 549, "Guide for the Design, Construction, and Repair of Ferrocement", ACI Structural Journal 85 (3), 1999, pp. 325-351.
10. Naaman, A. E.," Ferrocement and laminated Cementitious Composites", Book. 2000.
11. Kondraivendhan, B. and Pradhan, B.,"Effect of Ferrocement Confinement on Behavior of Concrete", Construction and Building Materials, 23, 2009, pp. 1218-1222.

12. Teng, S. and Wang, F.," Finite Element Analysis of Reinforced Concrete Deep Beams under Fatigue Loading", ACI Structural Journal, Vol.98, No. 3, 2001, pp.315-323.
13. Lam, Y.Y.," Behavior of Plain Concrete under Cyclic Compression Loading", Master thesis, Massachusetts Institute of Technology, 1980.
14. Charlies, H. N.," Structural Design for Dynamic Loads", McGraw Hill, Civil Engineering Series.
15. Richart, F. E., Brandtzaeg, A., and Brown, R. L., "A Study of the Failure of Concrete under Combined Compressive Stresses." Engineering Experiment Station Bulletin No. 185, University of Illinois, Urbana, IL. 1928.
16. lyengar, K. T. S. R, Desayi, R., and Reddy, K. N.,"Stress-Strain Characteristics of Concrete Confined in Steel Binders." Magazine of Concrete Research (London), 22 (72), 1970, pp. 173-184.
17. Ahmad, S. H. and Shah, S. P., "Complete Triaxial Stress-Strain Curves for Concrete." Proceedings, ASCE, Vol. 108, ST4, (1982a), pp. 728-742.
18. Ahmad, S. H. and Shah, S. P., "Stress-Strain Curves of Concrete Confined by Spiral Reinforcement." ACI Journal, Vol. 79, No. 6, (1982b), pp. 484-490.
19. Mander, J. B., Priestley, M. J. N. and Park, R. J. T., "Theoretical stress-strain model for confined concrete." Journal of Structural Engineering, ASCE, Vol.114, No.8, 1988, pp.1804-1826.
20. Bett, B.J., Klingner, R.E., & Jirsa, J.O.,"Lateral Load Response of Strengthened and Repaired Reinforced Concrete Columns", ACI Structural Journal, Vol. 85, No.5, 1988, pp.499-508.
21. Ersoy, U., Tankut, A.T. and Suleiman, R.," Behavior of Jacketed Columns", ACI Structural Journal, Vol. 90, No.3, 1993, pp. 288-293.
22. Rodriguez, M., and Park, R.," Seismic Load Tests on Reinforced Concrete Columns Strengthened by Jacketing", ACI Structural Journal, Vol. 91, No.2, 1994, pp.150-159.

23. Lehman, D.E., Gookin, S.E., Nacamuli, A.M. and Moehle, J.P.," Repair of Earthquake-Damaged Bridge Columns", ACI Structural Journal, Vol. 98, No.2, 2001, pp. 233-242.
24. Balaguru, P.," Use of Ferrocement for Confinement of Concrete", Journal of Ferrocement, Vol. 19, No. 2, April 1989, pp.135-140.
25. Mansur, M. and Paramasiva, P., "Ferrocement Short Column under Axial and Eccentric Compression," ACI Structural Journal, Vol. 87, No. 5, September- October, 1990, pp. 523-529.
26. Fahmy, E. H., Shaheen, Y.B. and Korany, Y.S., "Repairing Reinforced Concrete Columns Using Ferrocement Laminates" Journal of Ferrocement, Vol. 29, No. 2, April 1999.
27. Kabir, A. and Hasan, M.M.," Precast Ferrocement Jackets for Brick Masonry Columns", Affordable Village Building Technologies, February 1999, pp.41-49
28. Takiguchi, K., Abdullah and Fujita, S.," On Strengthening and Repair of Shear Failure Type R/C Columns with Circular Ferrocement Jacket", Journal of Structural Construction Engineering, Architectural Institute of Japan, No. 541, March 2001,pp.145-153.
29. Keisuke, T., Katsuki, T., Shingo, H. and Abdullah, "Behavior of Concrete Confined by Ferrocement Boxes", Architectural Institute of Japan, Structure, 2002.
30. Abdullah and Takiguchi, K.," An Investigation into the Behavior and Strength of Reinforced Concrete Columns Strengthened with Ferrocement Jackets", Cement and Concrete Composites, 25, 2003, pp. 233-242.
31. Kumar, P. R., Oshima, T., Mikami, S. and Yamazaki, T., "Seismic Retrofit of Square Reinforced Concrete Piers by Ferrocement Jacketing", Structure and Infrastructure Engineering-Maintenance, Management, Life-Cycle Design and Performance, Taylor and Francis group Ltd, No.4, 1, 2005, pp. 253-262.

32. Kazemi, M.T. and Morshed, R.," Seismic Shear Strengthening of R/C Columns With ferrocement Jacket", Cement and Concrete Composites, 27, 2005, pp. 834-842.
33. Kumar, P.R., Oshima, T., Mikami, S. and Yamazaki, T.,"Studes on RC and Ferrocement Jacketed Columns Subjected to Simulated Seismic Loading", Asian Journal of Civil Engineering, Vol. 8, No. 2, 2007, pp. 215-225.
34. Shah, A.A.," Applications of Ferrocement in Strengthening of Unreinforced Masonry Columns", International Journal of Geology, Volume 5, Issue 1, 2011, pp.21-27.
35. Knowles, R B., and Park, R., "Strength of Concrete Filled Steel Tubular Columns", ASCE Journal of the Structural Division, Vol. 95, ST12, 1969, pp. 2565-2587.
36. Knowles, R B., and Park, R., "Axial Load Design for Concrete Filled Steel Tubes", ASCE Journal of the Structural Division, Vol. 96, ST 10, 1970, pp. 2125-2153.
37. Prion, H.G.L., and Boehme, J., "Beam Column Behavior of Steel Tubes Filled with High Strength Concrete", Canadian Journal of Civil Engineering, 21 (2), 1994, pp. 207-218.
38. Schneider, S.P., "Axially Loaded Concrete-Filled Steel Tubes", Journal of Structural Engineering, Vol. 124, No. 10, October 1998, pp. 1125-1138.
39. Uy, B., "Strength of Short Concrete Filled High Strength Steel Box Columns", Journal of Constructional Steel Research, 57, 2001, pp. 113-134.
40. Johansson, M., and Gylltoft, K., "Mechanical Behavior of Circular Steel-Concrete Composite Stub Columns", Journal of Structural Engineering, Vol. 128, No. 8, August 2002, pp. 1073-1081.

41. Liu, D.," Behavior of High Strength Rectangular Concrete-Filled Steel Hollow Section Columns under Eccentric Loading", Thin-Walled Structures, 42, 2004, pp.1631-1644.
42. Lam, D., and Wong, K.K.Y., "Axial Capacity of Concrete Filled Stainless Steel Columns", ASCE Journal of Structures, 2005, pp. 1107-1120.
43. Ellobody, E., Young, B. and Lam, D.," Behavior of Normal and High Strength Concrete-Filled Compact Steel Tube Circular Stub Columns", Journal of Constructional Steel Research 62, 2006, pp. 706–715.
44. Yang, Y.F., and Han, L.H., "Experimental Behavior of Recycled Aggregate Concrete Filled Steel Tubular Columns", Journal of Constructional Steel Research, 62, 2006, pp. 1310-1324.
45. Gupta, P.K., Sarda, S.M., and Kumar, M.S., "Experimental and Computational Study of Concrete Filled Steel Tubular Columns under Axial Loads", Journal of Constructional Steel Research, 63, 2007, pp. 183-193.
46. Ellobody, E., "Nonlinear Behavior of Concrete-Filled Stainless Steel Stiffened Slender Tube Columns", Thin-Walled Structures, 45, 2007, pp. 259-273.
47. Shahawy, M., Mirmiran, A.and Beitelman, T.," Tests and Modeling of Carbon-Wrapped Concrete Columns", Composites: Part B 31, 2000, pp. 471-480.
48. Li, G., Kidane, S.,Pang, S., Helms, J.E. Stubblefield, M. A.," Investigation into FRP Repaired RC columns", Composite Structures, 62, 2003, pp. 83-89.
49. Lin, H. J. and Liao, C.I.," Compressive Strength of Reinforced Concrete Column Confined by Composite Material", Composite Structures, 65, 2004, pp. 239-250.
50. Li, G., "Experimental Study of FRP Confined Concrete Cylinders", Engineering Structures, 28, 2006, pp. 1001-1008.

51. Hadi, M.N.S.," Behavior of FRP Strengthened Concrete Columns under Eccentric Compression Loading", Composite Structures, 77 2007, pp. 92-96.
52. Wu, G., Wu, Z.S., Lu, Z.T., and Ando, Y.B.," Structural Performance of Concrete Confined with Hybrid FRP Composites", Journal of Reinforced Plastics and Composites, Vol. 27, No. 12, 2008, pp. 1323-1348.
53. Chakrabarti, A., Chandra, A. and Bharagava, P.," Finite Element Analysis of Concrete Columns Confined with FRP Sheets", Journal of Reinforced Plastics and Composites, Vol. 27, No. 12, 2008, pp. 1349-1373
54. Benzaid, R., Chikh, N. E. and Mesbah, H.," Behavior of Square Concrete Column Confined With GFRP Composite Warp", Journal of Civil Engineering and Management, 14(2), 2008, pp. 115-120.
55. Sadeghian, P. and Rahai, A.R., "Numerical Modeling of Concrete Cylinders Confined with CFRP Composites", Journal of Reinforced Plastics and Composites, Vol. 27, No. 12/2008, pp. 1309-1321.
56. Sadeghian, P., Rahai, A.R. and Ehsani, M.R., "Strength and Ductility of Unreinforced Concrete Columns Confined with CFRP Composites under Uniaxial Loading", Concrete Repair, Rehabilitation and Retrofitting II – Alexander et al (eds), Taylor & Francis Group, London, 2009, pp. 1277-1283.
57. Yu, F. and Niu, D.," Stress-Strain Model of PVC-FRP Confined Concrete Column Subjected to Axial Compression", International Journal of the Physical Sciences, Vol. 5, No.15, 2010, pp. 2304-2309.
58. Mostofinejad, D. and Saadatmannd, H.," A Procedure for Predicting the Behavior of FRP Confined Concrete Using the FE Method", Scientia Iranica (Transaction A:Civil Engineering), 17 (6), 2010.
59. Harmon, T., Slattery, K., and Ramakrishnan, S., "The Effect of Confinement Stiffness on Confined Concrete", Proceedings of the

Second. International RILEM Symposium (FRPRCS-2), Taerwe, L., (Ed.), Vol. l, 1995, pp. 584-592.

60. Mirmiran, A., and Shahawy, M., "A Novel FRP-Concrete Composite Construction for the Infrastructure", Proceeding of Structural Congress XIII, ASCE, Boston, MA, 1995, pp. 1663-1666.
61. Kargahi, M., "Fiber Reinforced Plastic (FRP) Shell as External Reinforcement for Concrete Columns", Master thesis, University of Central Florida, Orlando, FL., 1995.
62. Pico, O., "Confinement Effectiveness of square FRP Tubes in Hybrid Columns", Master thesis, University of Central Florida, Orlando, FL., 1997.
63. El Echary, H., "Length Effect on Concrete-Filled FRP Tubes Using Acoustic Emission", Master Thesis, University of Central Florida, Orlando, FL., 1997.
64. Kanatharana, J., and Lu, L.W., "Strength and Ductility of Concrete Columns Reinforced with FRP Tubes", Proceedings of the Second International on Composites in Infrastructure ICCI '98, 1998, pp. 370-384.
65. Saafi, M., Toutanji, H.A., and Li, Z., "Behavior of Concrete Columns Confined with Fiber Reinforced Polymer Tubes", ACI Materials Journal, Vol. 96, No. 4, 1999, pp. 500-509.
66. Marzouck, M., and Sennah, K., "Concrete-Filled PVC Tubes as Compression Members", Proceedings of the International Challenges of Concrete Construction Congress, Scotland, U.K., Vol. 4, 2002, pp. 31-37.
67. Hong, W.K., and Kim, H.C., "Behavior of Concrete Columns Confined by Carbon Composite Tubes", Canadian Journal of Civil Eng., 31, 2, 2004, pp. 178-188.
68. Li, G., Torres, S., Alaywan, W., and Abadie, C., "Experimental Study of FRP Tube-Encased Concrete Columns", Journal of Composite Materials, Vol. 39, No. 13, 2005, pp. 1131-1145.

69. Li, G., "Experimental Study of FRP Confined Concrete Cylinders", Engineering Structures, 28, 2006, pp. 1001-1008.
70. Mohamed, H., and Masmoudi, R., "Behavior of FRP Tubes-Encased Concrete Columns under Concentric and Eccentric Loads", Composites & Polycon, American Composites Manufacturers Association, 2009, pp. 1-8.
71. Sinha BP, Gerstle KH, Tulin LG. Stress-Strain Relations for Concrete under Cyclic Loading. J ACI 1964; 61(2):195–211.
72. Karsan ID, Jirsa JO.," Behavior of Concrete under Compressive Loadings", Journal of Structural Division, Vol. 95, ST12, 1969, pp.2543-63.
73. Maher, A. and Darwin, D.," Mortar Constituent of Concrete in Compression", ACI Journal, March-April 1982, pp.100-109.
74. Buyukozturk, O. and Tseng, T. M.," Concrete Biaxial Cyclic Compression", journal of Structural Engineering, Vol. 110, No. 3, March, 1984, pp. 461-476.
75. Perry, S. H., Al-Shaikh, A. H. and Cheong, H. k.," Response of Confined Concrete to Cyclic Loading at Various Slow Strain rates", Material Research Society, Vol.64, 1986, pp.245-255.
76. Otter, D. E. and Naaman, A. E., "Properties of Steel Fiber Reinforced Concrete under Cyclic Loading", ACI Materials Journal, 1988, pp. 254-261.
77. Bahn, B. Y., and Hsu, C.T.,"Stress-Strain Behavior of Concrete under Cyclic Loading", ACI Material Journal, Vol.95, 2, 1998, pp.178-193.
78. Shao, Y., Zhu, Z. and Mirmiran, A.," Cyclic Modeling of FRP-Confined Concrete with Improved Ductility", Cement & Concrete Composites, 28, 2006, pp. 959-968.
79. Sima, J. F., Roca, P. and Molins, C.," Cyclic Constitutive Model for Concrete", Engineering Structures, 30, 2008, pp. 695-706.

80. Varma, R. K., Barros, J. A. O., Cruz, J. S. and Ferreira, D. M.," A Model to Simulate the Cyclic Axial Compressive Behavior of RC Columns Confined with CFRP Sheets", Challenges of Civil Construction, Torres Marques (Eds), Porto, 2008. Web page: www.civil.uminho.pt/composites
81. Thayalan, P., Aly, T. and Patnaikuni, I.," Behavior of Concrete-Filled Steel Tubes under Static and variable Repeated Loading", Journal of Constructional Steel Research, 65, 2009, pp. 900-908.
82. Sadeghi, K. and Nouban, F.," A New Stress-Strain Law for Confined Concrete under Cyclic Loading", International Journal of Academic Research, Vol. 2, No. 4, July 2010,pp. 6-15.
83. Shukla, M.," Equations of Cyclic Reloading and Unloading Stress-Strain Curves of SFRC", International Journal of Earth Sciences and Engineering, Volume 04, No 06, SPL, October 2011, pp 847-850.
84. American Society of Testing and Materials (ASTM), ASTM C-191, West Conshohocken, PA., 2002.
85. American Society of Testing and Materials (ASTM)," Standard Test Method for Compressive Strength of Hydraulic Cement Mortars (Using 50-mm Cube Specimens)", ASTM C-109, West Conshohocken, PA., 2002.
86. المواصفة العراقية رقم (5) لسنة 1984 للاسمنت البورتلاندي (I.O.S. 5 / 1984)
87. American Society of Testing and Materials (ASTM), ASTM C-136, West Conshohocken, PA., 2001.
88. المواصفة العراقية رقم (45) لسنة 1984 لركام المصادر الطبيعية (I.O.S. 45 / 1984)
89. British Standard Institute, "Method of Testing Concrete", Part 118, BS-1881, 1983
90. ASTM C-305, "Mechanical Mixing of Hydraulic Cement and Mortar of Plastic Consistency", American Standard of Testing and Materials, 1965.
91. American Society of Testing and Materials (ASTM), ASTM C-39, West Conshohocken, PA., 2002.
92. Hinton, E. and Owen, D. R. J., "Finite Element Programming", Academic

Press Inc. Ltd., London, 1977.

93. Hinton, E. and Owen, D. R. J., "An Introduction to Finite Element Computations", Pine ridge Press Limited, Swansea, U. K., 1979.
94. Khudair, J. A., "Structural Behavior of Reinforced Flanged Continuous Deep Beams Failing in Shear", Ph.D.Thesis, University of Basrah, 2004.
95. Stasa, F. L., "Applied Finite Element Analysis for Engineers" Holt, Rinehart and Winston, 1985.
96. Ali, M. S., "Experimental and Theoretical Investigation of Concrete Slabs on Grade ", Ph.D.Thesis, University of Basrah, 2010.
97. Kwak, H. G. and Filip C. Filippou, "Finite Element Analysis of Reinforced Concrete Structures under Monotonic Loads", Report No. UCB/SEMM-90/14 Structural Engineering, Mechanics and Materials Department of Civil Engineering University of California, Berkeley, November 1990.
98. Nilson, A. H., "Nonlinear Analysis of Reinforced Concrete by the Finite Element Method", Journal of American Institute, Vol. 65, Sept., 1968, pp. 757-766.
99. Chen, W.F., "Plasticity in Reinforced Concrete", McGraw-Hill Book Company, 1985.
100. Chen, W. F. and Saleeb, A. F., "Constitutive Equations for Engineering Materials", West Lafayette, Indiana, December 1981.
101. Hemmaty, Y., "Modeling of the Shear Force Transferred Between Cracks in Reinforced and Fiber Reinforced Concrete Structures", Proceedings of the ANSYS Conference, Vol. 1, Pittsburgh, Pennsylvania, Aug. 1998.
102. American Concrete Institute (ACI). (2008) "Building Code Requirements for Structural Concrete" ACI 318-08, American Concrete Institute, Detroit.

103.Kupfer, H. P., Hilsdorf, H. K., and Rusch, H., "Behavior of Concrete under Biaxial Stresses", ACI journal, Proceedings, Vol. 66, No. 8, Aug. 1969, pp. 656-666.

104.ASCE-ACI Task Committee, "State of the Art Report on Finite ElementAnalysis of Reinforced Concrete", ASCE special Publication, New York, 1982.

105.ANSYS, "Analysis Guide", Version 11, Swanson Analysis System, Inc., 2007.

106. ACI Committee 224, "Cracking of Concrete in Direct Tension", ACI Journal, Proceeding Vol. 83, No. 1, Jan.-Feb., 1986, pp. 3-13.

107.Tasuji, M. E., and Nilson, A. H., "Stress-Strain Response and Fracture of Concrete in Biaxial Loading", ACI Journal, Proceeding Vol. 75, No. 3, July, 1978, pp. 306-312.

108.Arther H. Nilson, David Darwin, and Charles W. Dolan, "Design of Concrete Structures", 13th ed., Copyright 2003.

109.Willam, K. J. and Warnke, E. P., "Constitutive Model for the Triaxial Behavior of Concrete", Proceedings, International Association for Bridge and Structural Engineering, Vol. 19, ISMES, Bergamo, Italy, 1975, pp.174.

110.Ngo, D., and Scordelies, A. C., "Finite Element Analysis of Reinforced Concrete Beams", American Concrete Institute, Vol. 65, No. 3, 1967, pp. 757-766.

111.Bentize, M. A., Darwin, D., and Donahey, R. C., "Deflection of Composite Beams with Web Openings", Journal of Structural Engineering, ASCE, Vol. 124, No. 10, October, 1998, pp. 1139-1147.

112.Rashid, Y. R., "Analysis of Prestressed Concrete Pressure Vessels", Nuclear Engineering and Design, Vol. 7, No. 4, 1968.

113.Wolanski, A. J., "Flexural Behavior of Reinforced and Prestressed Concrete Beams Using Finite Element Analysis", Master Thesis, University of Marquette, 2004.

114. Desayi, P., and Krishnan, S., "Equation for the Stress-Strain Curve of Concrete", Journal of the American Concrete Institute, 61, March., 1964, pp.345-350.

115.Cervera, M. and Hinton, E., "Non-Linear Analysis of Reinforced Concrete Plates and Shells Using a Three Dimensional Model", In the Computational Modeling of Reinforced Concrete Structures, Eds. Hinton, E. and Owen, R., Pine ridge Press, Swansea, U. K., 1986, PP. 237-370.

116.Zienkiewicz, O. C., "The Finite Element Method", 3rd Ed., McGraw-Hill Book Company, New York, 1977.

117. Sakai, J. and Kawashima, K.," Unloading and Reloading Stress-Strain Model for Confined Concrete", Journal of Structural Engineering, ASCE, 132(1), 2006, pp.112-122.

118.Popovics, S., "Analytical Approach to Complete Stress-Strain Curves", Cement and Concrete Research, Vol. 3, No. 5, Sep., 1973, pp. 583-599.

119.Cusson, D., and Paultre, P., "High-Strength Concrete Columns Confined by Rectangular Ties," Journal of Structural Engineering, ASCE, Vol. 120, No.3, 1994, pp. 783-804.

للأحمال القصوى للخرسانة العادية هو بين 0.88 الى 1.094 للاعمدة الخرسانية المقواة بالفيروسمنت.

ودرست العديد من المتغيرات الخاصة بالعمود الخرساني وقشرة الفيروسمنت باستخدام طريقة العناصر المحددة لمعرفة مدى تأثيرها. فقد تم دراسة تأثير مقاومة الانضغاط للخرسانة، معامل المرونة للقشرة الفيروسمنتيق، و تاثير الحمل المسلط على القشرة الفيروسمنتية.

كما اقترحت الدراسة ايضا تطوير نماذج جديدة لعلاقة الاجهاد- الانفعال للاعمدة الخرسانية المقواة بالفيروسمنت تحت تاثير احمال م ستمرة (monotonic loads) وكذا لمنحنيي الافراغ واعادة التحميل.

الخلاصة

احد المتطلبات الاساسية لتقوية و رفع كفاءة المنشآت الخرسانية المسلحة هوتعزيز قدرة الأعمدة على تحمل الزيادة المتوقعة فى الاحمال المعرضة لها. حيث توجد تقنيات مختلفة لزيادة تحمل الأعمدة القائمة فى المباني، و تختلف تلك التقنيات من حيث المميزات و العيوب.

لذلك فأهداف هذا البحث هو دراسة كفاءة استخدام قشرة الفيروسمنت لزيادة الضغط الجانبي للعمود الخرساني.

وتشتمل الدراسة على جزئين؛ العمل المختبري والبحث النظري. وكان الغرض الرئيسي من العمل المختبري هو بحث السلوك الانشائي للأعمدة الخرس انية المقواة بقشرة الفيروسمنت تحت تأثير أحمال ضغط م حورية. وتضمن العمل المختبري فحص 48 عموداً تحت تحت تأثير حمل ضغط محوري ، وكانت المتغيرات المدروسة هي عدد طبقات الاسلاك (volume fraction) ومقاومة الانظغاط للملاط و حجم العمود ونوع الحمل المسلط . لقد وجد بان قشرة الفيروسمنت توفر حصرا جانبياً جيداً للخرسانة ممّا يزيد من مقاومة العمود ومطيليته. حيث تراوحت نسبة مقاومة العمود الم قوى بالفيروسمنت الى العمود العادي بين 1.132 و 2.291 للأعمدة المقواة بملاط ذي مقاومة 35MPa، في حين تراوحت هذه النسبة بين 1.364 و 2.34 للأعمدة الم قواة بملاط ذي مقاومة 45MPa. كما ناقشت الدراسة صلاحية (envelope curve) في تفسير سلوك الاعمدة تحت تاثير الاحمال الدورية.

وفي الجزء الثاني من الدراسة ، تم تحليل الاعمدة الخرسانية المفحوصة بالاعتماد على طريقة العناصر المحددة ثلاثية الأبعاد اللاخطية . وتم اعتماد برنامج (ANSYS11.0) لتحليل النموذج الثلاثي البعد . وجرت نمذجة كلا من العمود الخرساني وقشرة الفيروسمنت باستخدام عناصر من نوع (SOLID65) بثمانية عقد، ونمذجة صفائح التحميل بعناصر (SOLID45) أيضا بثمانية عقد. إما حديد التسليح للاسلاك ، فقد افترض على انه موزع (Smeared) داخل العناصر ثلاثية الأبعاد للفيروسمنت . كما افترض أن هناك ترابط تام بين العمود الخرساني و قشرة الفيروسمنت.

وجد بأن التمثيل المستخدم للاعمدة بطريقة العناصر المحددة يعطي قيم ذات اتفاق جيد مع النتائج المختبرية. وقد وجد إن نسب القيم للدراسة النظرية إلى قيم النتائج المختبرية

تصرف الاعمدة الخرسانية القصيرة المقواة بالفيروسمنت

اطروحة مقدمة إلى

كلية الهندسة – جامعة البصرة

وهي جزء من متطلبات نيل درجة دكتوراه فلسفة في

الهندسة المدنية (إنشاءات)

من قبل

عبدالخالق عبداليمة جعفر

شباط 2012